THE DEVELOPMENT OF AMPLIFIED VIBRATION-ABSORBING ISOLATORS FOR TONAL TIME-VARYING EXCITATION

by

Nicolaas Francois du Plooy

Submitted in partial fulfilment of the requirements for the degree

Philosophiae Doctor

in the

Faculty of Engineering, Built Environment and Information Technology

University of Pretoria

Pretoria

2004

Summary

The development of amplified vibration-absorbing isolators for tonal time-varying excitation

Candidate : NF du Plooy
Supervisor : Prof. PS Heyns
Department : Mechanical and Aeronautical Engineering
Degree : PhD

Vibration isolation is a procedure through which the transmission of oscillating disturbances or forces is reduced. The ideal isolator is one that will support the equipment being isolated without transmitting any dynamic forces. An isolator with infinite static stiffness and zero dynamic stiffness will achieve this goal. Although this ideal isolation cannot be obtained in practice, it can be approximated through a wide range of devices. This approximation occurs over a limited frequency band and methods of increasing this band were investigated. The goal of this thesis was to further our understanding of mechanical systems that can approximate the ideal isolator behaviour.

To compare the various devices the blocked transfer dynamic stiffness was defined. This value was found to represent the isolator properties without the additional complication of the equipment being isolated as happens in traditional transmissibility methods. Three classes of devices were distinguished namely isolators, vibration-absorbing isolators (VAI) and amplified vibration-absorbing isolators (AVAI). The last two types exploit nodalisation to reduce the dynamic stiffness over a limited frequency range. The focus of this work is the broadening of the effective low stiffness bandwidth of amplified vibration-absorbing isolators by adapting system characteristics. If the excitation is tonal time-varying these devices can be used successfully.

Two novel adaptive amplified vibration-absorbing isolators were introduced and studied in the time and frequency domains. The type I AVAI uses flexible reservoir walls to vary the isolation frequency. The type II device incorporates a heavy metal slug. Both devices use variable pressure air springs to change their stiffness. The use of air springs are convenient, offers low damping and can be used in an application such as a pneumatic rock drill handle to eliminate the need for a control system. Conceptual design methodologies for both damped and undamped fixed and adaptive isolation frequency AVAIs are presented. To determine the effects of tuning the equations were transformed in terms of constant frequency ratios and the variable stiffness ratio. The devices can be controlled using an optimisation approach, but care should be taken since the method could be unsuccessful in some cases.

The design was then applied to a pneumatic rock drill. This application was particularly demanding because the stiffness had to be large enough for the operator to remain in control of the drill, yet low enough to offer isolation. Extensive measurements of drill vibration at a test facility found that the

maximum acceleration values were 18.72 m/s^2. The maximum allowed under the proposed European Union legislation is 10 m/s^2 for short durations. The excitation consisted of a large tonal component and wide-band noise. The tonal component contributed ~50% of the total weighted equivalent acceleration experienced by the operator and a vibration absorbing isolator should therefore be an ideal solution. The measurements also showed that the excitation frequency is a function of the supply air pressure. By using the supply air pressure to feed the air spring the device could be made self-tuning. Numerical simulation showed that there is only a slight difference between using the supply pressure and forcing coincidence of the excitation and isolation frequencies. It was also found that the vibration levels could be reduced to below 10 m/s^2 in some cases.

Keywords: vibration, absorber, isolator, tonal time-varying, control, optimisation

Opsomming

Die ontwikkeling van 'n vibrasie-absorberende isolator met hefboomversterking vir enkelfrekwensie tyd-variante opwekking

Student : NF du Plooy
Promotor : Prof. PS Heyns
Departement : Meganiese en Lugvaartkundige Ingenieurswese
Graad : PhD

Vibrasie-isolasie is 'n prosedure wat ten doel het om die transmissie van ossillerende verplasings en kragte te verminder. Die ideale isolator sal toerusting staties ondersteun sonder dat dinamise kragte oorgedra word. 'n Isolator met oneindige statiese styfheid en geen dinamiese styfheid nie sal aan dié vereiste voldoen. Alhoewel ideale isolasie nie in die praktyk haalbaar is nie, kan dit benader word deur 'n verskeidenheid van toestelle. Hierdie benadering vind slegs oor 'n beperkte frekwensieband plaas en metodes wat dié band kan vergroot is bestudeer. Die doelwit van die proefskrif is om die bestaande kennis van meganiese stelsels wat die ideale isolator kan benader, uit te brei.

Om die verskillende toestelle met mekaar te vergelyk is die geblokkeerde-oordrag dinamiese styfheid gedefinieër. Daar is gevind dat hierdie waarde die isolator se eienskappe weerspieël sonder die komplikasie van die toerusting wat geïsoleer word, soos wat gebeur met die tradisionele transmissiemetodes. Drie groepe toestelle word onderskei, naamlik isolators, vibrasie-absorberende isolators (VAI) en vibrasie-absorberende isolators met hefboomversterking (AVAI). Die laaste twee tipes maak gebruik van nodalisering om die dinamsiese styfheid oor 'n beperkte frekwensieband te verminder. Die fokus van die werk is om die effektiewe lae-styfheid bandwydte te verlaag deur die isolator se eienskappe te wysig. In gevalle waar die opwekking gedomineer word deur 'n enkele frekwensie wat tyd-variant is, kan die toestelle met groot sukses gebruik word.

Twee unieke vibrasie-absorberende isolators met hefboomversterking is bestudeer in die tyd- en frekwensiedomeins. Die tipe I AVAI verander die styfheid van die reservoir wand om sodoende die isolasiefrekwensie te verander. Die tipe II AVAI maak gebruik van 'n swaar metaalprop om die absorbeerdermassa te vermeerder. Beide toestelle maak gebruik van veranderbare lugdrukvere om hul styfheid te verander. Die gebruik van lugvere is gerieflik, dra min demping by en kan saam met 'n lugdrukboor gebruik word op so 'n manier dat 'n beheerstelsel onnodig is. Konseptuele ontwerpmetodologië is voorgestel vir beide ongedemp en gedempte, veranderbare en vaste frekwensie toestelle. Om die effek van instemming beter te bestudeer is die vergelykings getransformeer in terme van konstante frekwensieverhoudings en die veranderbare-styfheidverhouding. Die toestelle is beheer deur van optimering gebruik te maak, maar hierdie metode moet omsigtig benader word aangesien die tegniek in sekere gevalle nie sal werk nie.

Die ontwerpmetodologië is vervolgens toegepas op 'n lugdrukrotsboor. Die toepassing is uitdagend aangesien die styfheid enersyds hoog genoeg moet wees sodat die operateur die boor effektief kan gebruik en andersyds laag genoeg moet wees sodat genoegsame isolasie verskaf word. 'n Groot aantal metings van boorvibrasie is gedoen by 'n toetsfasiliteit. Die maksimum geweegde ekwivalente versnelling wat gemeet is, was 18.72 m/s^2. Die maksimum wat toegelaat word deur voorgestelde wetgewing in die Europese Unie is 10 m/s^2, en dit net vir kort periodes. Daar is gevind dat hoë, noubandopwekking ~50% bydra tot die geweegde ekwivalente versnelling en 'n vibrasie-absorberende isolator blyk dus die ideale oplossing te wees. Die metings het ook getoon dat die opwekfrekwensie 'n liniêere funksie is van die toevoerdruk. Die toevoerdruk kan dus direk gebruik word om die lugveerstyfheid te bepaal en sodoende kan die behoefte vir 'n beheerstelsel uitgeskakel word. Numeriese simulasie het getoon dat deur dit te doen daar slegs 'n klein verskil in effektiwiteit is teenoor 'n situasie waar die beheerstelsel die opwek- en isolasie frekwensies ekwivalent geforseer het. Daar is ook gevind dat die vibrasie tot onder 10 m/s^2 verminder kan word in sekere gevalle.

Sleutelwoorde: vibrasie, absorbeerder, isolator, enkelfrekwensie tyd-variant, beheer, optimering

Acknowledgements

I would like to thank:

- Prof. Heyns for his guidance.
- My parents for understanding.
- Gavin Pemberton and Peter Hes for their assistance with design and measurements.
- Prof. Brennan for his valuable comments and hospitality.

This work was done with financial aid from Boart Longyear, SIMRAC and the Mellon Foundation.

Table of contents

Nomenclature

Symbol	Description	Unit
a	Acceleration	m/s^2
A_0	Orifice area	m^2
A_a	Port area	m^2
A_b	Reservoir area	m^2
A_e	Effective area	m^2
$a_{h,j}$	j^{th} ⅓ octave-band acceleration	m/s^2
$a_{h,w}$	Frequency-weighted hand-transmitted acceleration	m/s^2
A_r	Area ratio	
c	Damping coefficient	Ns/m
C	Discharge coefficient	
C_c	Constant discharge coefficient	
c_n	Complex Fourier coefficient	
d_0	Orifice diameter	m
d_a	Port diameter	m
d_b	Reservoir diameter	m
d_i	Inner diameter	m
d_o	Outer diameter	m
E	Young's modulus	Pa
e_i	i^{th} Unit vector	
F	Force amplitude	N
f	Frequency	Hz
f	Objective function value	
f_c	Control force	N
F_T	Transmitted force amplitude	N
G	Shear modulus	Pa
h	Hysteretic damping coefficient	N/m
h	Height	m
H	Transfer function	
i	$\sqrt{-1}$	
I	Moment of inertia	m^4
I_G	Mass moment of inertia about the centre of gravity	$kg.m^2$
k	Stiffness	N/m
k_G^r	Radial geometric stiffness	N/m
k_G	Axial geometric stiffness	N/m
k_{Gh}	Axial geometric stiffness excluding height effects	N/m
K_j	j^{th} ⅓ octave band weighting factor	
l	Port length (type I)	m
l	Slug length (type II)	m
l_c	Slug spring compressed length	m
l_e	Protrusion length	m

l_i	Inner length	m
l_o	Outer length	m
l_p	Port length (type II)	m
l_r	Reservoir length	m
l_T	Total length	m
$\dot{m}$	Mass flow rate	kg/s
m	Mass	kg
M	Narrow-band excitation amplitude	
n	Ratio of specific heats	
N	Normal load	N
p	Power	W
P, p	Pressure	Pa
P_0, P_i	Initial pressure	Pa
R	Rayleigh energy	J
R	Gas constant	J/kg.K
r	Radius	m
r_i	Inner radius	m
R_i	Reaction force i	N
r_o	Outer radius	m
S_{xx}	Power spectral density	
S_{xy}	Cross spectral density	
T	Kinetic energy	J
T_0	Initial temperature	K
T_r	Transmissibility	
T_s	Supply air temperature	K
V	Potential energy	J
V	Volume	m^3
W	One-sided power spectral density	$Unit^2/Hz$
X, Y, U	Harmonic excitation amplitude	m
x, u, y	Time-dependent displacement	m
α	Non-linearity parameter	
α	Lead screw helix angle	rad
α, β, γ	Gain	
δ_{st}	Static deflection	m
ΔW	Energy loss per cycle	J
$\Delta\omega_e$	Excitation bandwidth	rad/s
$\Delta\Omega_e$	Noise bandwidth	rad/s
ε	Noise amplitude	
ε	Radial clearance	m
ζ	Damping ratio	
η	Loss factor	
θ	Angle	rad
λ	Reduced area ratio	
μ_A	Area ratio	
μ_k	Stiffness ratio	

μ_m	Mass ratio	
ν	Poisson's ratio	
ρ	Density	kg/m^3
φ, θ	Rotation angle	rad
ω	Circular frequency	rad/s
ω_e	Excitation frequency	rad/s
ω_i	Isolation frequency	rad/s
Ω_i	Damped isolation frequency	rad/s
ω_n	Natural frequency	rad/s
Ω_n	Damped natural frequency or natural frequency of a two degree of freedom system	rad/s

1 Introduction to vibration-absorbing isolators

Vibration isolation is a procedure through which the transmission of oscillating disturbances or forces is reduced. This involves the insertion of a flexible member between the two vibrating bodies as shown in Figure 1.1. Most commonly this will be between the equipment and its supporting structure, where the vibration is emanating from either of the two and transmission to the other is undesirable. It can easily be anticipated that a very soft isolator will achieve this goal. However, the design of such an isolator is complicated by the fact that the equipment needs to be kept at a constant relative displacement to the structure at low frequencies.

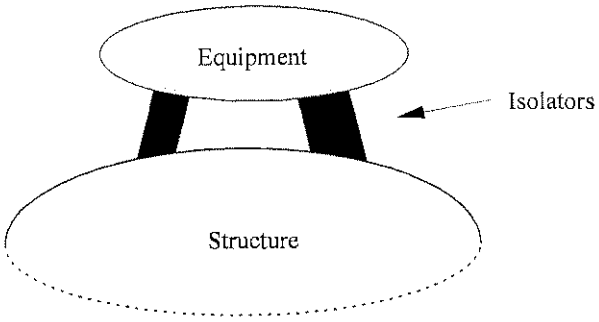

Figure 1.1: Isolation system

Miller & Ahmadian (1992) summarized the function of an isolator:

> *"In the simplest of terms, the ideal mount would have infinite stiffness at low frequencies and zero dynamic stiffness in the frequency range or the disturbance."*

Mead (2000) agreed:

> *"The study of vibration isolation must view the whole system in its three parts – the source system in which the vibration is generated, the receiver system in which the vibration is unwanted, and the interconnecting isolation system which must hold them together with adequate static stiffness and strength,* ***but with the smallest possible dynamic stiffness.***"

This goal can be illustrated graphically as shown in Figure 1.2.

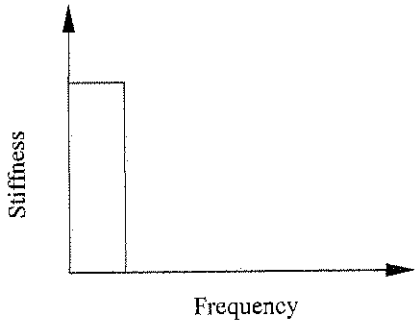

Figure 1.2: Stiffness *vs.* frequency relationship of an ideal isolator

As can be expected this discontinuous behaviour cannot be realised in practical systems. The goal of this thesis is to further our understanding of mechanical systems that can approximate this ideal isolator behaviour. Because of this approximation, a particular type of isolator will not necessarily be the best in all situations and additional parameters, such as the characteristics of the input, must be considered in order to arrive at an optimal solution.

Thus, when choosing a suitable isolator for a certain application it is important to define the isolation objective. One common aim would be to reduce the acceleration of sensitive equipment. This might be defined as a root-mean-square (rms) vibration criterion. Another aim might be to increase fatigne life. A further aim, which will be explored more fully in this thesis, relates to human vibration. In this case the output spectrum needs to be evaluated in terms of the ISO 5349 specification on hand-transmitted vibration. The optimal isolator choice will therefore depend on both the input spectrum as well as the evaluation criteria used. In cases where the excitation is tonal or narrow band an isolator with low dynamic stiffness at that frequency could be the best choice. In practice, however, random noise and harmonics will accompany most realistic inputs making the optimal choice less straightforward. The isolation philosophy is described graphically in Figure 1.3.

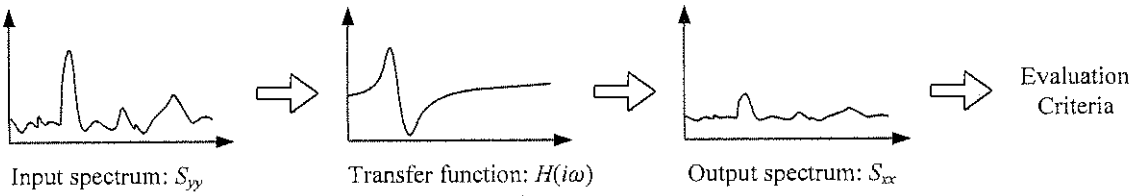

Figure 1.3: Isolation philosophy

A subset of tonal-excitation problems pertains to systems where the excitation frequency varies over a limited band. These changes can be a result of environmental changes such as ambient temperature or operational changes such as load. One possible solution to such a problem is to create an isolator that will continuously change its properties such that the region of lowest dynamic stiffness coincides with the excitation frequency. Such an isolator can be realised in a number of ways, the most general being an active isolator. It is, however, also possible to construct a passive isolator with adaptive properties (termed an adaptive isolator). Figure 1.4 illustrates how the adaptive algorithm seeks to minimise the objective of the isolator assuming that the input is stationary.

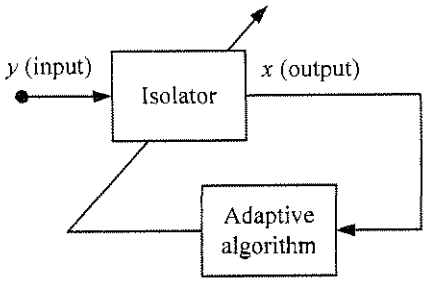

Figure 1.4: Adaptive isolator

The purpose of this chapter is to classify isolators in order to clarify the contribution of the thesis. The classification is not intended to be exhaustive, but examples will be given to illustrate isolator properties. Three approaches are identified namely passive, adaptive and active techniques. Passive

isolators are defined as resilient devices having no power requirements. Adaptive isolators can change its properties with some small power cost, while active isolators have a large power requirement. Passive techniques to reduce the dynamic stiffness of isolators will be introduced. These techniques are closely related to vibration absorbers and will therefore be termed vibration-absorbing isolators (VAI). The chapter will close by stating the aims of the research.

1.1 Background

In order to study the stiffness of isolators as a function of frequency it is necessary to define some terminology. Static stiffness refers to the deflection of the isolator when subjected to a constant force such as the weight of the equipment. Dynamic stiffness concerns the deflection when the system is moving and can be expressed as a function of frequency and is defined for frequencies larger than zero. The common definition of dynamic stiffness is the inverse of the direct receptance; F/Y in Figure 1.5 where the X, and Y refers to the excitation amplitude (Mead, 2000). It is, however, convenient to use the blocked ($X = 0$) transfer dynamic stiffness (F_T/Y) since it is independent of the mass of the attachment equipment (m_e). It is also possible to define the unblocked dynamic stiffness as $F_T/(X-Y)$. This has some advantages, which will be explored later. In this chapter a comparison of various isolation techniques will be discussed and it will be shown that the blocked transfer dynamic stiffness is a convenient measure to use. For the sake of brevity the blocked transfer dynamic stiffness will simply be referred to as the dynamic stiffness. When the dynamic stiffness is divided by the static stiffness the result is termed the normalised dynamic stiffness. This is an appropriate non-dimensional quantity.

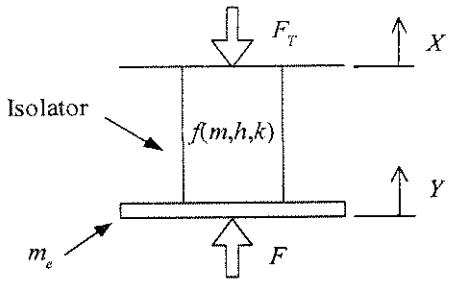

Figure 1.5: The definition of dynamic stiffness

For the system shown in Figure 1.5 the blocked and unblocked normalised dynamic stiffness lead to the same expressions (assuming the isolator mass is insignificant):

$$\frac{F_{T,unblocked}}{k(Y-X)} = 1 + i\eta \tag{1.1}$$

$$\frac{F_{T,blocked}}{kY} = 1 + i\eta \tag{1.2}$$

For some of the systems described later the blocked and unblocked dynamic stiffness is not equal. The unblocked dynamic stiffness has the advantage that it can be used to derive the system transmissibility. On the other hand, the blocked dynamic stiffness has the advantage that it only contains the properties of the isolator and not of the system being isolated. Therefore, it is independent of the natural

frequency of the system and as such explains the available parameters to reduce the transfer of motion clearly.

This study will further be limited to lumped-parameter systems i.e. rigid isolated masses suspended on massless isolators as shown in Figure 1.1. Such an approach is especially valid for low frequencies, which is the focus of this work. It will also be assumed that the resilient elements are massless, that is, massless spring and damping elements. The total isolation system need not be massless as it could include discrete masses, but these are expressly placed there to change the dynamics of the system and not to better idealise the spring or damping element behaviour. Due to the inclusion of masses the applied force (F) will not be equal to the transmitted force (F_T).

Most vibration texts consider both the transfer of force from a vibrating machine to its base as well as the transmission from a vibrating base to sensitive equipment. The first case is concerned with the force transmissibility, while the second considers motion transmissibility. For a single degree of freedom system the conclusions drawn from these two cases are essentially identical i.e. that the isolator stiffness should be as low as possible. This thesis will be limited to the motion transmissibility problem, without losing generality.

Several models exist to describe damping. The models that will be used in this work are:

1. Viscous damping $F_d = c\dot{x}$
2. Hysteretic damping $F_d = hx = k\eta x$
3. Coulomb or friction damping $F_d = -\text{sign}(\dot{x})\mu N$

When comparing the normalised dynamic stiffness of isolators in the frequency domain it is convenient to use hysteretic damping. It is not possible to use viscous damping for this purpose since non-dimensionalisation becomes impossible due to the addition of displacement and velocity units. In addition, although the linear viscous description of damping is mathematically convenient it is often not very realistic and it has been found that hysteretic damping better describes many common isolator materials, for instance, rubber (Rivin, 2001). In some cases time-domain simulation is used and in such cases the use of viscous damping will be necessary.

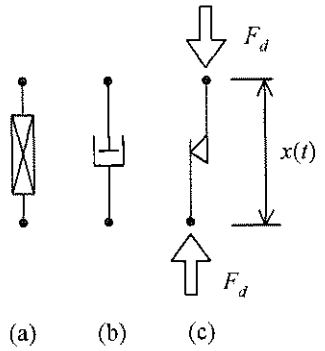

Figure 1.6: Damping models (a) hysteretic damper (b) viscous damper (c) Coulomb damper

Several models exist that describe the properties of an isolator. The most common element is the well-known Kelvin solid shown in Figure 1.7(c). Often elastomer behaviour is frequency dependent and can more accurately be described by the model shown in Figure 1.7(d) (Rivin, 2001).

The normalised dynamic stiffness for this model is [Equation (A.3)]:

$$\frac{F_T}{kY} = 1 + \frac{k'}{k}\frac{i\omega\frac{c}{k}}{\frac{k'}{k} + i\omega\frac{c}{k}} \tag{1.3}$$

The excitation (and response) is assumed to be of the form $y(t) = Ye^{i\omega t}$. To increase the readability of the thesis the derivation of the majority of the equations will be shown in appendices. Each chapter has its own appendix (i.e. Chapter 1, Appendix A etc.). References will indicate the equation in the relevant section of the appendix where the derivation can be found.

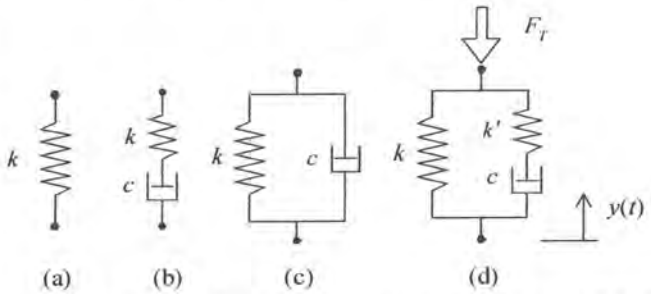

Figure 1.7: (a) Hook, (b) Maxwell, (c) Kelvin and (d) relaxation models (Rivin, 2001)

At low frequencies the model behaves as if the stiffness k' has no effect since the velocity across the damper is small. As the frequency increases the damper becomes solid and the stiffness k' appears parallel to stiffness k. The effect of frequency can be seen in Figure 1.8. This model does not take into account the effect of amplitude and temperature.

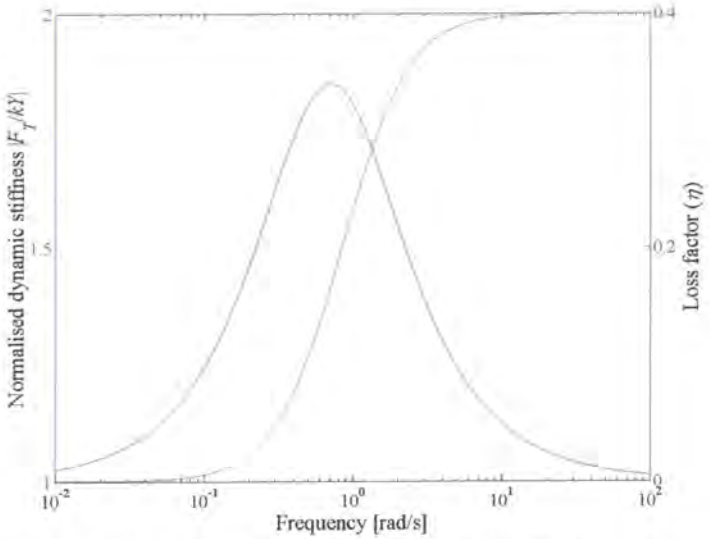

Figure 1.8: Normalised dynamic stiffness and loss factor of a relaxation model ($c/k = 1$ and $k'/k = 1$)

The quantities plotted in Figure 1.8 are the absolute values of the complex normalised dynamic stiffness and the loss factor. The loss factor is defined as the ratio of the imaginary and real parts of the complex dynamic stiffness as shown in Figure 1.9.

The loss factor is:

$$\eta = \frac{\mathrm{Im}\left(\frac{F_T}{kY}\right)}{\mathrm{Re}\left(\frac{F_T}{kY}\right)} = \tan(\theta) \tag{1.4}$$

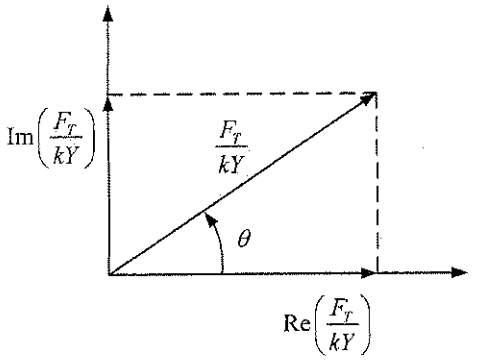

Figure 1.9: Complex dynamic stiffness phasor

Traditionally, isolation is discussed with reference to the single degree of freedom absolute transmissibility rather than dynamic stiffness (Rao, 1990). The single degree of freedom model is shown in Figure 1.10.

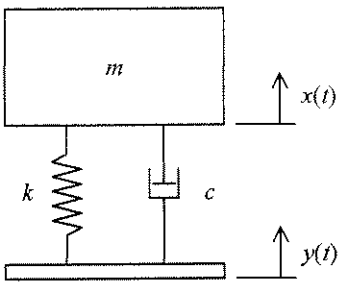

Figure 1.10: Mechanical model of a single degree of freedom isolator model

The transmissibility for a system with viscous damping is:

$$\frac{X}{Y} = \frac{1 + i2\frac{\omega}{\omega_n}\zeta}{1 + i2\frac{\omega}{\omega_n}\zeta - \left(\frac{\omega}{\omega_n}\right)^2} \tag{1.5}$$

where ζ is the damping ratio and ω_n the natural frequency. When using hysteretic damping the transmissibility is:

$$\frac{X}{Y} = \frac{1 + i\eta}{1 + i\eta - \left(\frac{\omega}{\omega_n}\right)^2} \tag{1.6}$$

For both these cases isolation occurs if the excitation frequency is larger than $\sqrt{2}\,\omega_n$ as shown in Figure 1.11.

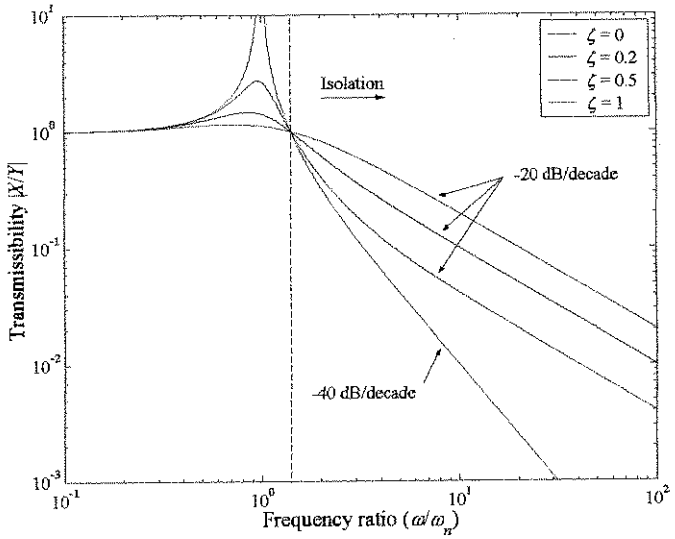

Figure 1.11: Single degree of freedom system transmissibility

In cases where the "rattle space" between of the isolated mass and its foundation is limited, the relative transmissibility is of importance. It is defined as $(X\text{-}Y)/Y$ and is related to the absolute transmissibility through:

$$\begin{aligned} T_r\big|_{REL} &= \frac{X-Y}{Y} \\ &= \frac{X}{Y} - 1 \\ &= T_r\big|_{ABS} - 1 \end{aligned} \tag{1.7}$$

In this thesis the absolute transmissibility will be used exclusively and will simply be referred to as the transmissibility. The relationship between the system transmissibility and the unblocked dynamic stiffness can be found by considering the force balance on the isolated mass as shown in Figure 1.12. The force acting on the mass can be calculated using the unblocked dynamic stiffness in Equation (1.1).

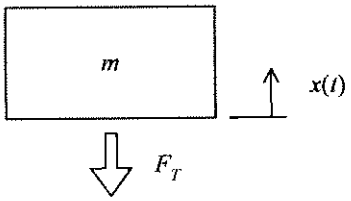

Figure 1.12: Force balance for the calculation of transmissibility

The result of the force balance is the transmissibility as shown before in Equation (1.6):

$$\begin{aligned} \sum F = F_T &= m\ddot{x} \\ k(1+i\eta)(Y-X) &= -\omega^2 mX \\ \frac{X}{Y} &= \frac{1+i\eta}{1+i\eta-\left(\frac{\omega}{\omega_n}\right)^2} \end{aligned} \tag{1.8}$$

By analysing several systems it was found that the blocked dynamic stiffness is a convenient method of comparison. In most cases it highlights the important parameters better than the transmissibility would have. There are, however, some exceptions where the transmissibility is modified by other factors than the dynamic stiffness, notably by "skyhook" damping and non-linear isolators. In such cases the effects will be explained by using transmissibility. The unblocked dynamic stiffness is only useful when the relationship between dynamic stiffness and transmissibility needs to be explained. In the following paragraphs the results of several unique derivations will be shown. These derivations relied heavily on existing vibration absorber literature, but had to be significantly adapted to fit the field of isolators.

1.2 Isolators

1.2.1 Passive isolators

Passive vibration isolation concepts can most easily be explained with reference to the basic isolator model shown in Figure 1.13.

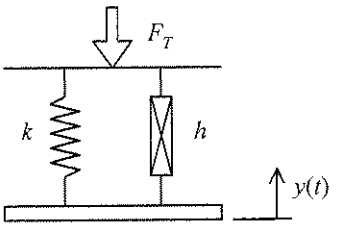

Figure 1.13: Mechanical model of a vibration isolator

The normalised dynamic stiffness is defined as the force transmitted by the isolator when a prescribed displacement (y) is applied:

$$\frac{F_T}{kY} = 1 + i\eta \tag{1.9}$$

Clearly, the normalised dynamic stiffness can never be less than 1 for a passive isolator. Additionally, materials tests have shown that for elastomers the loss factor will be a function of frequency and will generally increase with frequency resulting in an even more unfavourable situation as was shown in Figure 1.8 (Oyadiji & Tomlinson, 1994). Miller and Ahmadian (1992) also showed that elastomer an isolator's stiffness increases with frequency. Equation (1.9) implies that the stiffness must be as low as possible. There are, however, practical limits to the lowest stiffness that can be achieved in isolators. Improving these limits is not within the scope of this work and therefore, throughout this comparison, it will be assumed that the stiffness is as low as the technology used will allow.

The passive isolator can be augmented by adding an intermediate mass that will reduce the dynamic stiffness at high frequencies (Rivin, 2001). These devices are also known as two-stage mounts. The intermediate mass is inserted as shown in Figure 1.14. The stiffness values are chosen such that the normalised dynamic stiffness at zero Hz is the same as for the previous case, which allows fair comparison.

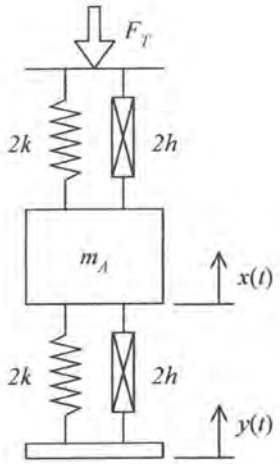

Figure 1.14: Mechanical model of an intermediate mass isolator

The normalised dynamic stiffness for this system is [Equation (A.9)]:

$$\frac{F_T}{kY} = \frac{(1+i\eta)^2}{1+i\eta-\left(\frac{\omega}{\omega_n}\right)^2} \qquad (1.10)$$

where: $\omega_n = \sqrt{\frac{4k}{m_A}}$

In Figure 1.15 it can be seen that the normalised dynamic stiffness will be less than one for all frequencies higher than $\sqrt{2}\,\omega_n$. The slope of the curve at high frequencies is -40 dB/decade, but this comes at the price of an area of high stiffness at low frequency. When the figure is compared to Figure 1.2 the approximation to the goal set out for this work is clear. By choosing the intermediate mass as large as possible the natural frequency of the isolator decreases and the isolation performance is optimised.

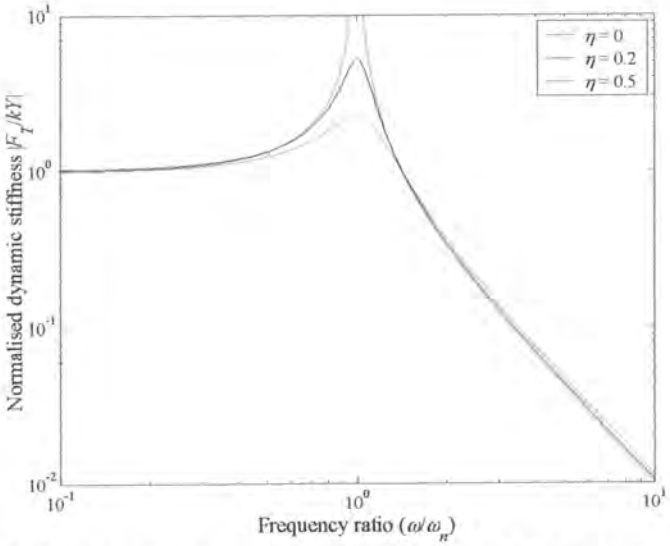

Figure 1.15: Normalised dynamic stiffness of an isolator with an intermediate mass

Several practical isolators display non-linear behaviour. This is often a consequence of their construction and not necessarily a performance requirement, as is the case with air springs. It is, however, possible to exploit non-linear behaviour to improve isolator performance. Two types of non-linear behaviour in isolators are identified. Firstly, a non-linear load-deflection characteristic is termed static non-linearity (Rivin, 2001). Examples of static non-linearity include Belleville springs, constant natural frequency isolators and motion-limiting bumpers (Babitsky & Veprik, 1998). Secondly, stiffness as well as damping that is frequency and amplitude dependent are categorised as dynamic non-linearities. Elastomeric materials commonly used for isolators exhibit this kind of behaviour as was illustrated in Figure 1.8.

An important aspect regarding non-linear behaviour of a single degree of freedom system with Duffing type stiffness is that the amplitude-frequency characteristic of the system "bends" at the natural frequency. This behaviour reduces the response at the natural frequency without the addition of damping, but at high amplitudes subharmonic oscillations will deteriorate isolation performance. Subharmonic oscillations cannot occur in systems where the damping exceeds a critical value depending on type and degree of non-linearity as well as amplitude of excitation (Rivin, 2001).

1.2.2 Adaptive isolators

Adaptive isolation entails the variation of stiffness and damping as shown in Figure 1.16. Adaptive isolation is also often termed semi-active isolation (Yu *et al.*, 2001).

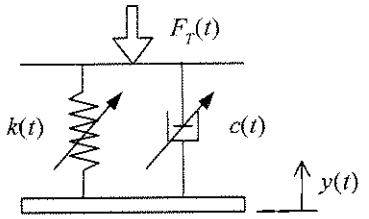

Figure 1.16: Mechanical model of a semi-active isolator

It is immediately clear that such a device cannot be used to reduce the normalised dynamic stiffness of the isolator. As such, these devices are not useful during steady state but can have advantages during transients. For instance, it is possible to increase the damping during start-up and rundown to reduce the response, while lowering damping when the excitation frequency is higher than $\sqrt{2}\,\omega_n$. Other instances where such devices can be used are in cases with conflicting requirements such as automotive suspensions, which need to be soft for comfort and hard to counteract body forces resulting from acceleration, braking and cornering. Cases where isolation is not the primary aim of the isolator falls outside the scope of this work.

1.2.3 Active isolators

Active isolation of vibration can be categorised as either feedback or feedforward techniques. Feedback control uses the response of the system as the input to the controller while feedforward control estimates the input directly. Generally, deterministic excitation is treated with feedforward

control and random excitation with feedback control (Fuller *et al.*, 1996). Two feedback techniques will be described. Absolute velocity feedback will be presented first (also termed "skyhook" damping). This is a well-known and effective technique to reduce system response at resonance (Karnopp, 1995). This technique does not reduce the dynamic stiffness, as does the second technique, which uses absolute input feedback.

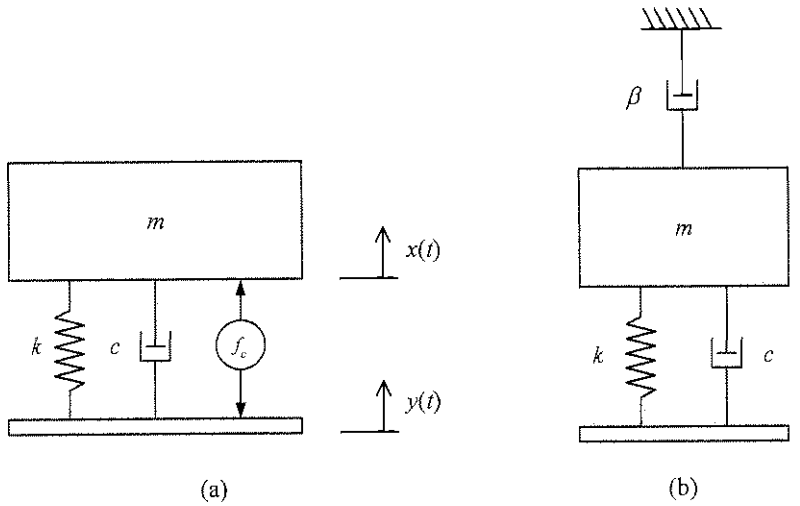

Figure 1.17: Mechanical model of an (a) active vibration isolator with absolute velocity feedback and (b) equivalent skyhook damper system

The control force (f_c) is a function of negative absolute velocity:

$$f_c(t) = -\beta \dot{x} \tag{1.11}$$

The system transmissibility is [Equation (A.14)]:

$$\frac{X}{Y} = \frac{1 + i2\dfrac{\omega}{\omega_n}\zeta}{1 + i2\dfrac{\omega}{\omega_n}\left(\zeta + \zeta_\beta\right) - \left(\dfrac{\omega}{\omega_n}\right)^2} \tag{1.12}$$

where: $\zeta = \dfrac{c}{2m\omega_n}$, $\zeta_\beta = \dfrac{\beta}{2m\omega_n}$

The most advantageous situation occurs when the system damping (ζ) is zero. In this case the high frequency roll-off remains -40 dB/decade regardless of the addition of damping by the control force as shown in Figure 1.18. If system damping exists the high frequency roll-off will be -20 dB/decade.

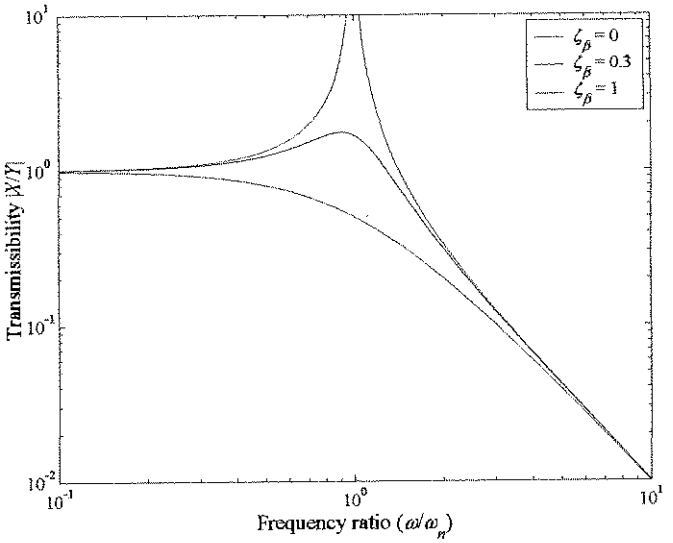

Figure 1.18: Transmissibility of an isolator with active damping ($\zeta = 0$)

Although many other active vibration isolator concepts exist, one is of particular interest since it is possible to arrange it in such a way that a system equivalent to the amplified vibration-absorbing isolator to be discussed in §1.4, is obtained. The model for this isolator is shown in Figure 1.19. It uses the input characteristics for the control force.

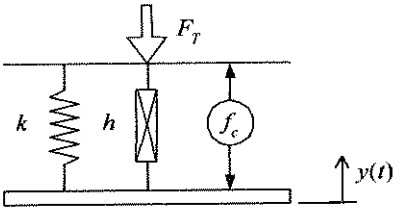

Figure 1.19: Mechanical model of an active isolator

The control force is:

$$f_c(t) = \alpha\ddot{y} + (\gamma + i\beta)y \tag{1.13}$$

where the parameters α, β and γ represent the gains.

The normalised dynamic stiffness is [Equation (A.18)]:

$$\frac{F_T}{(k+\gamma)Y} = 1 + i\frac{k\eta + \beta}{k+\gamma} - \left(\frac{\omega}{\omega_i'}\right)^2 \tag{1.14}$$

where: $\omega_i' = \sqrt{\dfrac{k+\gamma}{\alpha}}$

The undamped dynamic stiffness will be a minimum at the isolation frequency ω_i' as shown in Figure 1.20. It is possible to change the isolation frequency by varying the stiffness and acceleration feedback gains. Additionally, negative complex damping feedback can be used to reduce inevitable system

damping. These effects will be discussed in more detail in §1.4.2, which describes an adaptive device with similar properties but with some advantages, for instance, lower power requirement.

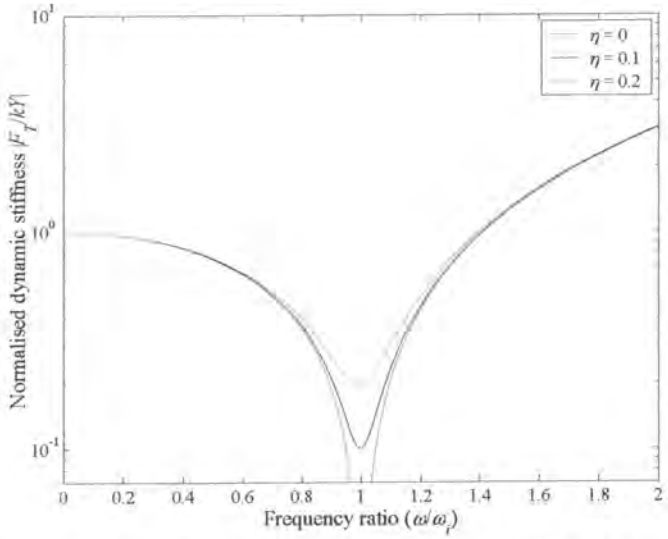

Figure 1.20: Normalised dynamic stiffness for an active isolator with absolute input acceleration feedback ($\alpha/k = 1$, $\gamma = 0$ and $\beta = 0$)

1.3 Vibration-absorbing isolators

Vibration absorbers are devices used to reduce the response of a structure by fixing a secondary spring mass system to the structure as shown in Figure 1.21. The first recorded use of vibration absorbers was to control the rolling motion of ships at sea (Watts, 1883). The vibration absorber was patented by Frahm (1909). The first theoretical analysis was done by Ormondroyd and Den Hartog (1928).

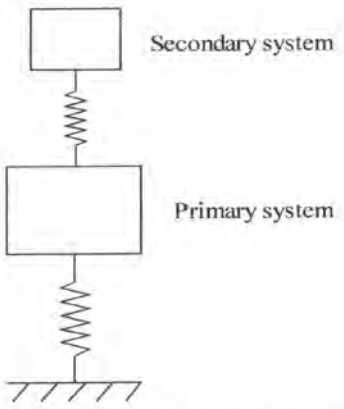

Figure 1.21: Vibration absorber

The secondary system is often called an auxiliary system. The objective of the absorber is to minimise the motion of the primary mass. This is achieved by tuning the natural frequency of the absorber to coincide with the excitation frequency. The result is a two degree of freedom system with zero response at the tuned frequency if no damping is present. Although vibration absorbers are classified as vibration control devices (Rao, 1990) they are not isolators since they are not fitted in the load path.

It is, however, possible to use a vibration absorber as part of a two-stage isolator as shown in Figure 1.22. This type of vibration control strategy is classified as nodalization by Mead (2000). He noted the similarity between nodalization and vibration isolators and the fact that it reacts the exciting force of the source by its own inertia forces.

Some authors (Mead, 2000 and Kidner and Brennan, 1999) prefer the term neutralizer to that of absorber because in their opinion "absorber" implies that the energy is dissipated. Ideally, in a low damping absorber, no energy will be dissipated. However, the word absorber is deeply entrenched in the literature and the device could therefore be called a Vibration-Absorbing Isolator (VAI) or a vibration-neutralizing isolator. In this work the term vibration-absorbing isolator will be used to describe the device. The relationship between the VAI and the vibration absorber is evident and the literature on vibration absorbers is extensive. A large proportion is applicable to the VAI, as will be shown next.

1.3.1 Passive vibration-absorbing isolators

The passive VAI is shown in Figure 1.22. Subscript A describes the intermediate (primary) mass and B the absorber (secondary) mass.

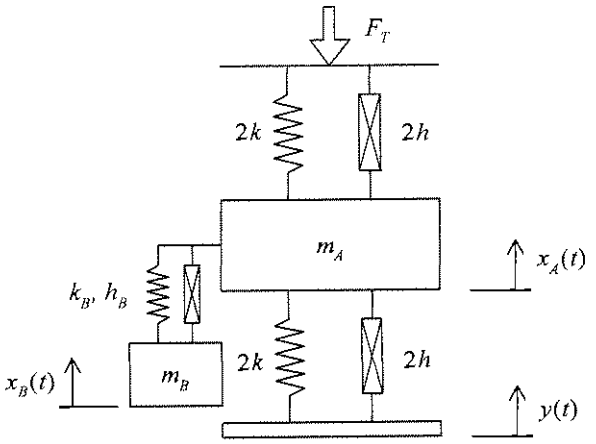

Figure 1.22: Mechanical model of a passive vibration-absorbing isolator ($h_B = \eta_B k_B$ and $h = \eta k$)

The normalised dynamic stiffness is given by [Equation (A.28)]:

$$\frac{F_T}{kY} = \frac{1 + i\eta_B - \left(\frac{\omega}{\omega_B}\right)^2}{\left[1 + i\eta + \frac{1}{4}\frac{k_B}{k}(1 + i\eta_B) - \left(\frac{\omega}{\omega_A}\right)^2\right]\left[1 + i\eta_B - \left(\frac{\omega}{\omega_B}\right)^2\right] - \frac{1}{4}\frac{k_B}{k}(1 + i\eta_B)} \tag{1.15}$$

where: $\omega_A = \sqrt{\frac{4k}{m_A}}$, $\omega_B = \sqrt{\frac{k_B}{m_B}}$

The main concern with the use of such a device is the small bandwidth over which the dynamic stiffness is low. Here the bandwidth is defined as the frequency range for which the normalized

dynamic stiffness is below 1 since that is the baseline for the best possible passive isolator. In Figure 1.23 it can be seen that the addition of damping decreases this bandwidth. Of course damping will be beneficial if the excitation frequency strays from the anticipated value.

The low-stiffness bandwidth could also be increased by increasing the mass ratio (m_B/m_A) as is shown in Figure 1.24. For a vibration absorber this will be difficult to do since the primary system mass is normally fixed and large. For the VAI it will be possible to choose a low intermediate mass (m_A) and therefore a large mass ratio is possible.

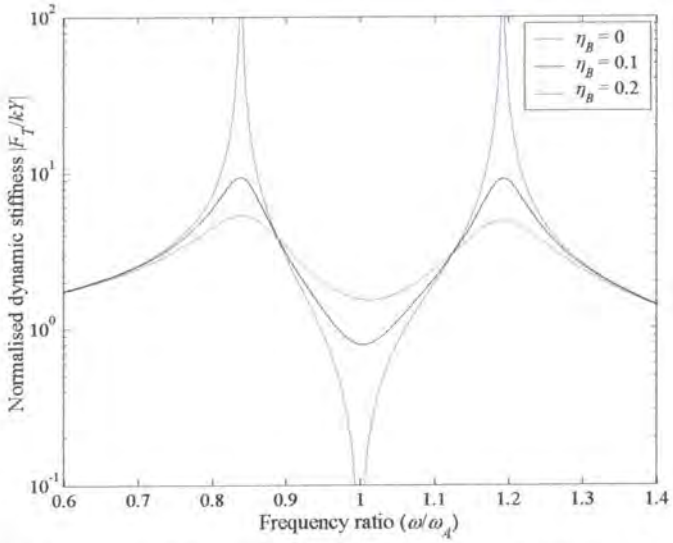

Figure 1.23: Normalised dynamic stiffness of a vibration-absorbing isolator as a function of absorber loss factor ($m_B/m_A = 1/8$, $\omega_A = \omega_B$ and $\eta = 0$)

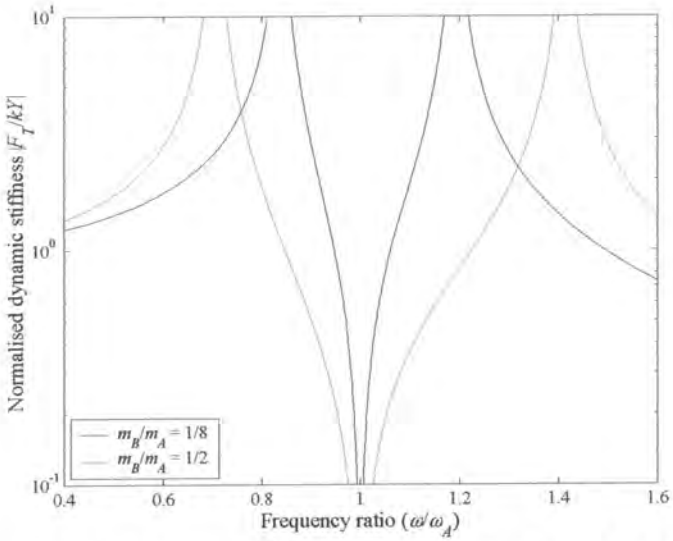

Figure 1.24: Normalised dynamic stiffness of a vibration-absorbing isolator as a function of mass ratio ($\eta = \eta_B = 0$ and $\omega_A = \omega_B$)

The bandwidth can be calculated by setting the normalised dynamic stiffness equal to 1 in Equation (1.15). There are four frequencies at which the undamped dynamic stiffness is equal to 1 as shown in Equation (1.16). Frequencies ω_2 and ω_3 define the bandwidth [Equations (A.30) and (A.32)].

$$\omega_1 = 0$$

$$\frac{\omega_2}{\omega_A} = \sqrt{\frac{1}{4}\mu_k + \left(\frac{\omega_B}{\omega_A}\right)^2} \tag{1.16}$$

$$\frac{\omega_3}{\omega_A}, \frac{\omega_4}{\omega_A} = \sqrt{\frac{\frac{1}{4}\mu_k + 2 + \left(\frac{\omega_B}{\omega_A}\right)^2 \mp \sqrt{\left[\frac{1}{4}\mu_k + 2 + \left(\frac{\omega_B}{\omega_A}\right)^2\right]^2 - 8\left(\frac{\omega_B}{\omega_A}\right)^2}}{2}}$$

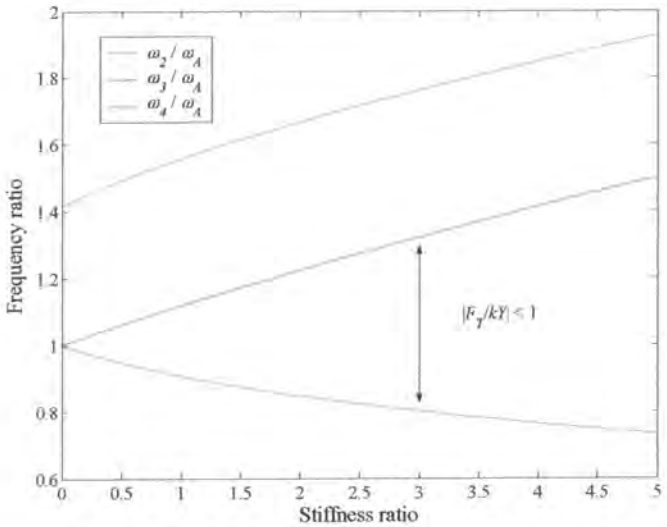

Figure 1.25: Frequencies at which the normalised dynamic stiffness is equal to 1 as a function of stiffness ratio (undamped, $\omega_B/\omega_A = 1$ and $\omega_1 = 0$)

The low stiffness bandwidth can be increased by attaching multiple vibration absorbers to the primary system as shown in Figure 1.26. The absorbers are tuned to a range of frequencies. It is possible to increase the suppression bandwidth by increasing the number of absorbers (Igusa & Xu, 1991 and Brennan, 1997a). Figure 1.27 shows a typical result for a system where the natural frequencies of a set of vibration absorbers are separated by η_q, the loss factor of the vibration absorbers. It is also clear from the figure that the resulting dynamic stiffness will be higher if the total mass of the absorbers is kept constant. The q^{th} natural frequency is:

$$\omega_q = \omega_A + (q-1)\eta_q \tag{1.17}$$

The q^{th} stiffness ratio is:

$$\frac{k_q}{k} = \frac{1}{N}\frac{\sum_{q=1}^{N} m_q}{m_A}\omega_q^2 \tag{1.18}$$

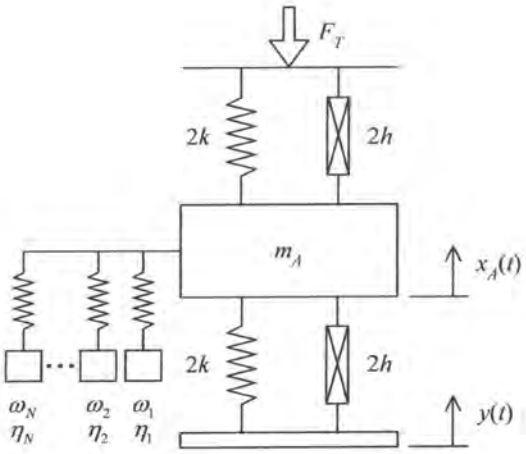

Figure 1.26: Mechanical model of a VAI with multiple vibration absorbers attached

The normalised dynamic stiffness for N absorbers can be written as [Equation (A.44)]:

$$\frac{F_T}{kY} = \frac{\left(1+i\eta_A\right)^2}{1+i\eta_A + \frac{1}{4}\sum_{q=1}^{N}\frac{k_q}{k}\left(1+i\eta_q\right) - \left(\frac{\omega}{\omega_A}\right)^2 - \frac{1}{4}\sum_{q=1}^{N}\frac{k_q}{k}\frac{\left(1+i\eta_q\right)^2}{1+i\eta_q - \left(\frac{\omega}{\omega_q}\right)^2}} \tag{1.19}$$

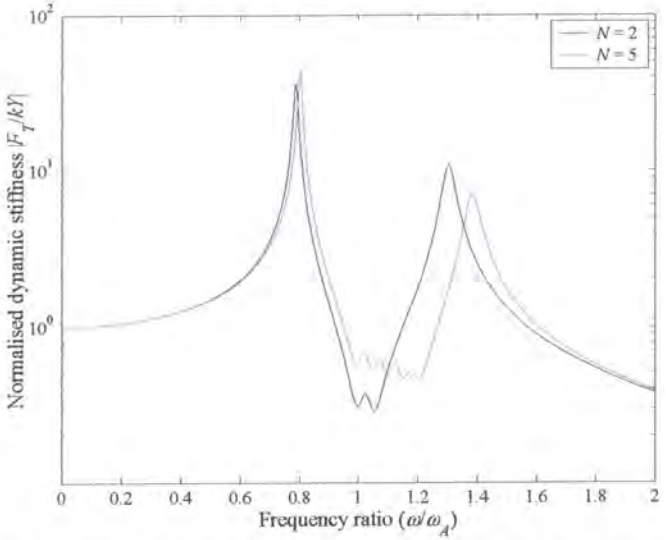

Figure 1.27: Normalised dynamic stiffness for a set of 2 and 5 vibration absorbers of equal total mass with natural frequencies separated by η_q starting at $\omega_A = 1$ ($\eta_1..\eta_q = 0.05$, $\eta = 0$ and $\Sigma m_q/m_A = 1$)

It has been shown that non-linear softening springs can be used to double the suppression bandwidth of a linear vibration absorber (Hunt & Nissen, 1981). For Duffing type non-linearity the spring restoring force (f_s) is given by:

$$f_s = k_B\left(x_A - x_B\right) + \alpha k_B\left(x_A - x_B\right)^3 \tag{1.20}$$

where α controls the degree of non-linearity. The normalised dynamic stiffness can be calculated by solving the following set of equations (Appendix A.3.3):

$$\begin{aligned}
&\ddot{x}_A + \frac{1}{2}\frac{k_B}{k}\frac{\zeta_B}{\omega_B}\omega_A^2(\dot{x}_A - \dot{x}_B) + \omega_A^2 x_A + \frac{1}{4}\frac{k_B}{k}\omega_A^2\left[x_A - x_B + \alpha(x_A - x_B)^3\right] = \frac{1}{2}\omega_A^2 y \\
&\ddot{x}_B - 2\zeta_B\omega_B(\dot{x}_A - \dot{x}_B) - \omega_B^2\left[x_A - x_B - \alpha(x_A - x_B)^3\right] = 0 \\
&\frac{f_T}{k} = 2x_A \\
&\text{where: } \zeta_B = \frac{c_B}{2m_B\omega_B},\quad \omega_A = \sqrt{\frac{4k}{m_A}},\quad \omega_B = \sqrt{\frac{k_B}{m_B}}
\end{aligned} \tag{1.21}$$

The normalised dynamic stiffness is shown in Figure 1.28 for various degrees of non-linearity.

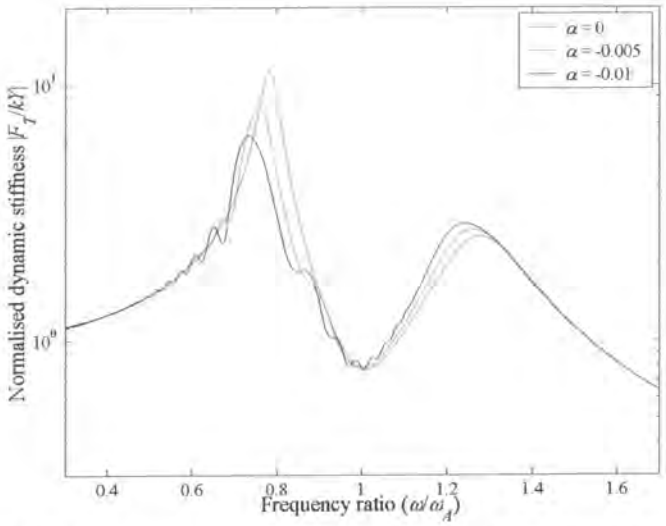

Figure 1.28: Normalised dynamic stiffness of a VAI with a non-linear absorber ($\zeta = 0.1$, $Y = 1$ and $\omega_A = \omega_B = k_B/k = 1$)

This section showed that it is possible to realise a device with a frequency range for which the dynamic stiffness is much less than one, even zero, in the ideal undamped configuration. It was also shown that the low stiffness bandwidth could be increased in a number of ways, each having its own disadvantage, notably addition of mass and added complexity. The adaptive vibration-absorbing isolator will address these problems, albeit with its own disadvantages, as will be shown next.

1.3.2 Adaptive vibration-absorbing isolators

Adaptive or tuneable vibration-absorbing isolators are devices that will automatically change their isolation frequency by changing either the absorber mass or stiffness. The advantage of tuning the absorber is that a low damping device can be used without the mass penalty normally required to increase the bandwidth. From Equation (1.15) it can be seen that the isolation frequency (ω_B) is equally sensitive to the absorber mass and stiffness. Practical implementations favour devices that changed stiffness, because it is easier to implement rather than attempting to change the absorber

mass. The technologies available to effect a change in stiffness are extensive, each with its own drawbacks and advantages. Methods that are available to vary stiffness can be categorised as follows:

1. Variable spring geometry:
    a. Compression of non-linear springs (Desanghere & Vansevenant, 1994).
    b. Moving a collar on a helical spring to control the number of active coils (Franchek *et al.*, 1995).
    c. Changing the moment of inertia of a beam or plate assembly (Walsh & Lamancusa, 1992 and Jensen, 1999).
    d. Varying spring displacement by changing its kinematics. Margolis (1992) used a variable fulcrum position for this purpose. Ribakov and Gluck (1998) changed the angle between the working direction and a set of angled helical springs to change their effective stiffness.
2. Variable physical property:
    a. Changing air spring pressure (Brennan, 1997b).
    b. Shape memory alloy Young's modulus modification, (Williams *et al.*, 2000).
    c. Using the magnetostrictive effect to vary the Young's modulus of a terfenol-D rod (Flatau *et al.*, 1998).
    d. Exploiting the temperature dependence of an elastomer's Young's modulus (Ketema, 1998).
    e. Magnetorheological elastomers under the influence of a magnetic field (Jolly *et al.*, 1996).
3. Electromagnets used to de-stiffen mechanical springs (Waterman, 1988).

Several variable damping methods have been published. Since variable damping is not useful for decreasing the low stiffness bandwidth it will not be discussed here. The model of an adaptive VAI with variable stiffness is shown in Figure 1.29.

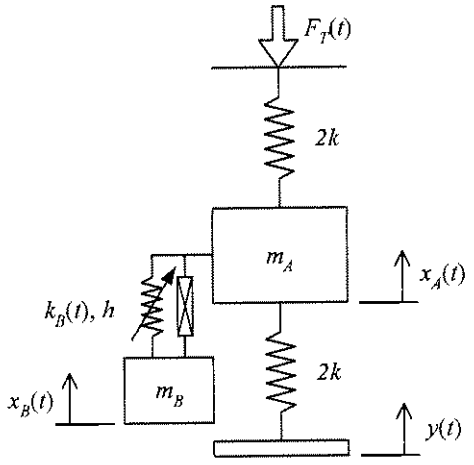

Figure 1.29: Mechanical model of an adaptive VAI

The normalised dynamic stiffness for the model shown in Figure 1.29 can be solved in the time domain using numerical integration. Such an analysis requires that the hysteretic damper be replaced by a viscous damper.

To calculate the transient behaviour the following set of equations must be solved [Equations (A.52) and (A.55)]:

$$\begin{aligned}
&\ddot{x}_A + \sqrt{\mu_m}\bar{\zeta}_B\omega_A\left(\dot{x}_A - \dot{x}_B\right) + \omega_A^2 x_A + \frac{1}{4}\mu_k(t)\,\omega_A^2\left(x_A - x_B\right) = \frac{1}{2}\omega_A^2 y \\
&\ddot{x}_B - \frac{\bar{\zeta}_B}{\sqrt{\mu_m}}\omega_A\left(\dot{x}_A - \dot{x}_B\right) - \frac{1}{4}\frac{\mu_k(t)}{\mu_m}\omega_A^2\left(x_A - x_B\right) = 0 \\
&\frac{f_T}{k} = 2x_A
\end{aligned} \tag{1.22}$$

where μ_k is the stiffness ratio k_B/k and μ_m is the mass ratio m_B/m_A. A simulation of the response of a system with an initial excitation frequency of 2π is shown in Figure 1.30. The excitation frequency is instantaneously doubled at 100 s and the stiffness is changed at 200 s such that the absorber is tuned to the new excitation frequency. In practice, there will be various delays associated with tuning and these will be discussed in more detail in §1.4.2. After tuning, some transient behaviour can be observed which must be controlled by the addition of damping.

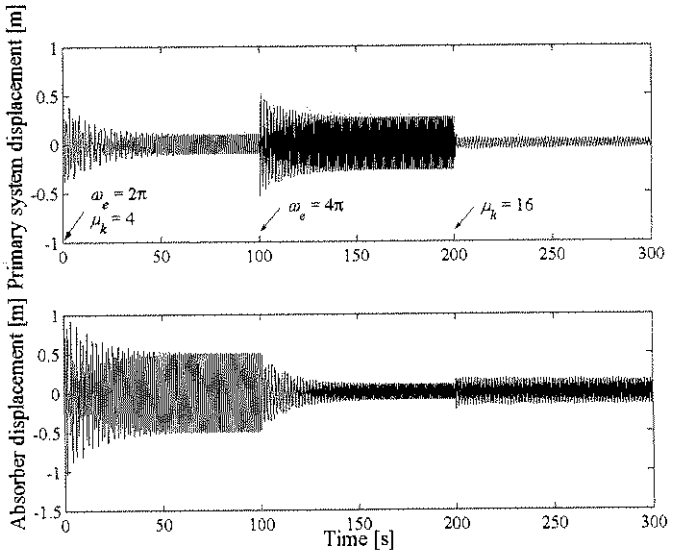

Figure 1.30: Transient response of a VAI ($\omega_A = 2\pi$, $\bar{\zeta}_B = 0.2$ and $Y = 1$)

If the assumption is made that the frequency changes will only occur occasionally and will be separated by long periods of steady state operation, it will be useful to derive the normalised dynamic stiffness. It is possible to find the normalised dynamic stiffness as a function of the intermediate mass natural frequency (ω_A) and the mass and stiffness ratios by rewriting Equation (1.15) [Equation (A.58)]:

$$\frac{F_T}{kY} = \frac{1 + i\eta_B - 4\dfrac{\mu_m}{\mu_k}\left(\dfrac{\omega}{\omega_A}\right)^2}{\left[1 + i\eta + \dfrac{1}{4}\mu_k\left(1 + i\eta_B\right) - \left(\dfrac{\omega}{\omega_A}\right)^2\right]\left[1 + i\eta_B - 4\dfrac{\mu_m}{\mu_k}\left(\dfrac{\omega}{\omega_A}\right)^2\right] - \dfrac{1}{4}\mu_k\left(1 + i\eta_B\right)} \tag{1.23}$$

where: $\mu_m = \dfrac{m_B}{m_A}$, $\mu_k = \dfrac{k_B}{k}$

This is a convenient equation with which to study the effect of absorber stiffness change on the dynamic stiffness of the VAI. The undamped frequency of minimum dynamic stiffness can be found by equating this equation to zero and will be termed the isolation frequency. The numerator can then be rewritten to yield the frequency ratio [Equation (A.56)]:

$$\frac{\omega_B}{\omega_A} = \frac{1}{2}\sqrt{\frac{\mu_k}{\mu_m}} \tag{1.24}$$

where ω_B is the isolation frequency. Figure 1.31 illustrates the effect when the stiffness ratio is changed from 2 to 6. At a stiffness ratio of 4 the isolation frequency is equal to the natural frequency of the intermediate mass (ω_A). To double the isolation frequency the stiffness ratio must be four times larger.

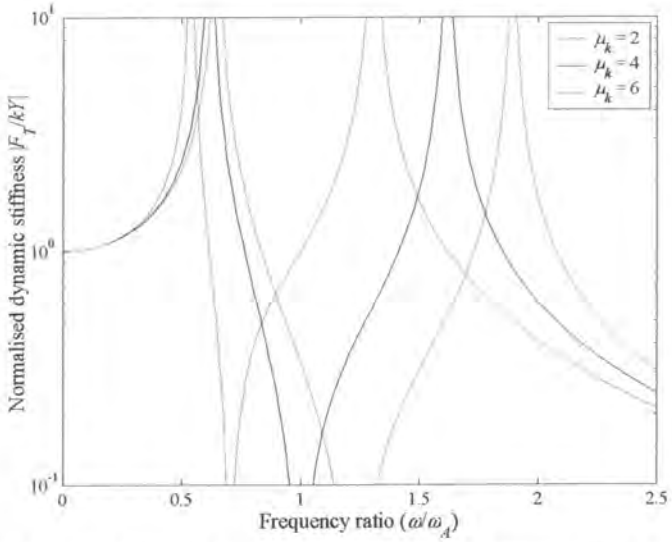

Figure 1.31: Effect of stiffness ratio on the normalised dynamic stiffness ($\mu_m = 1$, $\omega_A = 1$ and $\eta = \eta_B = 0$)

Figure 1.32 shows clearly that the adaptive VAI will be the most sensitive at low stiffness and mass ratios. At low mass ratios the adaptive VAI sensitivity increases, which strengthens the argument for tuning since for large mass ratios tuning will not be necessary.

Although it appears as if the adaptive VAI will be very sensitive at low stiffness ratios, its usefulness in this region will be limited by the proximity of the first frequency of large dynamic stiffness as illustrated in Figure 1.33 by the proximity of the black and blue lines for stiffness ratios less than 1. Depending on the application it could be decided that the separation is adequate above a stiffness ratio of, for instance, 1. If the stiffness change method chosen could vary the stiffness ratio from 1 to 6 the frequency ratio achievable will range from ~0.5 to ~1. Because of the proximity of the first frequency of large dynamic stiffness to the isolation frequency the full range of frequency ratios from 0 to ~1 is therefore not useful in practice. The frequencies of maximum dynamic stiffness are given by [Equation (A.61)]:

$$\frac{\Omega_1}{\omega_A}, \frac{\Omega_2}{\omega_A} = \sqrt{\frac{1+\frac{1}{4}\mu_k + \frac{1}{4}\frac{\mu_k}{\mu_m} \mp \sqrt{\left(1+\frac{1}{4}\mu_k + \frac{1}{4}\frac{\mu_k}{\mu_m}\right)^2 - \frac{\mu_k}{\mu_m}}}{2}} \tag{1.25}$$

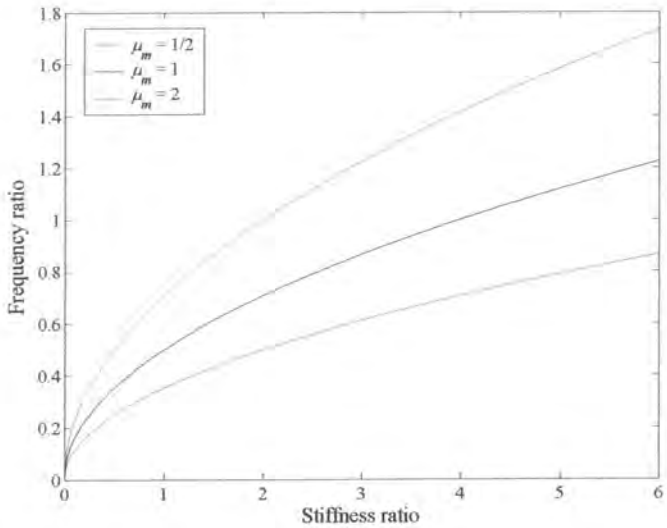

Figure 1.32: Undamped frequency ratio (ω_B/ω_A) *vs.* stiffness ratio for various mass ratios

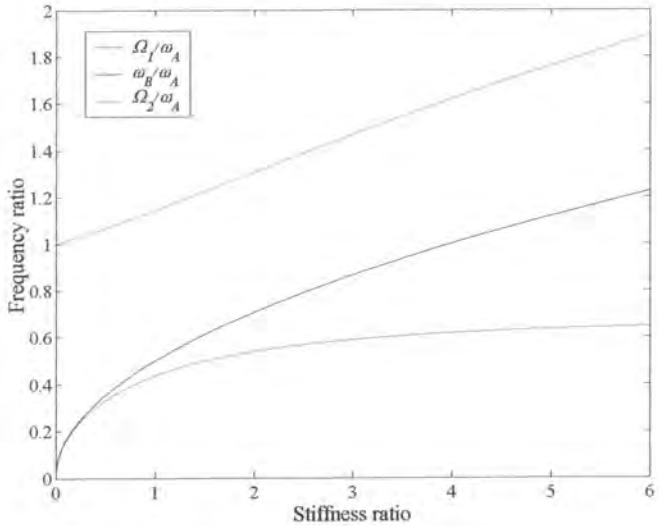

Figure 1.33: Undamped frequencies of maximum and minimum dynamic stiffness as a function of stiffness ratio ($\mu_m = 1$)

The envelope of the normalised dynamic stiffness can be calculated by finding the minimum stiffness at each frequency when changing the stiffness ratio from 0 to 6 and is shown in Figure 1.34. The normalised dynamic stiffness is less than 1 for a wide range of frequencies, but all frequencies will not be useful in a practical system because of the proximity of the first frequency of large dynamic stiffness at low stiffness ratios as discussed above.

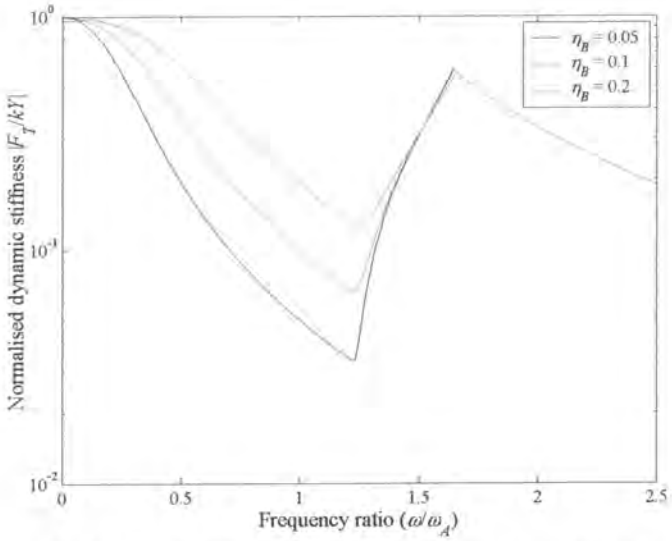

Figure 1.34: The normalised dynamic stiffness envelope *vs.* frequency ratio when changing the stiffness ratio (μ_k) from 0 to 6 ($\mu_m = 1$)

1.3.3 Active vibration-absorbing isolators

Active vibration absorbers consist of an actuator, most commonly in parallel with the passive spring supporting the absorber mass, as shown in Figure 1.35.

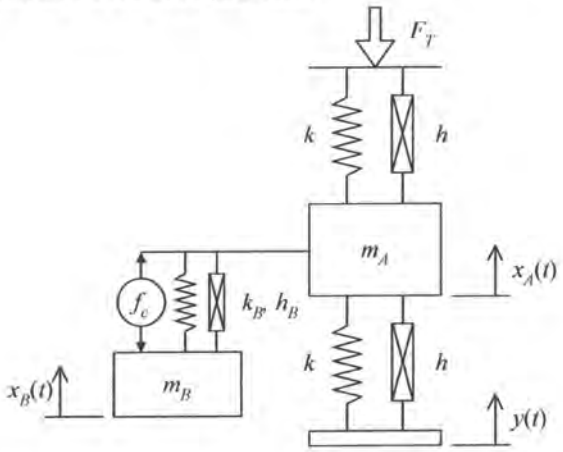

Figure 1.35: Mechanical model of an active vibration-absorbing isolator

The actuator provides a force acting on the absorber mass and must be controlled suitably. A wide variety of control methods have been used ranging from classic methods to fuzzy logic and neural networks. One possible method is to use acceleration, velocity and displacement feedback (Cunha & Rade, 2002). A shown before, the isolation frequency is a function of stiffness and mass and velocity feedback can therefore not be used to tune the device. Velocity feedback can be used to reduce damping and that will improve the isolation performance. Such a case will be considered later in this paragraph.

For tuning purposes the following control force can be used to change the effective stiffness and mass of the absorber:

$$f_c(t) = \alpha(\ddot{x}_B - \ddot{x}_A) + \gamma(x_B - x_A) \tag{1.26}$$

The advantages of using absolute instead of relative velocity feedback will be discussed later in this paragraph.

The dynamic stiffness for the undamped case is [Equation (A.70)]:

$$\frac{F_T}{kY} = \frac{1-\left(\frac{\omega}{\omega_B'}\right)^2}{\left[1+\frac{1}{4}\frac{k_B}{k}\left(1+\frac{\gamma}{k_B}\right)-\left(\frac{\omega}{\omega_A}\right)^2\right]\left[1-\left(\frac{\omega}{\omega_B'}\right)^2\right]-\frac{1}{4}\frac{k_B}{k}\left(1+\frac{\gamma}{k_B}\right)} \tag{1.27}$$

where: $\omega_A = \sqrt{\frac{4k}{m_A+\alpha}}$ $\omega_B' = \omega_B\sqrt{\frac{1+\frac{\gamma}{k_B}}{1+\frac{\alpha}{m_B}}}$

The following inequalities must be satisfied by the respective gains in order to satisfy the Routh-Hurwitz stability criterion [Equation (A.72)]:

$$\alpha > -\frac{m_B m_A}{m_A + m_B}$$
$$\frac{\gamma}{k_B} > -1 \tag{1.28}$$

It is also possible to reduce the response in the low-stiffness region by actively reducing damping as was shown by Kidner and Brennan (1999) for a vibration absorber. This can be done quite simply by using relative velocity feedback for the control force:

$$f_c(t) = \beta(\dot{x}_B - \dot{x}_A) \tag{1.29}$$

The dynamic stiffness then becomes [Equation (A.81)]:

$$\frac{F_T}{kY} = \frac{\left(1+i2\frac{\omega}{\omega_A}\zeta\right)^2\left[1+i2\frac{\omega}{\omega_B}\zeta_B-\left(\frac{\omega}{\omega_B}\right)^2\right]}{\left[1+\frac{1}{4}\frac{k_B}{k}+i2\left(\frac{\omega}{\omega_A}\zeta+\frac{1}{4}\frac{\omega}{\omega_B}\frac{k_B}{k}\zeta_B\right)-\left(\frac{\omega}{\omega_A}\right)^2\right]\left[1+i2\frac{\omega}{\omega_B}\zeta_B-\left(\frac{\omega}{\omega_B}\right)^2\right]-\frac{1}{4}\frac{k_B}{k}\left(1+i2\frac{\omega}{\omega_B}\zeta_B\right)^2} \tag{1.30}$$

where: $\zeta = \frac{c}{2m_A\omega_A}$, $\zeta_B = \frac{c_B}{2m_B\omega_B}\left(1+\frac{\beta}{c_B}\right)$

The absorber damping needs to be minimised, but as before, the gain (β) must comply with the Routh-Hurwitz criterion for stability [Equation (A.85)]:

$$\frac{\beta}{c_B} > -1 \tag{1.31}$$

From Equation (1.30) it can be seen that setting the velocity gain equal to the negative of the absorber viscous damping coefficient will result in zero absorber damping. This is favourable in the low stiffness region, but will also reduce damping at resonance, causing infinite stiffness (this was illustrated for the VAI in Figure 1.23 with $\eta_B = 0$). There is also the possibility of instability if the net damping becomes smaller than zero. Kidner and Brennan (1999) showed that it is possible to remove damping at isolation while keepings its benefits at resonance by using absolute velocity feedback:

$$f_c(t) = \beta \dot{x}_B \tag{1.32}$$

The normalised dynamic stiffness is now [Equation (A.93)]:

$$\frac{F_T}{kY} = \frac{\left(1+i2\zeta\frac{\omega}{\omega_A}\right)^2\left[1+i2\frac{\omega}{\omega_B}\zeta_B\left(1+\frac{\beta}{c_B}\right)-\left(\frac{\omega}{\omega_B}\right)^2\right]}{\left[1+\frac{1}{4}\frac{k_B}{k}+i2\left(\frac{\omega}{\omega_A}\zeta+\frac{1}{4}\frac{k_B}{k}\frac{\omega}{\omega_B}\zeta_B\right)-\left(\frac{\omega}{\omega_A}\right)^2\right]\left[1+i2\frac{\omega}{\omega_B}\zeta_B\left(1+\frac{\beta}{c_B}\right)-\left(\frac{\omega}{\omega_B}\right)^2\right]-\frac{1}{4}\frac{k_B}{k}\left[1+i2\frac{\omega}{\omega_B}\zeta_B\left(1+\frac{\beta}{c_B}\right)\right]\left(1+i2\frac{\omega}{\omega_B}\zeta_B\right)} \tag{1.33}$$

where: $\zeta_B = \frac{c_B}{2m_B\omega_B}$, $\zeta = \frac{c}{2m_A\omega_A}$

The stability is again given by Equation (1.31). Figure 1.36 shows that it will be most beneficial to have a system with high damping, but the trade-off is the cost of the power required to remove the damping:

$$p = \beta \dot{x}_B^2 \tag{1.34}$$

Importantly, the addition of primary system damping does not increase the stiffness at the isolation frequency, but will increase the high frequency roll-off and decrease the bandwidth and should therefore be minimised. Additional practical considerations include the maximum force output of the actuator and the large gain and damping needed.

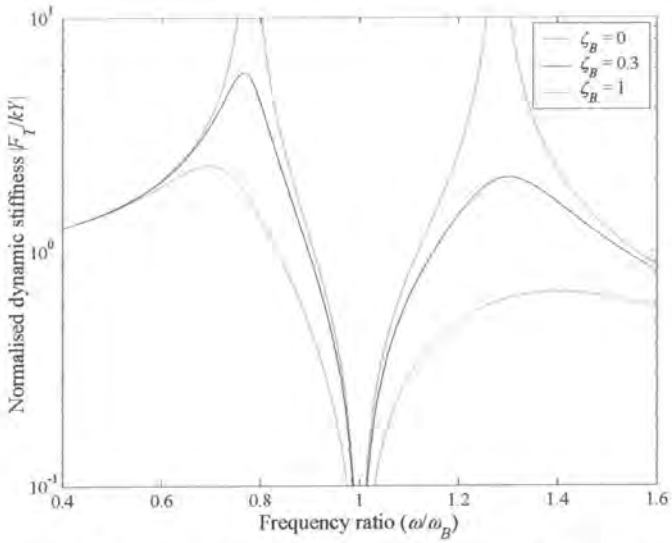

Figure 1.36 Normalised dynamic stiffness using absolute velocity feedback ($k_B/k = 1$ and $\zeta = 0$)

Other control methods have also been demonstrated. Sommerfeldt and Tichy (1990) describe a least-mean-squares (LMS) based control method for a two-stage vibration isolation mount that essentially is an active vibration absorber fitted in the load path. The advantage of the LMS algorithm control

method is that it will compensate for changes in the system and therefore control will be optimal at all times. This technique is similar to the method proposed in this work where physical properties are adapted to maintain optimal isolator stiffness at the excitation frequency. Other control methods have been suggested, specifically when applied to vibration absorbers and these might have benefits for vibration-absorbing isolators as well, although this was not investigated. These methods include an active dynamic vibration absorber incorporating a simple electromagnet arrangement used to enact a force on a pendulum (Mizuno & Araki, 1993). The control system used the theory of output regulation and could reduce the vibration to a low level over a wide range of frequencies, forcing it to zero at several specified frequencies. Burdisso and Heilmann (1998) found that a dual mass absorber with an active element inserted between the masses that are elastically coupled to the structure could have the same effectiveness as a single absorber, but with half the control effort. Filipović and Schröder (1998) demonstrated that a feedback compensator can be used to suppress a wide-band of frequencies. Olgac & Holm-Hansen (1993) introduced a delayed resonator where an actuator fitted between the primary and secondary masses is tuned using time delay and gaiu. They demonstrated that the delayed resonator could reduce the primary system response to zero.

1.4 Amplified vibration-absorbing isolators

1.4.1 Passive amplified vibration-absorbing isolators

The third distinction that will be made relate to devices that use absorber mass amplification. These are termed Amplified Vibration-Absorbing Isolators (AVAI) and the characteristics are in many respects similar to the VAI. The first important distinction that can be made is that the absorber mass is amplified using a lever mechanism, often termed a pendulum in literature (Braun, 1980). This makes it possible to reduce the mass of the device, but also amplifies damping associated with its movement. Interestingly it is not possible to increase the low stiffness bandwidth by having a large absorber mass. It is also important to note that the device has only one degree of freedom, the same as a simple isolator. A variety of physical implementations exist, as will be shown at the end of this paragraph, but all of them can be represented by an equivalent pendulum as shown in Figure 1.37.

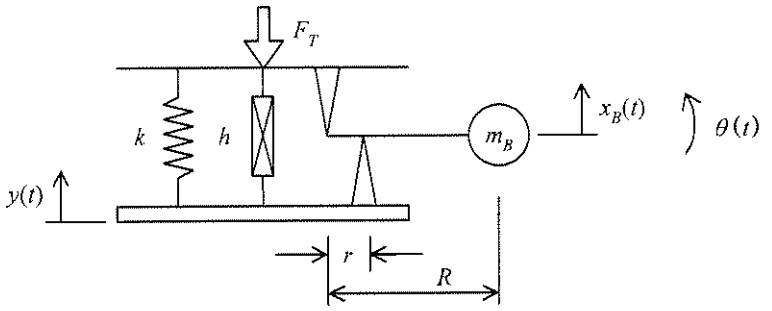

Figure 1.37: Mechanical model of a pendulum AVAI

The normalised dynamic stiffness for a pendulum type AVAI is given by [Equation (A.112)]:

$$\frac{F_T}{kY} = 1 + i\eta - \left(\frac{\omega}{\omega_i}\right)^2$$
$$\text{where:} \quad \omega_i = \sqrt{\frac{k}{m_B\left(\frac{R}{r}-1\right)\frac{R}{r} + \frac{I_G}{r^2}}} \tag{1.35}$$

where I_G is the moment of inertia about the mass centre of m_B. The characteristic of the AVAI is to reduce the dynamic stiffness over a limited frequency band as shown in Figure 1.38.

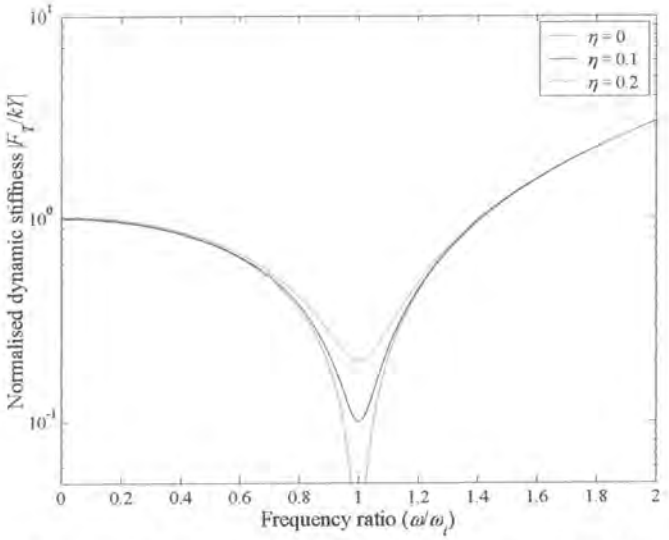

Figure 1.38: The normalised dynamic stiffness of an AVAI

The dynamic stiffness is less than one for:

$$0 < \omega < \sqrt{2}\omega_i \tag{1.36}$$

At high frequencies the AVAI will be very stiff. These properties make the AVAI ideal for narrow-band low-frequency excitation, which is often the most problematic case since it requires isolators with large static deflections. As for the VAI it would be beneficial if the low stiffness bandwidth could be increased. The low stiffness bandwidth is only slightly influenced by damping. However, it will be beneficial to have low damping at the isolation frequency.

Ideally the AVAI will be used when the excitation is tonal and time invariant. In such a case the parameters that determine the isolation frequency can be used for its design. A typical design procedure will be subject to certain size, mass and static deflection constraints while simultaneously trying to reduce the velocity of the absorber mass since this will increase damping in practical devices.

The dynamic stiffness is useful for comparison with other isolation methods, but it becomes important to study the transmissibility in order to get a more detailed description of AVAI behaviour, specifically, the response that must be evaluated using the set criteria. Adding a mass to be isolated to Figure 1.37 with degree of freedom $x(t)$ results in the model shown in Figure 1.40.

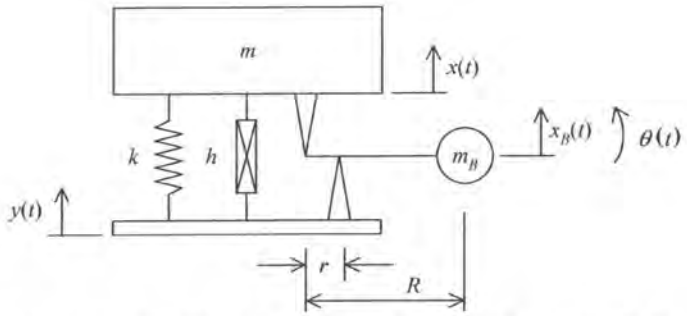

Figure 1.39: Mechanical model of a pendulum AVAI with the isolated mass included

The transmissibility is [Equation (A.108)]:

$$\frac{X}{Y}=\frac{1+i2\dfrac{\omega}{\omega_n}\zeta-\left(\dfrac{\omega}{\omega_i}\right)^2}{1+i2\dfrac{\omega}{\omega_n}\zeta-\left(\dfrac{\omega}{\omega_n}\right)^2} \tag{1.37}$$

$$\text{where: } \omega_n=\sqrt{\frac{k}{m+m_B\left(\dfrac{R}{r}-1\right)^2+\dfrac{I_G}{r^2}}}$$

The transmissibility is shown in Figure 1.40. The invariant point (A) is given by [Equation (A.109)]:

$$\frac{\omega_A}{\omega_i}=\sqrt{\frac{2}{1+\left(\dfrac{\omega_i}{\omega_n}\right)^2}} \tag{1.38}$$

Point B is where the benefit of the AVAI ends and is the same as was indicated before by Equation (1.36). Figure 1.40 clearly shows the benefit of the AVAI over a conventional isolator.

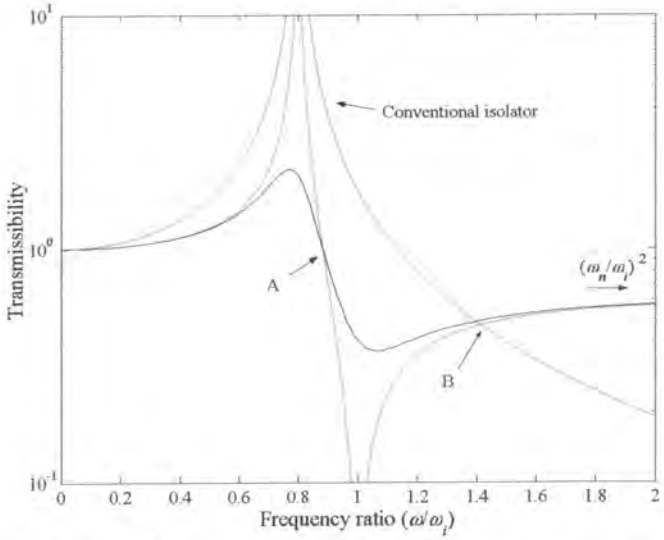

Figure 1.40: Damped (black) and undamped (red) AVAI transmissibility compared to a conventional isolator. A is the invariant point and B the cross over point ($\omega_n = 0.8$ and $\omega_i = 1$)

The high frequency transmissibility is given by the frequency ratio:

$$\left.\frac{X}{Y}\right|_{\omega\to\infty} = \left(\frac{\omega_n}{\omega_i}\right)^2 = \frac{m_B\left(\frac{R}{r}-1\right)\frac{R}{r}+\frac{I_G}{r^2}}{m+m_B\left(\frac{R}{r}-1\right)^2+\frac{I_G}{r^2}} \tag{1.39}$$

The only way to ensure that the high frequency transmissibility is low is to make certain that the effective absorber mass is much smaller than the mass of the system being isolated as shown by the above equation. At the isolation frequency the transmissibility is:

$$\left.\frac{X}{Y}\right|_{\omega=\omega_i} = \frac{i2\frac{\omega_i}{\omega_n}\zeta}{1-\left(\frac{\omega_i}{\omega_n}\right)^2+i2\frac{\omega_i}{\omega_n}\zeta} = \frac{1}{\frac{1-\left(\frac{\omega_i}{\omega_n}\right)^2}{i2\frac{\omega_i}{\omega_n}\zeta}+1} \approx \frac{i2\frac{\omega_i}{\omega_n}\zeta}{1-\left(\frac{\omega_i}{\omega_n}\right)^2} \approx i2\zeta\frac{\omega_n}{\omega_i} \tag{1.40}$$

The approximation shown in Equation (1.40) is not accurate at low values of the frequency ratio (ω_i/ω_n) as shown in Figure 1.41, but it aids in understanding the dependency of transmissibility on the parameters. It is obvious from Equation (1.40) that the natural frequency must be small in relation to the isolation frequency and that the damping ratio must be small to minimise the transmissibility.

The damped isolation frequency can be found by differentiating the absolute value of Equation (1.37) with respect to frequency [Equation (A.109)]:

$$\frac{\Omega_n}{\omega_n},\frac{\Omega_i}{\omega_n} = \sqrt{\frac{-\left(\frac{\omega_n}{\omega_i}\right)^2-1\pm\sqrt{\left[\left(\frac{\omega_n}{\omega_i}\right)^2-1\right]^2+8\zeta^2\left[\left(\frac{\omega_n}{\omega_i}\right)^2+1\right]}}{4\zeta^2+4\zeta^2\left(\frac{\omega_n}{\omega_i}\right)^2-2\left(\frac{\omega_n}{\omega_i}\right)^2}} \tag{1.41}$$

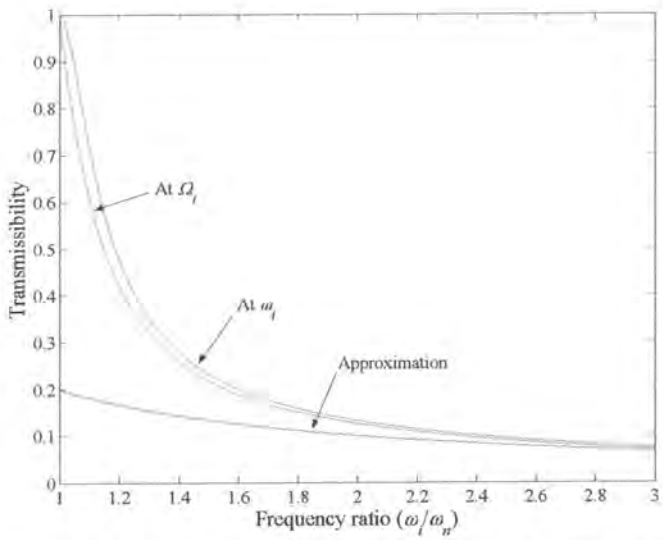

Figure 1.41: Approximation of the transmissibility at the isolation frequency (Equation (1.40)) as a function of frequency ratio ($\zeta = 0.1$)

For large values of frequency ratio (ω_i/ω_n) and damping the damped isolation frequency may not be defined as can be seen in Figure 1.42.

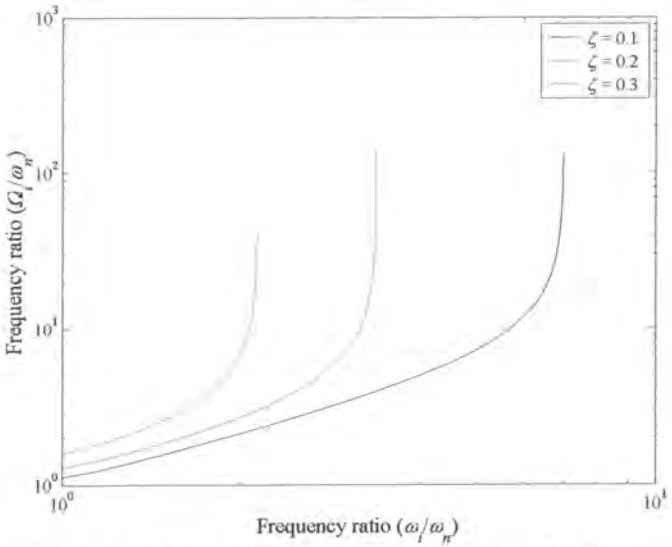

Figure 1.42: Damped frequency ratio *vs.* undamped frequency ratio

Adding pendulums in parallel will not have the same effect as was shown for the VAI in §1.3.1; in fact it is possible to reduce parallel pendulums to one equivalent pendulum. A number of discrete frequencies can, however, be suppressed if the pendulum absorber is extended by adding absorbers to the pendulum mass as shown in Figure 1.43 (Desjardins & Hooper, 1976).

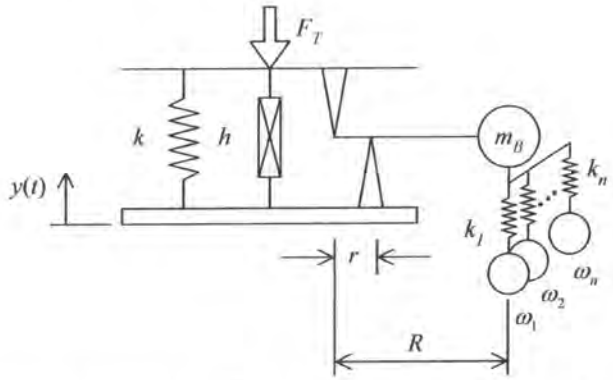

Figure 1.43: Mechanical model of an AVAI with multiple absorbers fitted to a pendulum

For a case with n absorbers attached to the pendulum mass the dynamic stiffness is [Equation (A.121)]:

$$\frac{F_T}{kY} = 1 + i\eta + \left(\frac{R}{r} - 1\right)\frac{R}{r}\sum_{q=1}^{n}\frac{k_q}{k}\left(1 + i\eta_q\right) - \left(\frac{\omega}{\omega_i}\right)^2 - \frac{R}{r}\left(\frac{R}{r} - 1\right)\sum_{q=1}^{n}\frac{k_q}{k}\frac{\left(1 + i\eta_q\right)^2}{1 + i\eta_q - \left(\frac{\omega}{\omega_q}\right)^2} \tag{1.42}$$

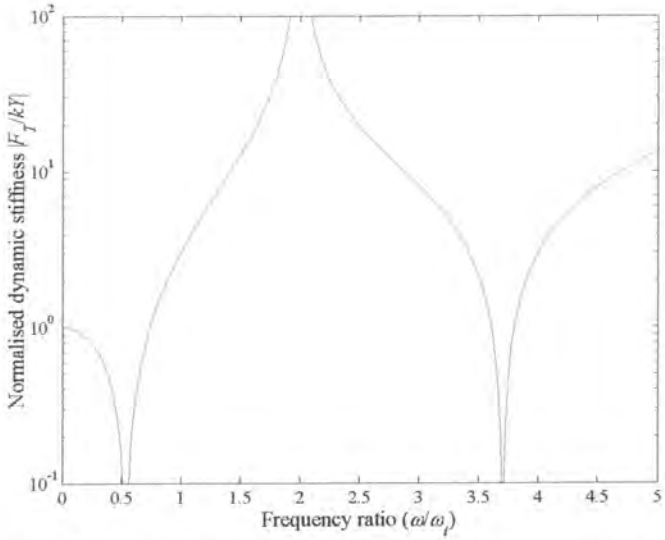

Figure 1.44: Normalised dynamic stiffness of a multi-frequency isolator with one absorber attached ($\omega_i = 1$, $\omega_1 = 2$, $R/r = 10$, $\eta = \eta_1 = 0$, $k_1/k = 0.1$)

The undamped frequencies of zero dynamic stiffness can be found by setting the normalised dynamic stiffness equal to zero. For one absorber these frequencies will be given by Equation (1.43) [Equation (A.120)]. This equation can be solved to find the system parameters that will give the required zero dynamic stiffness frequencies.

$$\frac{\omega'_{i1}}{\omega_i}, \frac{\omega'_{i2}}{\omega_i} = \sqrt{\frac{1+\left(\frac{R}{r}-1\right)\frac{R}{r}\frac{k_1}{k}+\left(\frac{\omega_1}{\omega_i}\right)^2 \mp \sqrt{\left[1+\left(\frac{R}{r}-1\right)\frac{R}{r}\frac{k_1}{k}+\left(\frac{\omega_1}{\omega_i}\right)^2\right]^2 - 4\left(\frac{\omega_1}{\omega_i}\right)^2}}{2}} \tag{1.43}$$

Figure 1.45 shows the effect of the absorber natural frequency on the isolation frequencies for two stiffness ratios.

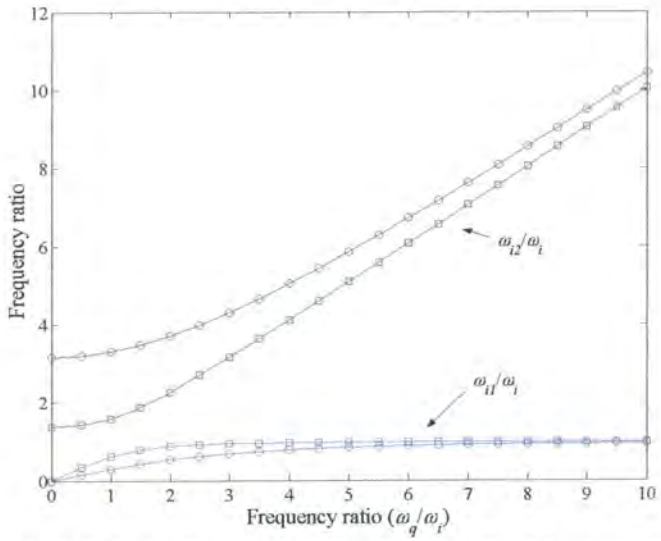

Figure 1.45: Isolation frequency ($k_1/k = 0.01$ □, $k_1/k = 0.1$ ○ and $R/r = 10$)

Softening non-linear springs can be used to increase the low stiffness bandwidth. Non-linear effects cannot be explained by using the dynamic stiffness and therefore the transmissibility will be calculated. This can be done by solving the equation of motion in the time domain using the Runge-Kutta algorithm and then calculating the transfer function using the H_1 estimator.

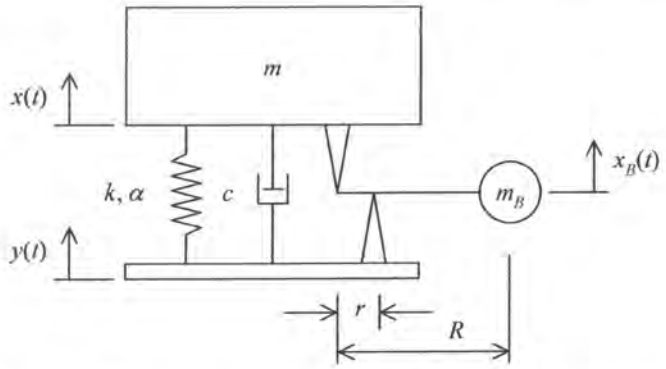

Figure 1.46: Mechanical model of an AVAI with non-linear spring

The equation of motion for a system with Duffing type non-linearity is [Equation (A.124)]:

$$\ddot{x}-\left(\frac{\omega_n}{\omega_i}\right)^2 \ddot{y}+2\zeta\omega_n\left(\dot{x}-\dot{y}\right)+\omega_n^2\left[\left(x-y\right)+\alpha\left(x-y\right)^3\right]=0 \tag{1.44}$$

Figure 1.47 shows the transmissibility of a softening system when excited by sine sweep excitation. It is clear that softening non-linearity increases the suppression bandwidth. A hardening spring will result in a decrease of the suppression bandwidth. Since this effect is highly dependent on the properties of the AVAI and the excitation amplitude it will be of limited use in most practical situations.

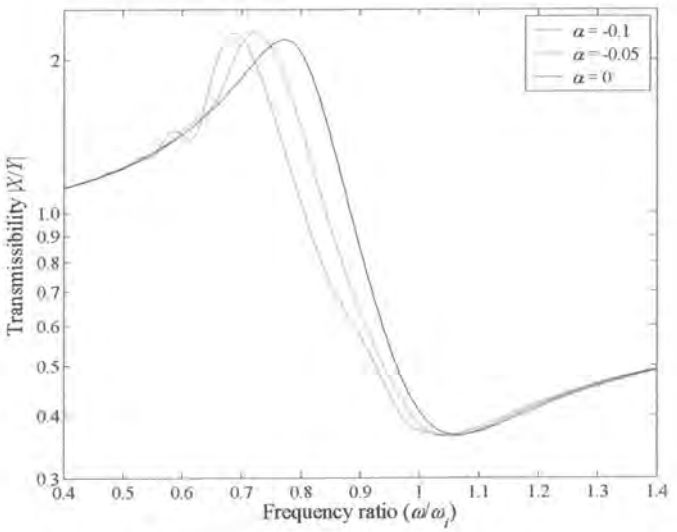

Figure 1.47: Effect of a softening spring on the transmissibility of an AVAI ($\zeta = 0.1$, $\omega_n = 0.8$, $\omega_i = 1$ and $Y = 1$)

AVAI can have a variety of physical realisations. These include nodal beams, mechanical pendulums, lead screw arrangements and various hydraulic devices. Some of these are shown in Figure 1.48. Figures (a) through (c) show schematic drawings of typical devices. Figures (d) through (f) show models of the major classes of devices and their isolation frequencies. Their relationship with Equation (1.35) is immediately apparent. Since all of these devices can realise the same low stiffness region, the final choice will include economic considerations.

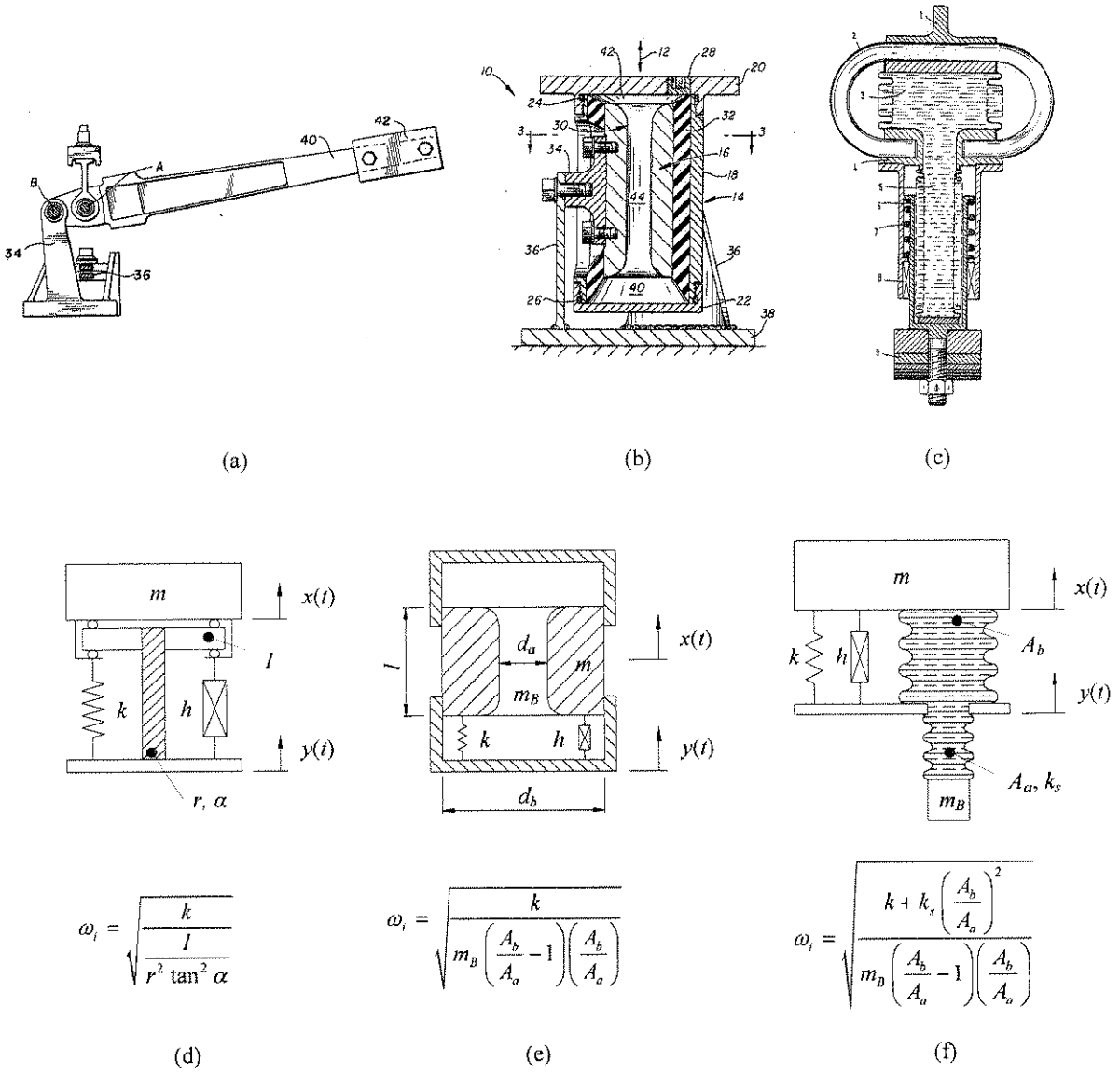

Figure 1.48: Practical implementations of the AVAI (a) pendulum type (Dejardins & Sankewitsch, 1982), (b and e) LIVE (Halwes & Simmons, 1980), (c and f) hydraulic amplification (Braun, 1980) and (d) motion transformation system (Rivin, 2001)

Hydraulic amplification isolators are also called fluid mounts and can be designed to have a static stiffness of 1.5 to 2 times that of an elastomeric isolator with a 10 times (20 dB) improvement in

isolation at the excitation frequency (Miller *et al.*, 1995). Fluid mounts are in use in cars, trucks and buses and more recently in aircraft as engine mounts and helicopter pylon isolators.

1.4.2 Adaptive amplified vibration-absorbing isolators

If the input excitation is tonal and time-varying it will be possible to adjust the AVAI such that the region of lowest stiffness coincides with the excitation frequency. The effect of varying the isolation frequency is illustrated in Figure 1.49. One advantage of the AVAI over the VAI is that the frequency ratio at which the normalised dynamic stiffness becomes more than 1 stays constant ($\omega_c/\omega_i = \sqrt{2}$). This significantly reduces the risk of tuning.

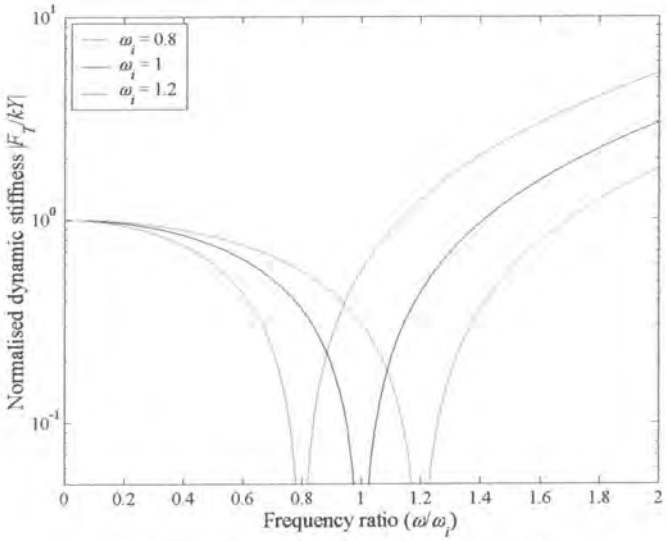

Figure 1.49: Effect of tuning the AVAI

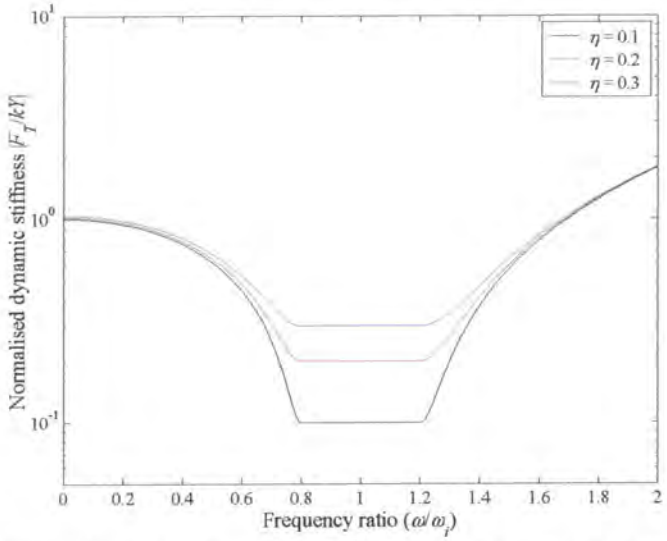

Figure 1.50: Envelope of minimum normalised dynamic stiffness for $0.8 < \omega/\omega_i < 1.2$

The objective of tuning is illustrated more clearly in Figure 1.50, which shows the envelope of normalised dynamic stiffness curves when changing the frequency ratio from 0.8 to 1.2. The effect of tuning is to increase the effective low stiffness bandwidth for this very specific class of excitation.

Another important advantage of the AVAI is that geometric variables are available for tuning, which increases the number of applicable technologies. In order to choose the best parameter to adjust, it is necessary to investigate the sensitivity of the isolation frequency to the variation of parameters shown in Equation (1.35). It is assumed that the moment of inertia is zero and that the mechanical advantage is much larger than 1. These assumptions lead to the following equation and the related sensitivities:

$$\omega_i \approx \sqrt{\frac{k}{m_B\left(\frac{R}{r}\right)^2}}, \qquad \omega_i \propto \sqrt{k}, \qquad \omega_i \propto \frac{1}{\sqrt{m_B}}, \qquad \omega_i \propto \frac{1}{\frac{R}{r}} \tag{1.45}$$

Equation (1.45) shows that the isolation frequency will be most sensitive to the mechanical advantage. This is also illustrated in Figure 1.51, which is a plot of Equation (1.46).

$$\frac{\omega_i}{\omega_i'} = \sqrt{\frac{k}{k'}\frac{m_B'}{m_B}}\left(\frac{\frac{R'}{r'}}{\frac{R}{r}}\right) \tag{1.46}$$

where the prime indicates the initial value.

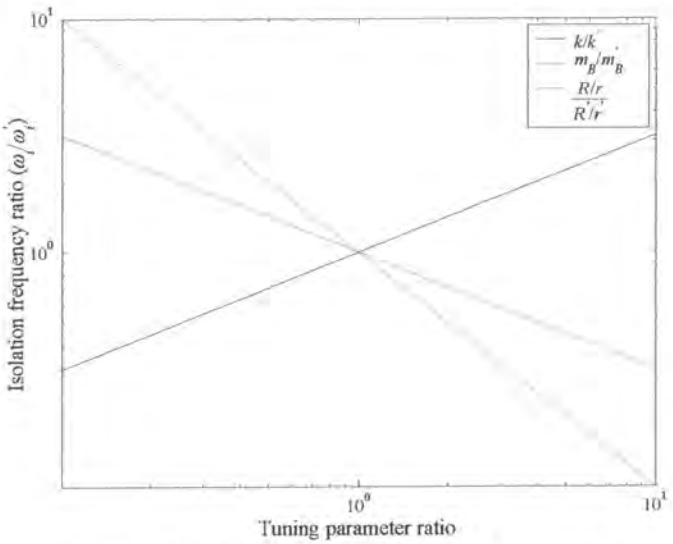

Figure 1.51: Sensitivity of the isolation frequency

Although Figure 1.51 shows a change in parameter ratio of 2 orders of magnitude, the amount achieved in practice will depend on the capability of the technology used. Also important are other constraints put on the system, for instance, there might be limited space available to lengthen the mechanical advantage or the change in static position by changing the stiffness, absorber mass or mechanical advantage may be undesirable. As with the VAI, changing the mass will be difficult while changing the mechanical advantage can be achieved easily through, for instance, a lead screw arrangement. Methods for changing the stiffness have been discussed before (§1.3.2).

Considering a Liquid Inertia Vibration Eliminator (LIVE) type AVAI it can be seen that the absorber mass is also a function of geometry as well as density:

$$\omega_i \approx \sqrt{\frac{kd_a^2}{\frac{\pi}{4}\rho l d_b^4}}, \qquad \omega_i \propto \sqrt{k}, \qquad \omega_i \propto d_a, \qquad \omega_i \propto \frac{1}{d_b^2}, \qquad \omega_i \propto \frac{1}{\sqrt{\rho}}, \qquad \omega_i \propto \frac{1}{\sqrt{l}} \tag{1.47}$$

The isolation frequency is very sensitive to the reservoir diameter, but changing it will be very difficult, if at all possible. The sensitivity to all the parameters is shown in Figure 1.52.

$$\frac{\omega_i}{\omega_i'} = \sqrt{\frac{k}{k'}\frac{\rho'}{\rho}\frac{l'}{l}\frac{d_a}{d_a'}\left(\frac{d_b'}{d_b}\right)^2} \tag{1.48}$$

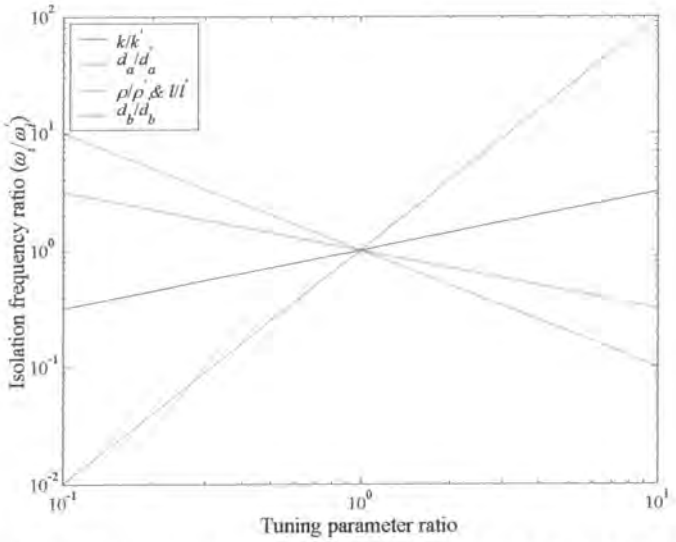

Figure 1.52: Sensitivity of the isolation frequency for a LIVE type AVAI

Figure 1.53(a) shows a proposed system to vary the port length of a LIVE type AVAI. Such a system needs careful design to minimise flow induced damping at the port inlet and outlet. Figure 1.53(b) shows a system that suggests that the port area can be changed by stretching a flexible member. It should be kept in mind that the fluid is incompressible and some compensating mechanism must be provided. In this case the fluid occupies the space between the flexible member and the port such that the total fluid volume remains constant. It has also been suggested that a chamber pressurised by nitrogen and connected by a small orifice to the reservoir to act as a volume compensator be used, specifically for heat expansion of the fluid (Ahmadian & Ahn, 1999).

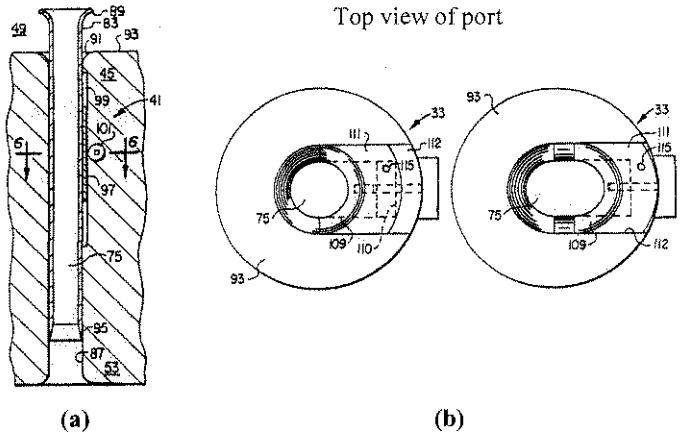

Figure 1.53: Adjustable (a) port length and (b) port area (Smith & Stamps, 1998)

Duclos *et al.* (1988) demonstrated a system using an electro-rheological fluid with a number of parallel ports, each with a valve that can be selectively switched so that the isolator can be tuned at a number of discrete frequencies. One problematic aspect with regards to tuning is that for some of the parameters the transmissibility at the isolation frequency is a function of the tuning parameter. Tuning could therefore increase the transmissibility at the isolation frequency so much that no benefit results.

It can be anticipated that an instantaneous change in excitation frequency or stiffness will result in impulsive loading of the system. This can be studied in the time domain by solving the equation of motion for the AVAI (Equation (1.44) with $\alpha = 0$):

$$\ddot{x} + 2\zeta\omega_n(t)\dot{x} + \omega_n^2(t)x = \left[\frac{\omega_n(t)}{\omega_i(t)}\right]^2 \ddot{y} + 2\zeta\omega_n(t)\dot{y} + \omega_n^2(t)y \tag{1.49}$$

When the stiffness is used as the tuning parameter the current isolation and natural frequencies can be expressed in terms of the initial values (using Equation (1.48) for the isolation frequency, the natural frequency follows similarly):

$$\omega_i = \sqrt{\frac{k}{k'}}\omega_i', \qquad \omega_n = \sqrt{\frac{k}{k'}}\omega_n' \tag{1.50}$$

The effect is illustrated in Figure 1.54. The AVAI is initially tuned to the excitation frequency. After a short transient the displacement settles. At 10 seconds the excitation frequency is doubled when the displacement passes through zero, exciting the system. In any practical system some delay between the change in excitation frequency and subsequent tuning is inevitable. Von Flotow (1994) identified three delays:

1. Logic delay: Associated with the time needed for data acquisition and to estimate if and how much mistuning has occurred.
2. Actuation delay: Changing any of the parameters needed to adapt the isolation frequency cannot happen instantaneously. In fact, instantaneous adaptation will excite the system impulsively, which could result in unacceptably large response.

3. Dynamic delay: The time taken by the system to reach steady-state conditions which can be found in terms of the exponential time constant as the number of periods before the system has settled:

$$T = \frac{1}{2\pi\zeta} \tag{1.51}$$

Clearly damping can be used to control the transient.

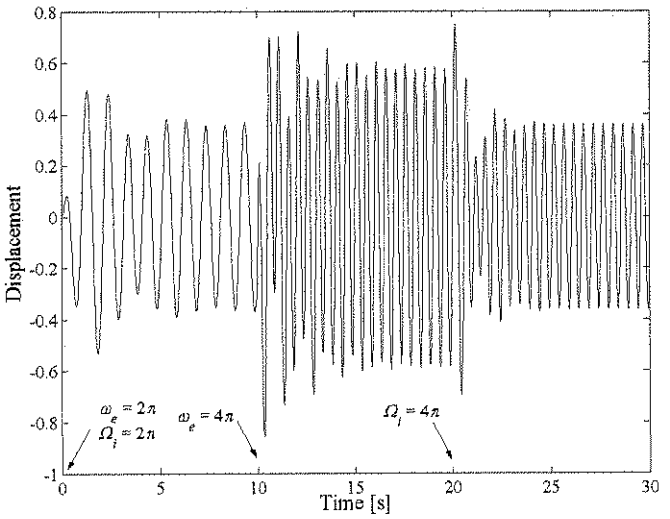

Figure 1.54: Transient response of an AVAI (initially tuned), subjected to an instantaneous frequency change at $t = 10$ and retnned at $t = 20$ s ($\omega_n/\omega_i = 0.8$, $\zeta = 0.1$ and $Y = 1$)

It is possible to extend the model of the AVAI by considering the effect of a flexible fulcrum as shown in Figure 1.55. At first glance it might seem superfluous, but it will be shown in Chapter 2 that such a configuration can be a reasonable compromise between constructability and tuning performance.

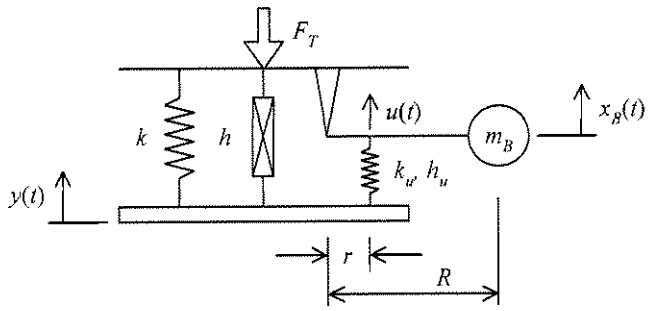

Figure 1.55: Mechanical model of an AVAI with flexible fulcrum

The system now has a degree of freedom which can be accounted for by the natural frequency of the pendulum mass (ω_u) [Equation (A.143)]:

$$\frac{F_T}{kY} = 1 + i\eta - \frac{\left(\frac{\omega}{\omega_l}\right)^2 (1 + i\eta_u)}{1 + i\eta_u - \left(\frac{\omega}{\omega_u}\right)^2} \tag{1.52}$$

$$\text{where: } \omega_l = \sqrt{\frac{k}{m_B\left(\frac{R}{r} - 1\right)\frac{R}{r} + \frac{I_G}{r^2}}}, \quad \omega_u = \sqrt{\frac{k_u}{m_B\left(\frac{R}{r}\right)^2 + \frac{I_G}{r^2}}}$$

The effect of adding the flexible fulcrum is shown in Figure 1.56.

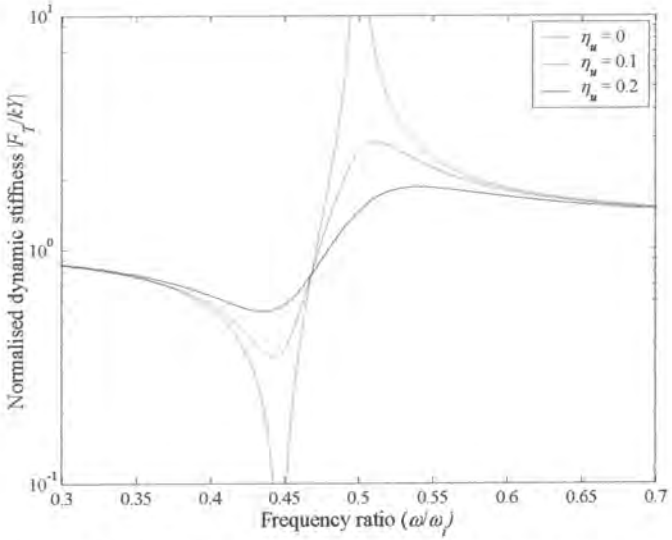

Figure 1.56: Normalised dynamic stiffness of the AVAI with flexible fulcrum ($\omega_u = 0.5$ and $\omega_l = 1$)

Equation (1.52) can be rewritten to show the effect of changing the fulcrum stiffness [Equation (A.144)]:

$$\frac{F_T}{kY} = 1 + i\eta - \frac{\left(\frac{\omega}{\omega_l}\right)^2 (1 + i\eta_u)}{1 + i\eta_u - \frac{k}{k_u}\left(\frac{\frac{R}{r}}{\frac{R}{r} - 1}\right)\left(\frac{\omega}{\omega_l}\right)^2} \tag{1.53}$$

As the stiffness ratio (k_u/k) increases, Equation (1.53) approaches that of the AVAI. Figure 1.57 shows that the low stiffness frequency range is a function of the stiffness ratio and therefore the risk of tuning is greater than in the case of the AVAI. The normalised dynamic stiffness is less than 1 when:

$$0 < \omega < \sqrt{\frac{2}{1 + 2\frac{k}{k_u}\left(\frac{\frac{R}{r}}{\frac{R}{r} - 1}\right)}}\,\omega_l \tag{1.54}$$

There is also the advantage that the high-frequency stiffness is finite for low stiffness ratios:

$$\left.\frac{F_T}{kY}\right|_{\omega\to\infty} = \frac{k_u}{k}\frac{1+i\eta_u}{\dfrac{\dfrac{R}{r}}{\dfrac{R}{r}-1}} \tag{1.55}$$

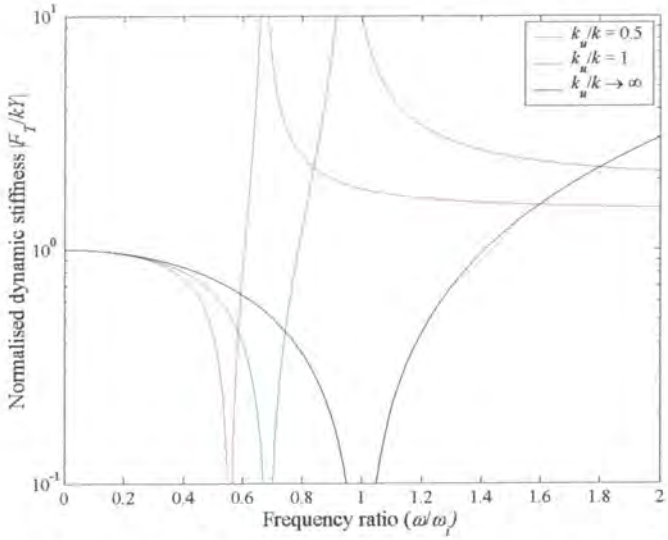

Figure 1.57: Effect of tuning the AVAI with flexible fulcrum ($R/r = 10$, $\omega_i = 1$ and $\eta = \eta_u = 0$)

Since the equation describing the actual isolation frequency as a function of stiffness ratio becomes unwieldy it is proposed that the system should be designed graphically as shown in Figure 1.58. This graph is, of course, dependent on several parameters and must be recreated for each specific case. For instance, the acceptable margin will be application specific and the range of stiffness change that can be achieved will depend on the method chosen for this purpose.

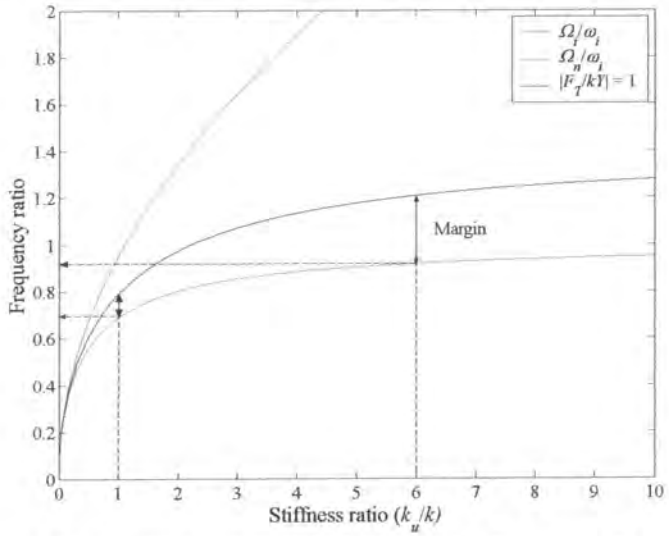

Figure 1.58 Design graph for the AVAI with flexible fulcrum with Ω_i the actual isolation frequency and Ω_n the frequency of maximum dynamic stiffness ($\eta = 0.1$, $\eta_u = 0$ and $R/r = 10$)

1.4.3 Active amplified vibration-absorbing isolators

As for the VAI it will be possible to apply various active control forces to the AVAI. Miller and Ahmadian (1992) noted that both traditional feedback and adaptive feedforward including LMS have been implemented to reject tonal disturbances. They further state that neural network based controllers will be essential when considering broadband vibration inputs. When considering traditional feedback control three cases will be identified. Firstly, tuning can be effected by using acceleration and displacement feedback. Secondly, damping can be removed by using relative velocity feedback. Thirdly, absolute velocity feedback can be used to add a "skyhook" damper to the system, reducing the transmissibility at both the natural and isolation frequencies.

The mechanical model describing the force transmitted for an active system is shown in Figure 1.59. The control force using input acceleration and displacement feedback to facilitate tuning is:

$$f_c = \alpha \ddot{y} + \gamma y \tag{1.56}$$

It will also be possible to use the acceleration and displacement of the pendulum mass x_B.

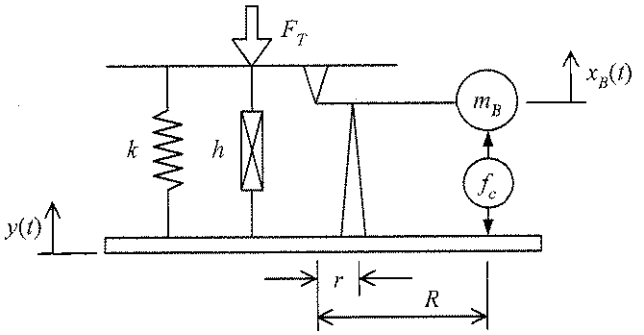

Figure 1.59: Mechanical model of an active AVAI for dynamic stiffness

The normalised dynamic stiffness of the active AVAI is [Equation (A.149)]:

$$\frac{F_T}{\left[k-\gamma\left(\frac{R}{r}-1\right)\right]Y} = 1+i\frac{\eta}{1-\frac{\gamma}{k}\left(\frac{R}{r}-1\right)}-\left(\frac{\omega}{\omega_i'}\right)^2$$

$$\omega_i' = \sqrt{\frac{k-\gamma\left(\frac{R}{r}-1\right)}{m_B\left(\frac{R}{r}-1\right)\frac{R}{r}+\frac{I_G}{r^2}-\alpha\left(\frac{R}{r}-1\right)}} \tag{1.57}$$

The above equation is similar to Equation (1.14). However, it has the advantage that the feedback gains are amplified by the mechanical advantage.

In practice it is difficult to build a device with low enough damping. As shown for the active VAI it is possible to use relative velocity feedback to reduce the damping (§1.3.3). The effect of velocity feedback must necessarily include a viscous damping model and will therefore be explained by considering the transmissibility of the system shown in Figure 1.60.

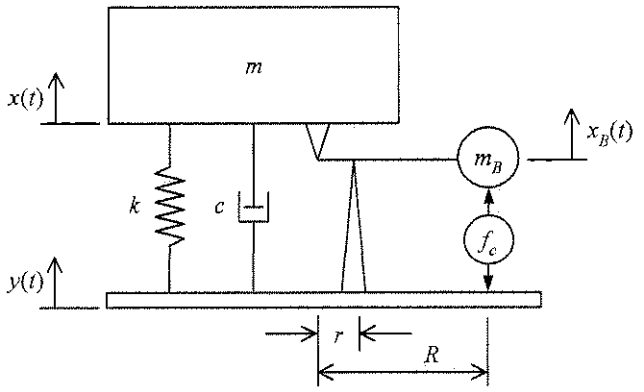

Figure 1.60: Mechanical model of an active AVAI for transmissibility

The control force is:

$$f_c = \beta(\dot{x} - \dot{y}) \tag{1.58}$$

The transmissibility is [Equation (A.155)]:

$$\frac{X}{Y} = \frac{1 + i2\frac{\omega}{\omega_n}\left[\zeta + \zeta_\beta\left(\frac{R}{r} - 1\right)\right] - \left(\frac{\omega}{\omega_i}\right)^2}{1 + i2\frac{\omega}{\omega_n}\left[\zeta + \zeta_\beta\left(\frac{R}{r} - 1\right)\right] - \left(\frac{\omega}{\omega_n}\right)^2} \tag{1.59}$$

where: $\zeta_\beta = \dfrac{\beta}{2\left[m + m_B\left(\frac{R}{r} - 1\right)^2 + \frac{I_G}{r^2}\right]\omega_n}$

From the above equation it can be deduced that if negative relative velocity feedback is used it will be possible to reduce the damping in the system to zero when [Equation (A.158)]:

$$\zeta_\beta = -\frac{\zeta}{\frac{R}{r} - 1} \tag{1.60}$$

If larger negative feedback is used the system will be unstable.

There are several advantages when using an active AVAI. The control force needed is less than that for the VAI because of the mechanical advantage of the pendulum. The tuning speed will be faster than that for an adaptive system and it should be possible to attain a larger range of isolation frequencies. McKeown *et al.* (1995) patented the active AVAI shown in Figure 1.61. This design used acceleration feedback to shift the isolation frequency up by 10% and down by 25% while consuming a maximum of 600 W. The system also used negative velocity feedback to reduce the damping such that the isolation approached 100%.

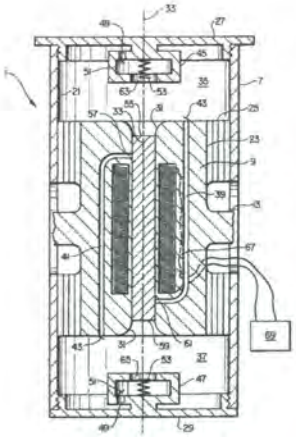

Figure 1.61: Cross section of a proposed active AVAI (McKeown *et al.*, 1995)

If absolute velocity feedback is used the control force is:

$$f_c(t) = \beta \dot{x} \tag{1.61}$$

The transmissibility is given by [Equation (A.163)]:

$$\frac{X}{Y} = \frac{1 + i2\dfrac{\omega}{\omega_n}\zeta - \left(\dfrac{\omega}{\omega_i}\right)^2}{1 + i2\dfrac{\omega}{\omega_n}\left[\zeta + \zeta_\beta\left(\dfrac{R}{r} - 1\right)\right] - \left(\dfrac{\omega}{\omega_n}\right)^2} \tag{1.62}$$

The effect of the damping added by the actuator is shown in Figure 1.62. It is interesting to note that the addition of damping is advantageous at the isolation frequency. Additionally, since damping is added and not removed the system is unconditionally stable.

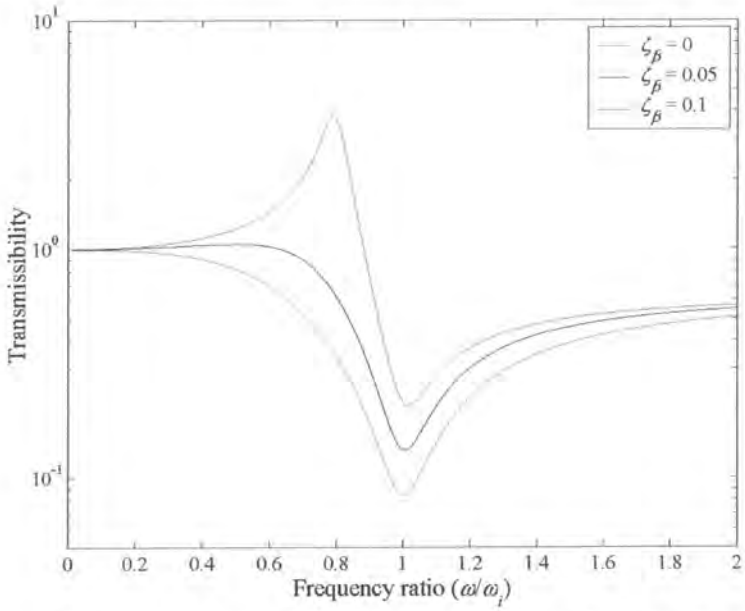

Figure 1.62: Transmissibility of an AVAI with absolute positive velocity feedback ($R/r = 10$, $\omega_n = 0.8$, $\omega_i = 1$ and $\zeta = 0.1$)

1.5 Thesis objectives

This chapter served as in introduction to methods that can be used to reduce the low stiffness bandwidth of isolators. It relied heavily on vibration absorber literature because these devices are related and very little has been published regarding their use as isolators. It introduced the normalised dynamic stiffness as a convenient and intuitive method to compare these devices. In most cases it was necessary to derive the equations because no references exist. This overview lays the foundation for the contribution of the thesis.

The focus of this work is the broadening of the effective low-stiffness bandwidth of amplified vibration-absorbing isolators (AVAIs) by adapting system parameters. The objectives are to:

1. Compare various isolator concepts using the transfer dynamic stiffness.
2. Develop mathematical models for two novel adaptive AVAIs.
3. Show how these devices can be controlled effectively using optimisation techniques.
4. Establish a design methodology for adaptive AVAIs for a pneumatic rock drill handle application.
5. Verify the mathematical models through experiment.

In order to achieve the above objectives, the following were done:

Comparison of isolators using the transfer dynamic stiffness

- Classify isolators according to their mechanical layout as either isolators, vibration-absorbing isolators or amplified vibration-absorbing isolators and according to their degree of autonomy as passive, adaptive or active.
- Define the blocked transfer dynamic stiffness as a measure of the suitability of an isolator for a specific excitation type.
- Compare isolators using the blocked transfer dynamic stiffness, specifically concentrating on various techniques to broaden the low stiffness bandwidth. For this purpose techniques established in the fields of isolators and vibration absorbers will be applied to the AVAI to show the benefits that can be obtained.
- Introduce the concept of adapting isolator properties to minimise the objective of the isolator. For the case of hand-transmitted vibration the objective is defined as the weighted equivalent acceleration given by ISO 5349.
- Study current techniques of adapting stiffness of springs as a foundation for applying such a technique to an adaptive AVAI.

Mathematical models for novel adaptive AVAIs

- Derive and verify the mathematical models of two novel adaptive AVAI designs. Here the emphasis will be on calculating the response of the devices and for this purpose the dynamic stiffness is abandoned in favour of the transmissibility properties of the AVAIs.
- Show that the first AVAI offers low construction cost, simplicity and robustness. Three cases will be investigated. The first option consists of flexible reservoir walls covering the full wall area, the second shows the effect of reducing the flexible section of the reservoir wall and the third considers a single flexible wall.

- Confirm that the second AVAI offers low mass at the expense of robustness. Three refinements to this design will be investigated. The first refinement derives the non-linear equation for a system with impact stops. The second investigates the effect of leakage on the transmissibility and the third explores a system utilising diaphragm seals to eliminate leakage.
- Develop general design methodologies for passive and adaptive damped and undamped devices using optimisation techniques.

Effective control of these devices using optimisation techniques

- Demonstrate that the adaptive AVAI can be controlled to ensure optimal transmissibility.
- Show that the objective function exhibits local minima, which must be handled appropriately to ensure convergence. Also compare different methods of estimating the objective function.
- Compare some common optimisation algorithms' ability to solve various excitation scenarios.

Design methodology for adaptive AVAIs for a pneumatic rock drill handle application

- Investigate current methods of vibration reduction for hand-operated tool handles.
- Present measurements of the Boart Longyear S215 rock drill vibration and analyse these as prescribed in ISO 5349.
- Qualitatively demonstrate the suitability of the both AVAIs for excitation containing broadband noise and narrowband tonal excitation.
- Develop a design methodology for the adaptive AVAI with specific application to a pneumatic rock drill. As part of this design methodology the effect of leakage on the stiffness, loss factor and tuning speed will be investigated through time domain simulation. Additionally, techniques for estimating the stiffness of rubber components for various loadings will be compared.
- Show that a rock drill handle can be set up in such a way that tuning is achieved through direct coupling with the supply line, making the use of a control system unnecessary.
- Compare the following: Tuning through air spring coupling to the supply line, an optimisation based control system and open-loop tuning to the frequency of maximum excitation through simulation using the measured vibration data.

Experimental verification of the mathematical models

- Experimentally verify and improve the mathematical models used to design the AVAIs.
- Estimate the system parameters by fitting the mathematical models to the experimental data.
- Show through experimentation that an optimisation control system can adapt the stiffness of the type I AVAI to find the optimal transmissibility.

It is believed that achieving the above objectives will extend and contribute to the current knowledge on these devices.

1.6 Thesis description

Chapter 2 will introduce the two innovative AVAIs that will be studied in this thesis. Mathematical models are derived in non-dimensional form and manipulated to clearly show their properties and

specifically the effects of tuning. This is done in a general way without considering application-specific issues. Chapter 3 will discuss possible control strategies. It will include numerical simulations that show which methods could be problematic and under which circumstances problems can occur. Chapter 4 will detail the design methodology for the pneumatic rock drill. An introduction to hand-arm vibration is given, specifically considering the diseases caused by vibration as well as the ISO specification used to assess the severity of tool vibration. A large set of measurements of a pneumatic drill commonly used in South-African gold mining industry is shown, which illustrate its operational behaviour. In this chapter application-specific issues will be addressed and the design methodology for each device will be applied. Chapter 5 will highlight experimental results obtained from the two devices. The experiments will show where assumptions made led to inaccurate modelling and how these can be improved. For the first prototype a control system will be implemented which will demonstrate that it can tune the device accurately. Chapter 6 will cover the conclusions.

2 Novel adaptive amplified vibration-absorbing isolators

The two novel types of adaptive AVAI that will be studied are shown in Figure 2.1, with the tuneable stiffness elements indicated. The type I modifies the continuity through the port using flexible reservoir walls. The primary spring stiffness (k in Figure 2.1(a)) remains constant. The main advantage of the addition of a degree of freedom to the LIVE isolator is that it simplifies the construction of the AVAI. The addition of the degree of freedom (u) to aid tuning is considered to be unique. The type II exploits the high density of a heavy metal slug in replacement of the fluid in the port. The main advantage of this approach is the reduced size of the device. As far as could be established the concepts for changing the stiffness of the springs in these ways for both the type I and type II AVAI are unique and innovative.

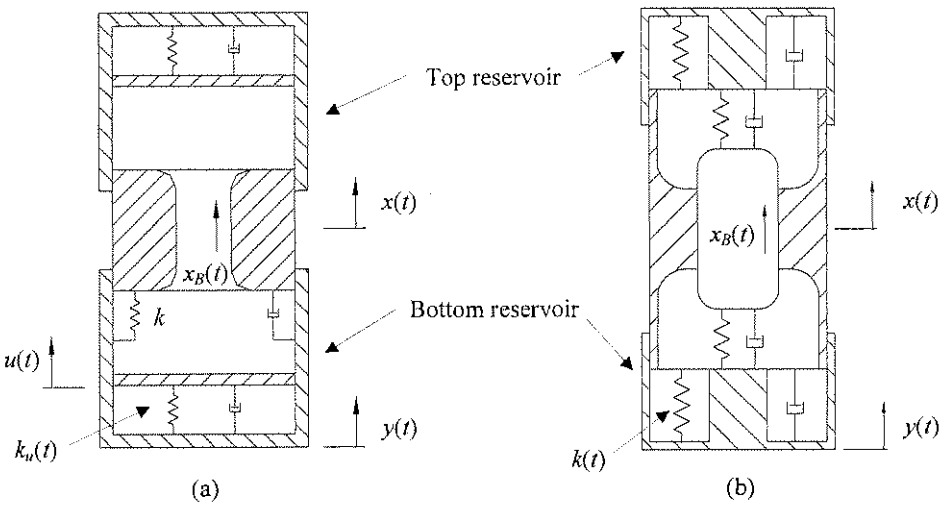

Figure 2.1: Adaptive AVAI (a) Type I: with adaptive reservoir wall stiffness (b) Type II: with adaptive stiffness and slug (moveable rigid bodies are hatched, flexible elements are indicated by springs and the top and bottom reservoirs are rigidly connected)

Chapter 1 showed the relationship between various isolator concepts using the blocked transfer dynamic stiffness. This method worked well for frequency domain comparison since the equations could be normalised easily in terms of non-dimensional parameters commonly used in the field of vibration. The dynamic stiffness was the best quantity to use for this evaluation because it focused on the isolator while disregarding the role of the equipment being isolated since it was assumed to be present in all cases. For this purpose the method proved to be both simple and intuitive.

Since it has already been established that there are advantages when using AVAI the need for the dynamic stiffness has passed. In this chapter the main consideration is the response of the equipment, simply finding the best isolator is not enough, the exact response is needed to assess if a design is feasible. As was shown in Chapter 1 the transmissibility cannot be calculated directly from the blocked transfer dynamic stiffness and it will therefore be derived from the equations of motion for each concept. The response must then be evaluated against a set of criteria to establish which isolator should be used as was shown in Figure 1.1. The specific characteristics of these devices will therefore

be considered using transmissibility and time domain integration. The main properties of the two AVAIs will be shown in this chapter with complete derivations shown in Appendix B.

2.1 Adaptive AVAI with variable reservoir wall flexibility (Type I)

The pendulum equivalent of this class of AVAI was discussed in §1.3.2 (Figure 1.55). Three devices will be discussed according to the type of flexibility added to the system:

1. Flexibility covering the full reservoir wall.
2. Flexibility covering a reduced area of the reservoir wall.
3. A single flexible wall.

The first device is more advantageous than the second and will be presented in detail. The second shows the effect of reducing the area of the flexible part of the reservoir wall. Such a device is less attractive than the first, but can be used to represent a real system more accurately. The single flexible wall device differs fundamentally from the first two in its principle of operation but has physical similarities that will be discussed.

2.1.1 Reservoir flexibility covering full wall

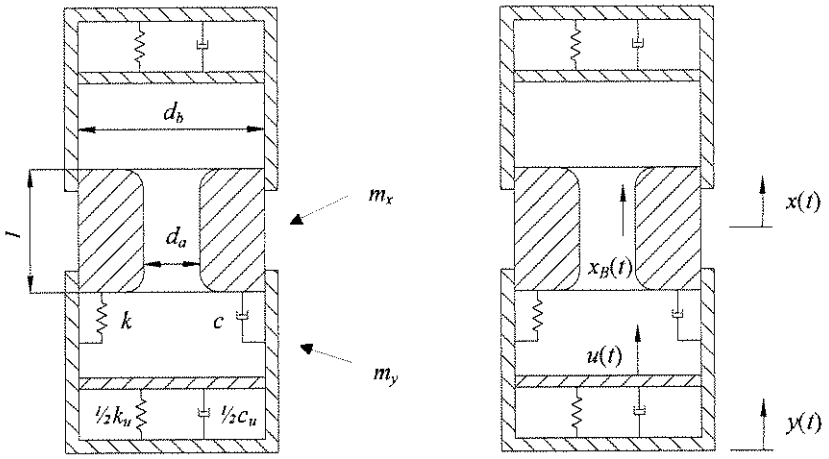

Figure 2.2: Mechanical model of an adaptive AVAI with flexibility covering the complete reservoir wall ($m_B = \rho A_a l$, $A_a = \pi d_a^2/4$ and $A_b = \pi d_b^2/4$)

In Figure 2.2 the u degree of freedom represents the displacement of the reservoir wall. Since the fluid is incompressible the fluid continuity through the port is [Equation (B.1)]:

$$x_B = \left(1 - \frac{A_b}{A_a}\right)x + \frac{A_b}{A_a}u \tag{2.1}$$

where A_b is the reservoir area and A_a the port area. Excitation can occur at the x or the y degree of freedom. In this chapter excitation will be assumed to be at the x degree of freedom because it has practical advantages for the experimental device that will be presented later. Equations for excitation

at the y degree of freedom are shown in Appendix B. If it is assumed that no external forces are acting on the system the equation of motion is [Equation (B.14)]:

$$\begin{bmatrix} m_y & 0 \\ 0 & m_B\left(\frac{A_b}{A_a}\right)^2 \end{bmatrix}\begin{bmatrix} \ddot{y} \\ \ddot{u} \end{bmatrix}+\begin{bmatrix} c+c_u & -c_u \\ -c_u & c_u \end{bmatrix}\begin{bmatrix} \dot{y} \\ \dot{u} \end{bmatrix}+\begin{bmatrix} k+k_u & -k_u \\ -k_u & k_u \end{bmatrix}\begin{bmatrix} y \\ u \end{bmatrix}=\begin{bmatrix} c\dot{x}+kx \\ -m_B\left(1-\frac{A_b}{A_a}\right)\frac{A_b}{A_a}\ddot{x} \end{bmatrix} \tag{2.2}$$

where m_y is the mass associated with y degree of freedom, m_B is the absorber mass, c and k denote the primary spring properties and c_u and k_u the reservoir spring properties. The above equation can be transformed to the frequency domain by assuming harmonic excitation:

$$\begin{bmatrix} -\omega^2 m_y + i\omega(c+c_u)+k+k_u & -(i\omega c_u + k_u) \\ -(i\omega c_u + k_u) & -\omega^2 m_B\left(\frac{A_b}{A_a}\right)^2 + i\omega c_u + k_u \end{bmatrix}\begin{bmatrix} Y \\ U \end{bmatrix}=\begin{bmatrix} i\omega c + k \\ \omega^2 m_B\left(1-\frac{A_b}{A_a}\right)\frac{A_b}{A_a} \end{bmatrix}X \tag{2.3}$$

Using the second equation in the set defined above it is possible to eliminate the U degree of freedom and to find the transmissibility between the input and the response [Equation (B.17)]:

$$\frac{Y}{X}=\frac{(k+i\omega c)\left[k_u+i\omega c_u-\omega^2 m_B\left(\frac{A_b}{A_a}\right)^2\right]-(k_u+i\omega c_u)\omega^2 m_B\left(\frac{A_b}{A_a}-1\right)\frac{A_b}{A_a}}{\left[k+k_u+i\omega(c+c_u)-\omega^2 m_y\right]\left[k_u+i\omega c_u-\omega^2 m_B\left(\frac{A_b}{A_a}\right)^2\right]-(k_u+i\omega c_u)^2} \tag{2.4}$$

Equation (2.4) can be non-dimensionalised by introducing the stiffness ratio and the frequencies ω_1, ω_2 and $\bar{\omega}_i$ [Equation (B.18)]:

$$\frac{Y}{X}=\frac{1-\left(\frac{\omega}{\omega_2}\right)^2-\left(\frac{\omega}{\bar{\omega}_i}\right)^2}{\left[1+\frac{k_u}{k}-\left(\frac{\omega}{\omega_1}\right)^2\right]\left[1-\left(\frac{\omega}{\omega_2}\right)^2\right]-\frac{k_u}{k}} \tag{2.5}$$

where: $\omega_1^2=\frac{k}{m_y}$, $\omega_2^2=\frac{k_u}{m_B\left(\frac{A_b}{A_a}\right)^2}$, $\bar{\omega}_i^2=\frac{k}{m_B\left(\frac{A_b}{A_a}-1\right)\frac{A_b}{A_a}}$

The defined frequencies have physical significance. The frequency ω_1 is the natural frequency of the primary system without the fluid. As was shown in Chapter 1 this frequency should be as low as possible, requiring a low primary stiffness (k). The second frequency is the natural frequency of the column of fluid in the port suspended by the membrane. This frequency is a function of the membrane stiffness, but it will be beneficial for explaining tuning to rewrite it in terms of a constant frequency (i.e. $\bar{\omega}_2 \neq f(k_u)$) and the stiffness ratio ($\mu_k = k_u/k$):

$$\omega_2^2=\frac{k_u}{k}\frac{k}{m_B\left(\frac{A_b}{A_a}\right)^2}=\mu_k\bar{\omega}_2^2 \tag{2.6}$$

The frequency $\bar{\omega}_i$ is the isolation frequency at infinite stiffness ratio and is the same as for a LIVE type AVAI. If the area ratio is large then the relationship between ω_2 and $\bar{\omega}_i$ is:

$$\omega_2^2 = \mu_k \frac{k}{m_B\left(\frac{A_b}{A_a}\right)^2} = \mu_k \bar{\omega}_2^2 \approx \mu_k \bar{\omega}_i^2 \tag{2.7}$$

The actual isolation frequency will be designated ω_i. The isolation frequency can be found by equating the numerator of Equation (2.5) to zero:

$$\left(\frac{\omega_i}{\omega_1}\right)^2 = \frac{1}{\left(\frac{\omega_1}{\bar{\omega}_i}\right)^2 + \frac{1}{\mu_k}\left(\frac{\omega_1}{\bar{\omega}_2}\right)^2} \tag{2.8}$$

By introducing the isolation frequency Equation (2.5) can be generalised:

$$\frac{Y}{X} = \frac{1-\left(\frac{\omega}{\omega_i}\right)^2}{\left[1+\mu_k-\left(\frac{\omega}{\omega_1}\right)^2\right]\left[1-\left(\frac{\omega}{\omega_2}\right)^2\right]-\mu_k} \tag{2.9}$$

Notably Equation (2.9) is similar to the equation describing the amplitude of a vibration absorber (Rao, 1990).

Vibration absorber theory generally identifies two distinct cases (Brennan, 1997b). Firstly, a resonance of the primary structure is excited and the absorber is used to add damping to the structure at frequencies in the region of the natural frequency. Such a device is often called a tuned damper. A second case occurs when a large force excites the system and in such a case the absorber is tuned to excitation frequency. Here only the second case will be considered since operation at resonance for an isolated system is unlikely. An important difference between a vibration absorber and the type I AVAI is that the isolation frequency (ω_i) for the present device is not equal to the absorber natural frequency (ω_2). The two frequencies are, however, related through their dependence on the mass and area ratios. This can be shown by considering the frequency ratios $\omega_1/\bar{\omega}_2$ and $\omega_1/\bar{\omega}_i$ [Equations (B.21) and (B.22)]:

$$\left(\frac{\omega_1}{\bar{\omega}_2}\right)^2 = \frac{m_B}{m_y}\left(\frac{A_b}{A_a}\right)^2 \tag{2.10}$$

$$\left(\frac{\omega_1}{\bar{\omega}_i}\right)^2 = \frac{m_B}{m_y}\left(\frac{A_b}{A_a}-1\right)\frac{A_b}{A_a} \tag{2.11}$$

The transmissibility can now be rewritten as:

$$\frac{Y}{X} = \frac{1-\frac{1}{\mu_k}\left(\frac{\omega_1}{\bar{\omega}_2}\right)^2\left(\frac{\omega}{\omega_1}\right)^2-\left(\frac{\omega_1}{\bar{\omega}_i}\right)^2\left(\frac{\omega}{\omega_1}\right)^2}{\left[1+\mu_k-\left(\frac{\omega}{\omega_1}\right)^2\right]\left[1-\frac{1}{\mu_k}\left(\frac{\omega_1}{\bar{\omega}_2}\right)^2\left(\frac{\omega}{\omega_1}\right)^2\right]-\mu_k} \tag{2.12}$$

A typical plot of Equation (2.12) is shown in Figure 2.3. It can be seen from the equation that the system will approach the transmissibility of the LIVE isolator as the stiffness ratio approaches infinity, since $1/\mu_k$ approaches zero.

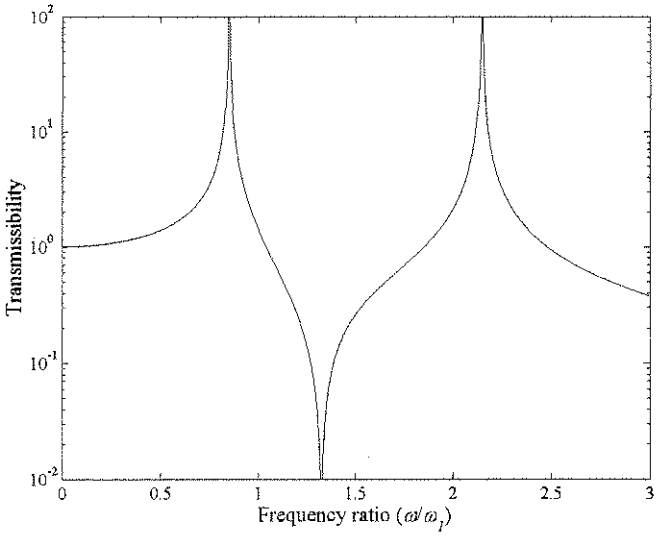

Figure 2.3: Undamped transmissibility curve ($m_B/m_y = 0.003$, $A_b/A_a = 10$ and $\mu_k = 1$ in Equation (2.12))

The objective of the design is for the excitation and isolation frequencies to coincide. The isolation frequency can be calculated by setting the numerator of Equation (2.12) to zero. Replacing the frequency ratios in the resulting equation with the ratios defined in Equation (2.10) and Equation (2.11) yields:

$$\frac{1}{\frac{m_B}{m_y}\left(\frac{A_b}{A_a}-1\right)\frac{A_b}{A_a}+\frac{1}{\mu_k}\frac{m_B}{m_y}\left(\frac{A_b}{A_a}\right)^2}=\left(\frac{\omega_i}{\omega_1}\right)^2 \tag{2.13}$$

Clearly there are multiple solutions for Equation (2.13), but all the ratios will have physical constraints in practice. Some constraints may even be discrete if standard parts are used, for instance, to achieve a certain area ratio. Since the primary natural frequency must be chosen as low as feasible the only parameters available for tuning are the mass, area and stiffness ratios. To find an appropriate choice it is necessary to investigate their effect on the frequencies of maximum transmissibility. The undamped frequencies of maximum transmissibility can be found by equating the denominator of Equation (2.12) to zero [Equation (B.24)]:

$$\left(\frac{\Omega_1}{\omega_1}\right)^2,\left(\frac{\Omega_2}{\omega_1}\right)^2=\frac{\frac{1+\mu_k}{\mu_k}\left(\frac{\omega_1}{\bar{\omega}_2}\right)^2+1\mp\sqrt{\left[\frac{1+\mu_k}{\mu_k}\left(\frac{\omega_1}{\bar{\omega}_2}\right)^2+1\right]^2-\frac{4}{\mu_k}\left(\frac{\omega_1}{\bar{\omega}_2}\right)^2}}{\frac{2}{\mu_k}\left(\frac{\omega_1}{\bar{\omega}_2}\right)^2} \tag{2.14}$$

Figure 2.4 and Figure 2.5 illustrate the effect of mass and stiffness ratios on the frequencies of maximum transmissibility as well as the isolation frequency. At low stiffness ratios and large mass ratios the isolation frequency approaches the first frequency of maximum transmissibility. It will be

beneficial if the isolation frequency is separated from the frequencies of maximum transmissibility, but in doing so the isolation frequency is increased. Since a low isolation frequency is normally required the primary system natural frequency must be as low as feasible to ensure coincidence. The effect of the area ratio will be similar to that of the mass ratio.

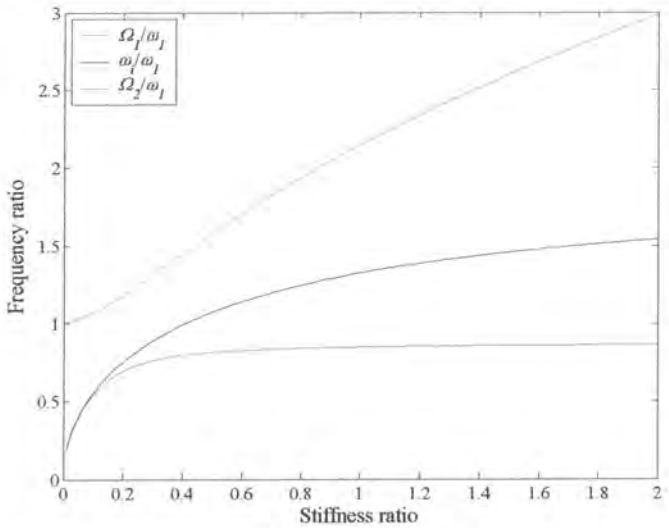

Figure 2.4: Frequencies of maximum and minimum transmissibility *vs.* stiffness ratio (μ_k) (m_B/m_y = 0.003 and A_b/A_a= 10)

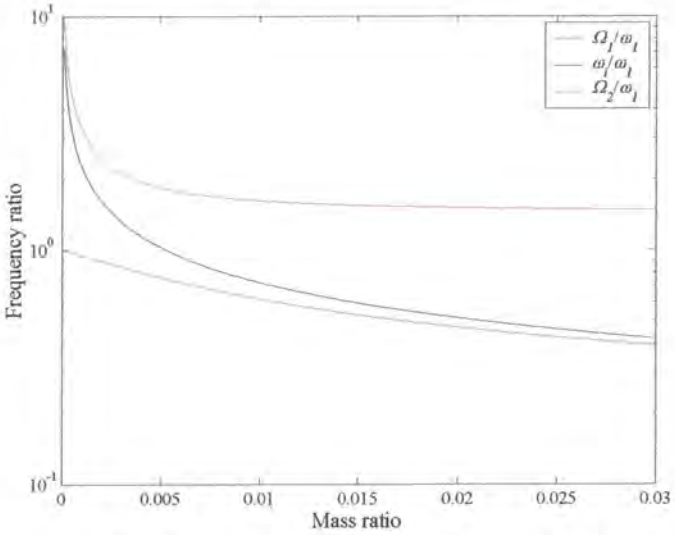

Figure 2.5: Frequencies of maximum and minimum transmissibility *vs.* mass ratio (m_B/m_y) (A_b/A_a= 10 and μ_k = 1)

The frequencies of maximum transmissibility can now be used to guide a more appropriate choice of parameter ratios to satisfy Equation (2.13). One method would be to require equal spacing between the isolation frequency and the two frequencies of maximum transmissibility. Mathematically this requirement can be expressed as:

$$\left(\frac{\omega_i}{\omega_1}\right)^2 - \left(\frac{\Omega_1}{\omega_1}\right)^2 = \left(\frac{\Omega_2}{\omega_1}\right)^2 - \left(\frac{\omega_i}{\omega_1}\right)^2 \tag{2.15}$$

Each of the above ratios can be written in terms of the parameter ratios as shown before in Equations (2.13) and (2.14), although not explicitly. It is necessary to solve the parameter ratios using a numerical method and for this purpose the equations are rewritten as follows:

$$\left(\frac{\Omega_1}{\omega_1}\right)^2 \frac{2\mu_m\mu_A^2}{\mu_k} - \frac{1+\mu_k}{\mu_k}\mu_m\mu_A^2 - 1 + \sqrt{\left[\frac{1+\mu_k}{\mu_k}\mu_m\mu_A^2 + 1\right]^2 - \frac{4\mu_m\mu_A^2}{\mu_k}} = 0$$

$$\left(\frac{\Omega_2}{\omega_1}\right)^2 \frac{2\mu_m\mu_A^2}{\mu_k} - \frac{1+\mu_k}{\mu_k}\mu_m\mu_A^2 - 1 - \sqrt{\left[\frac{1+\mu_k}{\mu_k}\mu_m\mu_A^2 + 1\right]^2 - \frac{4\mu_m\mu_A^2}{\mu_k}} = 0$$

$$\left(\frac{\omega_i}{\omega_1}\right)^2 \left[\mu_m(\mu_A - 1)\mu_A + \frac{\mu_m\mu_A^2}{\mu_k}\right] - 1 = 0 \qquad (2.16)$$

$$2\left(\frac{\omega_i}{\omega_1}\right)^2 - \left(\frac{\Omega_1}{\omega_1}\right)^2 - \left(\frac{\Omega_2}{\omega_1}\right)^2 = 0$$

where: $\mu_A = \frac{A_b}{A_a}$, $\mu_m = \frac{m_B}{m_y}$

In this set of equations there are 5 unknowns (μ_k, μ_A, μ_m, Ω_2/ω_1 and Ω_1/ω_1) and four equations, which requires that one parameter be prescribed. A typical design might prescribe the area ratio (μ_A) and calculate the required mass and stiffness ratios. The result for a design requiring an isolation frequency ratio ω_i/ω_1 = 1.5 and area ratio (μ_A) of 10 is shown in Figure 2.6. Clearly the frequency ratios of maximum transmissibility are equidistant from the isolation frequency ratio. The calculated values for the mass and stiffness ratios are μ_m = 0.00182 and μ_k = 0.65 respectively.

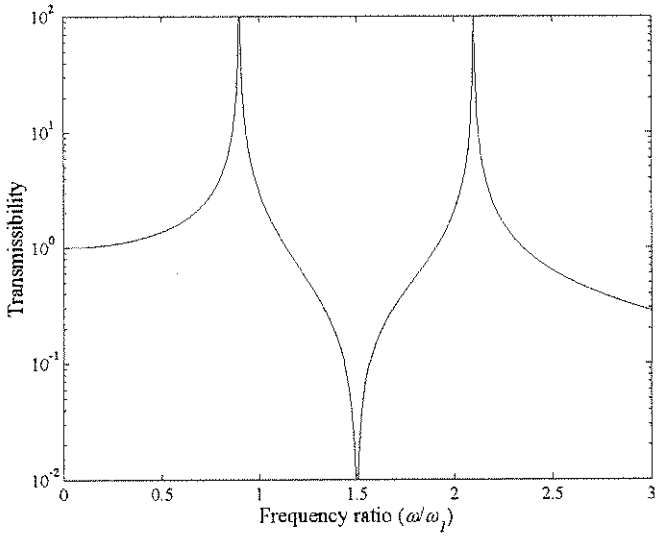

Figure 2.6: Design result for ω_i/ω_1 = 1.5

It is also possible for other requirements to exist such as limits on the stiffness, mass and area ratios as well as on the primary system natural frequency, in which case an optimisation approach can be used to find suitable parameters.

The approach described above is suitable for an undamped device. Although unwanted in most cases, damping will always be present in practical devices, and can influence the design substantially. The effect of damping will be considered next.

For the damped case the transmissibility can be non-dimensionalised by introducing the frequencies defined before and the damping ratios in Equation (2.4) [Equation (B.28)]:

$$\frac{Y}{X}=\frac{\left(1+i2\frac{\omega}{\omega_1}\zeta_1\right)\left[1+i2\frac{\omega}{\omega_2}\zeta_2-\left(\frac{\omega}{\omega_2}\right)^2\right]-\left(1+i2\frac{\omega}{\omega_2}\zeta_2\right)\left(\frac{\omega}{\overline{\omega}_i}\right)^2}{\left[1+\mu_k+i2\left(\frac{\omega}{\omega_1}\zeta_1+\mu_k\frac{\omega}{\omega_2}\zeta_2\right)-\left(\frac{\omega}{\omega_1}\right)^2\right]\left[1+i2\frac{\omega}{\omega_2}\zeta_2-\left(\frac{\omega}{\omega_2}\right)^2\right]-\mu_k\left(1+i2\frac{\omega}{\omega_2}\zeta_2\right)^2} \tag{2.17}$$

where: $\zeta_1=\dfrac{c}{2m_y\omega_1}$, $\zeta_2=\dfrac{c_u}{2m_B\left(\frac{A_b}{A_a}\right)^2\omega_2}$

The second damping ratio can be written in terms of the stiffness ratio:

$$\zeta_2=\frac{1}{\sqrt{\mu_k}}\frac{c_u}{2m_B\left(\frac{A_b}{A_a}\right)^2\overline{\omega}_2}=\frac{1}{\sqrt{\mu_k}}\overline{\zeta}_2 \tag{2.18}$$

It is convenient to rearrange Equation (2.17) in terms of the frequency ratio (ω/ω_1) and the stiffness ratio (μ_k) [Equation (B.29)]:

$$\frac{Y}{X}=\frac{\left(1+i2\frac{\omega}{\omega_1}\zeta_1\right)\left[1+i\frac{2}{\mu_k}\frac{\omega_1}{\overline{\omega}_2}\frac{\omega}{\omega_1}\overline{\zeta}_2-\frac{1}{\mu_k}\left(\frac{\omega_1}{\overline{\omega}_2}\right)^2\left(\frac{\omega}{\omega_1}\right)^2\right]-\left(1+i\frac{2}{\mu_k}\frac{\omega_1}{\overline{\omega}_2}\frac{\omega}{\omega_1}\overline{\zeta}_2\right)\left(\frac{\omega_1}{\overline{\omega}_i}\right)^2\left(\frac{\omega}{\omega_1}\right)^2}{\left[1+\mu_k+i2\frac{\omega}{\omega_1}\left(\zeta_1+\frac{\omega_1}{\overline{\omega}_2}\overline{\zeta}_2\right)-\left(\frac{\omega}{\omega_1}\right)^2\right]\left[1+i\frac{2}{\mu_k}\frac{\omega_1}{\overline{\omega}_2}\frac{\omega}{\omega_1}\overline{\zeta}_2-\frac{1}{\mu_k}\left(\frac{\omega_1}{\overline{\omega}_2}\right)^2\left(\frac{\omega}{\omega_1}\right)^2\right]-\mu_k\left(1+i\frac{2}{\mu_k}\frac{\omega_1}{\overline{\omega}_2}\frac{\omega}{\omega_1}\overline{\zeta}_2\right)^2} \tag{2.19}$$

The effect of damping on the transmissibility is illustrated in Figure 2.7 and Figure 2.8. The damping ratio ζ_1 is associated with the primary system before the addition of the absorber fluid. The source of this damping is the primary spring. For the combined system the primary spring damping will influence the response at all the frequencies of maximum and minimum transmissibility. The damping ratio ζ_2 is associated with the membrane and the fluid and will only influence the transmissibility at the second frequency of maximum transmissibility and the frequency of minimum transmissibility. The effect on the transmissibility at the isolation frequency is less than for the primary damping ratio ζ_1. It is also important to note that the addition of damping will have a significant effect on the isolation frequency. Normally this effect will not influence the design, since the AVAI is designed to have little damping. In a case where some damping is required it must clearly be accounted for to ensure optimal tuning.

In some cases high frequency transmissibility can enter the design requirements, for instance, to limit noise generation. It has already been shown for the single degree of freedom AVAI that the high frequency transmissibility is related to the ratio of natural to isolation frequencies and is independent of frequency. For the AVAI with flexible reservoir wall the high frequency roll-off is -20 dB/decade when damped and -40 dB/decade when undamped, which is the same as for a normal isolator.

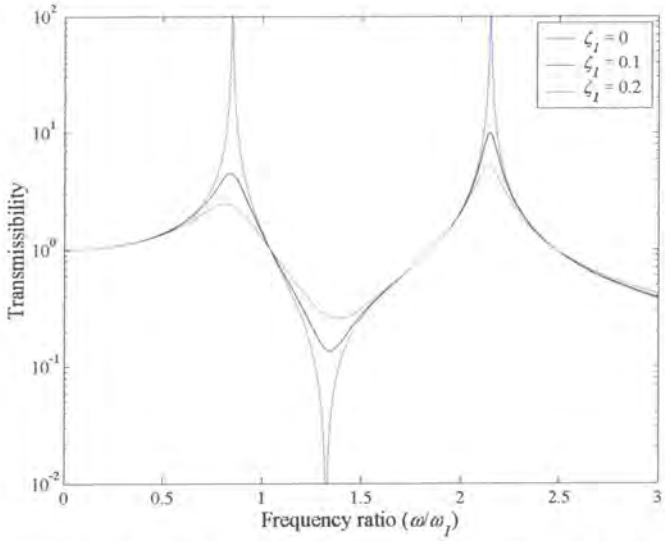

Figure 2.7: Transmissibility *vs.* damping ratio ζ_1 (m_B/m_y = 0.003, A_b/A_a= 10, ζ_2 = 0 and μ_k = 1)

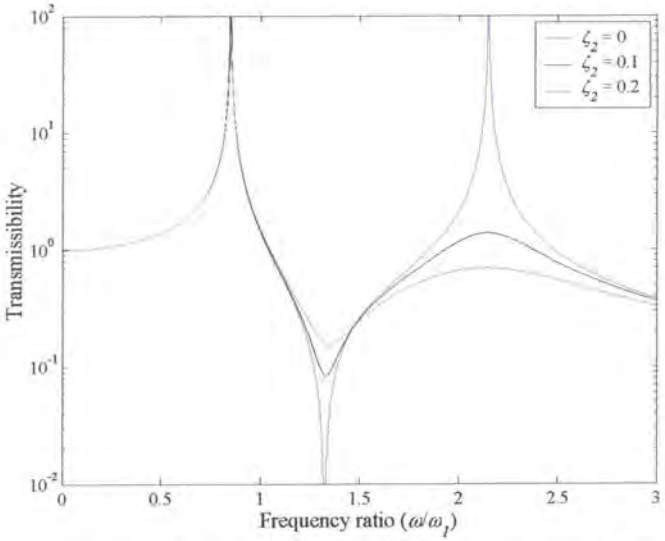

Figure 2.8: Transmissibility *vs.* damping ratio ζ_2 (m_B/m_y = 0.003, A_b/A_a= 10, ζ_1 = 0 and μ_k = 1)

It would be ideal to have a robust device that is insensitive to changes in excitation frequency. A high bandwidth device will fit this requirement. The bandwidth is defined as the normalised frequency range for which the transmissibility is within √2 of the minimum transmissibility at the isolation frequency:

$$B = \frac{\hat{\omega}_2 - \hat{\omega}_1}{\omega_t} \tag{2.20}$$

Analytical expressions for $\hat{\omega}_1$ and $\hat{\omega}_2$ can be found using Equation (2.19), but will be cluttered and will not be attempted. Instead the values will be obtained numerically. Figure 2.9 shows the effect of damping on the bandwidth, isolation frequency and frequencies of maximum transmissibility. It shows that for primary damping ratios of up to 0.1 the effect on the isolation frequency can be ignored for the

system considered. This might not be the case for other designs. As expected the bandwidth increases with damping.

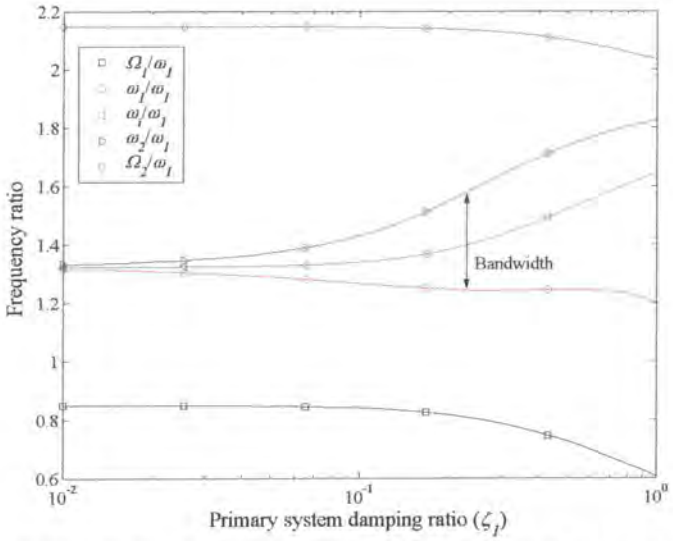

Figure 2.9: Frequency ratio *vs.* primary system damping ($m_B/m_y = 0.003$, $A_b/A_a = 10$, $\zeta_2 = 0$ and $\mu_k = 1$)

A device with large bandwidth only is, however, of little use if the isolation is not adequate, as will happen for a highly damped device. This is illustrated in Figure 2.10. Also shown is that use of the undamped isolation frequency will be adequate for designs with a damping ratio of less than 0.1.

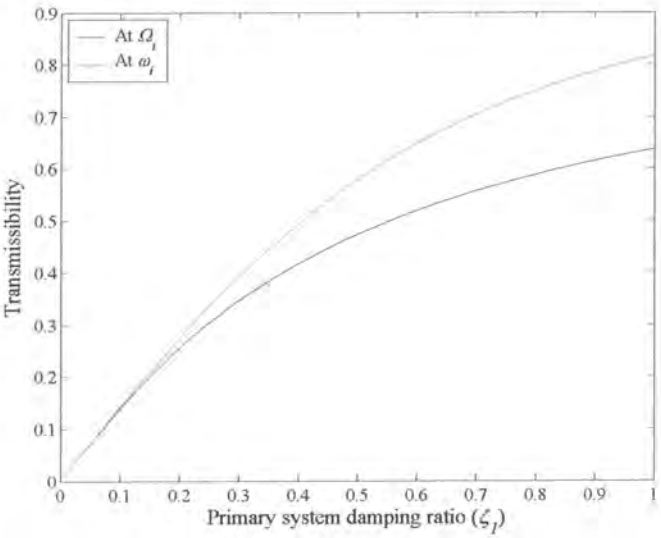

Figure 2.10: Transmissibility at the damped (Ω_i) and undamped (ω_i) isolation frequency as a function of primary system damping ($m_B/m_y = 0.003$, $A_b/A_a = 10$, $\zeta_2 = 0$ and $\mu_k = 1$)

To account for both the bandwidth and isolation in one parameter, Brennan (1997b) defined the robustness as the isolation bandwidth product:

$$R = B\left(1 - \left|\frac{Y}{X}\right|\right) \tag{2.21}$$

The robustness is shown in Figure 2.11.

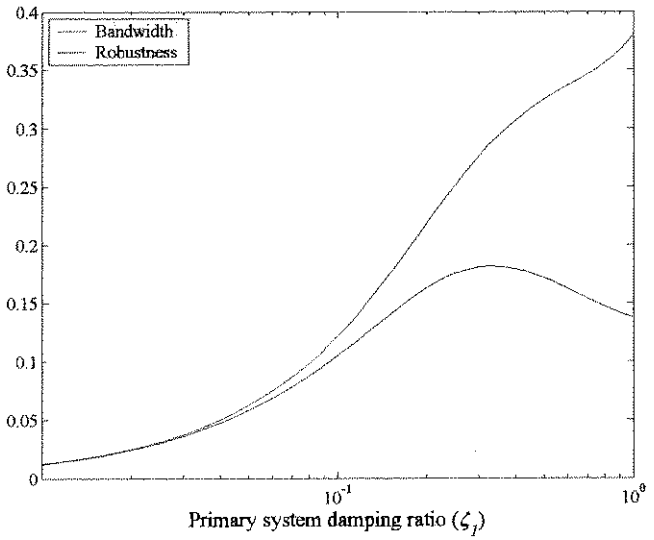

Figure 2.11: Bandwidth and robustness (m_B/m_y = 0.003, A_b/A_a= 10, ζ_2 = 0 and μ_k = 1)

Clearly an optimal value exist for this design, but practically a damping ratio of ~0.3 will not provide adequate isolation and a less robust design will be necessary. One way to increase both the bandwidth and the robustness is to increase the mass ratio as shown in Figure 2.12. This result should be interpreted with care, since it presupposes that a certain stiffness ratio can be realised. This might not be the case in practice, in which case an increase in mass ratio will result in inadequate separation between the isolation frequency and the first frequency of maximum transmissibility (Figure 2.5)

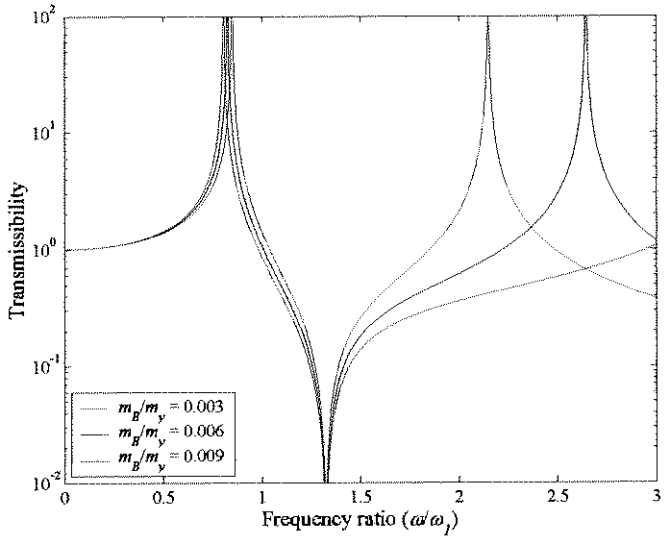

Figure 2.12: Transmissibility as a function of mass ratio ($\bar{\omega}_i/\omega_1$ = 1.3, A_b/A_a= 10 and $\zeta_1 = \zeta_2$ = 0)

Another constraint on the design is the membrane deflection. The transmissibility between the excitation and the membrane response is given by:

$$\frac{U}{X}=\frac{\left(1+i\frac{2}{\mu_k}\frac{\omega_1}{\bar{\omega}_2}\frac{\omega}{\omega_1}\bar{\zeta}_2\right)\left(1+i2\frac{\omega}{\omega_1}\zeta_1\right)-\left[1+\mu_k+i2\frac{\omega}{\omega_1}\left(\zeta_1+\frac{\omega_1}{\bar{\omega}_2}\bar{\zeta}_2\right)-\left(\frac{\omega}{\omega_1}\right)^2\right]\left(\frac{\omega_1}{\bar{\omega}_1}\right)^2\left(\frac{\omega}{\omega_1}\right)^2}{\left[1+\mu_k+i2\frac{\omega}{\omega_1}\left(\zeta_1+\frac{\omega_1}{\bar{\omega}_2}\bar{\zeta}_2\right)-\left(\frac{\omega}{\omega_1}\right)^2\right]\left[1+i\frac{2}{\mu_k}\frac{\omega_1}{\bar{\omega}_2}\frac{\omega}{\omega_1}\bar{\zeta}_2-\frac{1}{\mu_k}\left(\frac{\omega_1}{\bar{\omega}_2}\right)^2\left(\frac{\omega}{\omega_1}\right)^2\right]-\mu_k\left(1+i\frac{2}{\mu_k}\frac{\omega_1}{\bar{\omega}_2}\frac{\omega}{\omega_1}\bar{\zeta}_2\right)^2} \quad (2.22)$$

Figure 2.13 shows the transmissibility as a function of frequency ratio with the damped isolation frequency indicated. In this case the design must be able to pass through the first frequency of maximum transmissibility without damage to the membrane and must also be able to operate continuously with membrane deflections of similar size as the excitation. At low stiffness ratios the required deflection increases.

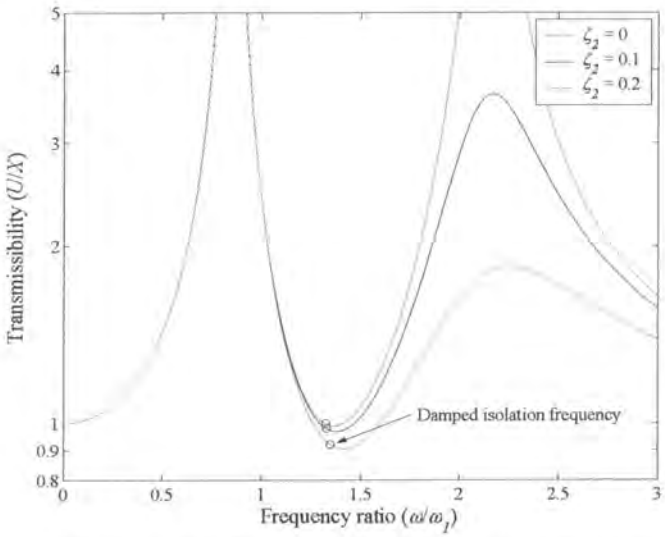

Figure 2.13: Transmissibility between the excitation and the membrane ($m_B/m_y = 0.003$, $A_b/A_a = 10$, $\zeta_1 = 0$ and $\mu_k = 1$)

When damping is included in the design it is possible to set bandwidth and transmissibility (or robustness) requirements for the design. One possible method for finding a suitable design will be discussed next. An optimisation approach will be used with the objective function defined as the transmissibility at a specified frequency. This will be done subject to some constraints. It is important to note that many other formulations can be used and these should be set up according to the design objectives. The constraints are listed in Table 2.1. The first two constraints will ensure proper separation of the frequencies of maximum transmissibility and the isolation frequency. The third constraint prescribes the required bandwidth.

Table 2.1: Definition of constraints

Parameter	Function	Constraint
First frequency of maximum transmissibility	$p_1(\bar{x})$	$< a\omega_i/\omega_1$
Second frequency of maximum transmissibility	$p_2(\bar{x})$	$> b\omega_i/\omega_1$
Bandwidth	$p_3(\bar{x})$	$> c$

The optimisation problem is shown in Equation (2.23). In this case five variables were used, but in practice it will be difficult to prescribe the damping terms. All of the variables were subjected to upper and lower bounds to ensure a realistic solution. It is also necessary to provide initial values that will ensure that the required prescribed isolation frequency is in-between the frequencies of minimum and maximum transmissibility. This can be guaranteed by solving the undamped design problem [Equation (2.16)] first.

$$f(\bar{x}) = \left| \frac{\left(1+i2\frac{\omega_i}{\omega_1}x_4\right)\left[1+i\frac{2\sqrt{x_1x_2^2}}{x_3}\frac{\omega_i}{\omega_1}x_5-\frac{x_1x_2^2}{x_3}\left(\frac{\omega_i}{\omega_1}\right)^2\right]-\left(1+i\frac{2\sqrt{x_1x_2^2}}{x_3}\frac{\omega_i}{\omega_1}x_5\right)x_1(x_2-1)x_2\left(\frac{\omega_i}{\omega_1}\right)^2}{\left[1+x_3+i2\frac{\omega_i}{\omega_1}\left(x_4+\sqrt{x_1x_2^2}x_5\right)-\left(\frac{\omega_i}{\omega_1}\right)^2\right]\left[1+i\frac{2\sqrt{x_1x_2^2}}{x_3}\frac{\omega_i}{\omega_1}x_5-\frac{x_1x_2^2}{x_3}\left(\frac{\omega_i}{\omega_1}\right)^2\right]-x_3\left(1+i\frac{2\sqrt{x_1x_2^2}}{x_3}\frac{\omega_i}{\omega_1}x_5\right)^2} \right|$$

$$g_1(\bar{x}) = p_1(\bar{x}) - a\frac{\omega_i}{\omega_1} \le 0$$

$$g_2(\bar{x}) = -p_2(\bar{x}) + b\frac{\omega_i}{\omega_1} \le 0 \qquad (2.23)$$

$$g_3(\bar{x}) = -p_3(\bar{x}) + c \le 0$$

$$x_1 = \frac{m_h}{m_y}, \quad x_2 = \frac{A_h}{A_a}, \quad x_3 = \frac{k_u}{k}, \quad x_4 = \zeta_1, \quad x_5 = \zeta_2$$

The optimal solution was found using the Matlab function `fmincon.m` and is shown in Figure 2.14 and Table 2.2. The choice of constraints must be realistic since it is easy to overconstrain the problem, which will then have no feasible solution. In this case the ratio of the first frequency of maximum transmissibility (Ω_1/ω_1) was chosen to be less than 70% of the isolation frequency ratio and the second frequency of maximum transmissibility (Ω_2/ω_1) was chosen to be more than 130% of the isolation frequency ratio. The frequencies of maximum transmissibility are found by calculating the maxima of the transmissibility equation (Equation (2.17)) defined by the solution of the optimisation problem (Equation (2.23)). The bandwidth is 6% of the isolation frequency and is also calculated using the transmissibility equation. These would be typical values used in an actual design. Since the calculated parameters are dimensionless, the result can easily be scaled to the actual desired isolation frequency.

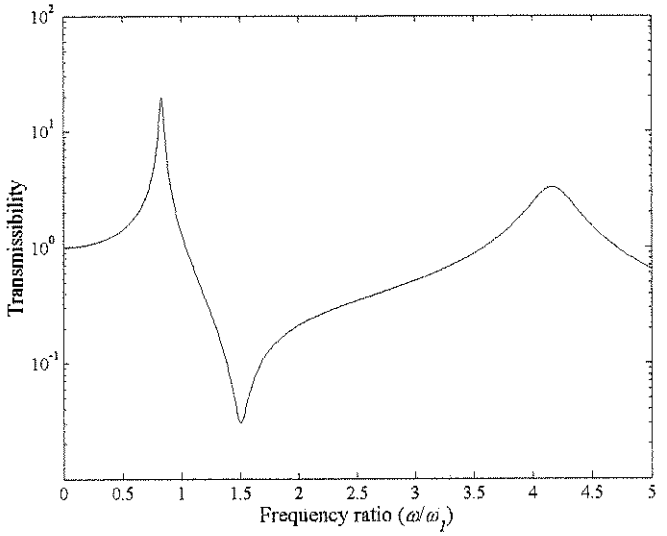

Figure 2.14: Optimal damped transmissibility curve

Table 2.2: Defined constants and solved parameter values

Constants	Parameter	Value
Ratio of first frequency of maximum transmissibility	a	0.7
Ratio of second frequency of maximum transmissibility	b	1.3
Bandwidth	c	0.06
Isolation frequency	ω_i/ω_1	1.5
Variables	Initial value (x_0)	Solution (x^*)
Mass ratio	0.0018	0.0069
Area ratio	10	7.739
Stiffness ratio	0.065	5
Primary damping ratio	0.05	0.02
Absorber damping ratio	0.05	0.078

If an increase in mass ratio is impractical and the excitation frequency is tonal time-varying, an adaptive device can be considered as a method for increasing the effective isolation bandwidth. The effect of changing the stiffness ratio for an undamped device is illustrated in Figure 2.15.

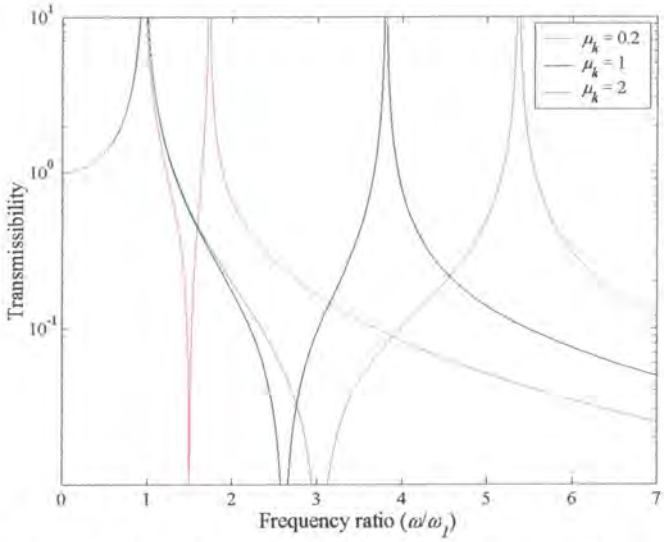

Figure 2.15: Effect of changing the stiffness ratio on the transmissibility (A_b/A_a= 16 and m_B/m_y = 0.00029)

At low stiffness ratios the bandwidth is low, but since the device can adapt to changes in frequency this will only be a problem if rapid frequency changes are expected. In order to design a device the excitation frequency range and the range of stiffness ratios that can be achieved must be known. The device is now designed for the lowest frequency ratio that must be achieved [Equation (B.23)]:

$$\mu_m = \frac{1}{\left(\frac{\omega_i}{\omega_1}\right)^2_{\min}\left[\left(\mu_A - 1\right)\mu_A + \frac{\mu_A^2}{\mu_k|_{\min}}\right]} \tag{2.24}$$

recalling that $\mu_m = m_B/m_y$, $\mu_A = A_b/A_a$ and $\mu_k = k_u/k$. Using the data from the undamped design with an isolation frequency ratio of $\omega_i/\omega_1 = 1.5$, $\mu_A = 16$ and $\mu_k|_{\min} = 0.2$ the mass ratio needed is $\mu_m = 0.00029$.

The highest frequency that can be achieved can now be calculated using Equation (2.13). If it is assumed to be $\mu_k|_{max} = 2$, then the maximum frequency ratio is $\omega_i/\omega_l = 3.05$. If the highest frequency cannot be attained the stiffness ratio must be increased, keeping in mind that there is an upper limit to the isolation frequency ratio [Equation (B.21)]:

$$\left(\frac{\bar{\omega}_i}{\omega_1}\right)^2 = \frac{1}{\mu_m(\mu_A - 1)\mu_A} \tag{2.25}$$

If it is impossible to increase the stiffness ratio or when the above limit has been reached the area ratio must be decreased. As the area ratio is decreased the calculated mass ratio will increase to maintain the isolation frequency ratio in Equation (2.24) and the upper limit of the isolation frequency ratio will increase as illustrated in Figure 2.16. The trade-off in the design is the size and mass of the device and to a lesser extent the bandwidth (for a constant stiffness ratio the bandwidth will decrease as the area ratio is decreased and the mass ratio increased).

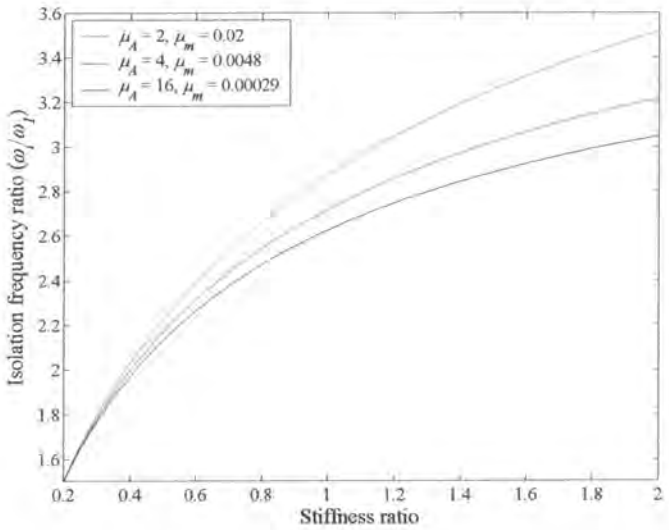

Figure 2.16: Range for various area ratios

Clearly the design method described above is iterative, but has the advantage that the designer can keep in touch with the values of mass ratio and area ratio required and those that can be achieved practically. Alternatively, the following set of equations can be solved numerically for the mass and area ratios [Equation (B.23)]:

$$\left(\frac{\omega_i}{\omega_1}\right)^2_{min} = \frac{1}{\mu_m\left[(\mu_A - 1)\mu_A + \frac{\mu_A^2}{\mu_k|_{min}}\right]}$$
$$\left(\frac{\omega_i}{\omega_1}\right)^2_{max} = \frac{1}{\mu_m\left[(\mu_A - 1)\mu_A + \frac{\mu_A^2}{\mu_k|_{max}}\right]} \tag{2.26}$$

It must, however, be kept in mind that there may not be a solution for the above equations if a too large frequency range is requested. Constraints similar to the single frequency design can also enter the design process, in which case optimisation can be used to find the best solution.

When damping is considered, it becomes clear that the transmissibility will be a function of the stiffness ratio, as illustrated in Figure 2.17. This phenomenon is a major disadvantage of the type I device as opposed to the type II AVAI.

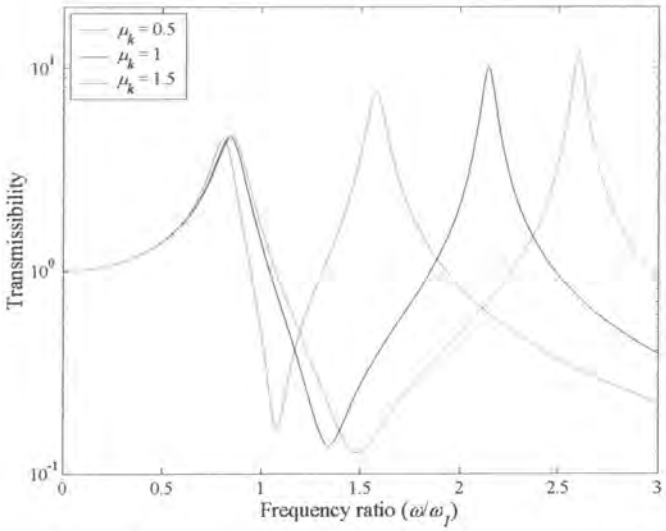

Figure 2.17: Effect of primary system damping on the transmissibility (A_b/A_a= 10, m_B/m_y = 0.003, ζ_1 = 0.1 and ζ_2 = 0)

The choice of area and mass ratios will be based on minimising the transmissibility at the isolation frequencies. The optimisation problem for the minimum isolation frequency ratio can be stated as:

$$f(x_1)=\left|\frac{\left(1+i2\frac{\omega_i}{\omega_1}\Big|_{\min}\zeta_1\right)\left[1+i\frac{2\mu_A\sqrt{x_1}}{\mu_k|_{\min}}\frac{\omega_i}{\omega_1}\Big|_{\min}\bar{\zeta}_2-\frac{x_1\mu_A^2}{\mu_k|_{\min}}\left(\frac{\omega_i}{\omega_1}\right)^2_{\min}\right]-\left(1+i\frac{2\mu_A\sqrt{x_1}}{\mu_k|_{\min}}\frac{\omega_i}{\omega_1}\Big|_{\min}\bar{\zeta}_2\right)x_1\left(\mu_A^2-1\right)\mu_{il}^2\left(\frac{\omega_i}{\omega_1}\right)^2_{\min}}{\left[1+\mu_k|_{\min}+i2\frac{\omega_i}{\omega_1}\Big|_{\min}\left(\zeta_1+\mu_A\sqrt{x_1}\bar{\zeta}_2\right)-\left(\frac{\omega_i}{\omega_1}\right)^2_{\min}\right]\left[1+i\frac{2\mu_A\sqrt{x_1}}{\mu_k|_{\min}}\frac{\omega_i}{\omega_1}\Big|_{\min}\bar{\zeta}_2-\frac{x_1\mu_A^2}{\mu_k|_{\min}}\left(\frac{\omega_i}{\omega_1}\right)^2_{\min}\right]-\mu_k|_{\min}\left(1+i\frac{2\mu_A\sqrt{x_1}}{\mu_k|_{\min}}\frac{\omega_i}{\omega_1}\Big|_{\min}\bar{\zeta}_2\right)^2}\right| \tag{2.27}$$

where x_1 is the mass ratio and the only design variable. At the maximum isolation frequency ratio a similar problem can be defined. For the problem shown above it is impossible to minimise both the transmissibility at the maximum and the minimum stiffness ratios simultaneously as the following example illustrates (Table 2.3). When the transmissibility at the minimum isolation frequency is minimised the result is that the transmissibility at the maximum isolation frequency is more than the optimal value possible. It would however make sense to tune it to the minimum value since the transmissibility decreases as the stiffness ratio is increased.

Table 2.3: Design results with $\mu_A = 16$

	Mass ratio (μ_m)	Minimum transmissibility	Maximum transmissibility
Tuned to minimum isolation frequency ratio ($\omega_i/\omega_1 = 1.5$)	0.000312	0.127139	0.064893
Tuned to maximum isolation frequency ratio ($\omega_i/\omega_1 = 3.05$)	0.000318	0.141605	0.064800

The effect of the area ratio at the minimum isolation frequency is shown in Figure 2.18. It is clear from this figure that the transmissibility at the isolation frequency can be improved noticeably by using a lower area ratio. However, the trade-off as discussed before remains.

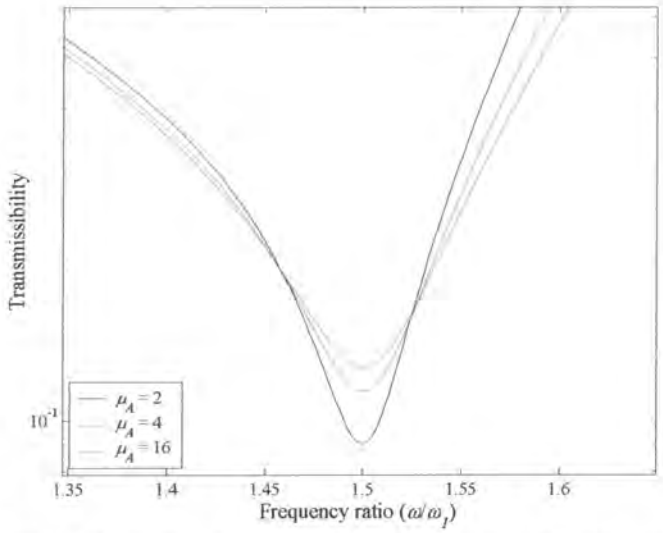

Figure 2.18: Transmissibility at the minimum isolation frequency

The envelopes for two designs are shown in Figure 2.19. The transmissibility is improved over the entire range of frequencies as the area ratio is decreased. The tuning range is also larger for a lower mass ratio, as was the case for the undamped design. Since the range is larger than that specified, the device can either be designed so that a lower minimum isolation frequency ratio or a higher maximum isolation frequency ratio can be achieved. At low stiffness ratios the isolation frequency ratio is more sensitive to the stiffness ratio and tuning will therefore be quicker. The device will also be slightly lighter. The lowest transmissibility that can be reached at a specific isolation frequency ratio will not be affected, but it will occur at a different stiffness ratio. The optimal design will therefore start at the minimum isolation frequency ratio and then minimise the area ratio within the mass and size constraints required by the application. It is also possible to set bandwidth or robustness requirements as for the fixed frequency design.

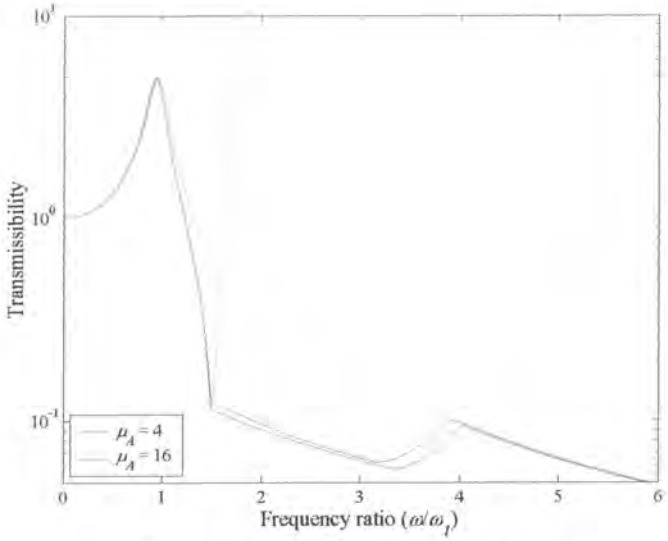

Figure 2.19: Transmissibility envelopes

For any of the above designs the physical parameters can be calculated from the various non-dimensional ratios. If the isolated mass is known the absorber mass can be calculated using the mass ratio. The absorber mass is also:

$$m_B = \rho A_a l \tag{2.28}$$

Once the fluid is chosen the size of the device can be calculated using the above equation and the area ratio. The design methods described in this section were mainly aimed at understanding the type I AVAI. In chapter 4 a more practical methodology will be described where the design starts at the maximum size and then calculates the performance that can be achieved, which can be evaluated against the performance requirements.

2.1.2 Reduced-area reservoir wall flexibility

This section will show what the effect will be if the membrane covers an area that is smaller than the reservoir wall as shown in Figure 2.20. There is no advantage to this arrangement in terms of transmissibility or frequency range over the previous case, but since it can better approximate actual system behaviour it will be discussed briefly. The fluid continuity is [Equation (B.32)]:

$$x_B = \left(1 - \frac{A_b}{A_a}\right)x + \frac{A_b - A_c}{A_a}y + \frac{A_c}{A_a}u \tag{2.29}$$

The damped transmissibility is [Equation (B.37)]:

$$\frac{Y}{X} = \frac{\left[k + i\omega c - \omega^2 m_B\left(\frac{A_b}{A_a} - 1\right)\left(\frac{A_b - A_c}{A_a}\right)\right]\left[k_w + i\omega c_w - \omega^2 m_B\left(\frac{A_c}{A_a}\right)^2\right] - \omega^2 m_B\left(\frac{A_b}{A_a} - 1\right)\frac{A_c}{A_a}\left[k_w + i\omega c_w + \omega^2 m_B\left(\frac{A_b - A_c}{A_a}\right)\frac{A_c}{A_a}\right]}{\left\{k + k_w + i\omega(c + c_w) - \omega^2\left[m_y + m_B\left(\frac{A_b - A_c}{A_a}\right)^2\right]\right\}\left[k_w + i\omega c_w - \omega^2 m_B\left(\frac{A_c}{A_a}\right)^2\right] - \left[k_w + i\omega c_w + \omega^2 m_B\left(\frac{A_b - A_c}{A_a}\right)\frac{A_c}{A_a}\right]^2} \tag{2.30}$$

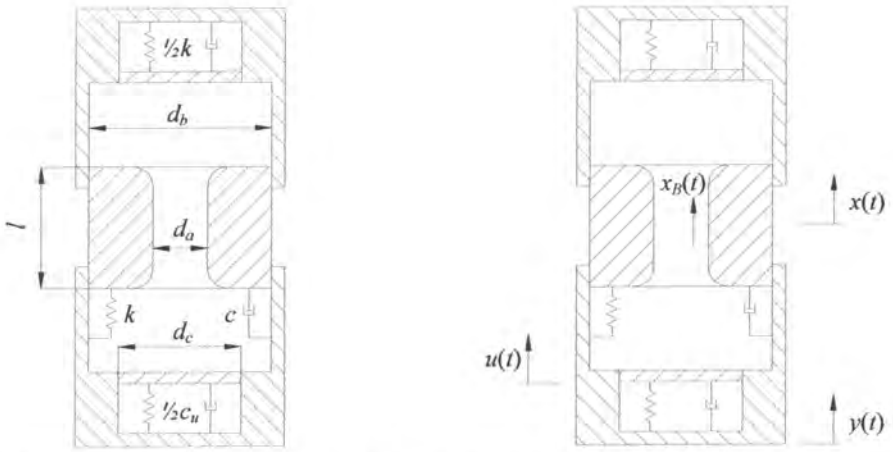

Figure 2.20: Mechanical model of an AVAI with reduced-area reservoir wall stiffness

The undamped non-dimensional transmissibility is [Equation (B.37)]:

$$\frac{Y}{X}=\frac{\left[1-(1-\lambda)\left(\frac{\omega}{\bar{\omega}_i}\right)^2\right]\left[1-\lambda^2\left(\frac{\omega}{\omega_2}\right)^2\right]-\lambda\left(\frac{\omega}{\bar{\omega}_i}\right)^2\left[1+(1-\lambda)\lambda\left(\frac{\omega}{\omega_2}\right)^2\right]}{\left[1+\mu_k-\left(\frac{\omega}{\omega_1}\right)^2-(1-\lambda)^2\mu_k\left(\frac{\omega}{\omega_2}\right)^2\right]\left[1-\lambda^2\left(\frac{\omega}{\omega_2}\right)^2\right]-\mu_k\left[1+(1-\lambda)\lambda\left(\frac{\omega}{\omega_2}\right)^2\right]^2} \tag{2.31}$$

where: $\lambda=\frac{A_c}{A_b}$, $\left(\frac{\omega_1}{\omega_2}\right)^2=\frac{1}{\sqrt{\mu_k}}\frac{m_B}{m_y}\left(\frac{A_b}{A_a}\right)^2$, $\left(\frac{\omega_1}{\bar{\omega}_i}\right)^2=\frac{m_B}{m_y}\left(\frac{A_b}{A_a}-1\right)\frac{A_b}{A_a}$

Equation (2.31) is equal to the transmissibility with full wall reservoir stiffness when $\lambda = 1$ (refer to Equation (2.5)). The equation for the damped transmissibility is shown in Appendix B.

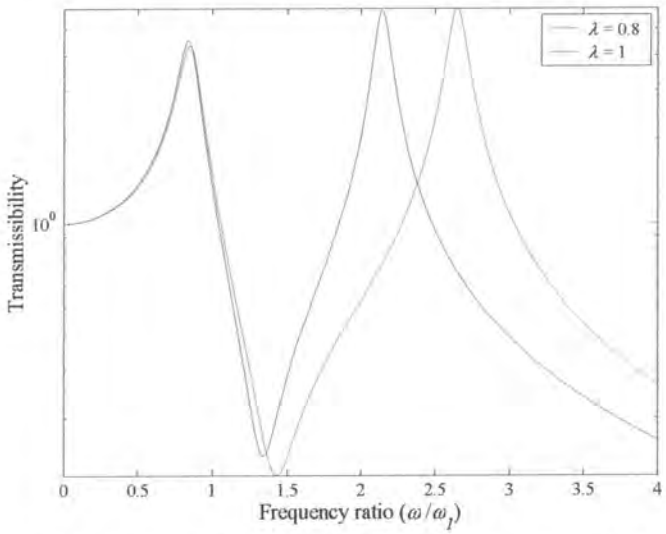

Figure 2.21: Transmissibility comparison ($\mu_k = 1$, $A_b/A_a = 10$, $m_B/m_y = 0.003$, $\zeta_1 = 0.1$ and $\zeta_2 = 0.01$ in Equation (B.38))

Figure 2.21 shows the effect of the reduced area ratio (λ) on the transmissibility. It appears as if the transmissibility is improved, but the comparison is biased since the isolation frequency is higher.

When plotting the minimum transmissibility against the isolation frequency as shown in Figure 2.22 the trend is clearer. Only at high stiffness ratios there is a slight improvement of the transmissibility at the same isolation frequency. At low stiffness ratios the disadvantage of having an area ratio of less than 1 is apparent. The effect on the isolation frequency is shown in Figure 2.23.

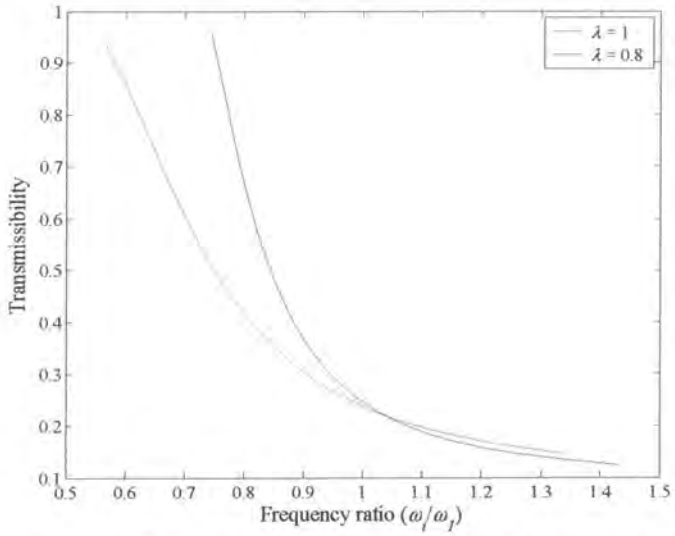

Figure 2.22: Minimum transmissibility *vs.* isolation frequency for stiffness ratios ranging from $\mu_k = 0.1$ to 1 ($A_b/A_a = 10$, $m_B/m_y = 0.003$, $\zeta_1 = 0.1$ and $\bar{\zeta}_2 = 0.01$)

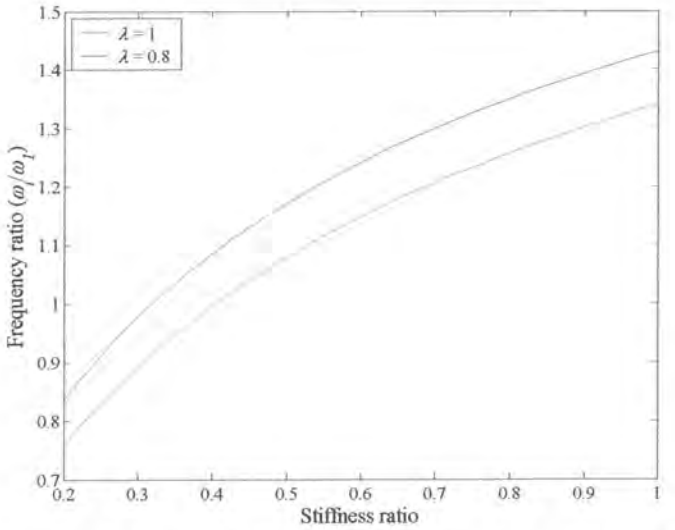

Figure 2.23: Isolation frequency *vs.* stiffness ratio for stiffness ratios ranging from $\mu_k = 0.1$ to 1 ($A_b/A_a = 10$, $m_B/m_y = 0.003$, $\zeta_1 = 0.1$ and $\bar{\zeta}_2 = 0.01$)

2.1.3 Single flexible wall

A special case occurs when only one flexible wall is used. Such a device is presently available from the Lord Corporation (Figure 2.24).

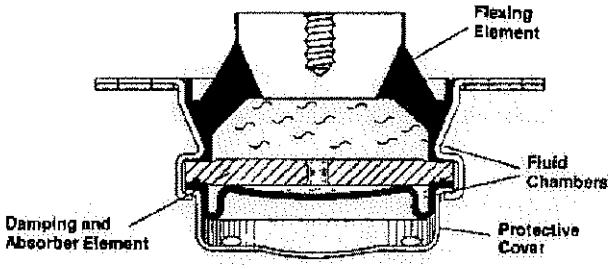

Figure 2.24: Sectional view of the fluidlastic® mount (Lord Corporation)

Several tuneable configurations have been patented. One used an adjustable length inertia track (Hodgson & Duclos, 1990) while another used variable compliance of an air filled chamber (Miller, 1987) as shown in Figure 2.25.

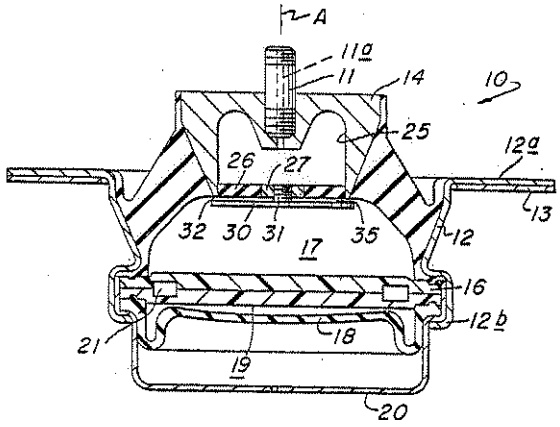

Figure 2.25: Variable compliance tuneable AVAI (Miller, 1987)

Strydom (2000) showed that this AVAI could also be made tuneable by charging the bottom chamber with air pressure. The model describing this device is shown in Figure 2.26.

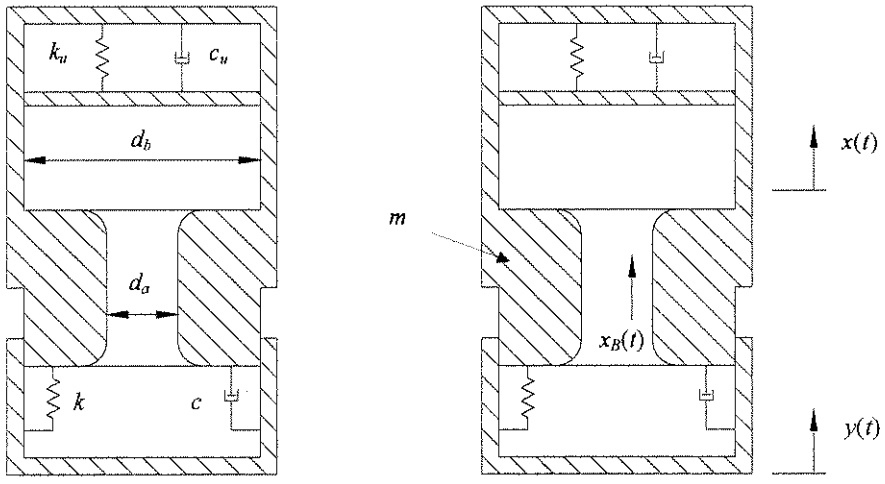

Figure 2.26: Mechanical model of one-sided stiffness

The continuity is not influenced by the membrane stiffness, as was the case before. It is simply:

$$x_B = \left(1 - \frac{A_b}{A_a}\right)x + \frac{A_b}{A_a}y \tag{2.32}$$

Incompressibility requires the membrane displacement to be equal to x. Incompressibility also requires that the effort required to change the distance between the x and y degrees of freedom will depend on the membrane stiffness.

The transmissibility is therefore the same as for the LIVE absorber [Equation (A.108)]:

$$\frac{X}{Y} = \frac{1 + i2\frac{\omega}{\omega_n}\zeta - \left(\frac{\omega}{\omega_i}\right)^2}{1 + i2\frac{\omega}{\omega_n}\zeta - \left(\frac{\omega}{\omega_n}\right)^2} \tag{2.33}$$

where: $\omega_i = \sqrt{\dfrac{k + k_u}{m_B\left(\frac{A_b}{A_a} - 1\right)\frac{A_b}{A_a}}}$, $\omega_n = \sqrt{\dfrac{k + k_u}{m + m_B\left(\frac{A_b}{A_a} - 1\right)^2}}$, $\zeta = \dfrac{c}{2\left[m + m_B\left(\frac{A_b}{A_a} - 1\right)^2\right]\omega_n}$

Although the construction of this device is different to the type II it is mathematically equivalent and its properties will be discussed in more detail in the following paragraphs. It does, however, have some practical properties that need some clarification. The main advantage is its simplicity of construction since it does not require a cylinder that can move axially inside another. One disadvantage is that it is difficult to transfer any moment that might be applied to the device with a soft spring that is only situated on one side of the device. The moment can, of course, be transferred through a bearing as long as it adds little damping. This will, however, result in loss of some of the advantage gained by its simple construction. If pressure is used to change the stiffness of the membrane, large static displacement will result which could be a problem in a practical device. The static displacement will be:

$$\delta_{st} = \frac{pA_b}{k} \tag{2.34}$$

2.2 Adaptive AVAI with slug (Type II)

The absorber mass and area ratio determine the overall size of the AVAI. A low area ratio minimizes the flow-induced losses through entrance, exit and friction effects. Achieving a large absorber mass is difficult using fluids due to the toxicity of heavy liquids. For these reasons it was decided to investigate a device that uses a heavy metal slug instead of a liquid. The use of a slug is not new, in fact the very first LIVE type isolators used slugs, which were later replaced by liquids (Halwes, 1981b). These designs were not adaptive. There are several problems with the use of slugs. Firstly the amplitude is limited, which puts a limit on the area ratio that can be used. In applications where the input is not known exactly provision must be made for over travel. A second problem with slug type devices is ensuring that the slug is centred vertically (Figure 2.27). Two methods will be described. The first uses slug springs to create a differential pressure on the top and bottom reservoirs, thereby

encouraging leakage to reach equilibrium. The second method uses rubber stops that will create a restoring force when the slug comes into contact with the stop.

2.2.1 Slug springs

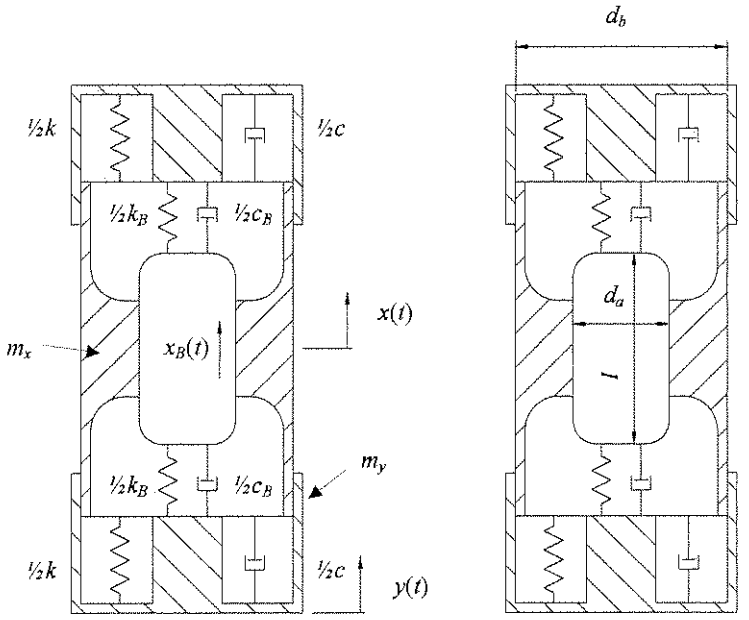

Figure 2.27: Mechanical model of an adaptive AVAI with a slug defined by length l and diameter d_a and slug spring properties defined by k_B and c_B

The continuity through the port (occupied by the slug) is [Equation (B.39)]:

$$x_B = \left(1 - \frac{A_b}{A_a}\right)x + \frac{A_b}{A_a}y \tag{2.35}$$

The equation of motion when assuming excitation at the y degree of freedom, is [Equation (B.46)]:

$$\ddot{x} + 2\zeta\omega_n x + \omega_n^2 x = \left(\frac{\omega_n}{\omega_i}\right)^2 \ddot{y} + 2\zeta\omega_n \dot{y} + \omega_n^2 y$$

$$\text{where: } \omega_i = \sqrt{\frac{k + k_B\left(\frac{A_b}{A_a} - 1\right)^2}{m_B\left(\frac{A_b}{A_a} - 1\right)\frac{A_b}{A_a}}}, \quad \omega_n = \sqrt{\frac{k + k_B\left(\frac{A_b}{A_a} - 1\right)^2}{m_x + m_B\left(\frac{A_b}{A_a} - 1\right)^2}}, \quad \zeta = \frac{c + c_B\left(\frac{A_b}{A_a} - 1\right)^2}{2\left[m_x + m_B\left(\frac{A_b}{A_a} - 1\right)^2\right]\omega_n} \tag{2.36}$$

Equation (2.36) shows the effect of the slug springs. Inclusion of such springs will increase the isolation (ω_i) and natural (ω_n) frequencies, which is undesirable since lowering the frequencies requires the addition of mass. The springs perform a necessary function of positioning the slug vertically and it should be possible to use low stiffness springs to achieve this goal. It will also be possible to use the slug spring for adapting the isolation frequency, especially since the isolation frequency will be very sensitive to this parameter. A practical device implementing such a concept

will, however, be a challenge because of space and low damping requirements. When using a slug spring additional care is necessary when a large area ratio is used to allow enough space for the spring in its compressed state.

If excitation occurs at the x degree of freedom the equation of motion is the same but the coordinates are swapped and the definition of the natural frequency and damping ratio is now given by [Equation (B.49)]:

$$\ddot{y}+2\zeta\omega_n\dot{y}+\omega_n^2 y=\left(\frac{\omega_n}{\omega_i}\right)^2\ddot{x}+2\zeta\omega_n\dot{x}+\omega_n^2 x$$

$$\text{where:}\quad \omega_n=\sqrt{\frac{k+k_B\left(\frac{A_b}{A_a}-1\right)^2}{m_y+m_B\left(\frac{A_b}{A_a}\right)^2}},\quad \zeta=\frac{c+c_B\left(\frac{A_b}{A_a}-1\right)^2}{2\left[m_y+m_B\left(\frac{A_b}{A_a}\right)^2\right]\omega_n} \tag{2.37}$$

The definition for the isolation frequency is the same as in Equation (2.36) for excitation at the y degree of freedom and the design will therefore remain unaffected. In the analysis that follows the ratio X/Y can therefore simply be inverted as long as the corresponding definition of the natural frequency and damping ratio is used. The transmissibility is (refer also to §1.4.1):

$$\frac{X}{Y}=\frac{1+i2\frac{\omega}{\omega_n}\zeta-\left(\frac{\omega}{\omega_i}\right)^2}{1+i2\frac{\omega}{\omega_n}\zeta-\left(\frac{\omega}{\omega_n}\right)^2} \tag{2.38}$$

The isolation frequency is clearly a function of damping as is shown in Figure 2.28.

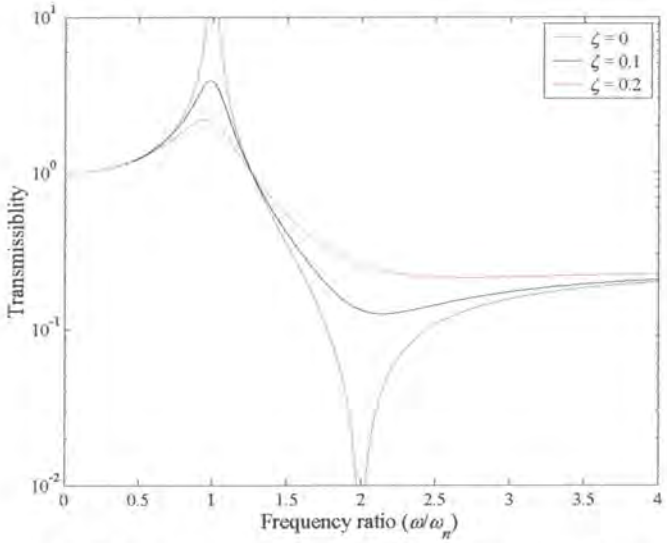

Figure 2.28: Effect of damping on the transmissibility ($\omega_n=1$ and $\omega_i=2$)

The frequency ratio is independent of stiffness and can be written for excitation at y as:

$$\left(\frac{\omega_n}{\omega_i}\right)^2 = \frac{m_B\left(\frac{A_b}{A_a}-1\right)\frac{A_b}{A_a}}{m_x + m_B\left(\frac{A_b}{A_a}-1\right)^2} = \frac{\frac{m_B}{m_x}\left(\frac{A_b}{A_a}-1\right)\frac{A_b}{A_a}}{1+\frac{m_B}{m_x}\left(\frac{A_b}{A_a}-1\right)^2} = \frac{\mu_m(\mu_A-1)\mu_A}{1+\mu_m(\mu_A-1)^2} \tag{2.39}$$

where: $\mu_m = \frac{m_B}{m_x}, \quad \mu_A = \frac{A_b}{A_a}$

and for excitation at x:

$$\left(\frac{\omega_n}{\omega_i}\right)^2 = \frac{m_B\left(\frac{A_b}{A_a}-1\right)\frac{A_b}{A_a}}{m_y + m_B\left(\frac{A_b}{A_a}\right)^2} = \frac{\frac{m_B}{m_y}\left(\frac{A_b}{A_a}-1\right)\frac{A_b}{A_a}}{1+\frac{m_B}{m_y}\left(\frac{A_b}{A_a}\right)^2} = \frac{\mu_m(\mu_A-1)\mu_A}{1+\mu_m\mu_A^2} \tag{2.40}$$

where: $\mu_m = \frac{m_B}{m_y}, \quad \mu_A = \frac{A_b}{A_a}$

Using the above relation the transmissibility can be rewritten in terms of the isolation frequency [Equation (B.50)]:

$$\frac{X}{Y} = \frac{1+i2\frac{\omega_i}{\omega_n}\frac{\omega}{\omega_i}\zeta - \left(\frac{\omega}{\omega_i}\right)^2}{1+i2\frac{\omega_i}{\omega_n}\frac{\omega}{\omega_i}\zeta - \left(\frac{\omega_i}{\omega_n}\right)^2\left(\frac{\omega}{\omega_i}\right)^2} \tag{2.41}$$

In §1.4.1 it was shown that a low frequency ratio (ω_n/ω_i) would minimise the transmissibility at the isolation frequency. This concept is reinforced by Figure 2.29. A design with a low frequency ratio can be realised when the mass ratio approaches zero or when the area ratio approaches 1. Implicit in this graph is the fact that the damping ratio is constant and not the viscous damping coefficient. This result is not unexpected and is similar to what was found for the type I AVAI. Of course, to ensure a low isolation frequency the exact opposite applies.

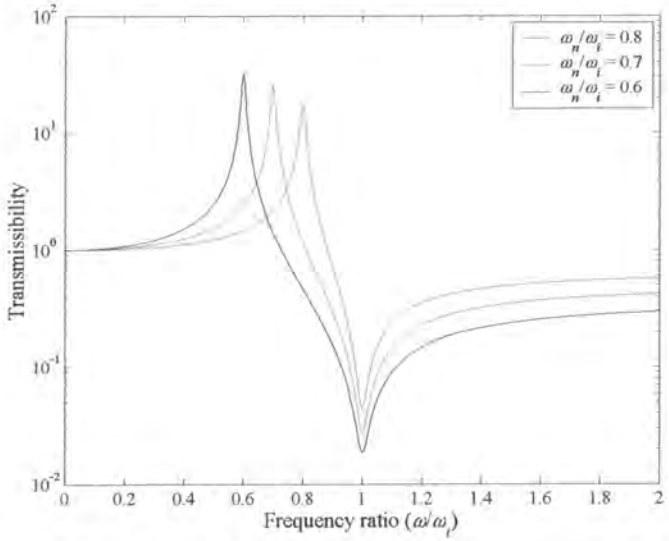

Figure 2.29: Transmissibility as a function frequency ratio ($\zeta = 0.01$)

The design for the type II device differs from the type I since it has an additional constraint on the slug travel. An equation will be set up that takes this constraint into account and can then be solved to yield the size of the device required. The absorber mass can be calculated as follows:

$$m_B = \rho A_a l = \frac{k + k_B\left(\frac{A_b}{A_a} - 1\right)^2}{\omega_i^2\left(\frac{A_b}{A_a} - 1\right)\frac{A_b}{A_a}} \tag{2.42}$$

where l is the length of the slug as shown in Figure 2.30. The excitation frequency is known and both the stiffness values must be as low as possible to decrease the absorber mass (m_B) and therefore the mass ratio. The area ratio is governed by the total length of the device. At isolation the amplitude of the isolated system (X) will be zero for an undamped device. The amplitude of the slug is:

$$X_B = \frac{A_b}{A_a} Y \tag{2.43}$$

If the slug amplitude is larger than the length of the slug protrusion (l_e) the slug will move into the port, which will create entrance losses and thereby increase damping. The compressed length of the slug spring can now be used to calculate the reservoir length:

$$l_r = l_c + 2l_e - Y \tag{2.44}$$

where l_c is the compressed length of the spring.

The port serves two purposes that will determine its length. When the AVAI is in a horizontal position the port length needs to be sufficient to ensure that the slug will not wedge when it is at its maximum displacement. Additionally, it offers some resistance to leak flow. A minimum port length must be specified to determine which designs are appropriate.

The total length of the AVAI can be found using Equations (2.43) and (2.44):

$$l_T = 2l_c + 2\left(\frac{A_b}{A_a} - 1\right)Y + l \tag{2.45}$$

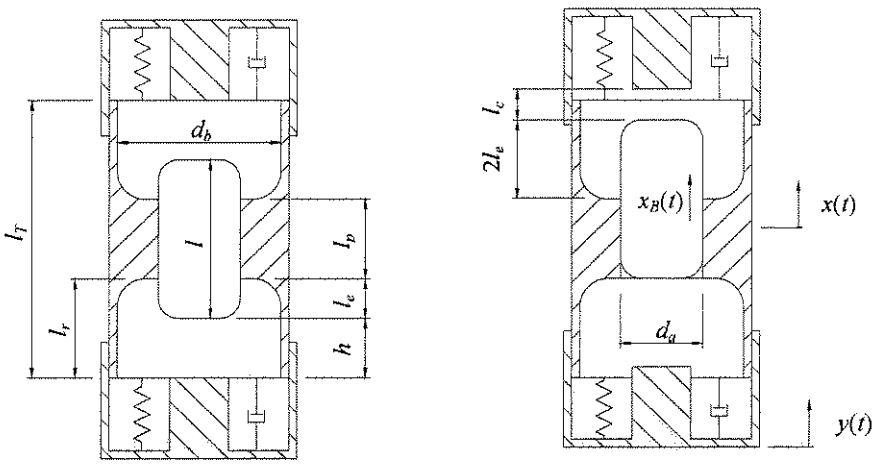

Figure 2.30: Definition of dimensions (length l_p and diameter d_a defines the port geometry)

One possible design approach would be to specify the overall device dimensions (l_T and d_b), excitation frequency (ω_e) and excitation amplitude (Y), spring stiffnesses (k and k_B), slug density (ρ), minimum port length and then to calculate the port diameter (d_a). Using Equation (2.44) and (2.42) the following design equation can be derived [Equation (B.62)]:

$$\begin{aligned}&\left(2l_c\omega_i^2 A_b\rho - 2Y\omega_i^2 A_b\rho - l_T\omega_i^2 A_b\rho - k - k_B\right)A_a^2 \\ &+\left(l_T\omega_i^2\rho A_b^2 - 2l_c\omega_i^2\rho A_b^2 + 4Y\omega_i^2 A_b^2\rho + 2k_B A_b\right)A_a - 2Y\omega_i^2\rho A_b^3 - k_B A_b^2 = 0\end{aligned} \tag{2.46}$$

It is evident that for a set of parameters four port diameters (d_a) will result from the solution of Equation (2.46), but some solutions might lack physical meaning since they result in complex or negative diameters or in port lengths shorter than the minimum required. The design approach will be explained using an example with a set of fixed parameters shown in Table 2.4. The set of parameters results in the two design spaces in terms of the overall size defined by length (l_T) and diameter (d_b) as shown in Figure 2.31 and Figure 2.32. In each figure design points are shown which are physically illustrated in Figure 2.33. The application will dictate which of the designs are the most appropriate in terms of geometry. The trade-off between two designs with identical outer dimensions lies in the total mass and area ratio. Large area ratios will result in high slug velocity (increasing damping) and low absorber mass. The absorber mass is shown in Figure 2.34 and Figure 2.35.

Table 2.4: Fixed design parameters

Parameter	Value
Frequency	10 Hz
Static deflection (δ_{st})	0.005 m
Isolated mass (m)	100 kg
Stiffness	mg/δ_{st}
Excitation amplitude	0.003 m
Slug spring (k_B)	$k/100$
Slug density	1000 kg/m^3
Spring compressed length (l_c)	0.01 m

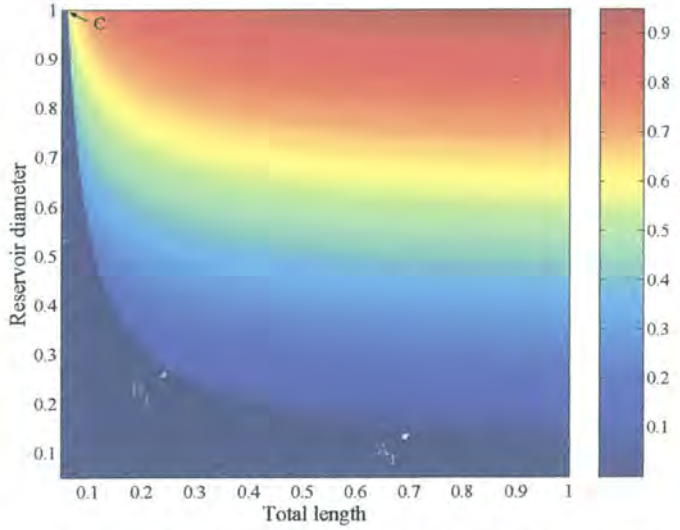

Figure 2.31: Port diameter for the first solution space ($l_p > 0$, $d_a = 0$ indicates complex or negative solution)

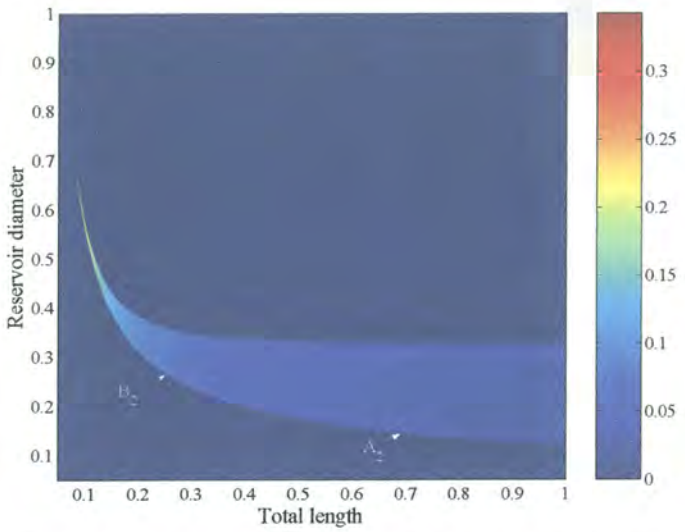

Figure 2.32: Port diameter for the second solution space ($l_p > 0$, $d_a = 0$ indicates complex or negative solution)

Table 2.5: Design parameters

	A_1	A_2	B_1	B_2	C
Total length (l_T)	0.700	0.700	0.260	0.260	0.100
Reservoir diameter (d_b)	0.150	0.150	0.260	0.260	1.000
Port diameter (d_a)	0.057	0.039	0.089	0.086	0.735
Slug length (l)	0.645	0.596	0.195	0.191	0.075
Slug protrusion (l_e)	0.021	0.045	0.026	0.027	0.006
Port length (l_p)	0.604	0.505	0.144	0.137	0.064
Area ratio (A_b/A_a)	6.9	15.1	8.5	9.1	1.9
Slug mass (m_B)	1.65	0.71	1.21	1.11	31.82

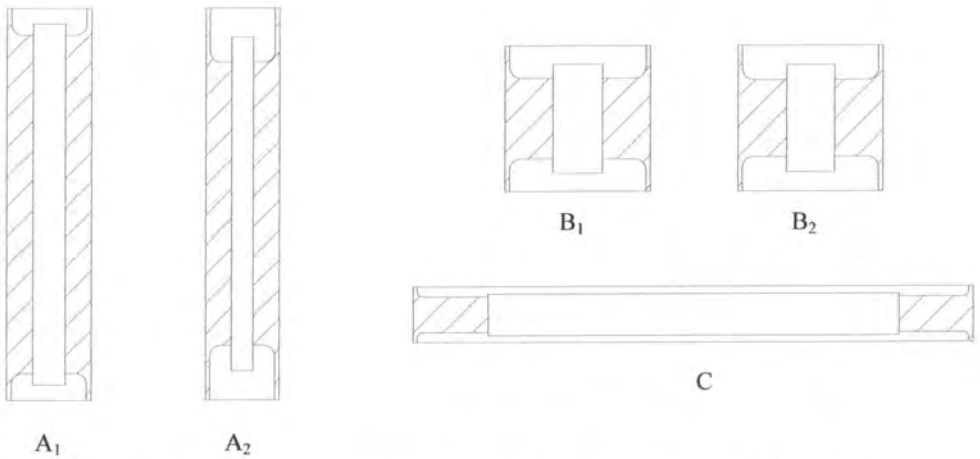

Figure 2.33: Five possible designs that fit the requirements of Table 2.4

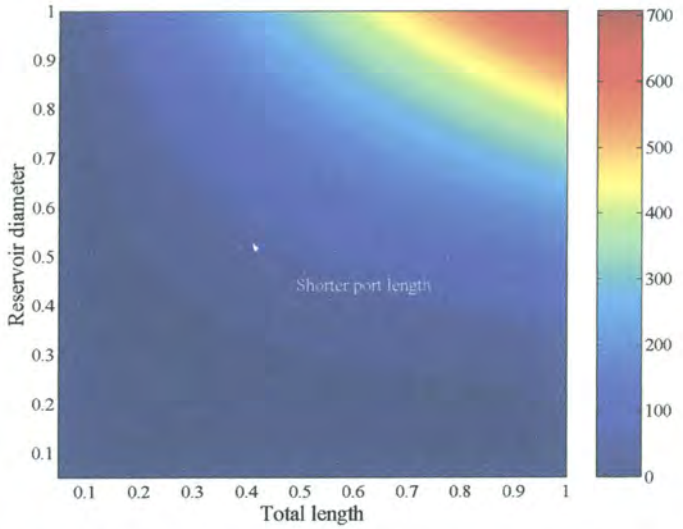

Figure 2.34: Absorber mass for the first solution space showing the direction in which the port length shortens ($l_p > 0$, $d_a = 0$ indicates complex or negative solution)

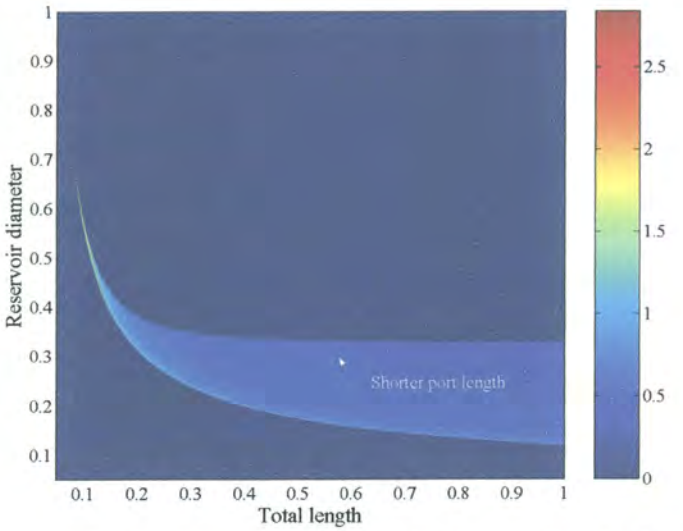

Figure 2.35: Absorber mass for the second solution space showing the direction in which the port length shortens ($l_p > 0$, $d_a = 0$ indicates complex or negative solution)

If a large amount of damping is present the damped isolation frequency must be set equal to the excitation frequency (Ω_i in Equation (2.47)). It is possible to use this equation to calculate the undamped isolation frequency, which can then be used in the same design procedure as shown before with the slug amplitude adapted to account for the fact that the motion of the mass is nonzero for a damped system.

$$\left(\frac{\Omega_i}{\omega_n}\right)^2 = \frac{-\left(\frac{\omega_n}{\omega_i}\right)^2 - 1 - \sqrt{\left[\left(\frac{\omega_n}{\omega_i}\right)^2 - 1\right]^2 + 8\zeta^2\left[\left(\frac{\omega_n}{\omega_i}\right)^2 + 1\right]}}{4\zeta^2 + 4\zeta^2\left(\frac{\omega_n}{\omega_i}\right)^2 - 2\left(\frac{\omega_n}{\omega_i}\right)^2} \tag{2.47}$$

To investigate the effects of changing the stiffness the transmissibility can conveniently be written in terms of the initial values (indicated by a prime) [Equation (B.55)]:

$$\frac{X}{Y}=\frac{1+i\frac{2}{\mu_k}\frac{\omega}{\omega_n'}\zeta'-\frac{1}{\mu_k}\left(\frac{\omega_n'}{\omega_i'}\right)^2\left(\frac{\omega}{\omega_n'}\right)^2}{1+i\frac{2}{\mu_k}\frac{\omega}{\omega_n'}\zeta'-\frac{1}{\mu_k}\left(\frac{\omega}{\omega_n'}\right)^2}$$

$$\text{where:}\quad \mu_k=\frac{k+k_B\left(\frac{A_b}{A_a}-1\right)^2}{k'+k_B'\left(\frac{A_b}{A_a}-1\right)^2},\quad \zeta'=\frac{c}{2\left[m_x+m_B\left(\frac{A_b}{A_a}-1\right)^2\right]\omega_n'},\tag{2.48}$$

$$\omega_i'=\sqrt{\frac{k'+k_B'\left(\frac{A_b}{A_a}-1\right)^2}{m_B\left(\frac{A_b}{A_a}-1\right)\frac{A_b}{A_a}}},\quad \omega_n'=\sqrt{\frac{k'+k_B'\left(\frac{A_b}{A_a}-1\right)^2}{m_x+m_B\left(\frac{A_b}{A_a}-1\right)^2}}$$

where k' is the initial value and k the current value. In the above equation it is assumed that the damping coefficient is constant. Figure 2.36 shows the effect of changing the stiffness ratio for an undamped device. From the figure it is clear that the natural frequency is a function of the stiffness change and consequently also the static deflection. This effect must be kept in mind, as it could be problematic in a practical device.

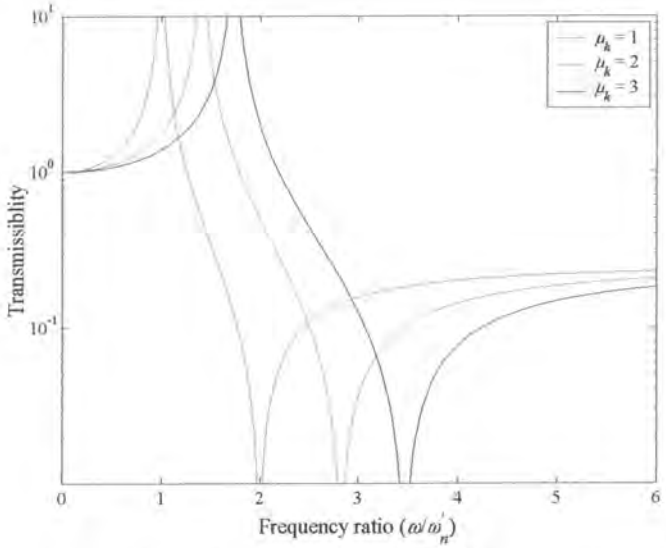

Figure 2.36: Transmissibility *vs.* frequency ratio for 3 stiffness ratios ($\omega_n'/\omega_i' = ½$ and $\zeta' = 0$)

Since it is difficult to design stable low stiffness springs it will be appropriate to use the passive design method to design the device for the lowest required frequency and then to calculate if the maximum frequency covers the required range. The isolation frequency ratio can be written in terms of the stiffness ratio (excitation at x) [Equation (B.63)]:

$$\left(\frac{\omega_i}{\omega_n'}\right)^2=\mu_k\left(\frac{\omega_i'}{\omega_n'}\right)^2=\mu_k\left(\frac{\omega_i}{\omega_n}\right)^2=\mu_k\frac{1+\mu_m\left(\mu_A-1\right)^2}{\mu_m\left(\mu_A-1\right)\mu_A}\tag{2.49}$$

The difference between the above equation and Equation (2.13) for the type I AVAI is that the mass and area ratios do not influence the tuning range. For the undamped case the only way to increase the tuning range is to increase the stiffness ratio.

The effect of changing the stiffness ratio for a damped design is shown in Figure 2.37. The provision is that the damping coefficient is independent of the stiffness ratio and frequency, which will not be the case in practice since the slug velocity will increase and the spring's loss factor can be frequency dependent.

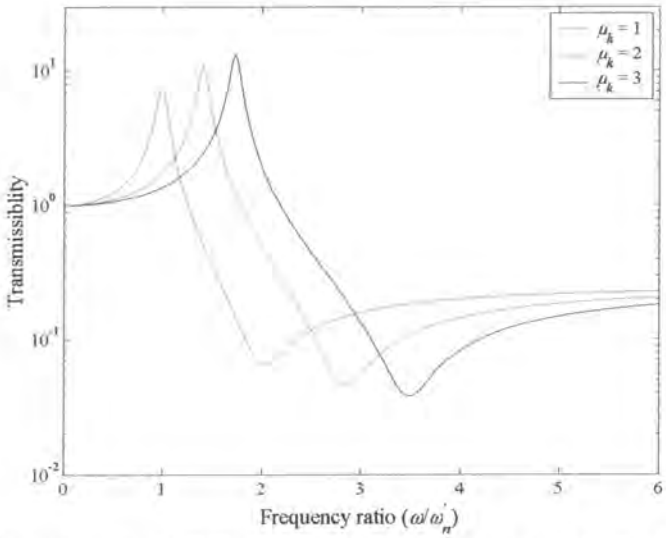

Figure 2.37: Damped transmissibility as a function of stiffness ratio ($\omega_n/\omega_i = ½$ and $\zeta' = 0.01$)

2.2.2 Slug stops

The use of flexible slug stops is one method of ensuring that the slug stays centred. When the slug hits the stop the pressure in the opposite chamber will increase, thereby forcing some fluid through he gap between the slug and the port. This action will tend to equalize the volume of fluid in the reservoirs, thereby centring the slug. Such a system will require a balancing act between a sufficient gap size to ensure adequate flow and one that will decrease the effectiveness of the device. Another method will be to construct channels with one-way valves that will open when the pressure rises to a certain level above that of normal operation. This will be at the cost of added complexity.

The addition of stops does not change the continuity equation. Both the spring and damper will only be active after the relative motion between the slug and reservoir is larger than the gap (h). The following Heaviside function describes this property:

$$\beta = \begin{cases} 0 \text{ if } \left| y - x + \frac{A_b}{A_a}(x-y) \right| < h \\ 1 \text{ if } \left| y - x + \frac{A_b}{A_a}(x-y) \right| \geq h \end{cases} \tag{2.50}$$

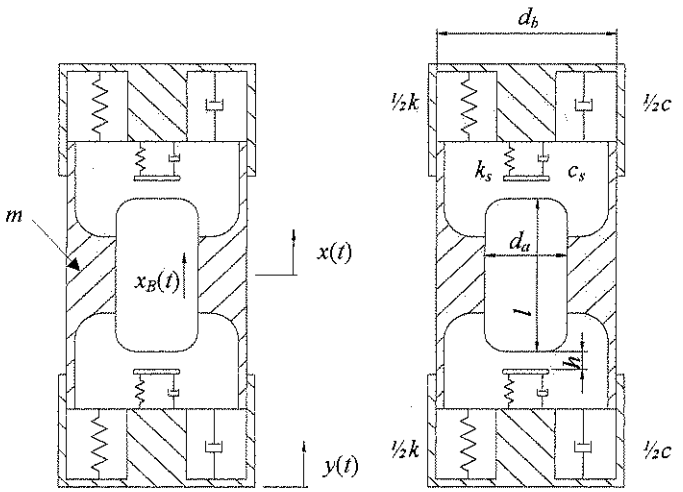

Figure 2.38: Mechanical model of a type II AVAI with slug stops

The spring force is [Equation (B.65)]:

$$f_s = \beta k_s \left\{ y - x + \frac{A_b}{A_a}(x - y) - \text{sign}\left[y - x + \frac{A_b}{A_a}(x - y) \right] h \right\} \tag{2.51}$$

The damping force is [Equation (B.66)]:

$$f_d = \beta c_s \left[\dot{y} - \dot{x} + \frac{A_b}{A_a}(\dot{x} - \dot{y}) \right] \tag{2.52}$$

The reservoir pressure that drives equalization of the fluid is [Equation (B.67)]:

$$p = \frac{1}{2A_a}(f_s + f_d - m_B \ddot{x}_B) \tag{2.53}$$

Equation (2.53) shows that the addition of stops will increase the pressure in the reservoir. Such a system is however non-linear, which makes its practical implementation problematic. The complete equation of motion is [Equation (B.69)]:

$$\ddot{x} = \left(\frac{\omega_n}{\omega_i}\right)^2 \ddot{y} - 2\zeta\omega_n(\dot{x} - \dot{y}) - \omega_n^2(x - y) - \omega_n^2 \frac{k_s}{k}\Delta_d \left(\frac{A_b}{A_a} - 1\right) - 2\zeta_s \omega_n \Delta_v \left(\frac{A_b}{A_a} - 1\right)$$

where: $\zeta = \dfrac{c}{2\left[m + m_B\left(\frac{A_b}{A_a} - 1\right)^2\right]\omega_n}$, $\zeta_s = \dfrac{c_s}{2\left[m + m_B\left(\frac{A_b}{A_a} - 1\right)^2\right]\omega_n}$

$$\omega_n = \sqrt{\frac{k}{m + m_B\left(\frac{A_b}{A_a} - 1\right)^2}}, \quad \omega_i = \sqrt{\frac{k}{m_B\left(\frac{A_b}{A_a} - 1\right)\frac{A_b}{A_a}}} \tag{2.54}$$

$$\Delta_d = \beta\left\{ y - x + \frac{A_b}{A_a}(x - y) - \text{sign}\left[y - x + \frac{A_b}{A_a}(x - y) \right] h \right\}$$

$$\Delta_v = \beta\left[\dot{y} - \dot{x} + \frac{A_b}{A_a}(\dot{x} - \dot{y}) \right]$$

Figure 2.39 shows the force and the relative motion. For this simulation the gap ratio was $h/Y = 10$ and the excitation amplitude (Y) equal to 1. As can be seen the force is zero when the relative motion is less than the gap length.

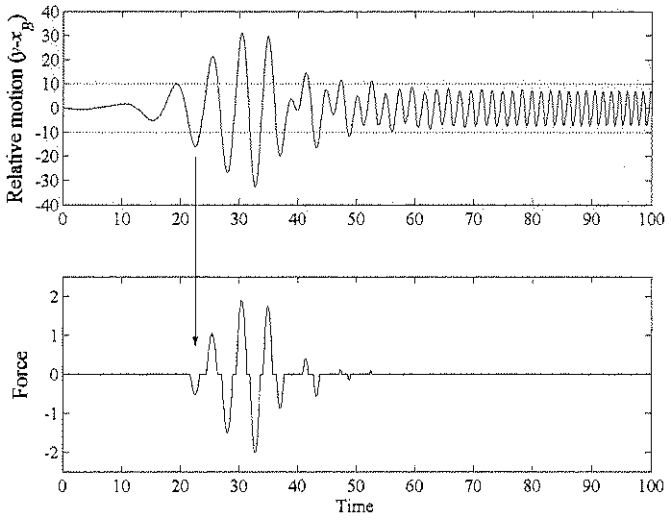

Figure 2.39: Stop force and relative motion of the slug and reservoir ($k_s/k = 0.01$, $h/Y = 10$, $Y = 1$, $\omega_n/\omega_i = 0.5$ and $\zeta = \zeta_s = 0$)

2.2.3 Leakage

The previous models assumed that a perfect seal exists between the slug and the port. The effect of leakage through this space will be considered next. It is assumed that the clearance is small in relation to the diameter of the slug.

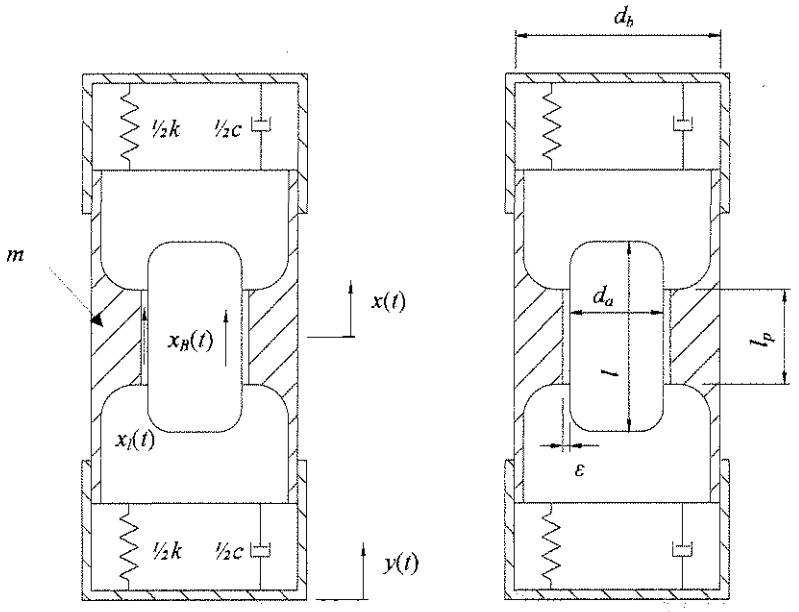

Figure 2.40: Mechanical model of a type II AVAI with leakage

If it is assumed that the gap between the port and the slug is small the leakage area is:

$$A_e = \varepsilon \pi d_a \tag{2.55}$$

where ε is the gap between the slug and the port.

The continuity equation is modified by the leak flow [Equation (B.71)]:

$$x_B = \frac{A_b}{A_a} y + \left(1 + \frac{\varepsilon \pi d_a - A_b}{A_a}\right) x - \frac{\varepsilon \pi d_a}{A_a} x_l \tag{2.56}$$

The kinetic energy now includes the mass of the leak flow [Equation (B.72)]:

$$T = \frac{1}{2}\left(m\dot{x}^2 + m_B \dot{x}_B^2 + m_l \dot{x}_l^2\right)$$
$$\text{where:} \quad m_B = \rho A_a l, \quad m_l = \rho_f \varepsilon \pi d_a l_p \tag{2.57}$$

m is the mass of the port, m_B the mass of the slug. m_l the mass of the fluid in the gap and is a function of the fluid density (ρ_f), area ($\varepsilon \pi d_a$) and the length of the port (l_p). $\dot{x}_l$ is the velocity of the liquid in the gap.

The mass of the leak flow is coupled to the slug and the port through damping created by the velocity dependent shear forces acting on these bodies. This is shown in Figure 2.41.

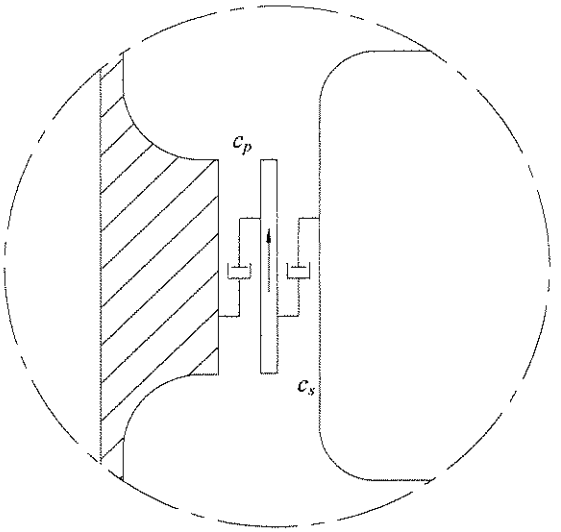

Figure 2.41: Fluid damping

The Rayleigh term is [Equation (B.76)]:

$$R = \frac{1}{2}\left[c\left(\dot{x} - \dot{y}\right)^2 + c_p\left(\dot{x}_l - \dot{x}\right)^2 + c_s\left(\dot{x}_B - \dot{x}_l\right)^2\right] \tag{2.58}$$

c_p is the damping resulting from the shear force between the fluid and the port and c_s the damping resulting from the shear force between the fluid and the slug.

The complete equation of motion is shown in Appendix B and leads to the definition of the following natural frequencies and damping ratios that will be used to non-dimensionalise the transmissibility:

$$\omega_l = \sqrt{\frac{k}{m_l + m_B\left(4\frac{\varepsilon}{d_a}\right)^2}},\quad \omega_i = \sqrt{\frac{k}{m_B\frac{A_b}{A_a}\left(\frac{A_b}{A_a} - 4\frac{\varepsilon}{d_a} - 1\right)}},\quad \omega_\varepsilon = \sqrt{\frac{k}{m_B\left(\frac{A_b}{A_a} - 4\frac{\varepsilon}{d_a} - 1\right)4\frac{\varepsilon}{d_a}}},$$

$$\omega_\varepsilon' = \sqrt{\frac{k}{m_B\frac{A_b}{A_a}4\frac{\varepsilon}{d_a}}},\quad \omega_n = \sqrt{\frac{k}{m + m_B\left(\frac{A_b}{A_a} - 4\frac{\varepsilon}{d_a} - 1\right)^2}},\quad \zeta_s = \frac{c_s}{2\left[m + m_B\left(\frac{A_b}{A_a} - 4\frac{\varepsilon}{d_a} - 1\right)^2\right]\omega_n},\qquad (2.59)$$

$$\zeta_p = \frac{c_p}{2\left[m + m_B\left(\frac{A_b}{A_a} - 4\frac{\varepsilon}{d_a} - 1\right)^2\right]\omega_n}$$

The transmissibility is given by [Equation (B.83)]:

$$\frac{X}{Y} = \frac{AB - CD}{EF - G^2},\qquad \text{where:}$$

$$\frac{A}{k} = i2\frac{\omega}{\omega_n}\left[\zeta_s\left(4\frac{\varepsilon}{d_a} + 1\right)^2 + \zeta_p\right] - \left(\frac{\omega_n}{\omega_l}\right)^2\left(\frac{\omega}{\omega_n}\right)^2$$

$$\frac{B}{k} = 1 + i2\frac{\omega}{\omega_n}\left[\zeta + \zeta_s\frac{A_b}{A_a}\left(\frac{A_b}{A_a} - 4\frac{\varepsilon}{d_a} - 1\right)\right] - \left(\frac{\omega_n}{\omega_i'}\right)^2\left(\frac{\omega}{\omega_n}\right)^2$$

$$\frac{C}{k} = i2\frac{\omega}{\omega_n}\left[\zeta_s\left(\frac{A_b}{A_a} - 4\frac{\varepsilon}{d_a} - 1\right)\left(4\frac{\varepsilon}{d_a} + 1\right) - \zeta_p\right] - \left(\frac{\omega_n}{\omega_\varepsilon}\right)^2\left(\frac{\omega}{\omega_n}\right)^2$$

$$\frac{D}{k} = i2\frac{\omega}{\omega_n}\zeta_s\frac{A_b}{A_a}\left(4\frac{\varepsilon}{d_a} + 1\right) - \left(\frac{\omega_n}{\omega_\varepsilon'}\right)^2\left(\frac{\omega}{\omega_n}\right)^2$$

$$\frac{E}{k} = 1 + i2\frac{\omega}{\omega_n}\left[\zeta + \zeta_p + \zeta_s\left(\frac{A_b}{A_a} - 4\frac{\varepsilon}{d_a} - 1\right)^2\right] - \left(\frac{\omega}{\omega_n}\right)^2$$

$$\frac{F}{k} = i2\frac{\omega}{\omega_n}\left[\zeta_s\left(4\frac{\varepsilon}{d_a} + 1\right)^2 + \zeta_p\right] - \left(\frac{\omega_n}{\omega_l}\right)^2\left(\frac{\omega}{\omega_n}\right)^2$$

$$\frac{G}{k} = i2\frac{\omega}{\omega_n}\left[\zeta_s\left(\frac{A_b}{A_a} - 4\frac{\varepsilon}{d_a} - 1\right)\left(4\frac{\varepsilon}{d_a} + 1\right) - \zeta_p\right] - \left(\frac{\omega_n}{\omega_\varepsilon}\right)^2\left(\frac{\omega}{\omega_n}\right)^2$$

$$\frac{\omega_n}{\omega_l} = \frac{\frac{m_l}{m_B} + \left(4\frac{\varepsilon}{d_a}\right)^2}{\frac{m}{m_B} + \left(\frac{A_b}{A_a} - 4\frac{\varepsilon}{d_a} - 1\right)^2},\quad \frac{\omega_n}{\omega_i'} = \frac{\frac{A_b}{A_a}\left(\frac{A_b}{A_a} - 4\frac{\varepsilon}{d_a} - 1\right)}{\frac{m}{m_B} + \left(\frac{A_b}{A_a} - 4\frac{\varepsilon}{d_a} - 1\right)^2},\qquad (2.60)$$

$$\frac{\omega_n}{\omega_\varepsilon} = \frac{4\frac{\varepsilon}{d_a}\left(\frac{A_b}{A_a} - 4\frac{\varepsilon}{d_a} - 1\right)}{\frac{m}{m_B} + \left(\frac{A_b}{A_a} - 4\frac{\varepsilon}{d_a} - 1\right)^2},\quad \frac{\omega_n}{\omega_\varepsilon'} = \frac{4\frac{\varepsilon}{d_a}\frac{A_b}{A_a}}{\frac{m}{m_B} + \left(\frac{A_b}{A_a} - 4\frac{\varepsilon}{d_a} - 1\right)^2}$$

When studying the effect of the gap on the transmissibility it is important to keep in mind that the mass ratio (m_l/m_B) is also a function of the gap size:

$$\frac{m_l}{m_B} = 4\beta\frac{\varepsilon}{d_a} \qquad \text{where:} \quad \beta = \frac{\rho_f l_p}{\rho l} \tag{2.61}$$

The main objective in using a slug was to exploit the large density of a heavy metal. It can therefore safely be assumed that the density of the fluid will be less than that of the slug. Since the slug is longer than the port, β will always be much less than 1. As the gap increases more of the effort will go towards accelerating the fluid, which has less mass, thereby increasing the isolation frequency. This can clearly be seen in Figure 2.42.

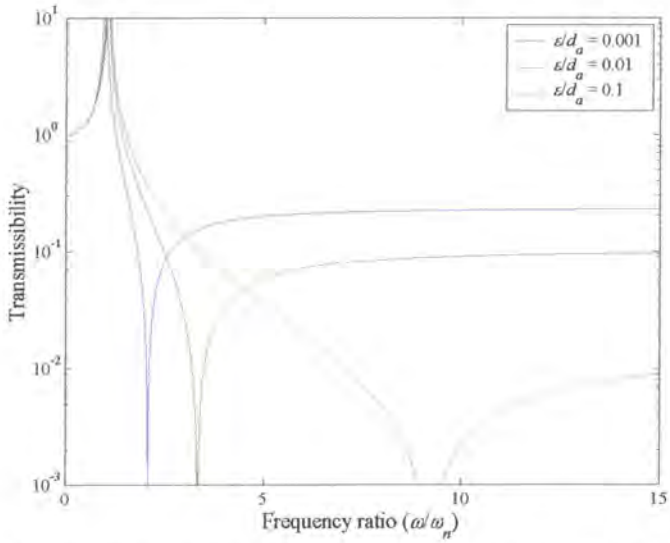

Figure 2.42: Transmissibility for various gap ratios ($\zeta = \zeta_s = \zeta_p = 0$, $m/m_B = 100$, $\beta = 0.01$ and $A_p/A_a = 10$)

Once damping is introduced the situation is very different, as shown in Figure 2.43. The leak flow mass is now coupled to the motion of the slug, equalising the acceleration of the two bodies.

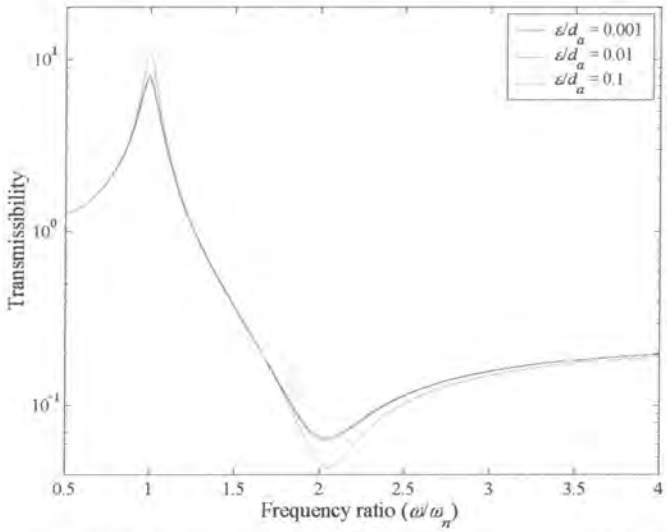

Figure 2.43: Transmissibility for various gap ratios ($\zeta = 0$, $\zeta_s = \zeta_p = 0.001$, $m/m_B = 100$, $\beta = 0.01$ and $A_b/A_a = 10$)

2.2.4 Slug with diaphragm seal

Rolling diaphragm seals are fabric-reinforced rubber seals that allow large axial movement with little damping and stiffness. Such a seal will not allow any leakage therefore ensuring that the slug stays centred with respect to the port. One disadvantage is that the device will become solid during over travel.

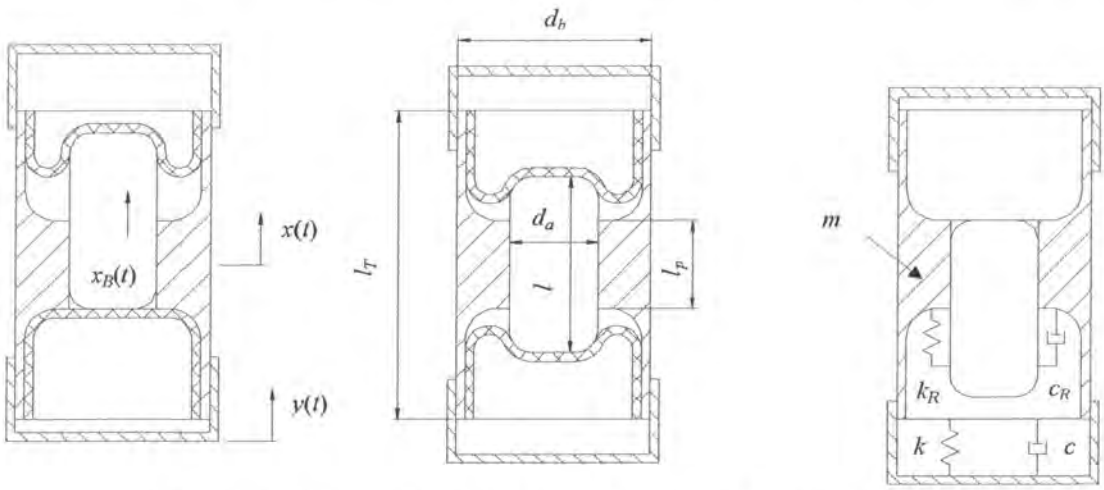

Figure 2.44: Mechanical model of a type II AVAI with a rolling diaphragm seal

By noting that a reinforced diaphragm cannot stretch, the continuity equation can be written as [Equation (B.85)]:

$$\begin{aligned} yA_b &= x_B A_a + \frac{1}{2}(x_B + x)(A_b - A_a) \\ x_B &= -\left(\frac{A_b - A_a}{A_b + A_a}\right)x + \frac{2A_b}{A_b + A_a}y \end{aligned} \tag{2.62}$$

The effect on the transmissibility is that the effective absorber mass is reduced (the diaphragm mass is neglected). In terms of a device without a diaphragm the effective absorber mass ratio is [Equation (B.96)]:

$$M_{ratio} = \frac{4}{\left(\frac{A_b}{A_a} + 1\right)^2} \tag{2.63}$$

The effective mass is therefore reduced for any area ratio larger than 1. Using a diaphragm will therefore increase the overall size of the device. Other practical problems exist such as commercial availability of suitable large-displacement small-diameter diaphragms.

An alternative to a rolling diaphragm is to insert a diaphragm that can stretch, for instance one made of thin latex rubber. In such a case the effective absorber mass will not be affected. There will, however, be relative motion between the latex and the slug, which will lead to damping. In addition, the number of cycles that such a latex diaphragm can be subjected to should be investigated.

2.3 Conclusion

This chapter showed the properties of two novel adaptive AVAI concepts. The type I AVAI used flexible reservoir walls to adapt the isolation frequency of the device. Conceptual design methodologies were illustrated for both damped and undamped fixed and adaptive isolation frequency devices. To determine the effects of tuning, the equations were transformed in terms of constant frequency ratios and the stiffness ratio, which was the only tuning parameter considered. For a fixed frequency device the system of equations is underdetermined and some parameters have to be prescribed or additional constraints should be introduced in the design. For adaptive devices it was shown that specific choice of the area and mass ratios can influence the tuning range. For damped adaptive AVAIs the transmissibility at the isolation frequency was minimised when the area ratio was minimised and the mass ratio maximised.

The type II AVAI used a metal slug to increase the absorber mass without the use of toxic heavy liquids. For this AVAI the main spring stiffness was made adaptive. The design methodology is different from the type I because the travel of the slug is restricted and must enter the design process to ensure that realistic area ratios are chosen. Three additional models were analysed. The first investigated the effect of rubber stops instead of slug springs. The second took account of leakage between the port and the slug. The effect of leakage was to increase the isolation frequency. The third showed the effect of using rolling diaphragm seals to eliminate leakage. The rolling diaphragm seal will result in a larger device since the effective mass is reduced.

3 Adaptive control methods

Several methods for the control of adaptive vibration absorbers have been studied. Most researchers suggested the use of open-loop rough tuning followed by a fine-tuning algorithm (Long *et al.*, 1994 and Franchek, 1995). Other methods that have been suggested include neural network and fuzzy logic control (Sun *et al.*, 1995). In this chapter several variations of the first method's application to the type I and type II AVAI will be discussed. An optimisation approach will be used, in contrast to the above work which used constant step size algorithms. The choice of variation on this method will depend on the characteristics of the input and the AVAI as will be shown. The scenarios investigated are:

1. The machine operates at a constant but unknown excitation frequency for an indefinite period after it is switched on. In such a case the AVAI will be tuned to this frequency at start-up only. An example is a pneumatic drill where the excitation frequency is a function of the supply air pressure and the drill is used at different locations with varying supply pressure.
2. The machine operates with a constant but unknown frequency for a period after which a near instantaneous change in frequency occurs to a new and unknown frequency. An example is if the operational frequency is a function of load in a batch process.
3. The properties of the AVAI changes with time, for instance, as the rubber spring heats up due to hysteresis. As the properties change, the isolation frequency is adapted to compensate. Similar conclusions are reached when the excitation frequency varies slowly with time.
4. A general case that does not require the above assumptions.

The control method that will be investigated is a physical implementation of optimisation where the objective function is the transmissibility (which is calculated from simulated or measured accelerometer data) and the variables are physical properties of the AVAI that can be adapted to minimise the objective function. The available variables can be classified as tuning and damping variables. Tuning variables are those that change the isolation frequency. For tonal excitation the isolator should have the lowest possible damping and therefore tuning only will be considered. In cases where wide-band excitation is present together with prominent tonal excitation, the addition of damping can be considered. In such cases it might even be beneficial to use the damping as a variable in the optimisation process. In this chapter it will be assumed that the excitation is tonal and that the amplitude is not necessarily constant.

3.1 Type I AVAI

If the excitation frequency is tonal and the stiffness is the only variable, the objective function can be written as the transmissibility given by Equation (2.19) with the stiffness ratio the only variable:

$$f(\mu_k)=\left|\frac{\left(1+i2\frac{\omega_e}{\omega_1}\zeta_1\right)\left[1+i\frac{2}{\mu_k}\frac{\omega_1}{\bar{\omega}_2}\frac{\omega_e}{\omega_1}\bar{\zeta}_2-\frac{1}{\mu_k}\left(\frac{\omega_1}{\bar{\omega}_2}\right)^2\left(\frac{\omega_e}{\omega_1}\right)^2\right]-\left(1+i\frac{2}{\mu_k}\frac{\omega_1}{\bar{\omega}_2}\frac{\omega_e}{\omega_1}\bar{\zeta}_2\right)\left(\frac{\omega_1}{\bar{\omega}_i}\right)^2\left(\frac{\omega_e}{\omega_1}\right)^2}{\left[1+\mu_k+i2\frac{\omega_e}{\omega_1}\left(\zeta_1+\frac{\omega_1}{\bar{\omega}_2}\bar{\zeta}_2\right)-\left(\frac{\omega_e}{\omega_1}\right)^2\right]\left[1+i\frac{2}{\mu_k}\frac{\omega_1}{\bar{\omega}_2}\frac{\omega_e}{\omega_1}\bar{\zeta}_2-\frac{1}{\mu_k}\left(\frac{\omega_1}{\bar{\omega}_2}\right)^2\left(\frac{\omega_e}{\omega_1}\right)^2\right]-\mu_k\left(1+i\frac{2}{\mu_k}\frac{\omega_1}{\bar{\omega}_2}\frac{\omega_e}{\omega_1}\bar{\zeta}_2\right)^2}\right| \tag{3.1}$$

where ω_e is the excitation frequency. A plot of the objective function as a function of stiffness ratio is shown in Figure 3.1. From the figure it can be seen that a low initial value will not allow convergence to the global minimum. This condition is caused by the second frequency of maximum transmissibility being lower than the excitation frequency as shown in Figure 3.2 where the transmissibilities for three different initial values are shown. Clearly, an initial condition of 0.2 will not allow for convergence to the minimum value if a local minimisation algorithm is used.

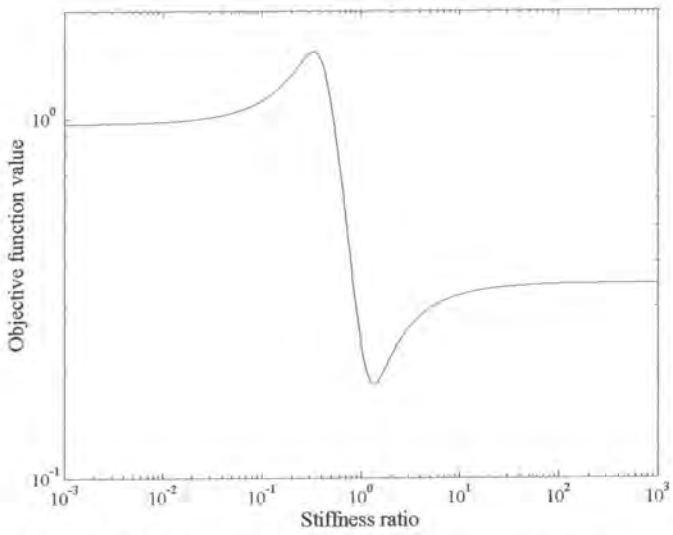

Figure 3.1: Objective function *vs.* stiffness ratio $\omega_e/\omega_1 = 1.4$ ($A_b/A_a = 10$, $m_B/m_y = 0.003$, $\zeta_1 = 0.1$ and $\overline{\zeta}_2 = 0.1$)

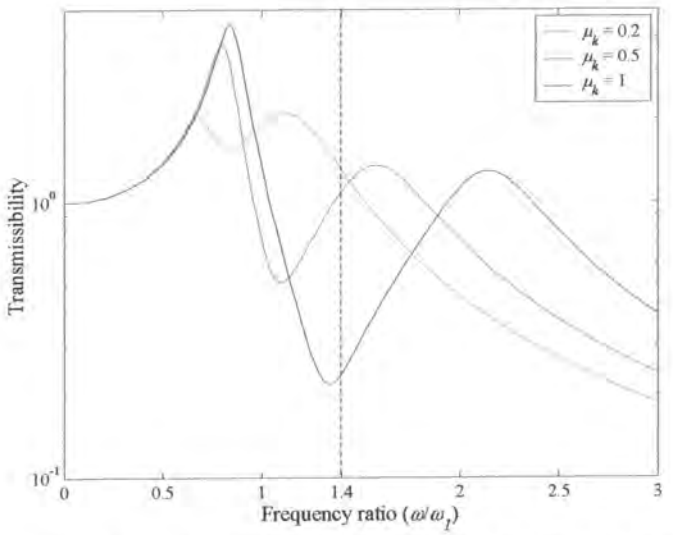

Figure 3.2: Transmissibility *vs.* frequency ratio for three initial values ($A_b/A_a = 10$, $m_B/m_y = 0.003$, $\zeta_1 = 0.1$ and $\overline{\zeta}_2 = 0.1$)

There are a number of solutions to this problem. A global optimisation strategy can be used, but this might be unacceptable in situations where the isolator cannot be allowed to operate close to regions of high transmissibility. Examples of global optimisation strategies are multiple start local optimisations or a genetic algorithm.

If the initial value can be guaranteed to be between the peaks of maximum transmissibility, the search direction of a gradient-based method will always be in the direction of the minimum. The following line search can therefore only find the optimal solution. It is possible that an unconstrained line search method may step too far, in which case the step size must be limited. To ensure that the initial value is between the frequencies of maximum transmissibility, the AVAI can simply be tuned to the maximum stiffness when initialised. The only risk with such a strategy is that it will put the excitation frequency near the first frequency of maximum transmissibility. If properly designed, the transmissibility should still be less than 1 even if tuned to the maximum isolation frequency. This can be seen from Figure 3.1 where for large stiffness ratios (and large isolation frequencies) the transmissibility is less than 1. It is also possible to initialise the optimisation algorithm by using the isolation frequency and stiffness ratio relationship found during a characterisation test. If changes in the physical properties of the device occur over time this relationship will not be exact anymore, but it should put the initial value close to the optimum as well as between the peaks of maximum transmissibility. It also requires that the excitation frequency be measured before initialisation.

It is possible to formulate a constrained optimisation problem to remove the risk posed by the local minimum. The necessary constraint is a lower bound on the stiffness ratio ($\hat{\mu}_k$) and can be calculated from [Equation (2.14)]:

$$\left(\frac{\Omega_2}{\omega_1}\right)^2 \frac{2}{\hat{\mu}_k}\left(\frac{\omega_1}{\bar{\omega}_2}\right)^2 - \frac{1+\hat{\mu}_k}{\hat{\mu}_k}\left(\frac{\omega_1}{\bar{\omega}_2}\right)^2 - 1 - \sqrt{\left[\frac{1+\hat{\mu}_k}{\hat{\mu}_k}\left(\frac{\omega_1}{\bar{\omega}_2}\right)^2 + 1\right]^2 - \frac{4}{\hat{\mu}_k}\left(\frac{\omega_1}{\bar{\omega}_2}\right)^2} = 0 \tag{3.2}$$

where Ω_2 is equal to the excitation frequency ω_e. In practice the above value will be found from a characterisation test and will therefore include the effect of damping. Once the problem has been set for a specific excitation frequency, continuous monitoring is necessary to ensure that the excitation frequency does not change. If the excitation frequency does change, it is necessary to recast the optimisation problem with a new lower bound. Only large changes in excitation frequency will require the process to be restarted, during which time the optimisation algorithm will maintain optimal tuning even if isolator physical properties changed slightly.

It is possible to simulate the control systems suggested above by solving the equation of motion and calculating the objective function from the simulated response. The process is explained in Figure 3.3. The optimisation algorithm calls the objective function. The objective function calculates the transmissibility by solving the equation of motion. The optimisation algorithm now estimates a new stiffness value and recalculates the objective function. During the second and subsequent objective function calls, the Runga-Kutta algorithm is restarted with the final value from the previous simulation as the initial value. This implies that the process of calculating the new stiffness ratio and changing the current stiffness ratio to the new stiffness ratio requires zero time. Although this is physically impossible, the purpose of the simulation is to study the performance of the optimisation algorithm and not the effect of delay and is therefore valid. The effect of delay will be to degrade performance and this simulation therefore represents the best case.

The set of equations that needs to be solved are [Equations (C.1) and (C.2)]:

$$\begin{aligned}\ddot{y}+2\left(\zeta_1+\frac{\omega_1}{\bar{\omega}_2}\bar{\zeta}_2\right)\omega_1\dot{y}-2\frac{\omega_1}{\bar{\omega}_2}\bar{\zeta}_2\omega_1\dot{u}+\omega_1^2\left(1+\mu_k\right)y-\omega_1^2\mu_k u-2\zeta_1\omega_1\dot{x}-\omega_1^2 x=0\\ \ddot{u}+2\bar{\zeta}_2\bar{\omega}_2\left(\dot{u}-\dot{y}\right)+\mu_k\bar{\omega}_2^2\left(u-y\right)-\left(\frac{\bar{\omega}_2}{\omega_1}\right)^2\ddot{x}=0\end{aligned} \tag{3.3}$$

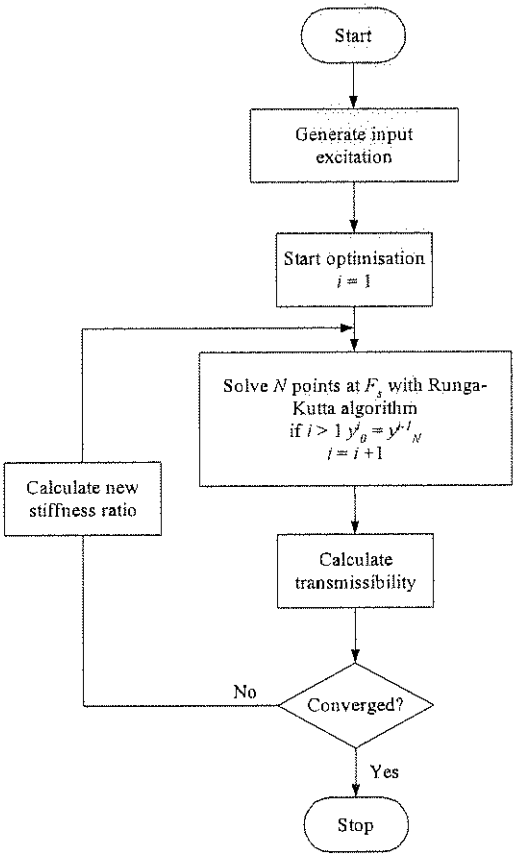

Figure 3.3: Control flow diagram

The properties of the system that was simulated are $\omega_1 = 1$, $A_b/A_a = 10$ and $m_B/m_y = 0.003$. This is the same system as was used in the previous chapter and only serves to illustrate the method. The solution was found with $F_s = 5$ Hz and the transmissibility was estimated using the H_1 estimator. H_1 evaluated at the excitation frequency is (Ewins, 2000):

$$H_1(\omega_e)=\frac{S_{xy}(\omega_e)}{S_{yy}(\omega_e)} \tag{3.4}$$

In a practical system it will be easier to use the ratio of rms output to input as an estimate of the transmissibility. The rms and maximum values calculations are, however, a function of frequency content and the number of data points used. At steady state the signals should only contain the excitation frequency, but due to impulsive excitation when the stiffness ratio is changed the two natural frequencies will also be excited. This has a larger effect on the maximum values calculation than the rms since the rms calculation averages the error. One possible solution is to use a band-pass

filter. Figure 3.4 shows four transmissibility estimates, a simple division of maximum values, a filtered and unfiltered rms and the H_1 estimate. Since the H_1 estimate is calculated at the excitation frequency only, it is considered to be the most accurate. The band-pass filtered rms can approach the H_1 estimate and might be easier to implement in practice.

Figure 3.5 shows that a minimum number of data points will be needed for an accurate estimate using the unfiltered rms method. The number of data points required will depend on the time taken to reach steady state conditions and therefore the damping present in the system.

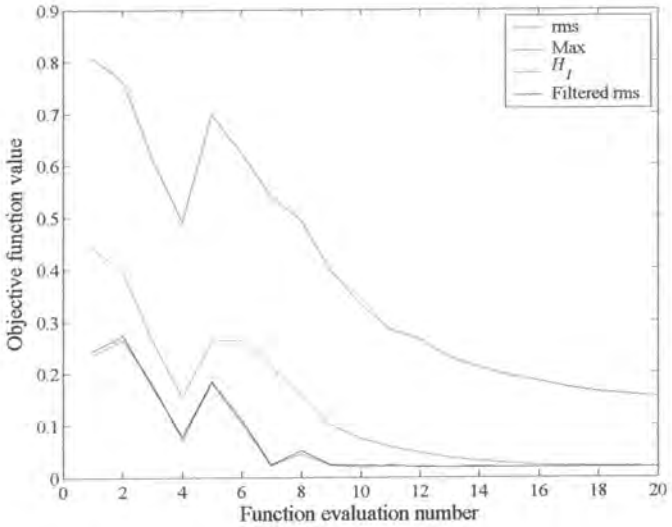

Figure 3.4 Comparison of objective function estimates at low damping ($N = 200$, $\omega_1 = 1$, $A_b/A_a = 10$, $m_B/m_y = 0.003$, $\zeta_1 = 0.01$ and $\overline{\zeta}_2 = 0.01$)

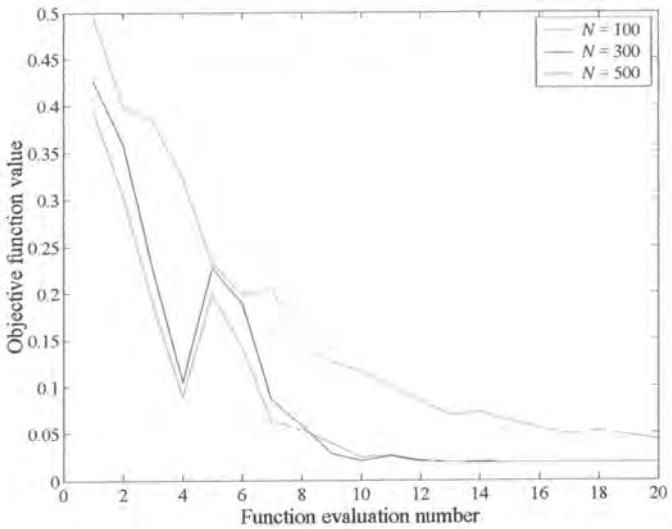

Figure 3.5 Comparison of objective function estimates at low damping for a different number of data points used for the rms transmissibility estimate ($\omega_1 = 1$, $A_b/A_a = 10$, $m_B/m_y = 0.003$, $\zeta_1 = 0.01$ and $\overline{\zeta}_2 = 0.01$)

Another way to formulate the objective function has been described by Long *et al.* (1994). When the angle between the input and output is -90°, the system is close to the minimum transmissibility as

shown in Figure 3.6. At high damping ratios there will be a difference between the optimal value using this method and the actual minimum transmissibility achievable, as indicated in the figure.

The objective function, formulated as the square of the difference between the actual phase angle and the required phase angle (-90°), is shown in Figure 3.7. The device needs to be tuned to the second minimum. Starting at a large stiffness ratio and limiting the step size will ensure that this minimum is reached.

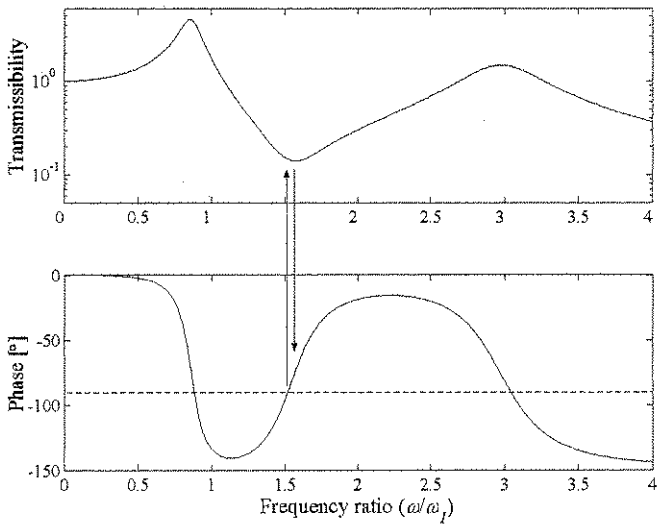

Figure 3.6: Transmissibility and phase angle indicating the difference in tuning frequency ($\omega_1 = 1$, $A_b/A_a = 10$, $m_B/m_y = 0.003$, $\zeta_1 = 0.1$, $\zeta_2 = 0.1$ and $\mu_k = 2$)

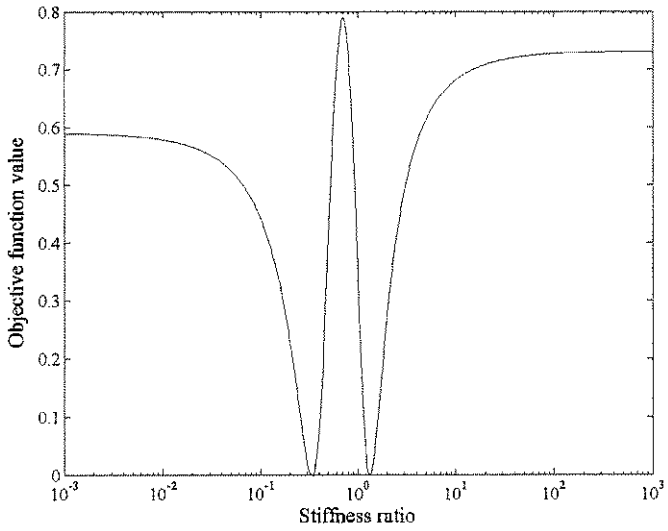

Figure 3.7: Quadrature objective function ($\omega_e = 1.4$, $A_b/A_a = 10$, $m_B/m_y = 0.003$, $\zeta_1 = 0.1$ and $\zeta_2 = 0.1$)

One major advantage of this method is the ease of implementation. The objective function can be formulated by integrating the input and response of the AVAI over a period of time T:

$$f = \frac{1}{T}\int_0^T x(t)\,y(t)\,dt \tag{3.5}$$

3.1.1 Tuning at start-up

A simulation of constant frequency excitation using the Matlab's constrained minimisation algorithm `fmincon.m` is shown in Figure 3.8. The excitation frequency ratio is constant at $\omega_e/\omega_1 = 1.4$. The objective function for this excitation frequency ratio was plotted in Figure 3.1. The simulation shows that an initial value of 0.2 will converge to the local minimum of $\mu_k^* = 0$. When a large initial value is specified, the global optimal value ($\mu_k^* = 1.34$) is approached within a couple of iterations. The results for the various initial values are shown in Table 3.1.

Table 3.1: Results of `fmincon.m` at constant excitation frequency ratio $\omega_e/\omega_1 = 1.4$

Initial value (μ_k^0)	Optimal value (μ_k^*)	$f(\mu_k^*)$
0.2	0.10	1.1088
1.0	1.36	0.1810
5.0	1.32	0.1806

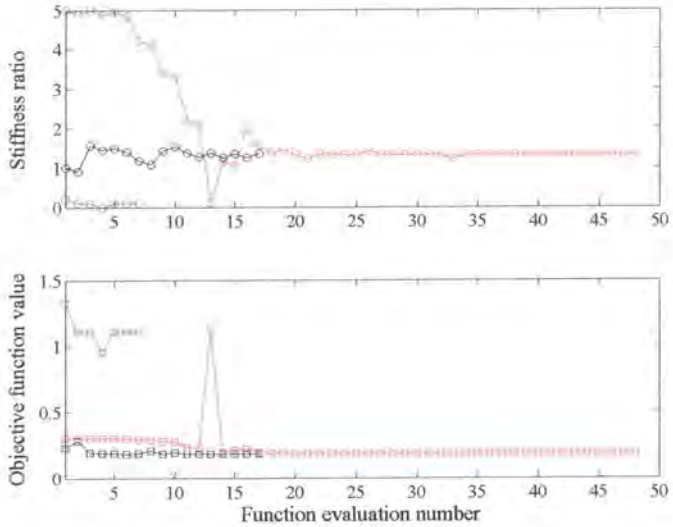

Figure 3.8: Convergence history of `fmincon.m` at constant frequency ratio $\omega_e/\omega_1 = 1.4$, and three initial conditions $\mu_k^0 = 0.2$, 1 and 5 ($\omega_1 = 1$, $A_b/A_a = 10$, $m_B/m_y = 0.003$, $\zeta_1 = 0.1$ and $\zeta_2 = 0.1$)

Recognising that the optimisation problem consists of one variable only, a simple method to use is a unimodal search technique. The search technique involves the efficient minimisation of the interval within which the solution is assumed to fall. If the AVAI is properly designed, the minimum must be in the interval given by the minimum and maximum stiffness ratios. Several methods exist of which the Fibonacci method could be shown to be optimal, but the simpler near-optimal golden section method is often preferred when implemented in optimisation algorithms. The convergence of the `fminbnd.m` algorithm in Matlab is shown in Figure 3.9. The algorithm is based on the golden section method and quadratic interpolation. The algorithm calculates the new stiffness ratio by successive operations that reduce the stiffness ratio interval until a preset convergence tolerance is reached. It can be inefficient when the solution is near one of the bounds and will only give local solutions. This method is easily implemented since the bounds of the stiffness ratio are known.

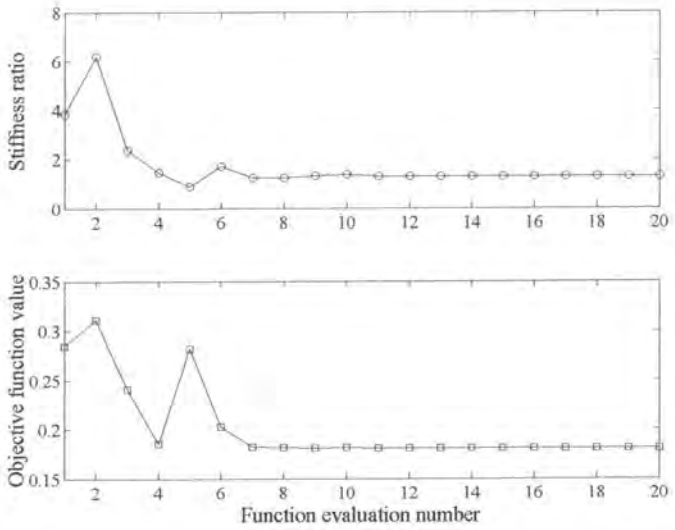

Figure 3.9: Convergence history of `fminbnd.m` at constant frequency ratio $\omega_e/\omega_1 = 1.4$ with bounds 0 and 10 ($\omega_1 = 1$, $A_b/A_a = 10$, $m_B/m_y = 0.003$, $\zeta_1 = 0.1$ and $\bar{\zeta}_2 = 0.1$)

To find the global minimum a genetic algorithm can be used. The result of the freely available algorithm `devec3.m` of Storn (1996) is shown in Figure 3.10.

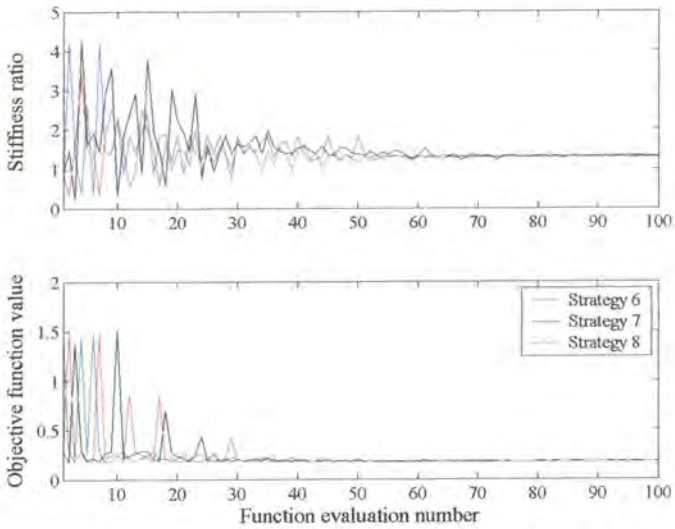

Figure 3.10: Convergence history of `devec3.m` at constant frequency ratio $\omega_e/\omega_1 = 1.4$ ($\omega_1 = 1$, $A_b/A_a = 10$, $m_B/m_y = 0.003$, $\zeta_1 = 0.1$ and $\bar{\zeta}_2 = 0.1$)

The algorithm is based an evolutionary process where the next generation is selected with bias towards the fittest choice of stiffness ratio. The strategies included crossover, which attempts to create a better solution from two previous solutions using parts of each. It differs from the previous technique in that it is suitable for problems with multiple local minima. The algorithm implements nine strategies of which the best three are shown. Some did not converge after 200 iterations. Although the algorithm was able to find the global optimum value, it did so after almost ten times more function evaluations than the previous method. Additionally, the transmissibility was larger than 1 during the optimisation

process. If this cannot be tolerated by the mechanical system under consideration, this method will not be acceptable. The methods discussed previously will ensure that such a condition cannot occur and are therefore safer to use.

3.1.2 Sudden excitation frequency change

If a step change in frequency occurs the algorithm must adapt the stiffness to the new optimal value for that excitation frequency. Since optimisation algorithms are not designed to handle changes in the objective function during optimisation, the standard Matlab routines did not exhibit the desired behaviour. A gradient-based algorithm that does not use explicit line searches was successfully used for this case. Details of the lfopc algorithm can be found in Snyman (1982). The algorithm handles constraints with a penalty function approach.

The gradient is determined using forward-difference (Nocedal & Wright, 1999):

$$\frac{\partial f}{\partial x_i} \approx \frac{f(x+\varepsilon e_i) - f(x)}{\varepsilon} \tag{3.6}$$

where e_i is the i^{th} unit vector and ε is chosen to be a small value. An additional advantage of this algorithm is that the step size can be controlled. This makes it easy to limit the risk that a too low stiffness ratio will be calculated during the optimisation process. A typical result is shown in Figure 3.11 and Table 3.2.

Table 3.2: Results of lfopc at constant excitation frequency ratio

Excitation frequency ratio (ω_e/ω_1)	Optimal value (μ_k^*)	μ_k after 7000 s of excitation at ω_e/ω_1
1.2	0.7710	0.7571
1.4	1.3414	1.3004

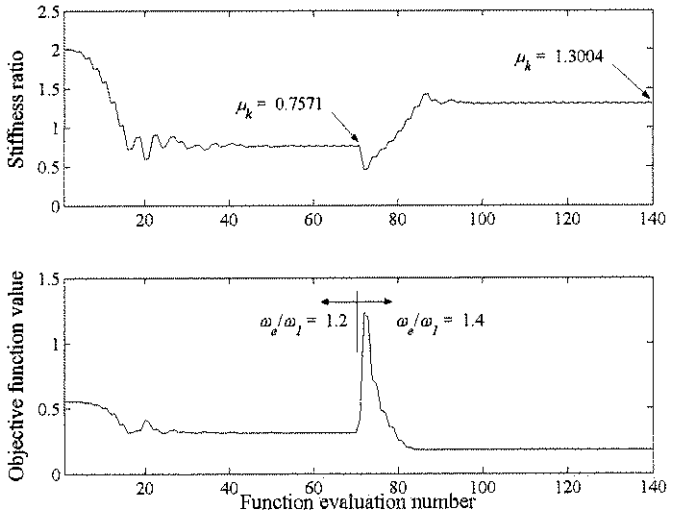

Figure 3.11: Convergence history of lfopc with a frequency step from $\omega_e/\omega_1 = 1.2$ to $\omega_e/\omega_1 = 1.4$ at 7000 s ($\omega_1 = 1$, $A_b/A_a = 10$, $m_D/m_y = 0.003$, $\zeta_1 = 0.1$ and $\bar{\zeta}_2 = 0.1$)

At 7000 seconds the excitation frequency ratio was changed from 1.2 to 1.4. The algorithm adapted the stiffness ratio to the optimum of the new excitation frequency within a couple of function evaluations. The step size was limited to 0.3 while the other parameters were left at their default. The time history is shown in Figure 3.12.

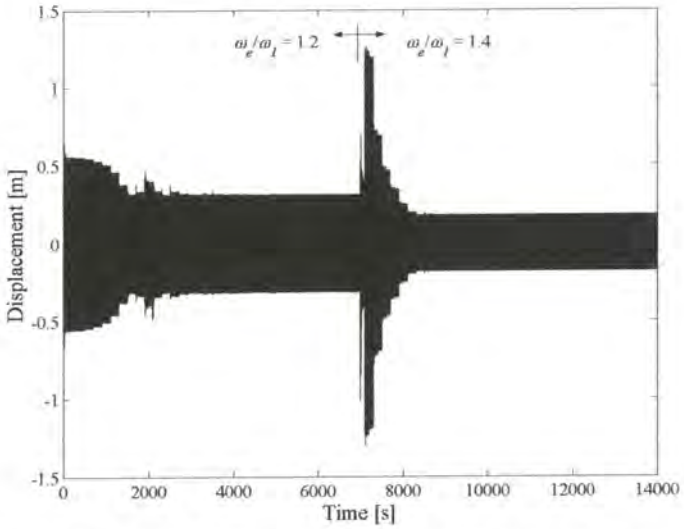

Figure 3.12: Time history of the isolated system displacement for Ifopc with a frequency step from ω_e/ω_1 = 1.2 to 1.4 at 7000 s ($\omega_1 = 1$, $A_b/A_a = 10$, $m_B/m_y = 0.003$, $\zeta_1 = 0.1$ and $\bar{\zeta}_2 = 0.1$)

3.1.3 Slow change in excitation frequency or AVAI properties

When a slow change in excitation frequency occurs the optimisation method will not always have the desired result since optimisation requires that the objective function should only be a function of the variables being optimised. If the optimisation algorithm is not restarted the calculated gradients will be incorrect. Two results are shown in Figure 3.13.

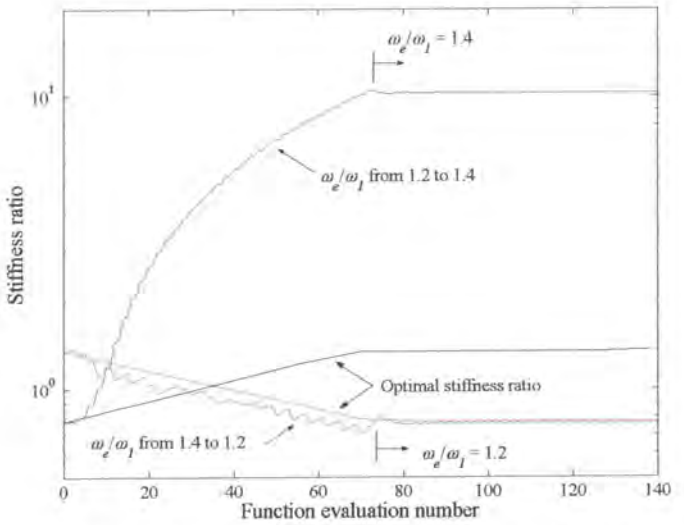

Figure 3.13: The tuning result for a slow change in excitation frequency ($\omega_1 = 1$, $A_b/A_a = 10$, $m_B/m_y = 0.003$, $\zeta_1 = 0.1$ and $\bar{\zeta}_2 = 0.1$)

For a case where the excitation frequency ratio varied from 1.4 to 1.2 over 7000 seconds, the tuning result seems reasonable. For a case where the excitation frequency ratio varied from 1.2 to 1.4, the stiffness ratio calculated was incorrect. For a case where a slow change in frequency is expected, open-loop tuning must be implemented as will be discussed in §3.1.4.

Figure 3.14 shows the effect of a changing system parameter on the convergence history. The primary system natural frequency was changed from 1 to 1.2 during the first 6000 seconds, after which it was kept constant. The algorithm was able to follow the optimal stiffness ratio even with incorrect gradient information. If the change were in the opposite direction the convergence would not have been to the correct value as was the case for a slow change in excitation frequency.

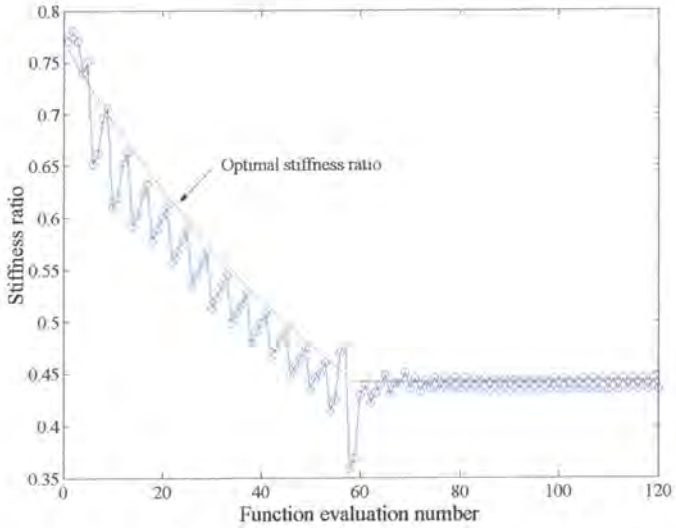

Figure 3.14: Convergence history of lfopc with ω_1 changing from 1 to 1.2 from function evaluation 1 to 60 ($\omega_e = 1.2$, $A_b/A_a = 10$, $m_B/m_y = 0.003$, $\zeta_1 = 0.1$ and $\bar{\zeta}_2 = 0.1$)

3.1.4 General tuning method

Although it has been shown that for certain conditions a restart of the optimisation algorithm after a change in excitation frequency is not necessary, it is the safest option since it will ensure that the optimisation algorithm starts near the optimal point. If the frequency varies slowly or frequently this method will not be efficient. In such a case open-loop rough tuning followed by a fine-tuning algorithm should be used. The rough tuning can be done using either a look-up table or a curve fit of the stiffness ratio (μ_k) *vs.* isolation frequency (ω_i). The rough tuning only needs to set the stiffness ratio near the optimal value as shown in Figure 3.15. If the initial value is close to the optimal value after the change in excitation frequency occurred, convergence could be achieved after only a few objective function evaluations.

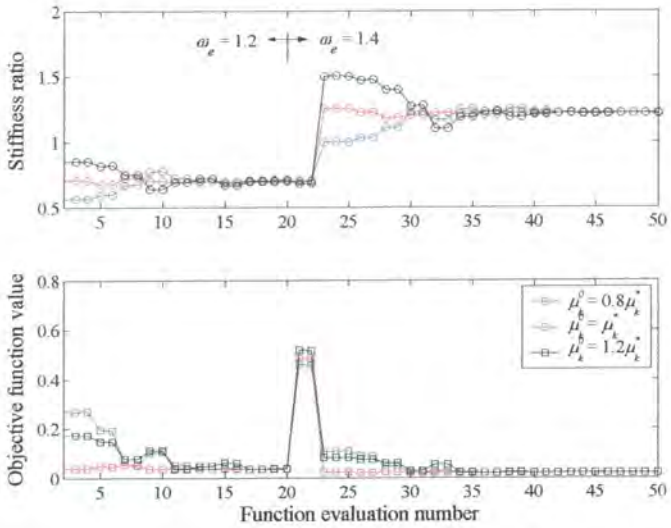

Figure 3.15: Convergence history of lfopc with a frequency step from $\omega_e/\omega_1 = 1.2$ to $\omega_e/\omega_1 = 1.4$ at 2000 s ($\omega_1 = 1$, $A_b/A_a = 10$, $m_B/m_y = 0.003$, $\zeta_1 = 0.1$ and $\bar{\zeta}_2 = 0.1$)

The system can be made more robust by continuous updating of the look-up table using the results of each optimisation process. The flow diagram for such a process is shown in Figure 3.16.

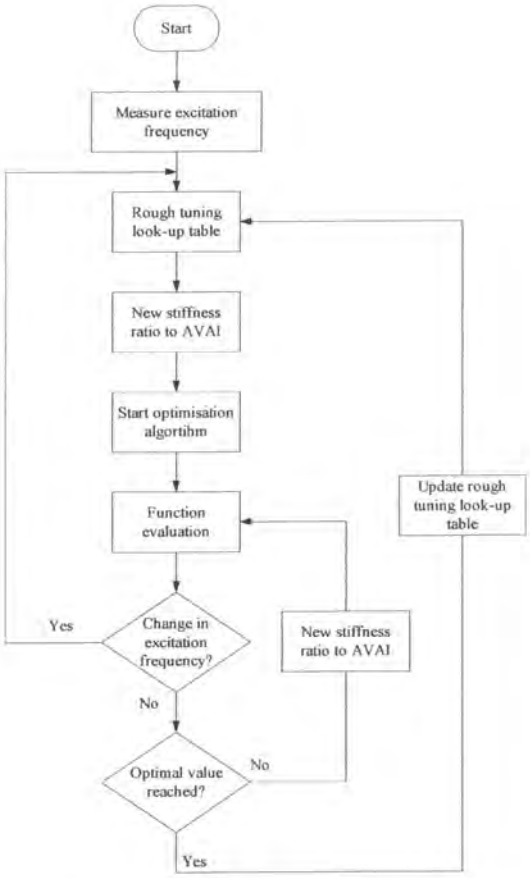

Figure 3.16: General tuning method

During optimisation the excitation frequency must be monitored continuously to make sure than an erroneous value is not entered in the look-up table. The frequency change must be evaluated with a certain tolerance to account for small changes in the excitation frequency and small errors in the estimation process. The maximum error that can be allowed is a function of the bandwidth and the rate of change in frequency.

3.2 Type II AVAI

The control for the type II AVAI is in most respects exactly the same as for the type I. This chapter will not repeat the discussion of the previous paragraphs; instead the few differences will be highlighted. The most important difference is the objective function [Equation (2.48)]:

$$f(\mu_k) = \left| \frac{1 + i\frac{2}{\mu_k}\frac{\omega_e}{\omega_n'}\zeta' - \frac{1}{\mu_k}\left(\frac{\omega_n'}{\omega_i'}\right)^2\left(\frac{\omega_e}{\omega_n'}\right)^2}{1 + i\frac{2}{\mu_k}\frac{\omega_e}{\omega_n'}\zeta' - \frac{1}{\mu_k}\left(\frac{\omega_e}{\omega_n'}\right)^2} \right| \tag{3.7}$$

The objective function is shown in Figure 3.17. If compared to the objective function of the type I AVAI, it can be seen that the problem with the local minimum is reversed and that a large initial stiffness value will make it impossible for a local minimiser to find the optimum stiffness ratio.

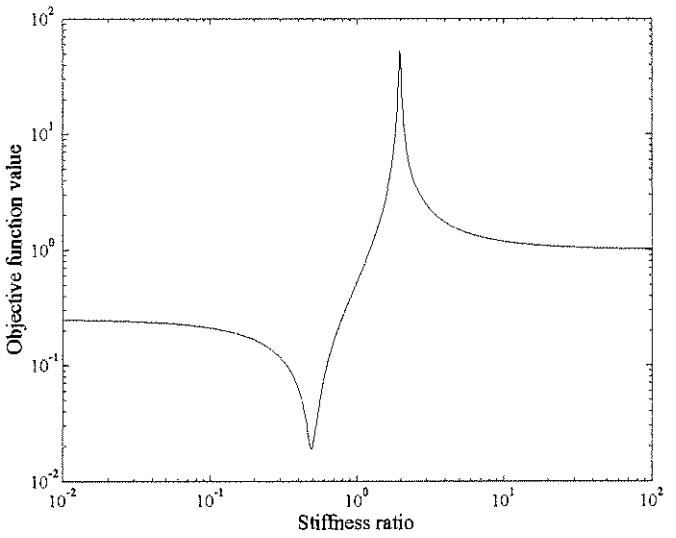

Figure 3.17: Objective function *vs.* stiffness ratio $\omega_e/\omega_n' = 1.4$ ($\omega_n'/\omega_i' = ½$ and $\zeta' = 0.01$)

The techniques to address this problem have been discussed in §3.1. For the last method that was discussed an upper bound on the stiffness ratio ($\hat{\mu}_k$) must be calculated. For the type I AVAI this constraint is [Equation (2.47)]:

$$\hat{\mu}_k = \frac{4\frac{\zeta'^2}{\mu_k} + 4\frac{\zeta'^2}{\mu_k}\left(\frac{\omega_n'}{\omega_i'}\right)^2 - 2\left(\frac{\omega_n'}{\omega_i'}\right)^2}{-\left(\frac{\omega_n'}{\omega_i'}\right)^2 - 1 + \sqrt{\left[\left(\frac{\omega_n'}{\omega_i'}\right)^2 - 1\right]^2 + 8\frac{\zeta'^2}{\mu_k}\left[\left(\frac{\omega_n'}{\omega_i'}\right)^2 + 1\right]}}\left(\frac{\Omega_n}{\omega_n'}\right)^2 \tag{3.8}$$

where Ω_n is equal to the excitation frequency ω_e. To estimate the transmissibility the following equation of motion must be solved [Equation (C.8)]:

$$\ddot{y} + 2\zeta'\omega_n'\dot{y} + \mu_k\omega_n' y = \left(\frac{\omega_n'}{\omega_i'}\right)^2 \ddot{x} + 2\zeta'\omega_n'\dot{x} + \mu_k\omega_n' x \tag{3.9}$$

The results for the lfopc algorithm for four initial conditions are shown in Figure 3.18. No constraint was used to illustrate the problem posed by the local minimum when a high initial value for the stiffness ratio is used.

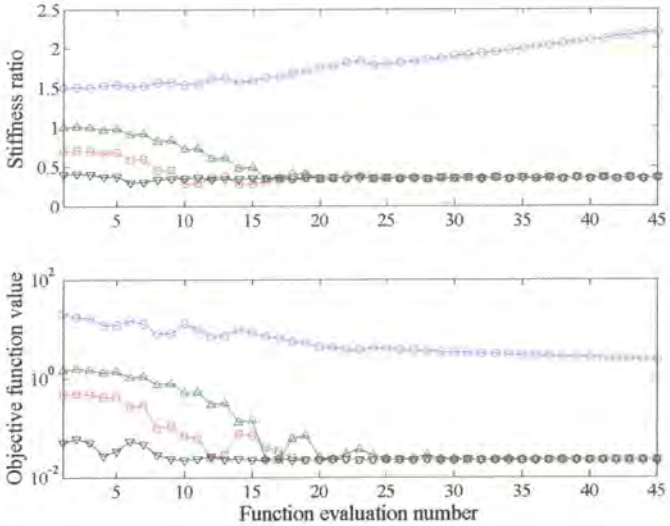

Figure 3.18: Adaptation results for 4 initial conditions $\omega_e/\omega_n' = 1.2$ ($\mu_k^0 = 0.4, 0.7, 1, 1.5$, $\omega_n'/\omega_i' = ½$ and $\zeta' = 0.01$)

For the type II AVAI the same general tuning method as described in Figure 3.16 can be applied to ensure both optimal and fast tuning.

3.3 Conclusion

This chapter showed how optimisation can be used as a control method for the AVAI. Several pitfalls exist which have been discussed in detail. Even though the objective functions differ, the same control methods can be applied to the type I and type II AVAIs. For the most general case it was suggested that open-loop tuning using a look-up table be used as a rough tuning method. If the excitation

frequency remains constant, a fine-tuning algorithm will find a new optimal stiffness for that excitation frequency. If such an optimal value is found, the look-up table is updated. The methods concentrated on using the transmissibility value as the objective function. If the input amplitude is known to be constant, it is possible to use only one sensor to measure the response of the system to provide the objective function value.

4 Design methodologies of AVAIs for a pneumatic rock drill handle

4.1 Introduction

In this chapter the design methodologies of two AVAIs will be described. These methodologies will concentrate on the design requirements of a handle for a pneumatic rock drill. Many of the more practical aspects of the design of these devices are application-specific, but the basic requirement of coincidence of the excitation and isolation frequencies is universal as is the method of achieving coincidence. The rock drill design is particularly demanding because the input contains significant amplitudes at frequencies other than the impact frequency. Furthermore, the low overall mass and size required as well as cost and robustness are necessary constraints.

This chapter will start with a discussion of the effects of tool vibration on the operators of hand-held machinery. Current strategies for the reduction of hand tool vibration will be reviewed. It will then continue with measurements that were done for a specific drill that is in widespread operation in South African gold mines. These measurements were done to assess the current exposure of operators to vibration and will be used as the baseline for any reduction method. The design methodologies used for the two handles will then be discussed and evaluated. Here the problems related to noise in the input will be addressed as well as the many practical aspects particular to each design.

4.2 Vibration reduction of tool handles

Exposure of the fingers and hands to long periods of shock or vibration can lead to a number of disorders threatening the operators of hand-held tools with irreversible damage. Five disorders are described by Griffen (1998) and are listed in Table 4.1. Combinations of these disorders are referred to as Hand-Arm Vibration Syndrome (HAVS). The disorder that has received the most attention from researchers is the vascular disorder Vibration White Finger (VWF). VWF is characterised by the occasional whitening (blanching) of the fingertips especially when exposed to a cold environment. Attacks are often accompanied by numbness and tingling and in rare cases gangrene has been reported. VWF is also associated with primary Raynaud's disease, which is a hereditary disease not caused by vibration. Currently there is no treatment for the disease and prevention is therefore essential, which means that workers must be reassigned as soon as symptoms are noticed.

Table 4.1: Disorders associated with HAVS

Type	Disorder
A	Circulatory
B	Bone and joint
C	Neurological
D	Muscle
E	General (e.g. central nervous system)

Due to the debilitating effect of VWF it has been classified as an industrial disease in 1985 in the United Kingdom (Raw, 1999). In 1999 the UK government agreed to pay £500 million to 30 000 former coal mine workers suffering from the disease. In South Africa there has been concern that the widespread use of pneumatic drills in underground mining operations can lead to similar personal suffering and claims. A comprehensive study of vibration levels of several different rock drills used in South African mines measured an average weighted equivalent acceleration of 24 m/s^2 in underground operation (Van Niekerk, Heyns & Heyns, 2000). The Commission of European Communities' proposed directive on physical agents (1994) prescribes an action level of weighted 8-hour equivalent acceleration ($a_{h,w(eq,8h)}$) of 2.5 m/s^2 and a threshold value of 5 m/s^2. The 8-hour value is calculated using the time exposed to the high levels as a ratio of an 8-hour workday. Short duration vibration can therefore be higher than the stated values, but there are absolute limits of 10 and 20 m/s^2 corresponding to the action and threshold values as illustrated in Figure 4.1. The action level involves measures to reduce the vibration while the threshold value is an absolute limit where work must be stopped.

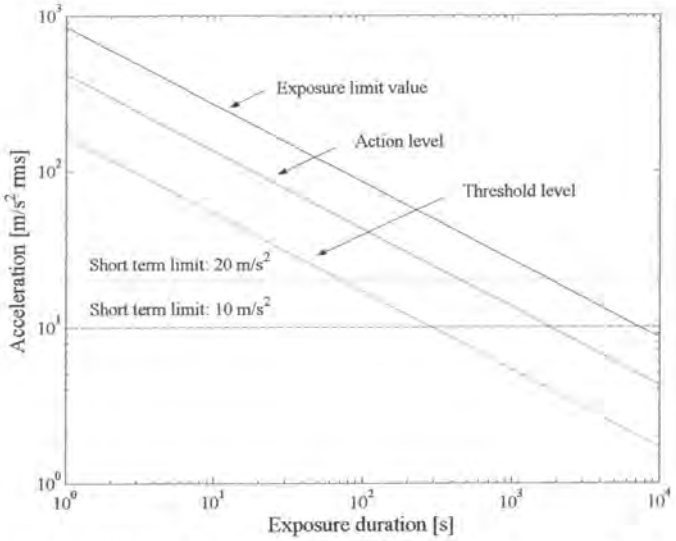

Figure 4.1: Threshold level, action level and exposure limit of the proposed EU directive on physical agents

There are two options available to meet these criteria namely, limiting exposure time or reducing the vibration level. Since the weighted equivalent acceleration of pneumatic drills used in South African mines are already above the short-term value the only option is the latter.

The standard pneumatic drill handle is shown in Figure 4.2(a). No isolation is provided and the steel handle is simply bolted to the back end of the drill. Simple solutions such as elastomeric handle wraps and gloves have been shown to have negligible isolation effect. This is because they isolate at high frequencies, typically larger than 250 Hz, where the hand is less sensitive to damage. Gloves are sometimes recommended because they keep the hands warm, which may lessen the damage (Griffen, 1998).

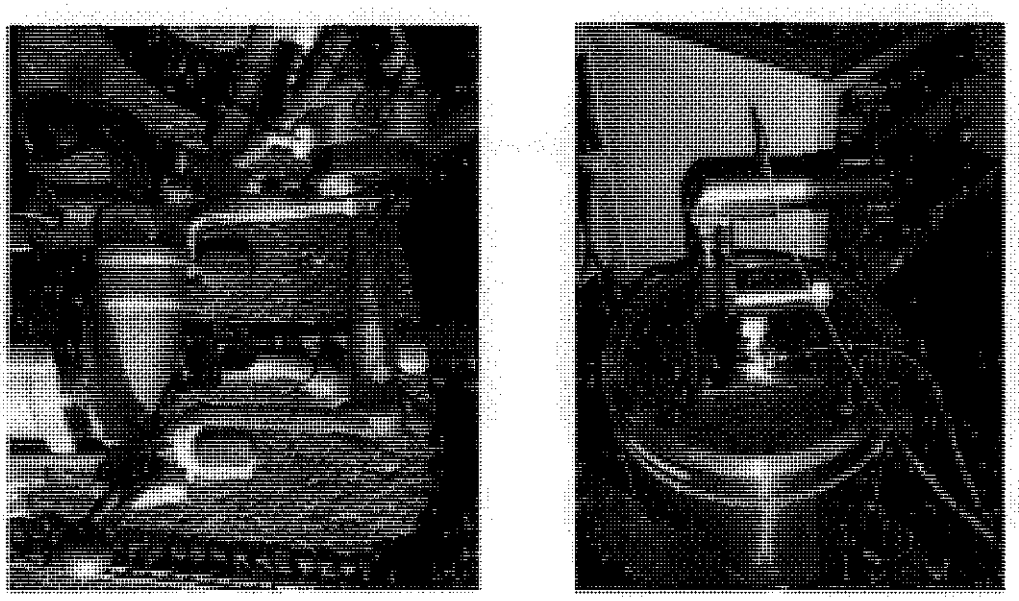

(a) (b)

Figure 4.2: (a) Standard handle, (b) isolated handle in transmissibility test set-up

If an operator is expected to drill continuously for 8-hours the vibration levels must be limited to 10% of the current value, which will be a considerable achievement. A proposed isolated handle is shown in Figure 4.2(b). The development of this handle is described by Prajapati and Hes (1999). The main problem with using isolators in this application is that a low natural frequency is directly in conflict with the static deflection requirement. A low static deflection is necessary for the operator to remain in control of the tool. The natural frequency is related to the static deflection:

$$\omega_n = \sqrt{\frac{F}{m\delta_{st}}} \tag{4.1}$$

where δ_{st} is the static deflection, F the thrust force of the operator and m the combined mass of the handle and the operator's hand. The displacement transmissibility for an undamped system at the excitation frequency (ω_e) is (Chapter 1):

$$\frac{X}{Y} = \frac{1}{1-\left(\frac{\omega_e}{\omega_n}\right)^2} \tag{4.2}$$

For a 10% transmissibility the excitation frequency ratio must be 3.2. For a pneumatic drill with an operating frequency of 35 Hz the required natural frequency will be 11 Hz. According to Griffin (1990) the apparent mass of the hand at 35 Hz is ~0.4 kg. The handle mass was measured as 1.745 kg and the total sprung mass is therefore 2.145 kg. For a thrust force of 150 N the static deflection will be ~15 mm. Such a large deflection will not be acceptable for safe tool use. Often preload of the spring is used to limit the deflection experienced by the operator. In this case the preload was measured to be ~12 kg. The only problem with using preload is that it is difficult to be certain that the operator always pushes with the same force.

Other solutions have been reported, for instance, Alabuzhev *et al.* (1989) suggested vibration reduction using quasi-zero stiffness handles on jackhammers and riveting tools. Barber (1992) also reported other methods, which required fundamental design changes to the machine to reduce the vibration experienced by the operator. Palej *et al.* (1993) showed that an active pneumatic spring could have a dynamic stiffness 20 times lower than its static stiffness and subsequently reduced vibration of a riveter 4 times. Raw (1999) achieved a 45% vibration reduction on a road-breaking tool by using a lead-silicone composite material to cover its handle, each suspended lead particle essentially acting as a vibration absorber. Andersson (1990) showed an 85% reduction in acceleration for a hammer drill using an isolated handle. Bisutti (2001) showed that the addition of mass could greatly reduce the vibration of hand tools. In his design water is pumped from a storage tank to the tool at the moment it is switched on and back when switched off. This addition of mass achieved a 60% reduction of handle vibration. Gwinn and Marjoram (1999) describes several isolated handle concepts. The first shown in Figure 4.3 uses a softening spring as the isolation element (annotation 44A). The purpose of the softening spring is to provide a lower spring rate at the operating point after the application of the thrust force by the operator. The moment put on the handle is transferred using a bearing (annotation 40A and 40B). In Figure 4.4 a vibration absorber is put in the load path forming a VAI. The mass of the absorber is shown as annotation 86. Figure 4.5 describes a handle with a fixed frequency LIVE type isolator, similar to the one proposed in this thesis. The design is greatly complicated by the air supply that runs through the handle. This necessitates a seal, in this case two O-rings (annotation 84), which will add considerable amounts of damping to the system.

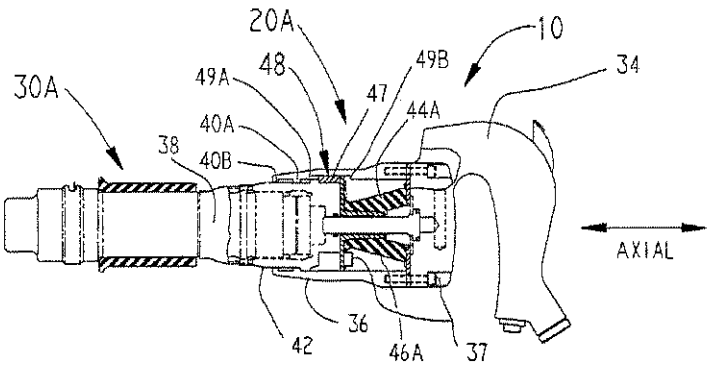

Figure 4.3: Isolated handle (Gwinn & Marjoram, 1999)

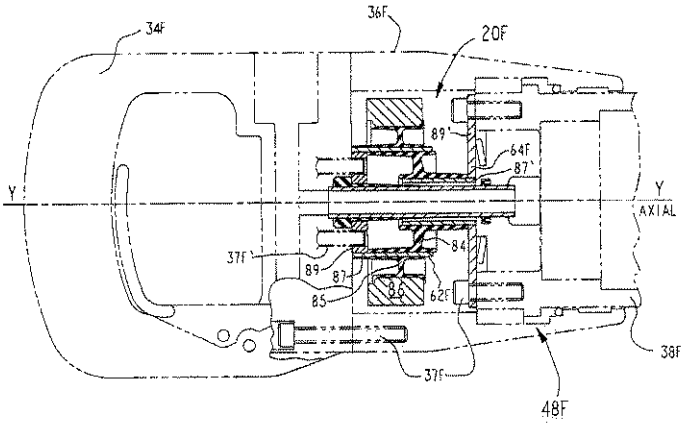

Figure 4.4: Handle with VAI (Gwinn & Marjoram, 1999)

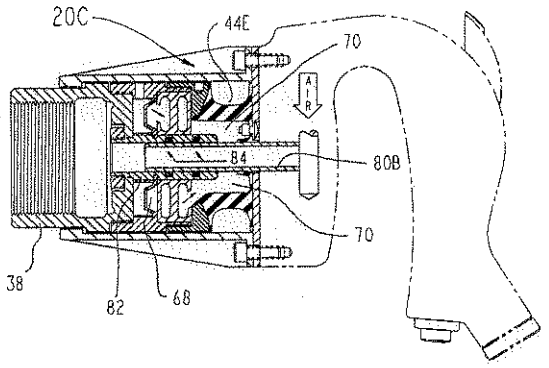

Figure 4.5: Handle with AVAI (Gwinn & Marjoram, 1999)

It is important to note that the pneumatic rock drill's operation differs from most other pneumatic tools in that the forward thrust is provided by a pneumatic piston called a jack-leg. The operator is required to counterbalance the vertical force and normally does this by leaning on the handle with his right hand, while his left hand is used to operate the jack-leg pressure control valve (Figure 4.6). It seems therefore that it will be important for the handle to be able to transfer this moment to the drill, while the axial stiffness is less important. Some axial stiffness is, however, still necessary since the drill is often jerked to remove the drill steel from the face. A minimum stiffness of 100 N/mm should be sufficient since it will allow a static deflection of 3 mm at a force of 30 kg.

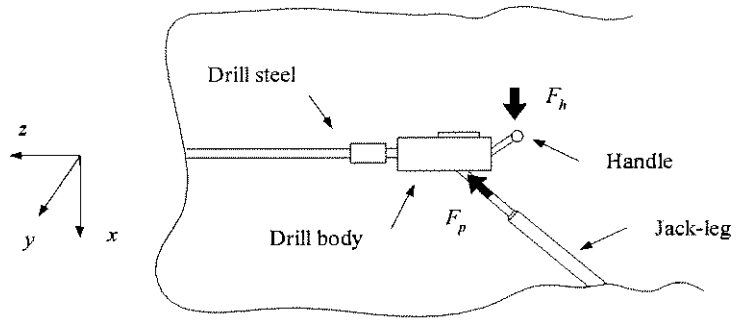

Figure 4.6: Pneumatic rock drill operation

4.3 Vibration measurement of a Boart Longyear S250 pneumatic rock drill

At the start of this work the standard regarding measurement and assessment of hand transmitted vibration was ISO 5349:1986. The measurements were done using the guidelines in this standard. ISO 5349:2001 was published in June 2001 and differs from the previous standard in many respects. The most important difference is that the evaluation of the weighted rms acceleration is done in vector fashion, while previously only the dominant axis was used. The experimental work followed the procedure of the earlier standard and to allow for continuity the theoretical part will be developed using the same standard. In the following paragraphs the assessment procedure will be described

specifically for the current drill handle. Later the response of the new handle will be compared to this reference design to show the improvement that is possible.

The measurement set-up is shown in Figure 4.7 and Figure 4.8. The drill is a percussive tool with the z-direction the axis of operation. The x-direction is vertical and the y-direction horizontal. Three Brüel & Kjær type 4393 charge accelerometers were used to measure the operational vibration of the handle. The accelerometers were mounted on mechanical filters with a cut-off frequency of 3000 Hz in accordance with the standard's guideline for percussive tools. The handle did not have any additional isolation material (Figure 4.2a) and is usually used with a work glove that offers negligible isolation. The pressure was also measured to establish the relationship between excitation frequency and supply pressure. It was additionally found that the pressure measurement could be used to calculate the excitation frequency. Such an approach could be much cheaper than using a piezoelectric accelerometer.

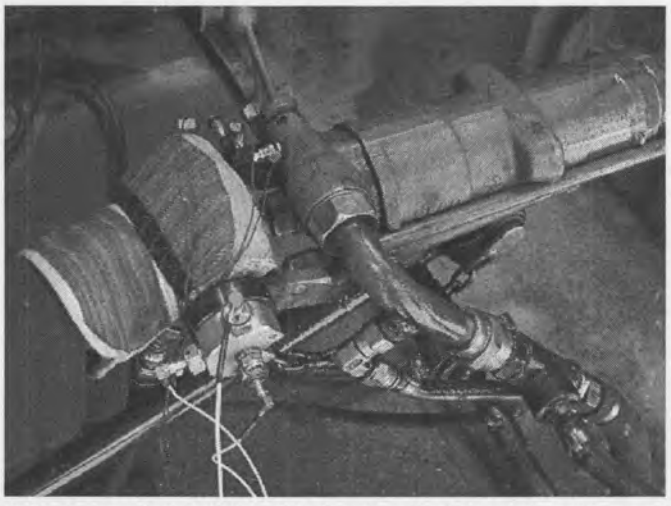

Figure 4.7: Instrumented drill handle showing the tri-axial accelerometer set-up

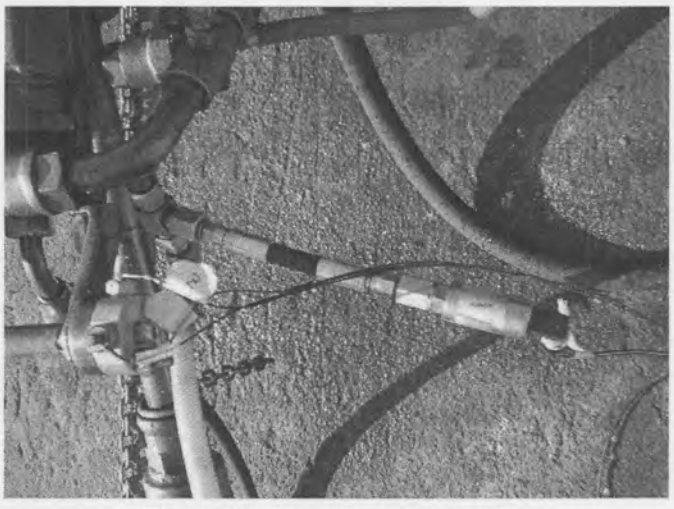

Figure 4.8: Pressure sensor location

The test started with a collaring operation shown in Figure 4.9. The collaring establishes a starting hole for the drilling operation. After collaring the second operator lets go of the drill steel and the drilling commences. The memory of the Siglab 20-42 FFT analyser allowed for 32 seconds of data to be sampled at 5120 Hz on 4 channels. The specified frequency range of 5-1500 Hz is easily covered. This corresponded to an almost complete hole of ~1.8 m at the maximum pressure tested. At lower pressure the drill speed is lower. Because the drill performance is different in different types of rock a standard Norite block is used for all testing. Four drills were measured. Three of these were new and their operational characteristics will probably vary with time. The fourth was a drill used for development work and consequently well run in.

Figure 4.9: Collaring operation

As would be expected the acceleration in the z-direction was the largest, but in the other two directions significant values were measured which could have an impact on the design under the new ISO standard. A typical measurement is shown in Figure 4.10. The acceleration values have been integrated to show the handle velocity and displacement. Although 95% of the displacement amplitudes were less than 2 mm for all operating conditions, the absorber has to be able to cope with maximum values of up to 8 mm.

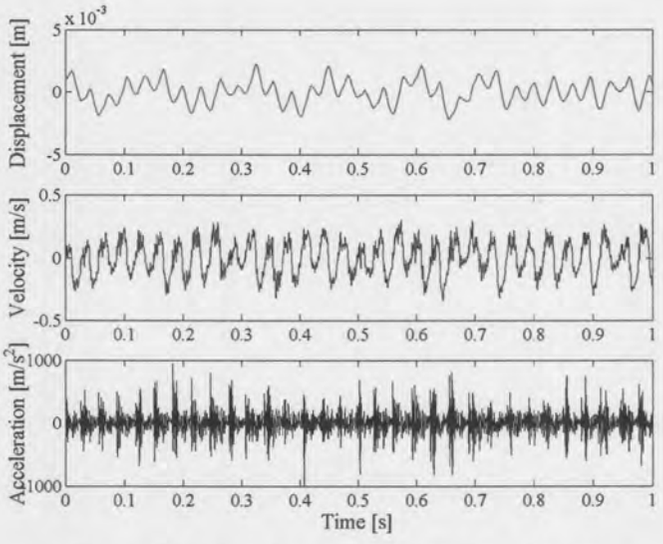

Figure 4.10: Typical measurement in the z-direction

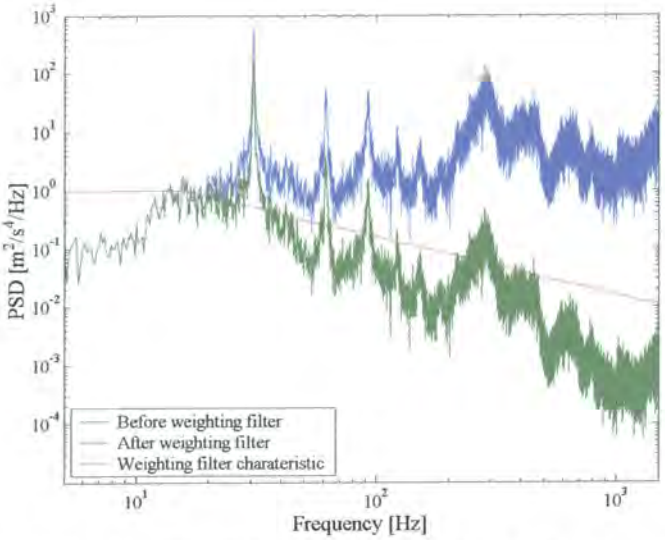

Figure 4.11: Typical PSD of the acceleration in the *z*-direction before and after the application of the weighting filter (Δf = 0.125 Hz, 4 averages)

A typical Power Spectral Density (PSD) of the acceleration is shown in Figure 4.11. The frequency of the impact dominates the spectrum. The large values at frequencies above the excitation frequency is not very important since current evidence indicates that the hand is less sensitive to vibration injury at these frequencies. The weighting curve corresponding to the hand's sensitivity is also shown in the figure. Frequencies below 16 Hz have a weighting of 1. The weighted acceleration can be found by using the relationship:

$$a_{h,w}(f) = a(f)|H(f)| \tag{4.3}$$

where $a_{h,w}(f)$ is the weighted acceleration and $a(f)$ the unweighted acceleration and $H(f)$ the weighting filter characteristic. The rms value of the Fourier transform can be calculated using Parseval's formula (Mead, 2000):

$$a_{h,w} = \sqrt{c_0^2 + \frac{1}{2}\sum_{n=1}^{\infty}|c_n|^2} \tag{4.4}$$

where c_n is the complex Fourier coefficient:

$$c_n = \frac{2}{T}\int_0^T a(t)e^{-in\omega_0 t}dt \tag{4.5}$$

Alternatively the power spectral density of the acceleration can be used:

$$a_{h,w} = \sqrt{\int_0^{\infty} W_a(f)|H(f)|^2 df} \tag{4.6}$$

where $W_a(f)$ is the one-sided power spectral density. In the time domain the rms acceleration can be calculated using a set of digital ⅓ octave band filters.

The weighting is done using:

$$a_{h,w} = \sqrt{\sum_{j=1}^{n} \left(K_j a_{h,j}\right)^2} \tag{4.7}$$

where K_j is the j^{th} ⅓ octave band weighting factor and $a_{h,j}$ is the rms acceleration measured in the j^{th} ⅓ octave band. The ISO 5349:2001 specification prescribes a weighting filter that can be used in the time domain without using ⅓ octave band analysis, which is easier to use and more accurate. Any of the above frequency-domain or time-domain methods can be used, but the narrow-band methods will be more accurate since the approximate nature of the octave band analysis is eliminated.

The test procedure for each drill involved increasing the supply pressure from 300 to 600 kPa in increments of 50 kPa. At each pressure 32 seconds of data were recorded for each of the four drills. Although the weighted rms acceleration values varied widely, the variation in frequency covered the same band between 28.75 and 37.5 Hz for all the drills. This is important if the handle is to be mass-produced. The weighted acceleration for the various supply pressures is shown in Table 4.2. The excitation frequency can be estimated using a transformation to the frequency domain such as a PSD or a Fourier transform and picking the maximum value or by using zero crossings in the time domain. Zero crossings of a band-pass filtered displacement signal will be faster for similar accuracy than a frequency-domain method.

Table 4.2: Comparison of weighted acceleration and frequency band values of the four drills

Drill	Weighted acceleration [m/s^2]		Excitation frequency [Hz]	
	Minimum	Maximum	Minimum	Maximum
1	10.51	18.16	30.625	36.250
2	9.38	13.37	30.000	36.875
3	8.91	17.28	28.750	37.500
4	8.28	18.72	28.750	37.500

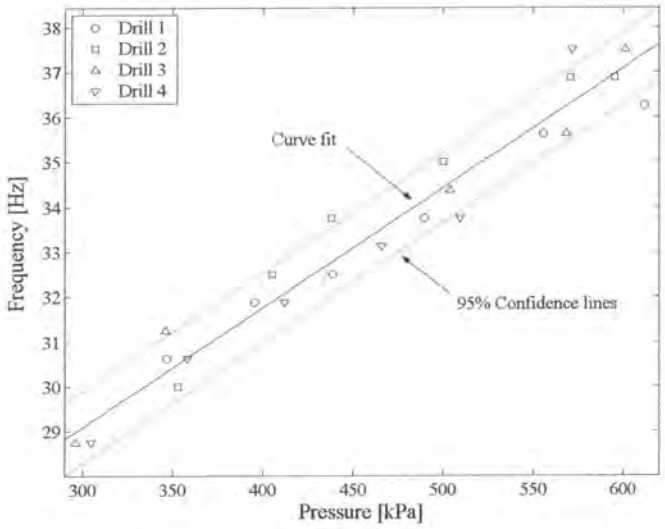

Figure 4.12: Curve fit of frequency *vs.* pressure values

When the excitation frequency *vs.* pressure is plotted a clear trend emerges as shown in Figure 4.12. As the supply pressure increases, the excitation frequency increases linearly. Since four machines where tested of which one was well run in there is reason to believe that well-maintained machines will fall within the 95% confidence lines. If the handle is designed so that the bandwidth enveloped the excitation frequencies, then good performance for any drill can be ensured. The main innovation of the AVAI as applied to the handle lies in the fact that the stiffness of the air spring can be made to be a function of the supply line air pressure and therefore it will be self-tuning. This is a major advantage in an environment where the use of an electronic control system will be expensive.

4.4 Type I amplified vibration-absorbing isolator

This section will document the design of the type I AVAI. Firstly, from measured data it was clear that the excitation does not consist of a single frequency and that the effect of noise in the input must be assessed. The following paragraph will analyse the effect of noise in the input. Subsequently, the insight gained from the general approach will be used to simulate the exact handle response using the measured input.

4.4.1 Narrow-band excitation with noise

As shown in §4.3 the excitation consists of large magnitude excitation over a limited frequency band as well as low and high frequency noise and harmonics. In general excitation of this type can be enveloped as shown in Figure 4.13. For the following discussion the AVAI response will be calculated in a non-dimensional sense in order to preserve generality. Firstly, it is assumed that the average of the narrow-band excitation ($\bar{\omega}_e$) is half of the total bandwidth ($\Delta\Omega_e$). This assumption is done simply to illustrate the effect of noise and bandwidth and does not directly pertain to the handle excitation.

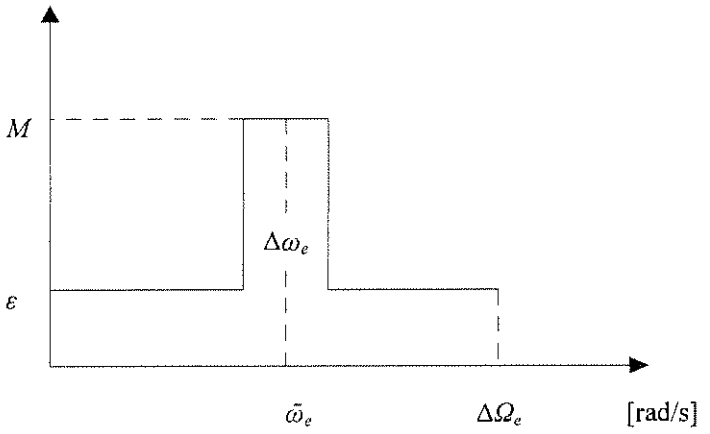

Figure 4.13: Power spectral density envelope

The following two non-dimensional ratios can now be defined. The ratio of noise (ε) to peak magnitude (M) is:

$$n = \frac{\varepsilon}{M} \tag{4.8}$$

The ratio of excitation bandwidth ($\Delta\omega_e$) to noise bandwidth ($\Delta\Omega_e$):

$$B = \frac{\Delta\omega_e}{\Delta\Omega_e} \tag{4.9}$$

The one-sided PSD of the response is:

$$W_x(i\omega) = W_y(i\omega)\left|H(i\omega)\right|^2 \tag{4.10}$$

where x describes the response and y the input and H is the transfer function of the isolator. The mean square of the response can be calculated in the frequency domain (Rao, 1990):

$$\bar{X} = \int_0^{\Delta\Omega_e} W_x(i\omega)\,d\omega = \int_0^{\Delta\Omega_e} W_y(i\omega)\left|H(i\omega)\right|^2 d\omega \tag{4.11}$$

The ratio of output to input mean square response is:

$$\bar{R} = \frac{\bar{X}}{\bar{Y}} = \frac{\int_0^{\Delta\Omega_e} W_y(i\omega)\left|H(i\omega)\right|^2 d\omega}{\int_0^{\Delta\Omega_e} W_y(i\omega)\,d\omega} \tag{4.12}$$

The numerator of Equation (4.12) can be expanded as follows:

$$\begin{aligned}\int_0^{\Delta\Omega_e} W_y(i\omega)\left|H(i\omega)\right|^2 d\omega = {} & \int_0^{\Delta\Omega_e/2-\Delta\omega_e/2} W_y(i\omega)\left|H(i\omega)\right|^2 d\omega + \int_{\Delta\Omega_e/2-\Delta\omega_e/2}^{\Delta\Omega_e/2+\Delta\omega_e/2} W_y(i\omega)\left|H(i\omega)\right|^2 d\omega \\ & + \int_{\Delta\Omega_e/2+\Delta\omega_e/2}^{\Delta\Omega_e} W_y(i\omega)\left|H(i\omega)\right|^2 d\omega\end{aligned} \tag{4.13}$$

Integrating by parts for one of the terms in Equation (4.13) gives:

$$\begin{aligned}\int_0^{\Delta\Omega_e/2-\Delta\omega_e/2} W_y(i\omega)\left|H(i\omega)\right|^2 d\omega = {} & W_y(i\omega)\Big|_0^{\Delta\Omega_e/2-\Delta\omega_e/2} \int_0^{\Delta\Omega_e/2-\Delta\omega_e/2}\left|H(i\omega)\right|^2 d\omega \\ & - \int_0^{\Delta\Omega_e/2-\Delta\omega_e/2} \frac{dW_y(i\omega)}{d\omega}\left(\int_0^{\Delta\Omega_e/2-\Delta\omega_e/2}\left|H(i\omega)\right|^2 d\omega\right)d\omega \\ \text{but}\quad \frac{dW_y(i\omega)}{d\omega} = 0 & \\ \therefore\quad \int_0^{\Delta\Omega_e/2-\Delta\omega_e/2} W_y(i\omega)\left|H(i\omega)\right|^2 d\omega = {} & W_y(i\omega)\Big|_0^{\Delta\Omega_e/2-\Delta\omega_e/2} \int_0^{\Delta\Omega_e/2-\Delta\omega_e/2}\left|H(i\omega)\right|^2 d\omega\end{aligned} \tag{4.14}$$

The total response is now:

$$\begin{aligned}\int_0^{\Delta\Omega_e} W_y(i\omega)\left|H(i\omega)\right|^2 d\omega = {} & W_y(i\omega)\Big|_0^{\Delta\Omega_e/2-\Delta\omega_e/2} \int_0^{\Delta\Omega_e/2-\Delta\omega_e/2}\left|H(i\omega)\right|^2 d\omega \\ & + W_y(i\omega)\Big|_{\Delta\Omega_e/2-\Delta\omega_e/2}^{\Delta\Omega_e/2+\Delta\omega_e/2} \int_{\Delta\Omega_e/2-\Delta\omega/2}^{\Delta\Omega_e/2+\Delta\omega/2}\left|H(i\omega)\right|^2 d\omega + W_y(i\omega)\Big|_{\Delta\Omega_e/2+\Delta\omega_e/2}^{\Delta\Omega_e} \int_{\Delta\Omega_e/2+\Delta\omega_e/2}^{\Delta\Omega_e}\left|H(i\omega)\right|^2 d\omega\end{aligned} \tag{4.15}$$

Solving for the input described in Figure 4.13:

$$\int_0^{\Delta\Omega_e} W_y(i\omega)\,d\omega = 2\varepsilon\left(\Delta\Omega_e - \Delta\omega_e\right) + M\Delta\omega_e \tag{4.16}$$

The ratio ($\bar{R}$) of output ($\bar{X}$) to input ($\bar{Y}$) mean square response is now:

$$\bar{R} = \frac{\frac{\varepsilon}{M}\int_0^{\Delta\Omega_e/2-\Delta\omega_e/2}\left|H(i\omega)\right|^2 d\omega + \int_{\Delta\Omega_e/2-\Delta\omega_e/2}^{\Delta\Omega_e/2+\Delta\omega_e/2}\left|H(i\omega)\right|^2 d\omega + \frac{\varepsilon}{M}\int_{\Delta\Omega_e/2+\Delta\omega_e/2}^{\Delta\Omega_e}\left|H(i\omega)\right|^2 d\omega}{2\frac{\varepsilon}{M}\left(\Delta\Omega_e - \Delta\omega_e\right) + \Delta\omega_e} \tag{4.17}$$

When the AVAI is compared to a single degree of freedom isolator the result is:

$$\frac{\bar{R}_{AVAI}}{\bar{R}_{SDOF}} = \frac{\frac{\varepsilon}{M}\int_0^{\Delta\Omega_e/2-\Delta\omega_e/2}\left|H_{AVAI}(i\omega)\right|^2 d\omega + \int_{\Delta\Omega_e/2-\Delta\omega_e/2}^{\Delta\Omega_e/2+\Delta\omega_e/2}\left|H_{AVAI}(i\omega)\right|^2 d\omega + \frac{\varepsilon}{M}\int_{\Delta\Omega_e/2+\Delta\omega_e/2}^{\Delta\Omega_e}\left|H_{AVAI}(i\omega)\right|^2 d\omega}{\frac{\varepsilon}{M}\int_0^{\Delta\Omega_e/2-\Delta\omega_e/2}\left|H_{SDOF}(i\omega)\right|^2 d\omega + \int_{\Delta\Omega_e/2-\Delta\omega_e/2}^{\Delta\Omega_e/2+\Delta\omega_e/2}\left|H_{SDOF}(i\omega)\right|^2 d\omega + \frac{\varepsilon}{M}\int_{\Delta\Omega_e/2+\Delta\omega_e/2}^{\Delta\Omega_e}\left|H_{SDOF}(i\omega)\right|^2 d\omega} \quad (4.18)$$

Since for the type I AVAI the first natural frequency is constant, this frequency will be used for comparison with a conventional isolator. The transmissibility for an isolator was given in Chapter 1. The parameters used for the comparison are summarised in Table 4.3. The values were chosen to allow comparison of the methods and to draw general conclusions as to the suitability of the AVAI for this type of excitation.

Table 4.3: Values used for the comparison

Description	Parameter	Value
Centre frequency of excitation	$\bar{\omega}_e$	10
Noise bandwidth	$\Delta\Omega_e$	20
Mass ratio	m_B/m_y	0.003
Area ratio	A_b/A_a	5
Second damping ratio	$\bar{\zeta}_2$	0.01
Stiffness ratio	μ_k	0.36...0.4

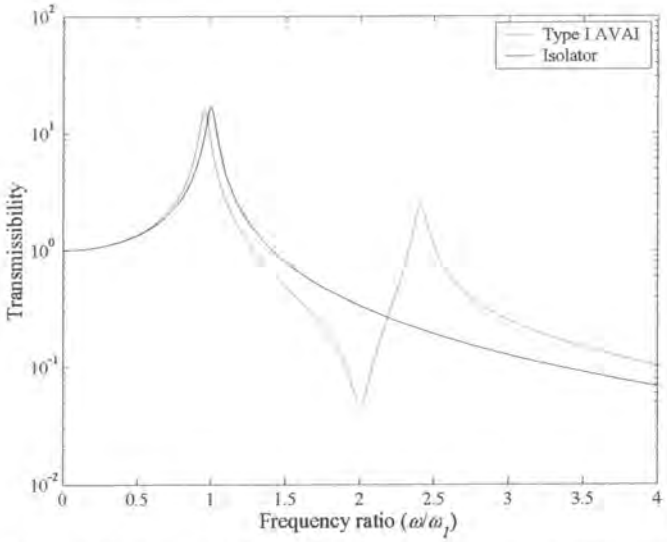

Figure 4.14: Type I AVAI and isolator used in the comparison

The two transmissibilities that are compared are shown in Figure 4.14. Clearly, for an undamped case the mean square response will be infinite due to the infinite response at the natural frequencies. It can also immediately be seen that the isolator will provide the best isolation if the bandwidth of the noise is infinite.

The ratio of ratios ($\bar{R}_{AVAI}/\bar{R}_{SDOF}$ in Equation (4.18)) is a measure of the benefit of the AVAI over an isolator and can be plotted as a function of three of the non-dimensional ratios namely damping,

excitation bandwidth ratio and noise ratio. One of the non-dimensional ratios must be held constant while the other two are being varied to create a contour plot showing the combination of variables that create an advantage for the AVAI. In Figure 4.15 through Figure 4.17 it can be seen that there is a benefit for the AVAI at small excitation bandwidth ratios (blue region), while at large excitation bandwidth ratios there is an advantage for the isolator (red region). This is not unexpected since the AVAI has been shown to be effective over a very limited bandwidth. It is interesting to note that for each excitation bandwidth ratio an optimal damping value exists. For a practical application where the noise floor and excitation bandwidth ratio are known, the optimal damping ratio can therefore be read from such a graph. It can also be seen that the optimal damping ratio is lower for the same excitation bandwidth ratio as the noise ratio is reduced. This is also not unexpected since the introduction of damping will reduce the response at the natural frequency (which will be infinite at zero damping) and even small noise ratios will therefore dominate the response. Figure 4.18 through Figure 4.20 show the effect of reducing the noise ratio if the excitation bandwidth ratio is fixed. The first two figures show similar trends i.e. some damping is necessary even at low noise ratios and the required damping increases as the noise ratio is increased. The last graph shows that a large excitation bandwidth ratio cannot be corrected using damping and an AVAI is therefore inappropriate in such a case.

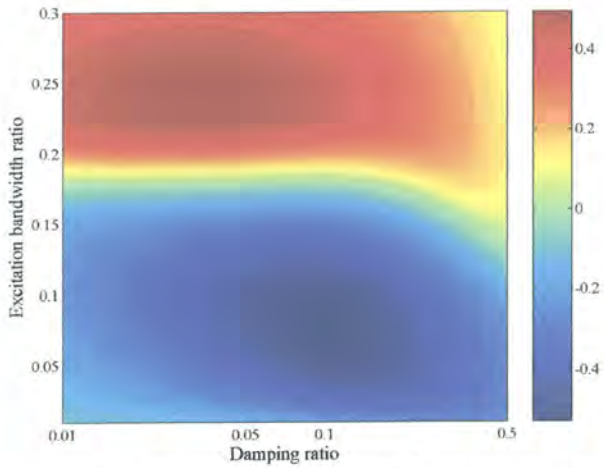

Figure 4.15: The logarithm of the ratio of ratios for a case with noise ratio 10^{-3}

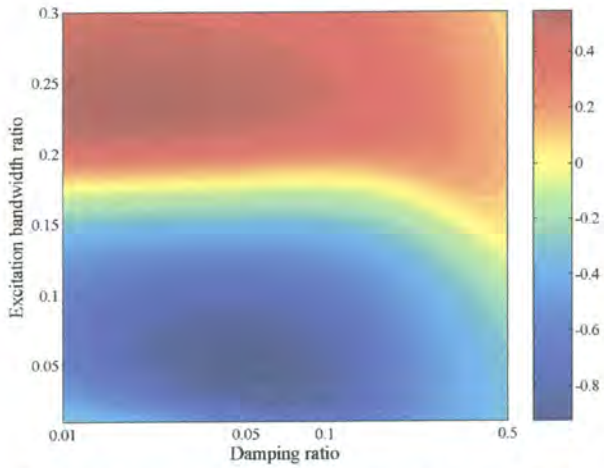

Figure 4.16: The logarithm of the ratio of ratios for a case with noise ratio 10^{-4}

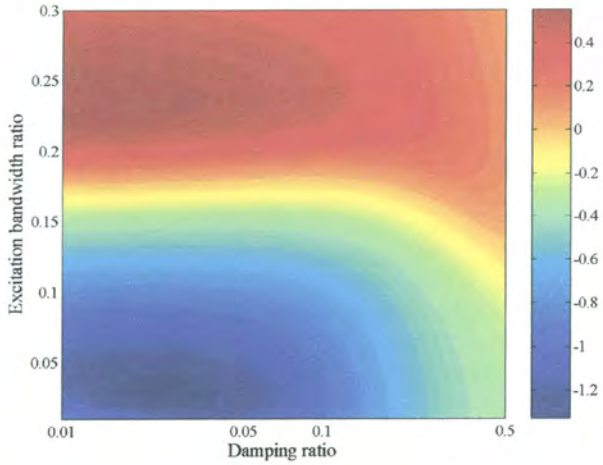

Figure 4.17: The logarithm of the ratio of ratios for a case with noise ratio 10^{-5}

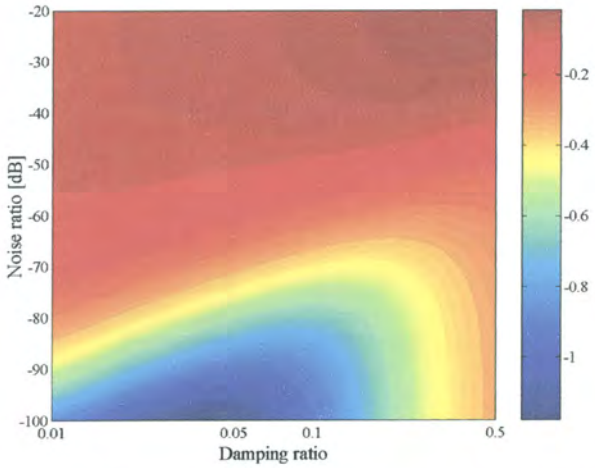

Figure 4.18: The logarithm of the ratio of ratios for a case with excitation bandwidth ratio 0.01

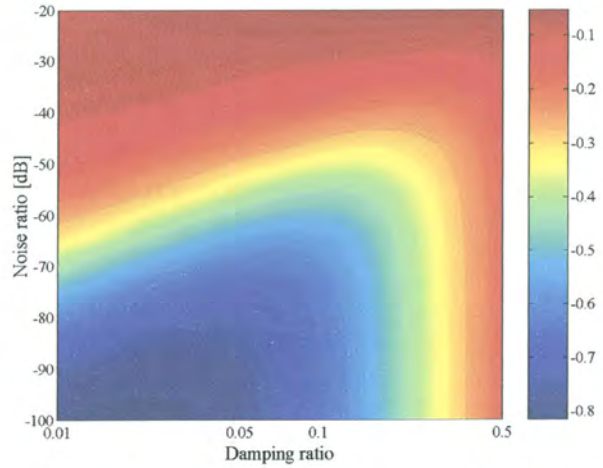

Figure 4.19: The logarithm of the ratio of ratios for a case with excitation bandwidth ratio 0.1

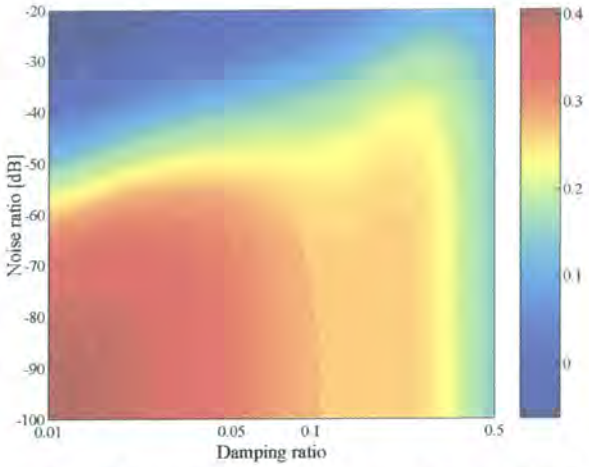

Figure 4.20: The logarithm of the ratio of ratios for a case with excitation bandwidth ratio 0.2

Figure 4.15 through Figure 4.20 show that an optimal value of damping exists for each noise and excitation bandwidth ratio. It seems as if a damping specification should enter the design as an additional parameter to those considered in Chapter 2. However, it will be very difficult to realise in a practical device. Inevitably some damping will be present, which can only be removed with the addition of energy as discussed in Chapter 1. If damping needs to be added, this can easily be done in a device that uses fluid in the port by obstructing the flow (for instance with the addition of a variable pitch butterfly valve in the port). The controllable addition of damping will be more difficult for a slug type device. For a type I device it could be possible to make both the damping and stiffness variable so that the optimal values for both will always be guaranteed. For the present work the design will attempt to reduce the damping as much as possible so that the addition of damping or variable damping can easily be considered in future work. The main sources of flow-related damping are the entrance and exit losses of the port as well as friction in the port. Careful design can reduce these losses. Overall damping is, however, dominated by the elastomeric material of the spring that is used, which can be minimised by choosing a low damping material.

4.4.2 Type I AVAI design

The design is shown schematically in Figure 4.21. The normal design approach for LIVE type isolators as well as vibration absorbers is to build devices and then to tune each before it is used. For absorbers this is often done by adding or subtracting mass. For a LIVE type isolator this can be done by sleeving the port. The purpose of the present design is to characterise the influence of assumptions made during the design. If the absorber can be designed accurately in the first instance, the amount of modification needed can be minimised. The assumptions made will be different for each design, but it could be possible to find design rules for certain classes of devices (i.e. type I), which could then at least give the designer the ability to scale its dimensions.

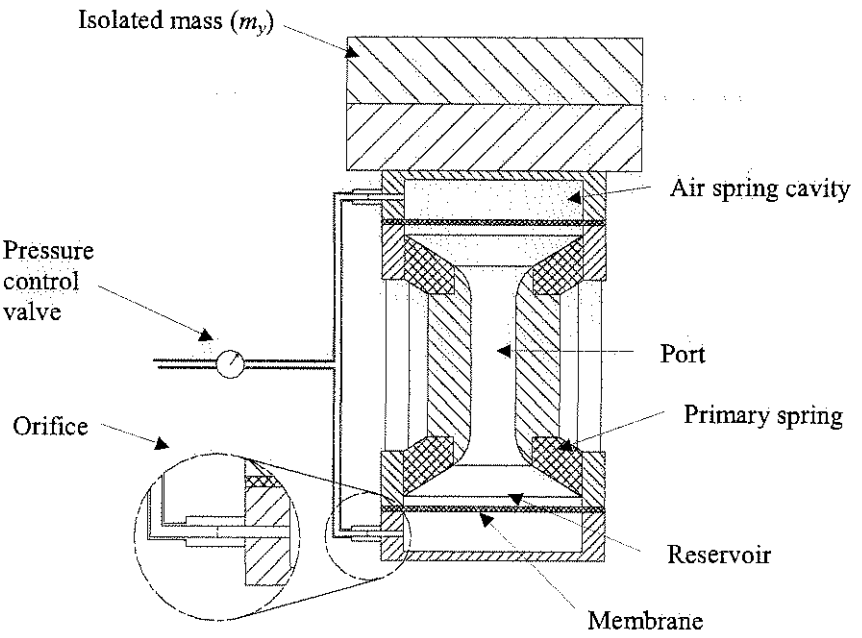

Figure 4.21: Schematic of type I AVAI design

Of all the parameters determining the design the stiffness is the most difficult to estimate accurately. For the type I AVAI the stiffness elements are the primary spring, the membrane stiffness and the stiffness contributed by the air spring. The primary spring stiffness is a function of geometry, boundary conditions and dynamic material properties. The description of dynamic material properties requires extensive testing. As a first estimate static material properties will be used.
The membrane stiffness can be calculated using the pressure deflection equation for a clamped circular plate (Young & Budynas, 2002):

$$k_m = \frac{64\pi E t^3}{3d_b^2\left(1-\nu^2\right)} \tag{4.19}$$

with t the membrane thickness, E the modulus of elasticity and ν the Poisson's ratio. A soft rubber (Nitrile) was used for the membrane of which the maximum Young's modulus was estimated to be less than 20 MPa. For a 2 mm thick rubber membrane the stiffness will be much smaller than that of the air spring.

The air spring stiffness for a closed double-acting air spring is a function of displacement (Figure 4.22) [Equation (D.4)]:

$$k_a(x) = nP_iA_bh^n\left[\left(\frac{1}{h-x}\right)^{n+1}+\left(\frac{1}{h+x}\right)^{n+1}\right]$$

$$\text{for } x \ll h \tag{4.20}$$

$$k_a = \frac{2nP_iA_b}{h}$$

where n is the ratio of specific heats (1.4 for air), P_i the initial air pressure and h the undeflected air spring height.

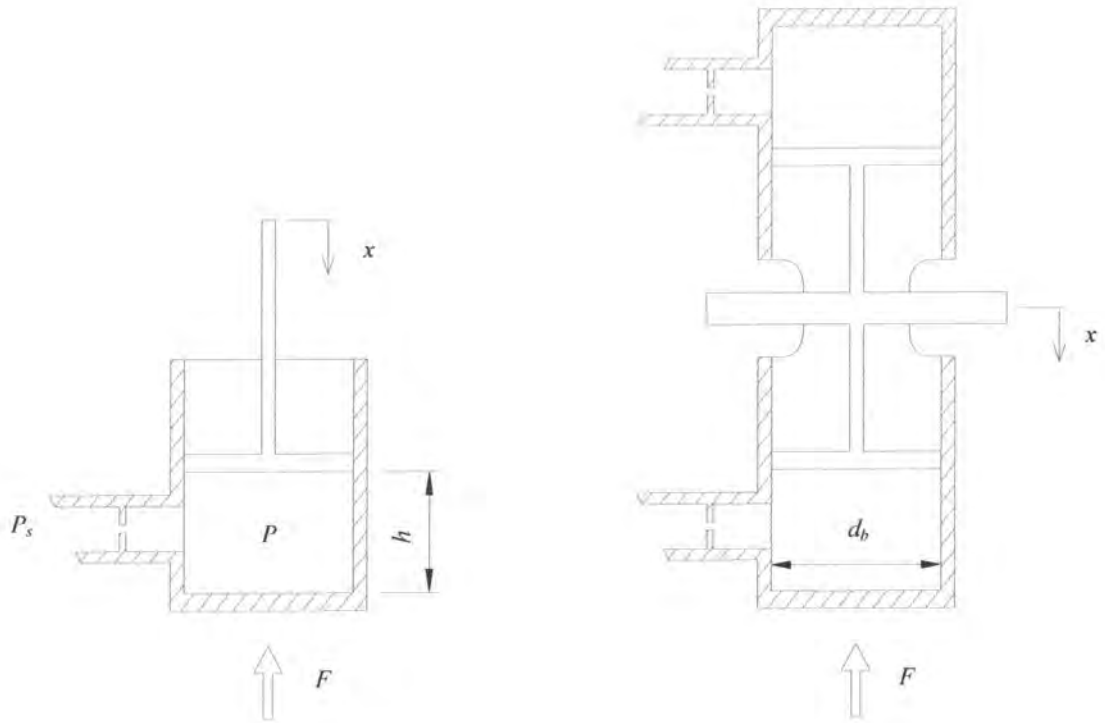

Figure 4.22: Single and double acting air springs

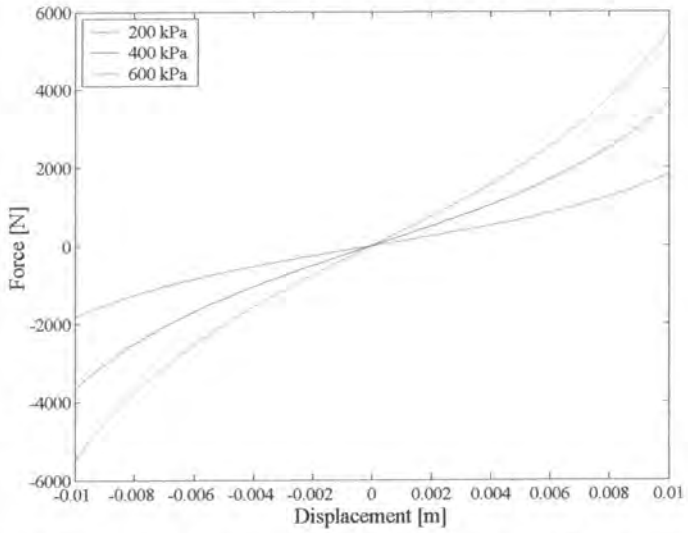

Figure 4.23: Spring force as a function of displacement (h = 20 mm and d_b = 75 mm)

Examination of Equation (4.20) shows that the two practical methods of changing the air spring stiffness are to modify either the pressure or the air spring height. Ting-Kong (1999) investigated a vibration absorber that changed air spring height and Longbottom *et al.* (1987) patented a vibration

absorber that changed the air pressure in the spring using an arrangement of valves. Since the operational frequency of the drill is related to the air pressure, it is proposed that the air spring be connected directly to the supply pressure through a flow restriction. The flow restriction will ensure that the pressure in the spring can rise on compression instead of simply pushing the air back into the supply line, while a change in the supply line pressure will cause the pressure in the spring to equalise after some time delay. This assembly will essentially achieve the same objective as the vibration absorber described by Longbottom *et al.*, without the complexity of a valve arrangement. The disadvantage is a longer time delay in changing the pressure, additional damping and lower stiffness.

Air spring damping is known to be very low, for example, Firestone commercial air spring literature states a damping ratio of 0.03. Damping in an air spring originates from heat transfer and from material losses in the rubber composite bellows. Above 3 Hz the compression process is adiabatic and heat transfer losses will become negligible (Cavanaugh, 1976). In this design the losses through the port is an additional source of damping. These losses can be minimised by using a small orifice. There will be a trade-off between the amount of damping added and the time delay and a decision here will have to take the application considered into account.

Two sets of theory exist that can be used to describe flow in and out of an air spring. Cavanaugh (1976) assumed that the air spring is connected to an auxiliary tank through a capillary, while Palej *et al.* (1993) considered a connection through an orifice. The capillary theory results in algebraic equations, which can easily be solved while the flow through an orifice requires that a non-linear differential equation be solved. A capillary can further be distinguished from an orifice because the flow resistance results from wall friction rather than gas momentum. Although the theory is certainly more complicated, it is much easier to source an orifice and for this design a standard liquid petroleum (LP) gas bottle orifice of 0.15 mm diameter was used.

The mass flow rate through an orifice is given by (Palej *et al.*, 1993):

$$\dot{m} = \begin{cases} CA_0P_s\left\{\dfrac{2n}{n-1}\dfrac{1}{RT_s}\left[\left(\dfrac{P}{P_s}\right)^{2/n} - \left(\dfrac{P}{P_s}\right)^{(n+1)/n}\right]\right\}^{1/2} & \text{for } \sigma_c < \dfrac{P}{P_s} \le 1 \\ CA_0P_s\left[\dfrac{n}{RT_s}\left(\dfrac{2}{n+1}\right)^{(n+1)/(n-1)}\right]^{1/2} & \text{for } 0 \le \dfrac{P}{P_s} \le \sigma_c \end{cases} \tag{4.21}$$

where P_s is the supply pressure, T_s is the absolute supply air temperature, P is the pressure in the spring, R is the gas constant, C the discharge coefficient and A_0 the orifice area. When the pressure in the spring becomes larger than the pressure in the supply line the spring pressure becomes the supply pressure P_s and the supply line the pressure P. In general, the discharge coefficient is a function of the pressure ratio. The product CA_0 is the reduced flow area of the *vena contracta* and the discharge coefficient is therefore always less than 1.

Equation (4.21) can be approximated as follows (Wang & Singh, 1987):

$$\dot{m} = C_c A_0\left[\left|P_s^2 - P^2\right|\frac{1}{RT_s}\right]^{\frac{1}{2}}\operatorname{sign}(P_s - P) \tag{4.22}$$

where C_c is a constant discharge coefficient. A comparison of the two flow rate equations is shown in Figure 4.24. Experimental work by Grace and Lapple (1951) has found that a discharge coefficient of 0.82 is within 2% accurate for an application where the orifice is mounted in a line.

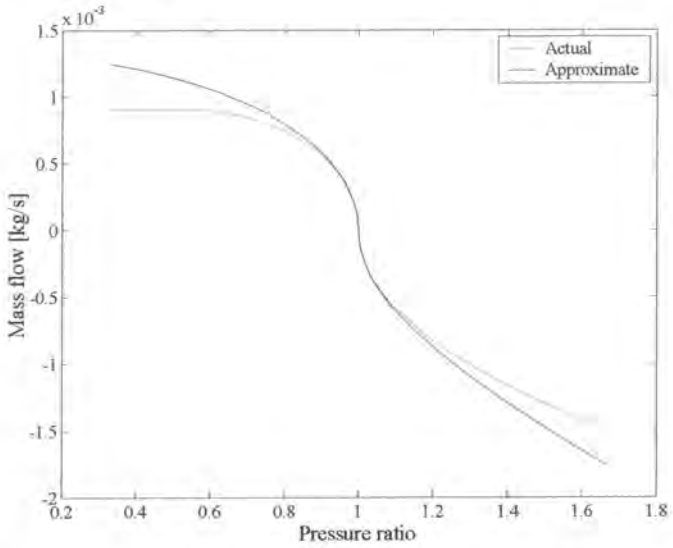

Figure 4.24: Mass flow rate as a function of pressure ratio. The actual curve given by Equation (4.21) and the approximate curve by Equation (4.22) (P_s = 600 kPa, R = 287, T_s = 25°C and C = 0.82)

The differential equation describing the pressure in the air spring is given by (Wang & Singh, 1987):

$$\dot{P} = \frac{1}{V}\left\{ n\dot{m}R\left[\frac{P}{P_0}\right]^{\frac{n-1}{n}} T_0 - nP\dot{V} \right\} \tag{4.23}$$

where P_0 and T_0 are the initial pressure and temperature inside the spring and V is the current volume of air inside the spring. When flow from the spring to the supply line occurs, the gas temperature inside the spring must be used in the mass flow equation. The gas temperature can be found by using the equation for a polytropic thermodynamic process:

$$PT^{n/(1-n)} = P_0 T_0^{n/(1-n)} \tag{4.24}$$

When solving this differential equation the force *vs.* displacement relationship can be calculated for a given displacement input. When the forced displacement is sinusoidal with a constant amplitude and frequency the curve exhibit hysteresis as shown in Figure 4.25. The curve shown is that which is reached after ~50 cycles when the air temperature in the spring has stabilised.

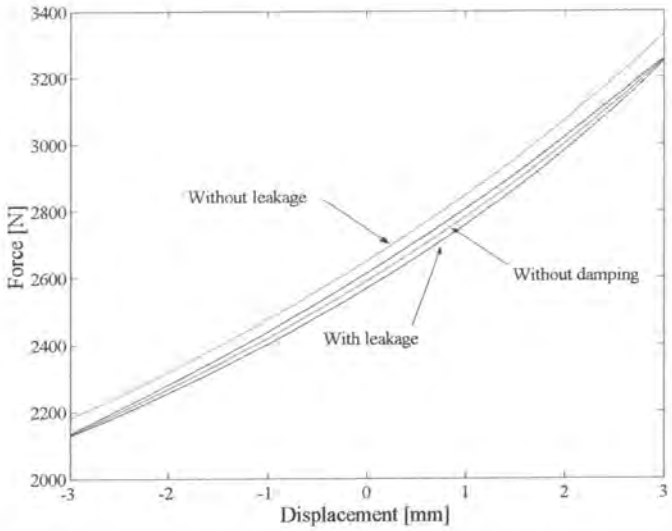

Figure 4.25: Hysteresis curve at 50 Hz compared with an air spring without leakage (d_b = 75 mm, h = 20 mm, X = 3 mm, $T_s = T_0$ = 25°C, P_s = 600 kPa, C = 1 and R = 287 J/kg.K)

The hysteretic damping constant can be calculated by integrating the area bordered by the hysteresis loop (Rao, 1990):

$$h = \frac{\Delta W}{\pi X^2} \tag{4.25}$$

where ΔW is the energy loss during one cycle and X is the excitation amplitude. The loss factor can be found by dividing the hysteretic damping constant by the stiffness. In this case the stiffness is significantly non-linear, but in order to get a basic understanding of the effect of the orifice design on the loss factor it will be assumed to be independent of displacement (i.e. displacement much smaller than the spring height). The effect of orifice diameter is illustrated in Figure 4.26.

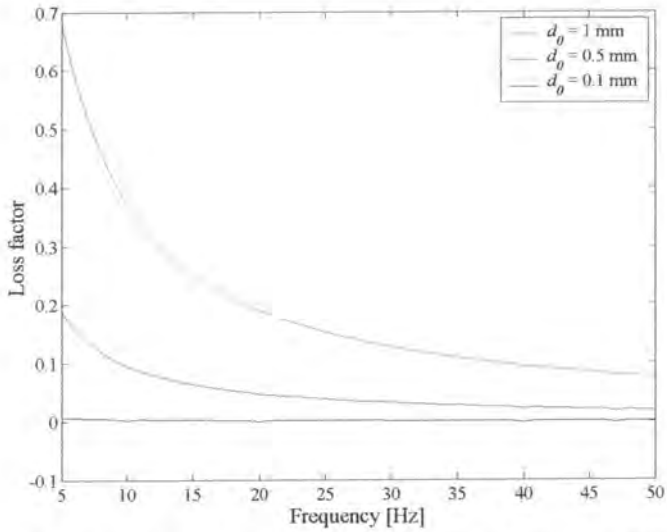

Figure 4.26: Loss factor as a function of frequency and orifice diameter (d_b = 75 mm, h = 20 mm, X = 3 mm, $T_s = T_0$ = 25°C, P_s = 600 kPa, C = 1 and R = 287 J/kg.K)

As would be expected, the loss factor decreases as the orifice diameter decreases. Figure 4.27 shows the effect of orifice diameter on the time taken for the pressure in the air spring to rise to that of the supply line. As would be expected the smaller the diameter, the longer the delay will be. It may also be expected that the air spring will be slightly less stiff than a spring without leakage, as is illustrated in Figure 4.28.

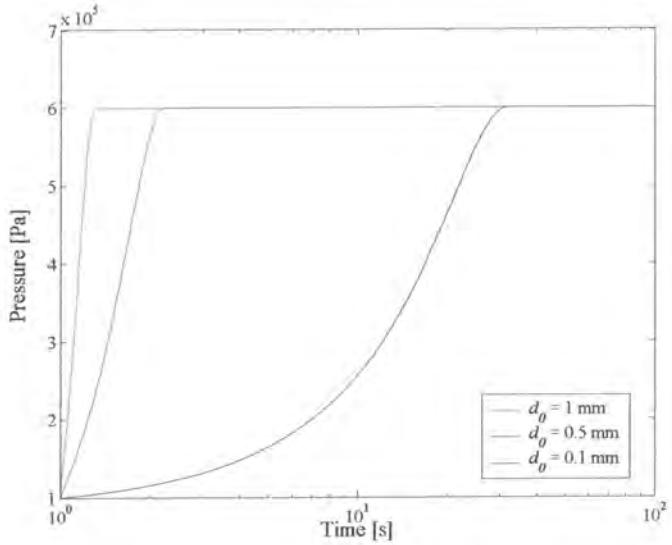

Figure 4.27: Pressure rise from 100 to 600 kPa as a function of orifice diameter d_0 (d_b = 75 mm, h = 20 mm, X = 3 mm, $T_s = T_0$ = 25°C, P_s = 600 kPa, C = 1 and R = 287 J/kg.K)

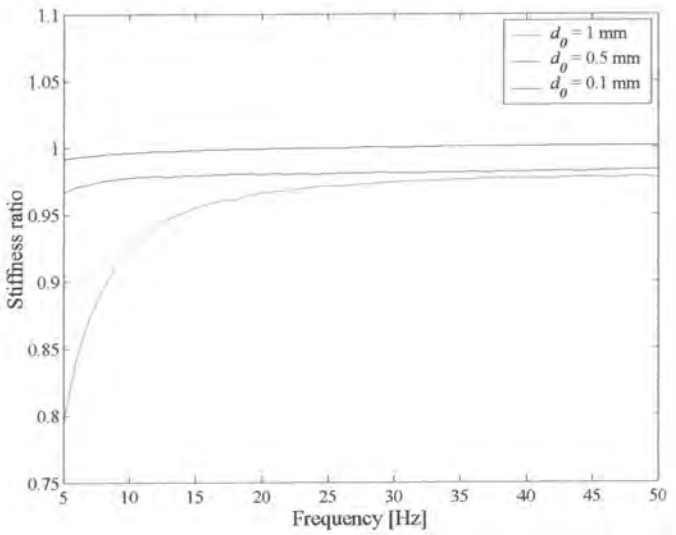

Figure 4.28: Ratio between stiffness of an air spring with and without leakage (d_b = 75 mm, h = 20 mm, X = 3 mm, $T_s = T_0$ = 25°C, P_s = 600 kPa, C = 1 and R = 287 J/kg.K)

Lastly, it is important to keep in mind that up till now the change in volume of the air spring was assumed to be the area multiplied by the displacement, which is not the case for the present design. The air spring volume change is defined by the shape of the membrane and can be written as a function of the displacement of the centre of the membrane (x_c):

$$V = \frac{1}{3} A_b x_c \tag{4.26}$$

The derivation of the displaced volume assumes a fixed boundary for the membrane and is shown in Appendix E.

The primary spring stiffness is a function of the elastomer material property as well as geometry. Time-independent material behaviour for elastomers is generally described in terms of strain energy density functions. The well-known Ogden polynomial model correlates well with experimental data up to 700% strain. Clearly, the maximum strain for the spring will not be that large and it is possible to use linear assumptions to obtain a design value for the stiffness. It is important to keep in mind that elastomers are incompressible and their Poisson's ratio is therefore close to 0.5. The relationship between shear modulus and the modulus of elasticity is:

$$G = \frac{E}{2(1+\nu)} \tag{4.27}$$

The shear modulus is therefore ⅓ of the modulus of elasticity for nearly incompressible materials. As stated before it is required that the stiffness is low and therefore the softest possible low damping rubber will be used. The softest readily available was unfilled natural rubber with hardness 35 Shore A. From Davey and Pane (1964) the modulus of elasticity for his type of rubber can be estimated as ~1.2 MPa.

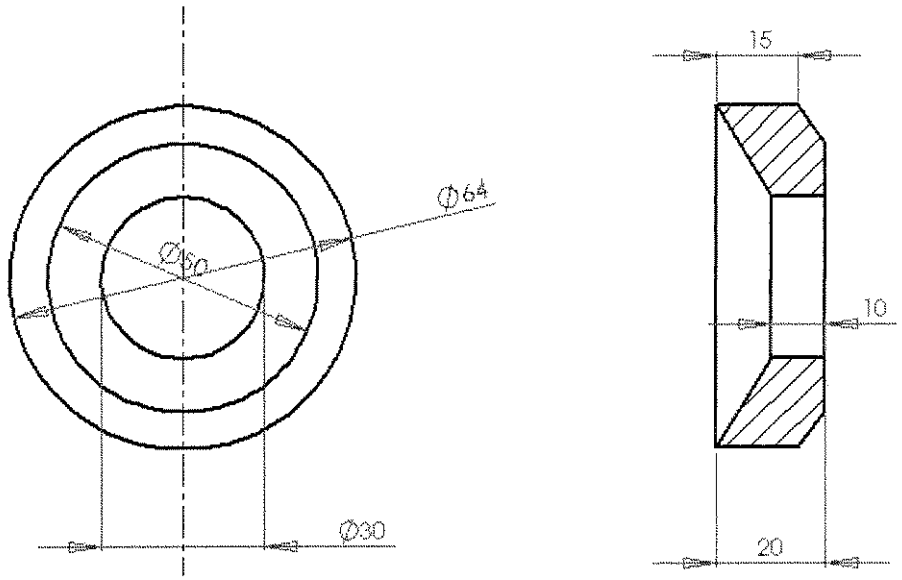

Figure 4.29: Primary spring geometry

The primary spring geometry is shown in Figure 4.29. Due to the boundary condition it will be difficult to find an exact solution for the stiffness. Instead, a number of assumptions will be made and this will be compared with finite element (FE) results to show that they are valid for design purposes. The effect of geometry on the stiffness for a cylindrical spring can be found by summing the stiffness of series springs from the inner to the outer radius (Figure 4.30).

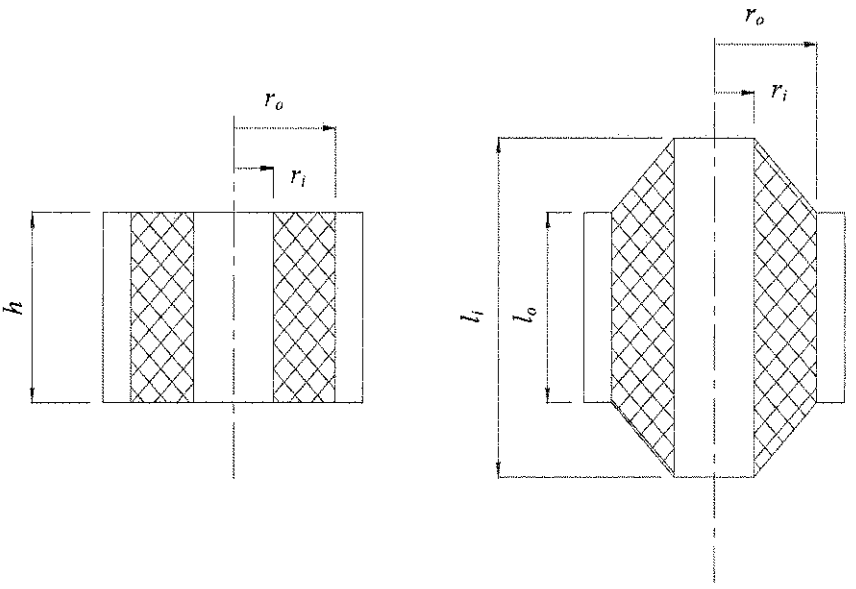

Figure 4.30: Cylindrical spring

A section of the spring at radius r will have a rectangular cross section and assuming that shear effects dominates, the stiffness is (Gere & Timoshenko, 1991):

$$\delta k = \frac{2\pi rhG}{\delta r} \tag{4.28}$$

The total stiffness of the series springs is:

$$\frac{1}{k} = \frac{1}{2\pi G}\int_{r_i}^{r_o}\frac{1}{rh}dr \tag{4.29}$$

If the height is constant the stiffness is:

$$k = \frac{2\pi Gh}{\ln\left(\frac{r_o}{r_i}\right)} \tag{4.30}$$

To separate the effect of the radius ratio from that of material property and height, the geometric stiffness coefficient is defined as:

$$k_{Gh} = \frac{k}{Gh} = \frac{2\pi}{\ln\left(\frac{r_o}{r_i}\right)} \tag{4.31}$$

If the effect of bending is taken into account, the stiffness is given by (Davey & Pane, 1964):

$$k_{Gh} = \frac{k}{Gh} = \frac{1}{\frac{1}{Q_1} + \left(\frac{r_o}{h}\right)^2 \frac{1}{Q_2}} \tag{4.32}$$

where:

$$Q_1 = \frac{2\pi}{\ln\left(\frac{r_o}{r_i}\right)} \tag{4.33}$$

$$Q_2 = \frac{16\pi \left(\frac{r_o}{r_i}\right)^2 \left[\left(\frac{r_o}{r_i}\right)^2 - 1\right]}{3\left\{\left[\left(\frac{r_o}{r_i}\right)^2 - 1\right]^2 - 4\left(\frac{r_o}{r_i}\right)^2 \left[\ln\left(\frac{r_o}{r_i}\right)\right]^2\right\}} \tag{4.34}$$

The geometric stiffness for a tapered section is (Davey & Pane, 1964):

$$k_G = \frac{k}{G} = \frac{2\pi(l_o r_i - l_i r_o)}{(r_o - r_i)\left[\ln(l_o r_i) - \ln(l_i r_o)\right]} \tag{4.35}$$

If the dimensions in Equation (4.35) are chosen such that $l_i r_i = l_o r_o$ then the spring will have uniform shear stress, which can be advantageous. The primary spring stiffness is a function of the ratio of inside and outside diameters as well as the height of the spring, as shown in Figure 4.31. Clearly, for thin sections bending behaviour will dominate and must be accounted for. It must also be kept in mind that thin sections will stretch when the reservoir is pressurised through the motion of the port, which will make the design less efficient. For this reason it is not possible to make a very flexible spring by simply increasing the radius ratio or by decreasing the spring height. A second reason is that the bending stiffness will also decrease significantly, which will make the handle difficult to use in the manner described in §4.2.

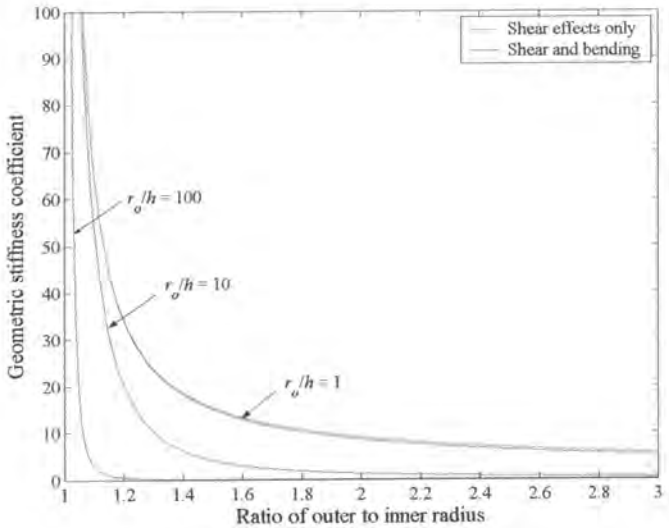

Figure 4.31: Geometric stiffness coefficient

For a general section, as was used in this design, the function describing the height as a function of the radius must be found and then used in Equation (4.29), which can then be integrated numerically. The stiffness can also be found using the exact geometry and the finite element method. For this purpose a finite element model was solved using the MSC.Marc commercial finite element code. The results are summarised in Table 4.4. The compression values were calculated by assuming that the port outer diameter defines the spring inner diameter ($d_i = 2r_i = 50$ mm). This assumption should be valid because the elastomer is incompressible and little deformation will be present past the port outer diameter. In extension it was assumed that the spring inner diameter is defined by the tapered section ($d_i = 30$ mm). The assumptions are confirmed by the finite element analysis shown in Figure 4.32. The extended part shows deformation past the outer diameter of the spring, while in compression there is very little. The force displacement graph as found using finite elements is shown in Figure 4.33. The relationship is fairly linear up to 2 mm, which is adequate since 95% of the measured amplitudes were below 2 mm. This analysis assumes that the material will behave linearly below 2 mm.

Table 4.4: Geometric stiffness using various methods

	Equation	Geometric stiffness (k/G) [m]		
		Extension	Compression	Mean
Exact integration	(4.29)	0.0996	0.3933	0.2465
Rectangular cross section with average height	(4.30)	0.1037	0.3930	0.2483
Rectangular cross section with average height, including bending	(4.32)	0.0723	0.3739	0.2231
Tapered section	(4.35)	0.1285	0.3933	0.2609
Finite element method				0.2969

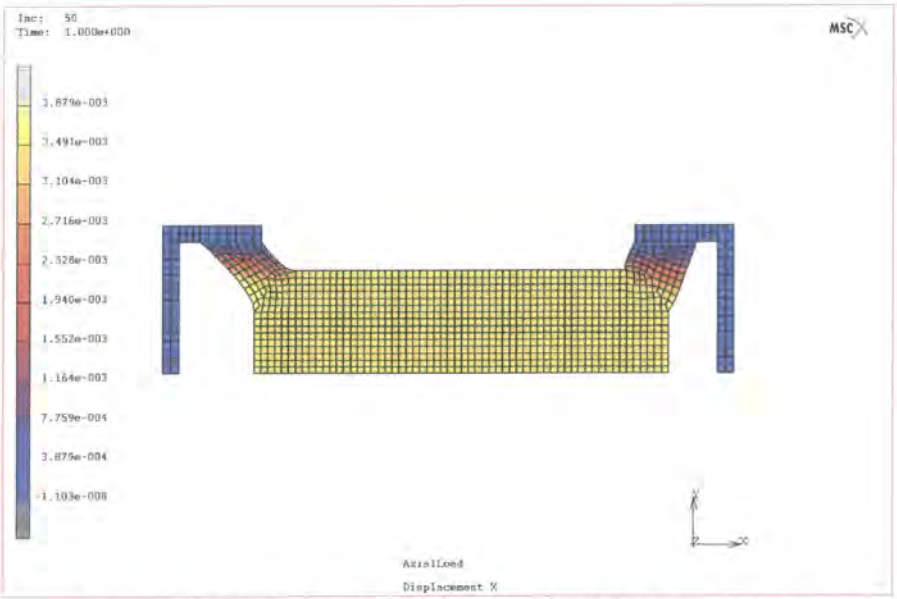

Figure 4.32: Final state of the spring when loaded in the x-direction

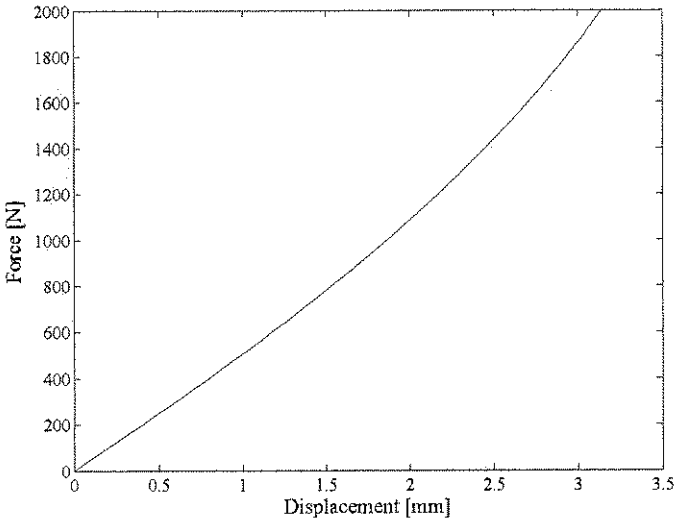

Figure 4.33: Force *vs.* displacement result from the FE model

The effect of a moment acting on the handle is illustrated in Figure 4.34. It is difficult to estimate the amount of angular deflection that will interfere with operator efficiency and comfort. The prudent course of action is to minimise this deflection as much as possible. Appendix D.4 estimates the load required to balance the force of the jack-leg acting on the drill handle. The estimate shows that the load can approach 80 kg, which is comparable to the mass of the operator and is therefore achievable.

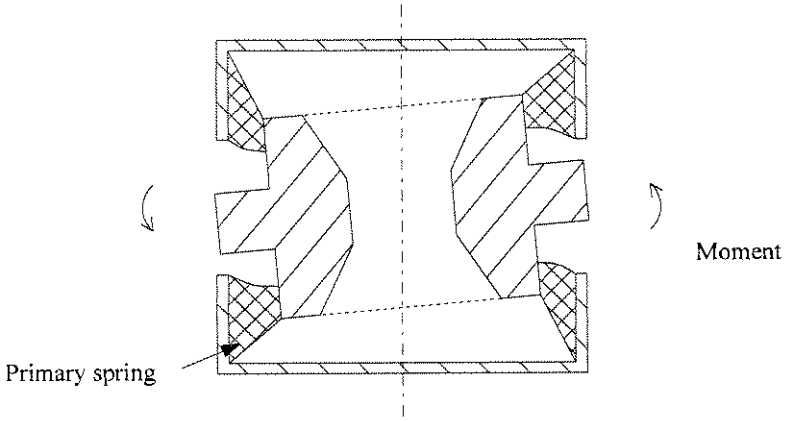

Figure 4.34: Effect of a moment put on the AVAI

The angle through which the handle will rotate can be estimated by calculating the moment balance on the AVAI as shown in Figure 4.35 [Equation (D.11)].

$$\theta = \sin^{-1}\left[\frac{-\frac{F}{k_2}\left(\frac{a}{b}-\frac{1}{2}\right)-\frac{F}{k_1}\left(\frac{a}{b}+\frac{1}{2}\right)}{b}\right] \tag{4.36}$$

For the present design the dimensions are a = 186.76 and b = 105.72 mm.

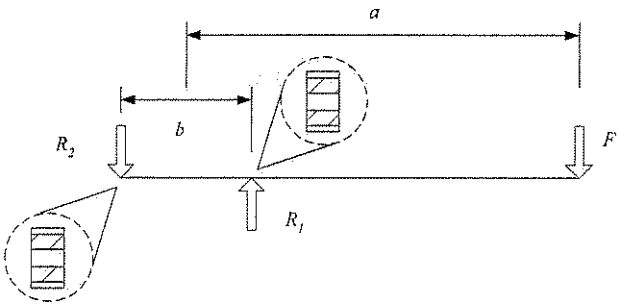

Figure 4.35: Moment acting on the handle

The radial stiffness of the cylindrical spring shown in Figure 4.30 was approximated as follows by Gobel (Davey & Pane, 1964):

$$k_G^r = \frac{k_r}{G} = \frac{7.5\pi h}{\ln\left(\frac{r_o}{r_i}\right)}\left[1 + \frac{0.0097h^3}{(r_o - r_i)^3}\right] \tag{4.37}$$

Adkins and Gent proposed the following empirical equation (Davey & Pane, 1964):

$$k_G^r = \frac{k_r}{G} = \frac{H\pi h\left[\left(\frac{r_o}{r_i}\right)^2 + 1\right]}{J\left[\left(\frac{r_o}{r_i}\right)^2 + 1\right]\ln\left(\frac{r_o}{r_i}\right) - M\left[\left(\frac{r_o}{r_i}\right)^2 - 1\right]} \tag{4.38}$$

where $H = 80$, $J = 25$ and $M = 9$ for a short bush.

Table 4.5: Radial geometric stiffness comparison

	Equation	Geometric stiffness (k_r/G) [m]
Gobel	(4.37)	1.6273
Adkins and Gent	(4.38)	0.9717
Finite element method		1.1360

Using the above stiffness values in Table 4.5 it was estimated that the maximum angle would be less than 7°, which seems adequate.

The most advantageous feature of this design is that assembly is much simpler than previous designs. Previous designs required the assembly of two cylinders that moved inside one another, which complicated both assembly and manufacture. The type I design, however, uses spacing rods to separate the two reservoirs, as shown in Figure 4.36. The port is connected via a cradle to the actuator. The cradle assembly was designed to be stiff so that it would not influence the response of the handle. Either end could have been connected to the handle or the actuator, but the most benefit will be gained by connecting the heaviest part to the handle. By connecting it in this way the mass on the drill side is 5.39 kg and on the handle side 7.46 kg. The mass of the hand was ignored during design and testing since it will have a very small effect.

For the type I AVAI it was decided to use water as the absorber fluid. Other possible heavy liquids are listed in the Appendix D. To minimise corrosion, a small amount of glycol was added to the water. The effect of the glycol on the density of the mixture was negligible. The effect of port inlet and outlet geometry is to increase the isolation frequency and was analysed in Du Plooy (1999). For this design the effect of the port geometry is small and can be neglected.

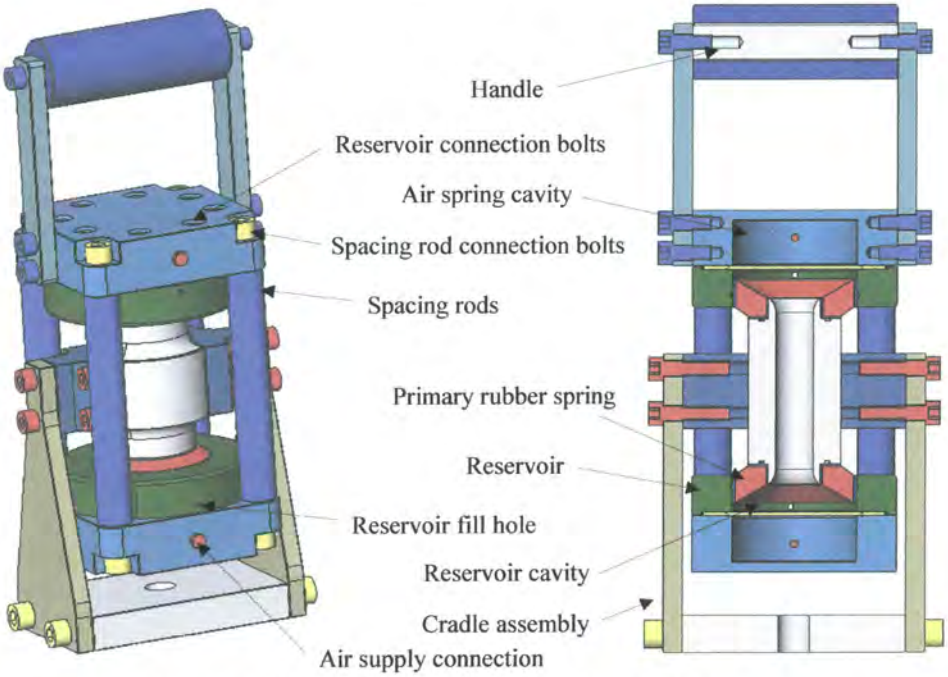

Figure 4.36: Important features of the type I AVAI design

A major problem in previous designs was leakage of the absorber fluid. Leakage occurred because the bond between the metal and the polyurethane spring used in that design failed after a small number of cycles. To ensure that this does not happen the primary spring was press-fitted and sealed using O-rings as shown in Figure 4.37. The press-fit was also required because the natural rubber used in this design could not be bonded to a thick metal part.

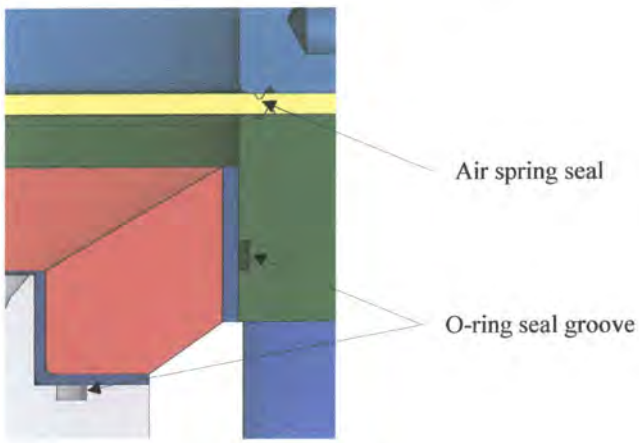

Figure 4.37: Seals for the air spring and reservoir area

An exploded view of the type I AVAI is shown in Figure 4.38.

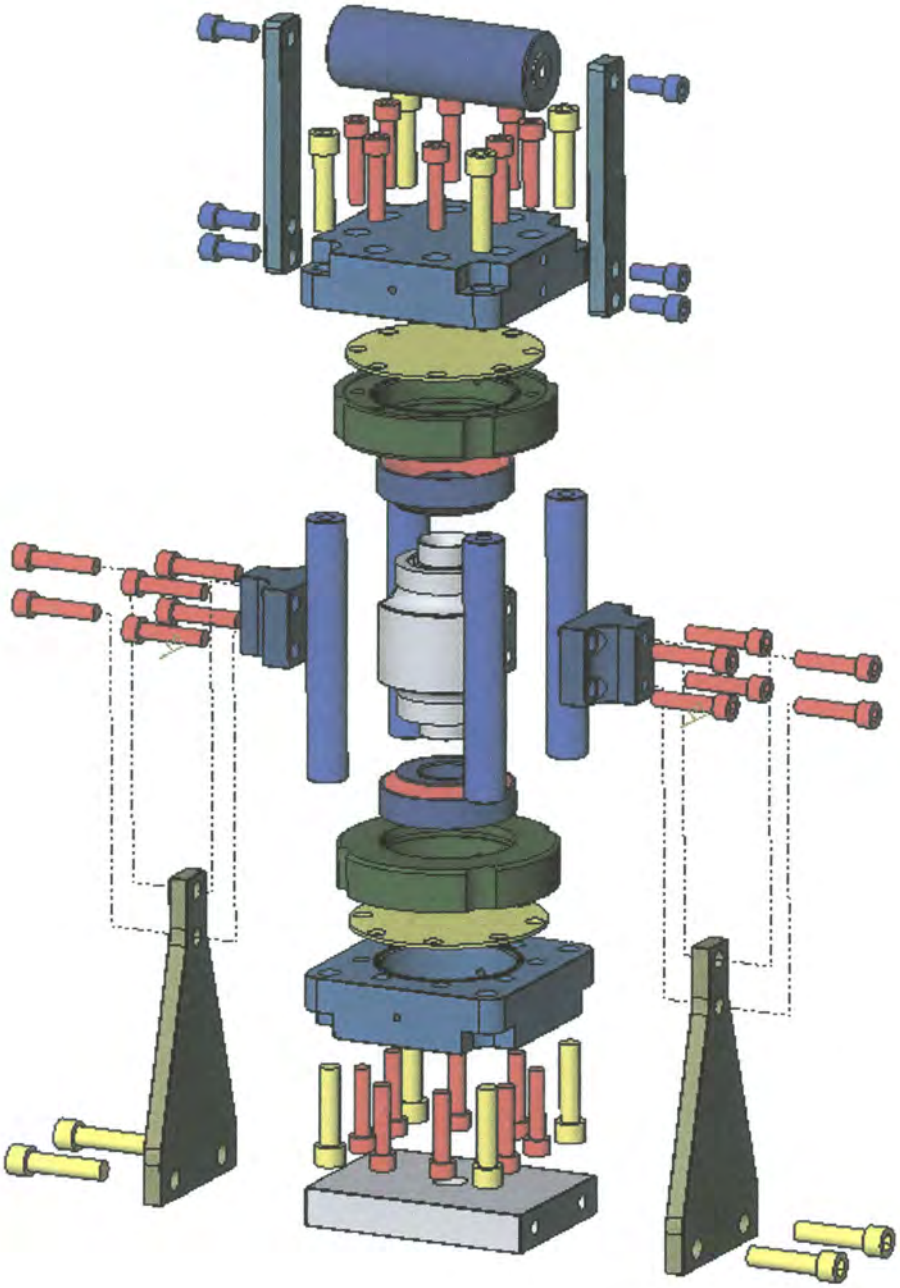

Figure 4.38: Exploded view of the type I AVAI

The major dimensions of the AVAI, are shown in Figure 4.39. The length of the AVAI is determined by the space needed for the operators hand, the port, reservoir and air spring length and the gap needed between the AVAI and the back of the drill. The length of the air spring and reservoir was discussed before. The gap between the drill and the handle is determined by the amplitude of the displacement of the drill, which was estimated to be a maximum of 8 mm. The length of the port is determined by the ratio of port and reservoir diameters. It is possible to shorten the device by increasing the diameter, but this will decrease the distance between the springs, which will affect its rotation angle when the moment is applied.

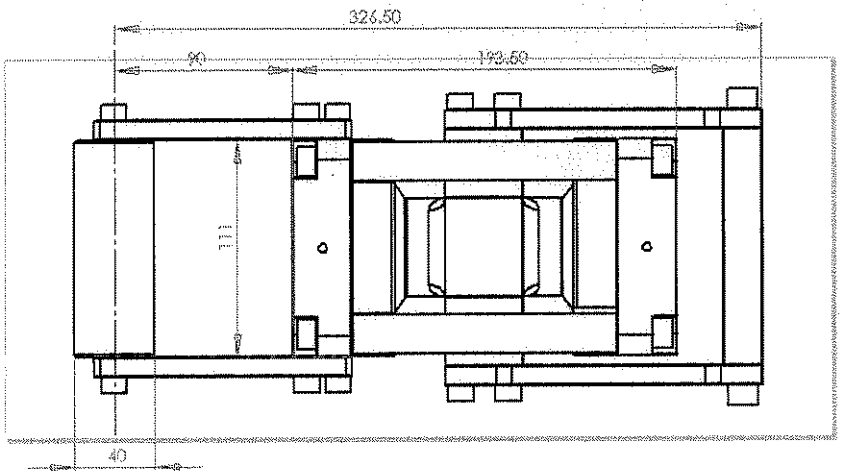

Figure 4.39: Major dimensions

The design dimensions are shown in Figure 4.40. A large air spring height was chosen because it could easily be made smaller later, while making it larger would be difficult. In fact, after testing the spring height was changed to 5 mm by fixing a plastic disc inside the spring.

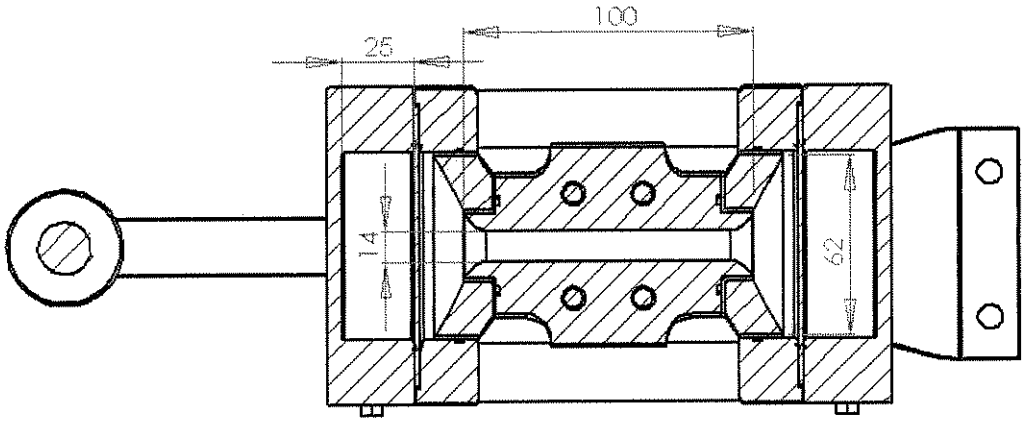

Figure 4.40: Design dimensions

The preceding section showed how the spring stiffness of the primary spring and the air spring could be estimated. Although the formulas could be used for an initial design, it is clear that there is some uncertainty in the exact values. For this reason the absorber will be designed so that it can be modified easily. After manufacture it is possible to reduce the air spring height as well as the port diameter.

The effect of the air spring can be examined by considering the total stiffness of the two rubber membranes and the air spring (Equations (4.19) and (4.20)):

$$k_u = 2\frac{64\pi Et^3}{3d_b^2\left(1-\nu^2\right)} + \frac{2nP\frac{A_b}{3}}{h} \tag{4.39}$$

where t is the membrane thickness, $d_b = 62$ mm is the reservoir diameter, $h = 25$ is the reservoir height, n is the ratio of specific heats and P is the pressure in the air spring and is assumed to be equal to the supply line pressure during steady state operation. For an operating pressure between 300 and 600 kPa the membrane stiffness will be between ~5 and 45 times less than the air spring stiffness. The choice of membrane material should be such that the stiffness of the membrane is minimised while providing an adequate seal under the severe environmental conditions of a mine. The reason for minimising the membrane stiffness is to reduce its contribution to the total damping of the air spring. Lubricants in the air supply rule out the use of natural rubber. Typical elastomer sheet materials are Nitrile and silicone and both can be used in this application. The effect of the air spring height on the isolation frequency can be found by solving the air spring stiffness and then calculating the isolation frequency:

$$\omega_i = \sqrt{\frac{1}{\left(\frac{1}{\bar{\omega}_1}\right)^2 + \frac{1}{\mu_k}\left(\frac{1}{\bar{\omega}_2}\right)^2}} \tag{4.40}$$

When calculating the frequencies in the above equation the area ratio used is the reduced area ratio that compensates for the conical geometry of the primary spring. The reduced area ratio is:

$$A_r = \frac{1}{3}\frac{A_b}{A_a}\left[\left(\frac{d_o}{d_b}\right)^2 + \frac{d_o}{d_b} + 1\right] \tag{4.41}$$

where $d_o = 30$ mm is the inner diameter of the conical section, A_a is the port diameter defined by $d_a = 14$ mm. The effect of air spring height on the isolation frequency is shown in Figure 4.41.

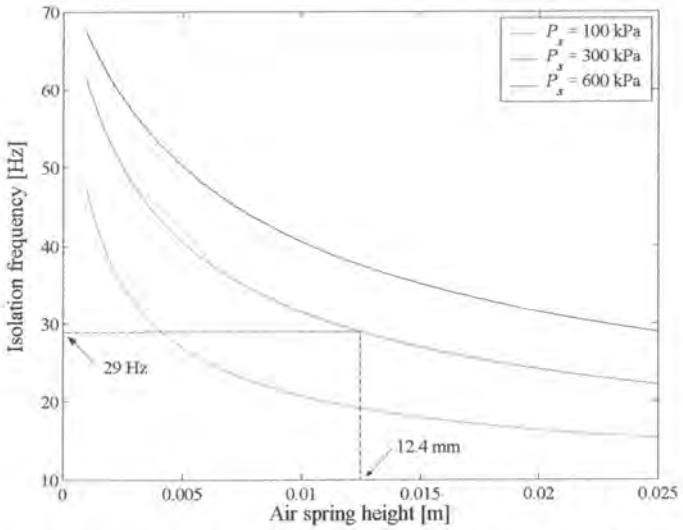

Figure 4.41: Isolation frequency *vs.* air spring height

The frequency range covered by the change in pressure is a function of the air spring height. The required frequency change from 300 to 600 kPa is ~8.5 Hz with the isolation frequency equal to 29 Hz at 300 kPa. Figure 4.42 shows that heights between 2.7 and 13 mm will have the required range.

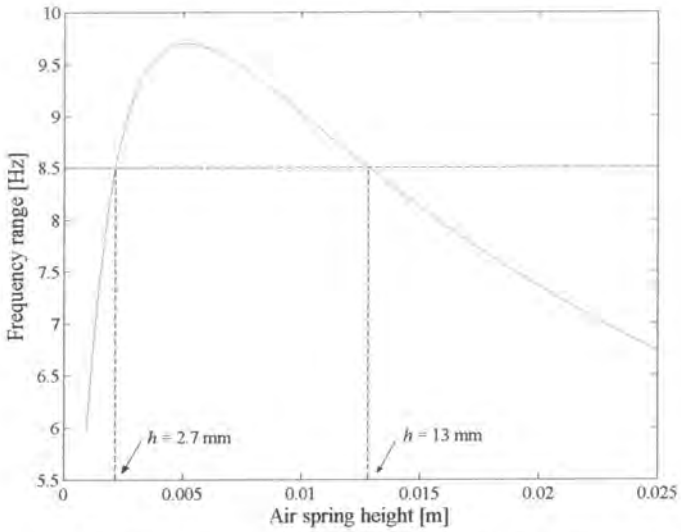

Figure 4.42: Frequency range (P_s = 300 and 600 kPa) *vs.* air spring height

By choosing the air spring height to be 13 mm the isolation frequency will be close to the excitation frequency (refer Figure 4.12) over a wide frequency range, as shown in Figure 4.43. Also shown in the figure is the bandwidth, which can be seen to envelop most of the excitation frequencies. The damped and undamped isolation frequencies are plotted and since the difference is small it is recommended that the undamped isolation frequency be used for design purposes. In production there will be significant differences between individual AVAIs. To compensate for this the AVAI could be designed with an air spring height that can be varied externally with a mechanism. Each AVAI can then be tuned before being used. Tuning could also be effected by keeping the air spring at atmospheric pressure and varying its height, as shown by Ting-Kong (1999).

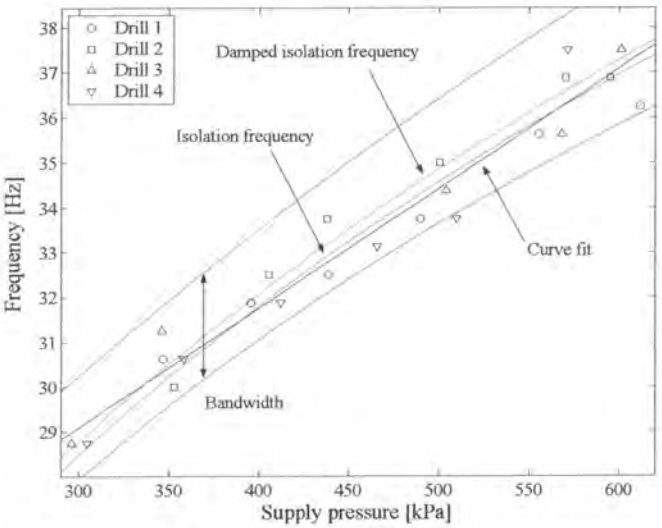

Figure 4.43: Excitation and isolation frequency *vs.* supply line pressure (h = 13 mm)

To estimate the benefit of adding an AVAI, the response to the measured excitation was simulated. Three cases were considered. In the first case the device is tuned using the supply line pressure i.e. the spring stiffness as a function of air spring pressure shown in Equation (4.39) was used. This should be the least effective method since differences between individual drills and the estimated average is not taken into account as can be seen from Figure 4.43. A second simulation shows the effect when the AVAI is tuned using a control system that forces coincidence of the isolation and excitation frequencies while the damping ratio is kept constant. The excitation frequency is determined by calculating the FFT of the input excitation and finding the frequency at which the maximum occurs. The transmissibility is then minimised at the excitation frequency using an optimisation algorithm to calculate the optimal stiffness. The third case employs a control system to minimise the weighted rms acceleration by adjusting both the stiffness and the damping. The simulation used the PSD method to calculate the weighted rms acceleration. The weighted rms was minimised using both the stiffness and damping as variables in an optimisation algorithm. The methods are summarised in Table 4.6.

Table 4.6: Summary of tuning methods

Method	Stiffness	Damping
1	Derived from supply line pressure	Constant
2	Optimal	Constant
3	Optimal	Optimal

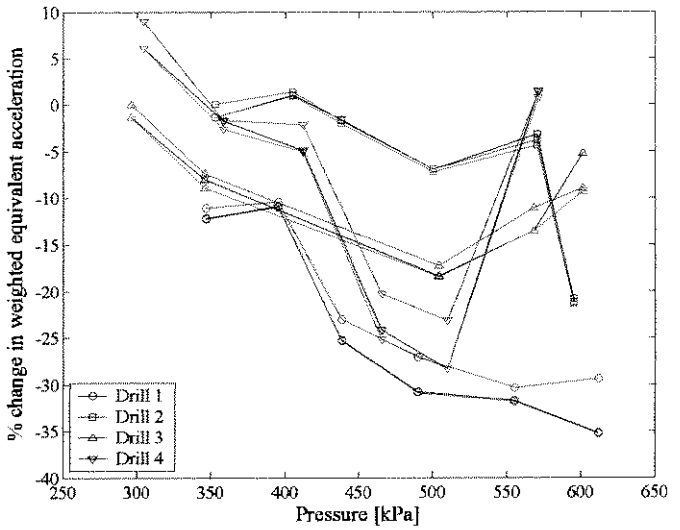

Figure 4.44: Percentage change in the weighted equivalent acceleration with the addition of a type I AVAI using the supply line for tuning (red), tuning the device using the excitation frequency (black) and perfect tuning (blue)

The percentage change in weighted rms acceleration for an AVAI tuned using the supply line pressure only is shown in Figure 4.44 in red. The most benefit is achieved at higher pressures and at best a ~35% reduction was achieved. At low pressures it is possible that the AVAI can increase the weighted equivalent acceleration. The percentage change in weighted equivalent acceleration for an AVAI tuned to the excitation frequency is shown in Figure 4.44 in black. This result is better than if the supply line

only was used. This case does not necessarily represent the maximum benefit possible, since a situation can exist where a detuned AVAI results in lower weighted rms acceleration.

For such a case the objective function will be the weighted rms acceleration and most ideally, both the stiffness and damping will be adjusted to minimise this quantity. A typical objective function for such a case is shown in Figure 4.45. Clearly, a minimum value does exist and if the AVAI can be adjusted to this value it will be perfectly tuned for this application. Simulation for a perfectly tuned case found that there is little benefit in choosing such a method. This is shown in Figure 4.44 in blue. This might not always be the case and for some applications it could be beneficial to use such an objective function instead of more simplistic methods. The net result of tuning the type I AVAI using the supply line pressure is shown in Figure 4.46. The target of 10 m/s^2 is not reached in the majority of circumstances.

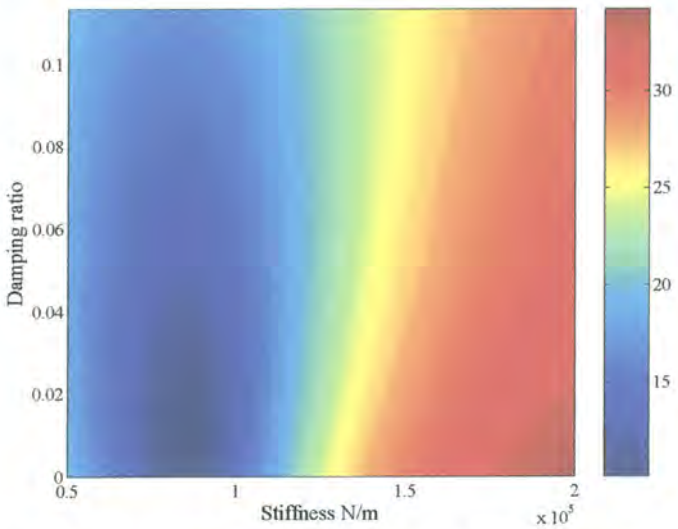

Figure 4.45: A typical objective function for an AVAI with adjustable stiffness and damping

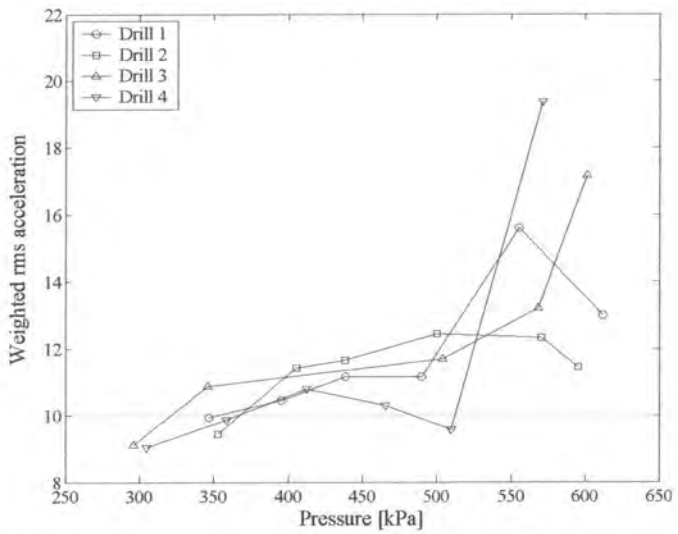

Figure 4.46: Simulated weighted rms acceleration for a type I AVAI tuned using the supply line pressure

4.5 Type II amplified vibration-absorbing isolator

This section will document the design of the type II absorber, where initially the effect of noise in the input will be assessed and thereafter the actual design will be discussed.

4.5.1 Narrow-band excitation with noise

The parameters used in the comparison between the type II AVAI and an isolator is shown in Table 4.7. The isolator stiffness ratio was held constant at the lowest value used for the tuned AVAI to allow for fair comparison. For each case the AVAI was tuned to the centre of the excitation frequency ($\bar{\omega}_e$) by changing the stiffness ratio. A comparison of the isolator and type II AVAI are shown in Figure 4.47.

Table 4.7: Parameter values used for the comparison

Description	Parameter	Value
Centre frequency of excitation	$\bar{\omega}_e$	10
Frequency bandwidth	$\Delta\Omega_e$	20
Mass ratio	ω_n/ω_i'	0.5
Stiffness ratio	μ_k	21.6...25

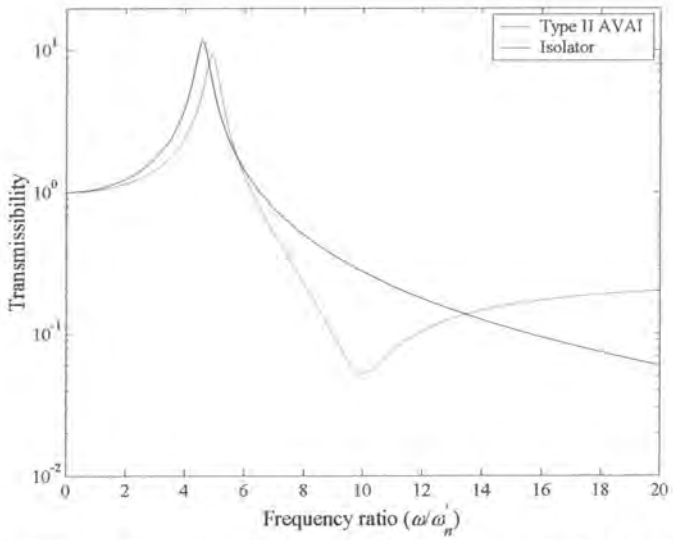

Figure 4.47: Type II AVAI and isolator used in the comparison

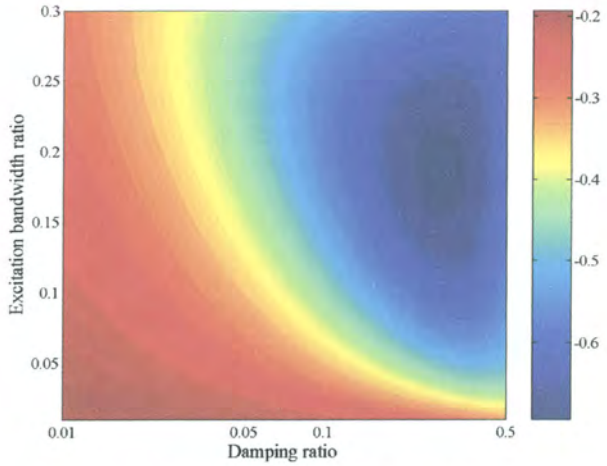

Figure 4.48: The logarithm of the ratio of ratios for a case with noise ratio 10^{-3}

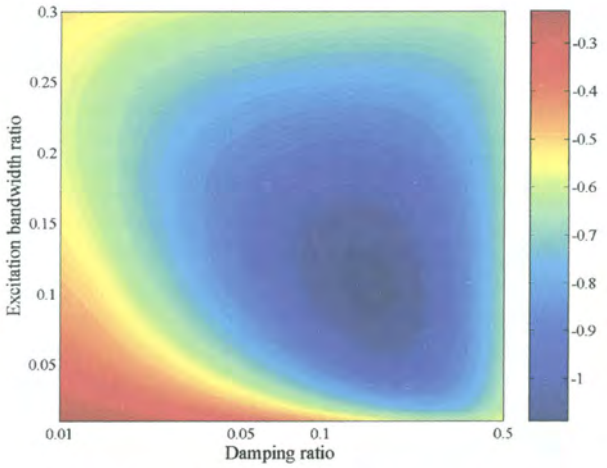

Figure 4.49: The logarithm of the ratio of ratios for a case with noise ratio 10^{-4}

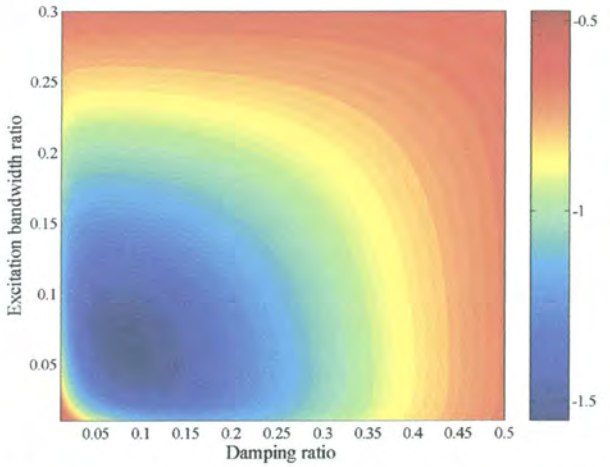

Figure 4.50: The logarithm of the ratio of ratios for a case with noise ratio 10^{-5}

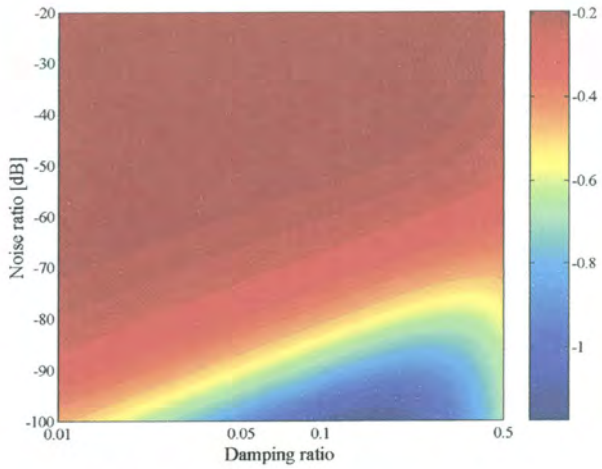

Figure 4.51: The logarithm of the ratio of ratios for a case with excitation bandwidth ratio 0.01

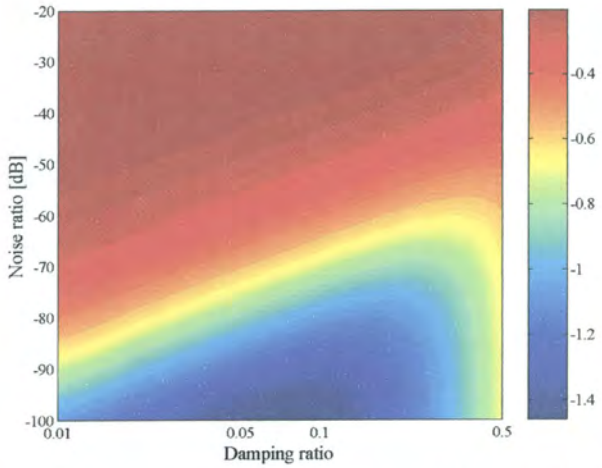

Figure 4.52: The logarithm of the ratio of ratios for a case with excitation bandwidth ratio 0.1

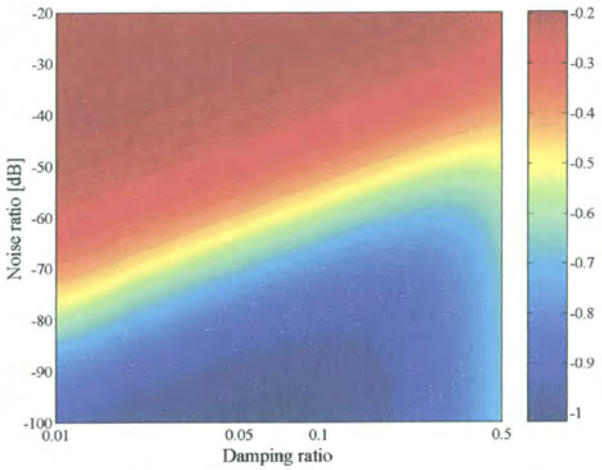

Figure 4.53: The logarithm of the ratio of ratios for a case with excitation bandwidth ratio 0.2

Figure 4.48 through Figure 4.50 show the damping required as a function of excitation bandwidth ratio when the noise ratio is kept constant. The figures show that as the noise ratio is increased, more damping is needed. It also shows that the benefit of using an AVAI is the most at small noise ratios and small excitation bandwidth ratios. Figure 4.51 through Figure 4.53 confirm that the damping must be increased as the noise ratio increases. Figure 4.48 through Figure 4.53 show that an optimal value of damping exists for each noise and excitation bandwidth ratio. In each of the cases considered here it was more advantageous to use a tuneable AVAI. As was discussed in §4.4.1, it will be difficult to prescribe a damping ratio during the design process.

4.5.2 Type II AVAI design

A schematic of the type II AVAI is shown in Figure 4.54. It consists of a port with a Teflon bearing in which a tungsten carbide slug with a sliding fit is mounted. The tungsten carbide is ground to a smooth finish and has a density of ~14500 kg/m^3. The Teflon bearing is press-fitted and then machined to provide the sliding fit. The air spring is similar to the one used in the type I AVAI and consists of a pressure supply line connected to the air spring cavity via an orifice. The reservoir is filled with fluid, which transfers the motion to the slug, resulting in the amplification of the slug motion. Preferably the fluid will have low viscosity and provide some lubrication, but due to the filling method used it was not possible to use oil, and water had to suffice. A small gap exists between the slug and the Teflon bearing through which leakage can occur. The initial design proposed the use of slug stops as shown in Figure 4.55. The purpose of the slug stop is to equalise the volume of fluid in the two reservoirs. After considerable difficulty with the experimental work it was decided to replace these with slug springs. The only disadvantage of using slug springs is that they can add damping to the system through turbulence in the fluid. They will also cause an increase in the isolation frequency, but by choosing their stiffness to be small this effect will be negligible.

It may be possible to provide a positive seal between the slug and the port by using a metal bellow or a rolling diaphragm seal, but this will be costly. The large amplitude and number of cycles needed might even make this method infeasible. It could also be possible to provide a pressure-activated leakage path between the two reservoirs. When the slug impacts the stop, leakage will occur between the two reservoirs. Instead of becoming completely solid, the leakage will provide additional damping and decrease the shock load due to the impact.

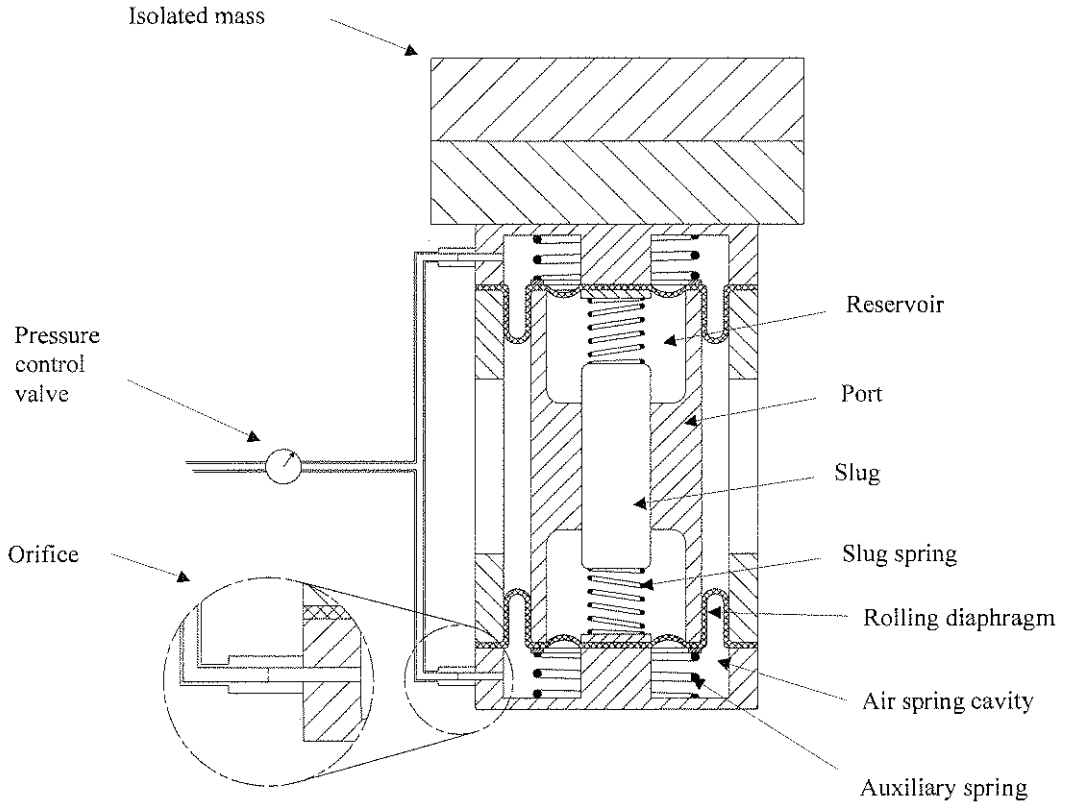

Figure 4.54: Schematic of type II AVAI design

The flexibility between the port and the reservoir is provided by a rolling diaphragm seal. This seal also acts as the air spring boundary. Rolling diaphragms are zero-leakage seals that offer very little frictional damping since the relative motion between the seal and the contact surface is small. Additionally, the diaphragms are reinforced with polyester that do not stretch and will therefore have a low loss factor. These seals have a limited number of standard sizes, which will put a constraint on this design that was not present for the type I AVAI.

The volume of the spring is determined by the average of the inner and outer diameter of the rolling diaphragm and the diameter of the inner diaphragm mount as shown in Figure 4.55. The port and the groove in the sleeve must be machined according to the manufacturer's specification to ensure that the diaphragms seal properly and have adequate durability. When the seal rings are fitted the seal tends to bulge. This is advantageous because it provides some low stiffness flexibility between the reservoir and the port. The maximum relative amplitude is ~2 mm. The maximum motion possible can be increased by fitting a custom made diaphragm with a second convolution in the reservoir area. This second convolution should face towards the air spring as shown in Figure 4.56. Such a diaphragm configuration will however make it impossible to transfer a moment from the handle to the drill. As discussed in §4.2 the drill handle must transfer a large moment and this will have to be done in some different way if this method is used.

It is possible to provide a bearing to transfer the moment. The bearing will have to be low friction such as a linear ball bearing or an air bearing. An air bearing could work well since air is readily available, but air consumption must be low for it to economically feasible. However, the space available for an air bearing is also very limited.

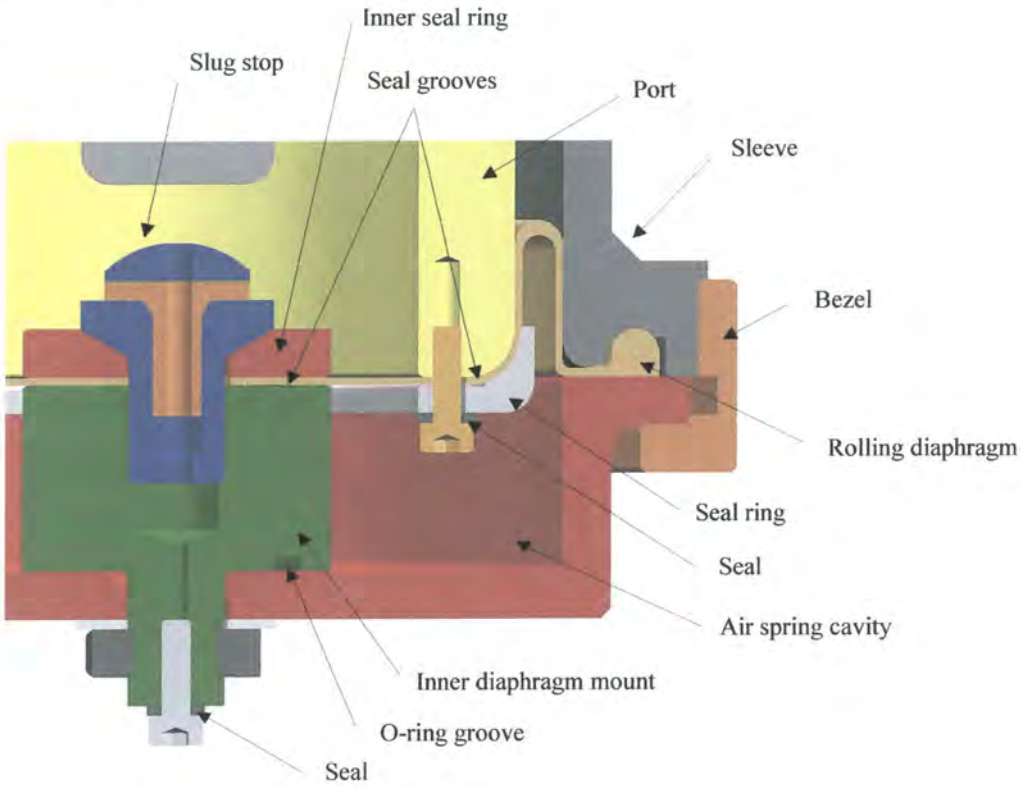

Figure 4.55: Air spring design

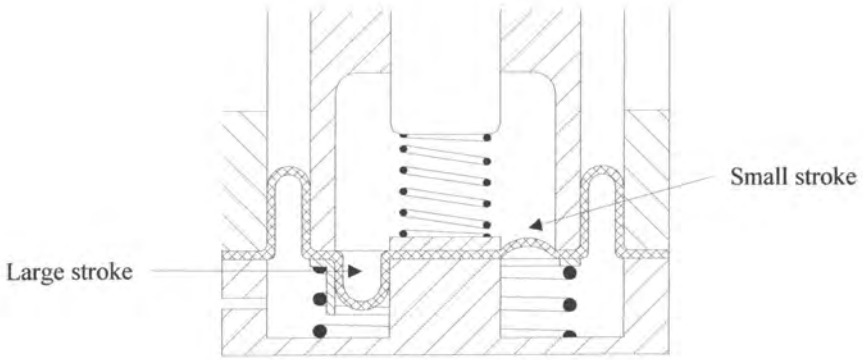

Figure 4.56: Possible diaphragm designs

The purpose of the auxiliary spring in Figure 4.54 is to centre the port vertically. In an application where the load is not variable the auxiliary spring will be chosen to off-set the mass of the supported machine. Under variable load the springs must ensure that the port will always be in a position where the maximum displacement amplitude can be accommodated.

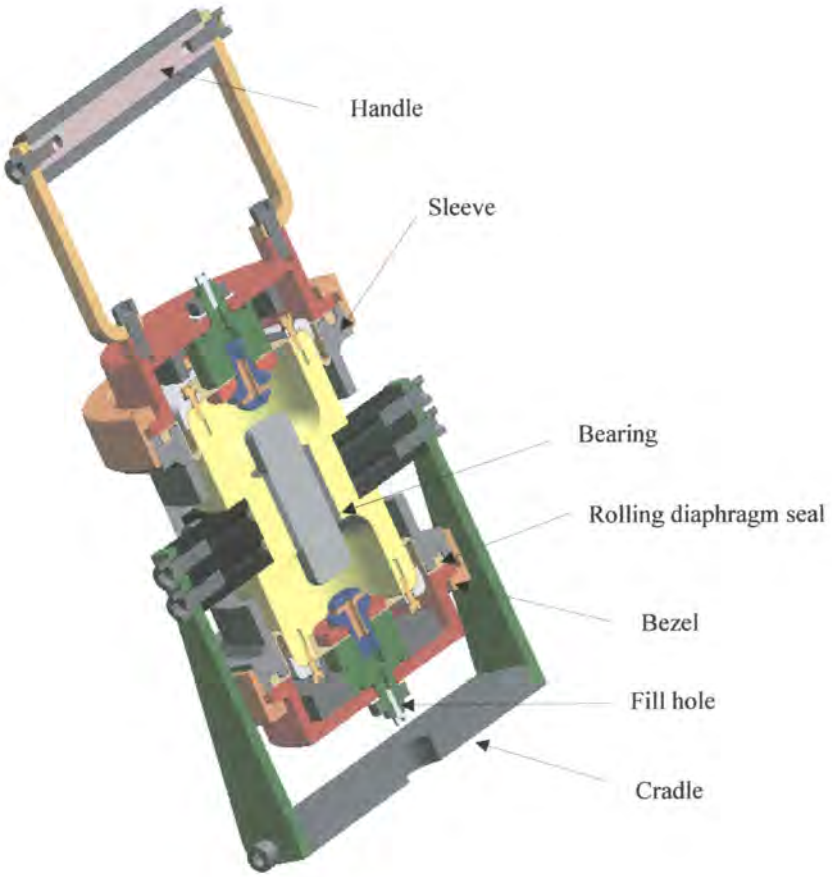

Figure 4.57: Important features of the type II AVAI design

The reservoir must be filled without trapping air bubbles, which will be compressible and decrease the effective reservoir area. This proved to be a challenge. Options available include pressurising the fluid in the reservoir, vacating the air in the reservoir cavity before filling it with fluid, or assembling the reservoir parts while submerged. The last method is difficult to execute, but does not put additional strain on the design and was therefore preferred. Securing the air spring cavity to the sleeve can be done in a number of ways, as long as the rolling diaphragm seal can be accommodated. For this design it was decided to use a bezel rather than bolts on a flange to reduce the diameter of the device as shown in Figure 4.55. Because the bezel was chosen the air spring cavities were not separated by spacing rods as for the type I design, but by a flanged section of hollow bar (sleeve) as shown in Figure 4.57. The sleeve was also necessary to provide a supporting surface for the rolling diaphragm.

Freudenberg's standard rolling diaphragms are available from an outer diameter of 16 mm up to 200 mm. To ensure optimal use of space the reservoir diameter must be as large as possible, but it is limited by the sealing requirements for the diaphragm seal. The seal is bolted onto the port using a seal ring. Four M3 cap screws were used which proved difficult to work with (smaller crews should not be considered). To ensure that no leakage occurs at the cap screw a washer was added which consisted of

a flat metal ring with an internally bonded trapezoidal rubber seal. Initially the holes were positioned too close to the reservoir and it did not seal properly. The holes were moved closer to the radius, which solved the leakage problem. Thus, with significant difficulty the diameter of the reservoir could be maximised to 50 mm using a 70 mm inside diameter rolling diaphragm. The rolling diaphragm is relatively fragile and caution must be exercised not to twist it while tightening the bezel or the inner seal ring.

If it is assumed that the diaphragm deforms as shown in Figure 4.58, an effective reservoir area can be calculated.

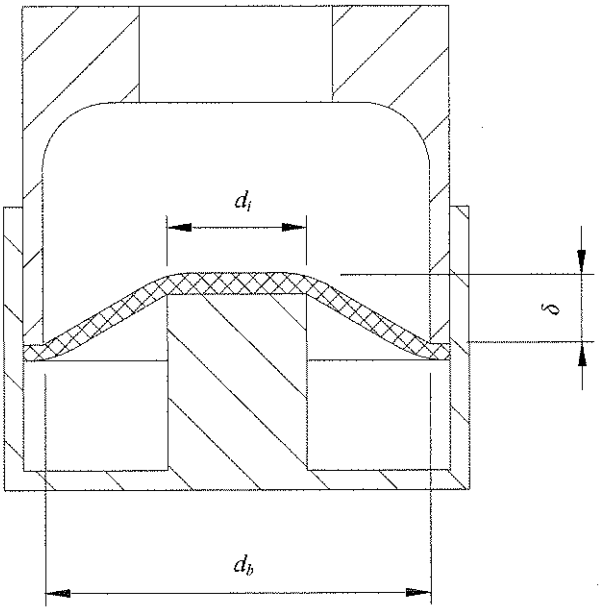

Figure 4.58: Dimensions for the calculation of the effective area

The effective reservoir area is [Equation (D.14)]:

$$A_e = \frac{\pi}{12}\left(\frac{d_b^3}{d_b - d_i} - \frac{d_b d_i^2}{d_b - d_i} + d_i^2\right) \tag{4.42}$$

The effective area ratio can be maximised by choosing the inner diameter d_i as large as possible. A large inner diameter will, however, limit the displacement that can be achieved. The major dimensions of the design are shown in Figure 4.59 and Table 4.8. The device is smaller and considerably lighter than the type I design. Two slugs were manufactured; one with a diameter of 16 mm and one of 20 mm. Changing the slug size requires the remanufacture of the bearing only.

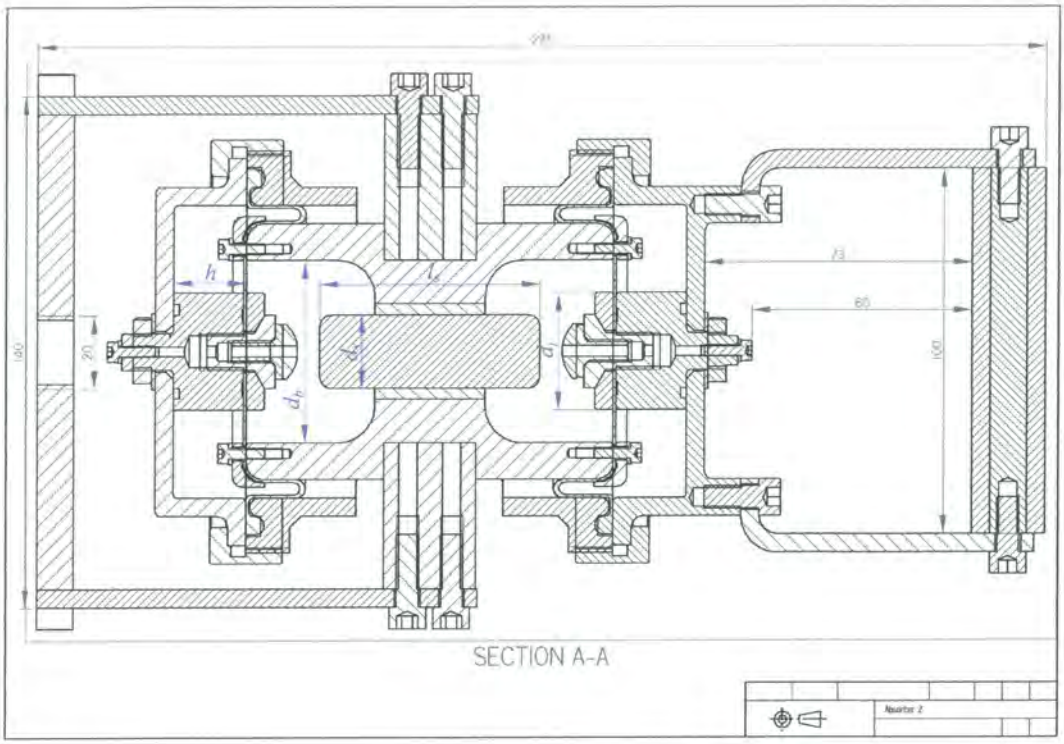

Figure 4.59: Major dimensions of the type II AVAI

Table 4.8: Type II design parameters

	Variable	Value
Slug diameter [mm]	d_s	16, 20
Reservoir outer diameter [mm]	d_b	50
Reservoir inner diameter [mm]	d_i	32
Isolated mass [kg]	m	3.5
Density [kg/m^3]	ρ	14500
Slug length [mm]	l_s	60
Effective area ratio	A_e/A_a	4.27, 6.67
Air spring outer diameter [mm]	d_s	75
Air spring height [mm]	h	20
Damping ratio	ζ	0.05

The travel required by the slug is dependent on the area ratio and the input displacement as shown in chapter 2. The AVAI is designed for a base input of 2 mm as discussed in §4.3. Assuming that the device is perfectly tuned and including the effects of damping, the relative displacement between the handle and the base is 1.74 mm. The slug travel will be 7.43 mm for the 20 mm slug and 11.61 mm for the 16 mm slug. The present design has provision for 12 mm of travel, which is deemed adequate for prototype purposes.

The design requires that the damped isolation frequency coincide with the excitation frequency for all the supply pressures. If no auxiliary spring is used then the results will typically be as shown in Figure 4.60. It is not possible to change the slope and the y-axis intercept independently by only changing the

air spring dimensions. One possibility is to change the area ratio or slug diameter in conjunction with the air spring dimensions. Since there are several implications when changing these values, for instance, slug travel, it is proposed that an auxiliary spring should be used instead. The air spring height and the auxiliary spring stiffness can now be used to independently change the slope and y-axis intercept. The total stiffness can be written as:

$$k = k_p P_s + k_c \tag{4.43}$$

where k_p is the coefficient defining the air spring dimensions and k_c represents the auxiliary spring. The values for k_p and k_c can be calculated by considering two sets of supply pressure (P_s) and excitation frequency (Ω_e) data points defined by the curve fit in Figure 4.60 [Equation (D.21)]:

$$\begin{bmatrix} k_p \\ k_c \end{bmatrix} = \frac{\left[m + m_B \left(\frac{A_b}{A_a} \right)^2 \right]}{\frac{-\left(\frac{\omega_n}{\omega_i} \right)^2 - 1 - \sqrt{\left[\left(\frac{\omega_n}{\omega_i} \right)^2 - 1 \right]^2 + 8\zeta^2 \left[\left(\frac{\omega_n}{\omega_i} \right)^2 + 1 \right]}}{4\zeta^2 + 4\zeta^2 \left(\frac{\omega_n}{\omega_i} \right)^2 - 2\left(\frac{\omega_n}{\omega_i} \right)^2}} \begin{bmatrix} P_1 & 1 \\ P_2 & 1 \end{bmatrix}^{-1} \begin{bmatrix} \Omega_{e1}^2 \\ \Omega_{e2}^2 \end{bmatrix} \tag{4.44}$$

The result of such a design is shown in Figure 4.61. The damped isolation curve coincides with excitation frequency curve fit at the design points of 290 and 620 kPa. Instead of using only two points it is also possible to calculate the stiffness to minimise the least squares difference between the isolation and excitation curves. In this case it does not appear to be worth the effort since all the measured excitation frequencies fit comfortably within the bandwidth. Of course, as the damping is reduced the bandwidth will decrease making the matching process more difficult.

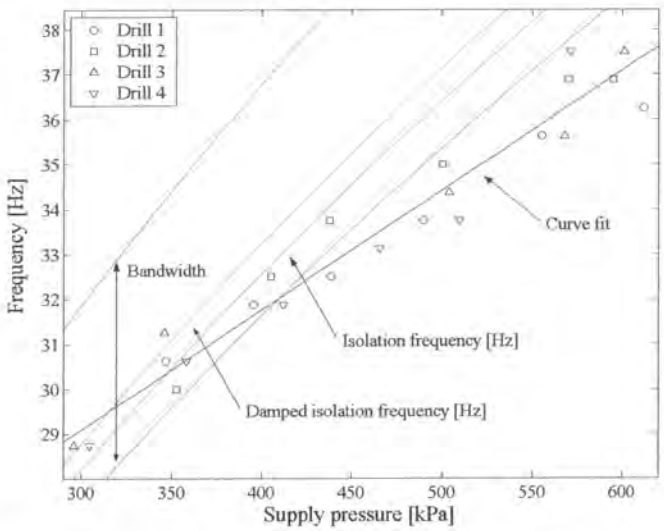

Figure 4.60: Excitation vs. isolation frequency for a system without an auxiliary spring (d_a = 16 mm and h = 14.6 mm)

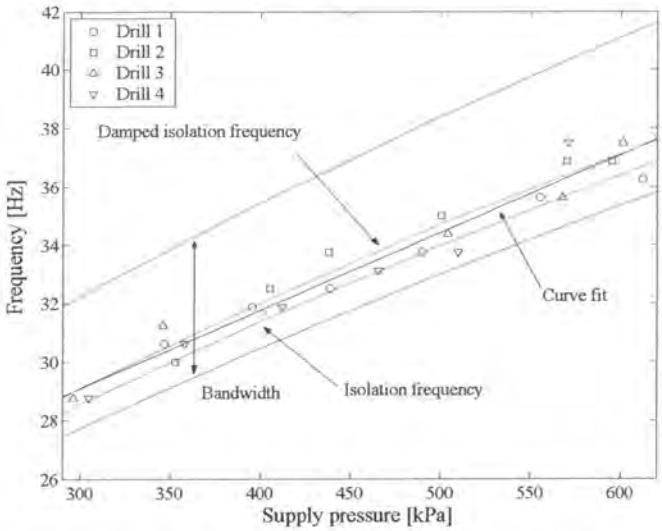

Figure 4.61: Excitation vs. isolation frequency for a system with an auxiliary spring (d_a = 16 mm, h = 22.6 mm and k_c = 80320)

When the design is complete the challenge that remains is to manufacture an airspring and auxiliary spring that fit the specifications. Tolerance values on springs, helical or otherwise, can be quite large and it would be necessary to tune each device at considerable expense. Of course, if a control system is used, exact matching becomes less important since the control system can compensate. In such a case the initial design only needs to be in the vicinity of the frequency range covered as long as it is exceeded by the device's isolation frequency range capability.

The performance of a system tuned using the supply line is shown in Figure 4.62 in red. The benefit ranged from 5% to 50%, but importantly it was never detrimental as in the case of the type I AVAI. By tuning the device to the excitation frequency only slight benefit is gained as shown in Figure 4.62 in black. When optimising both the damping and stiffness to minimise the weighted rms acceleration the performance is significantly better, as indicated by the blue curve. This is in contrast with the type I AVAI where the gain was not considerable. The weighted rms acceleration with the addition of the type II AVAI is shown in Figure 4.63. The acceleration values are below 10 m/s^2 at low supply pressure.

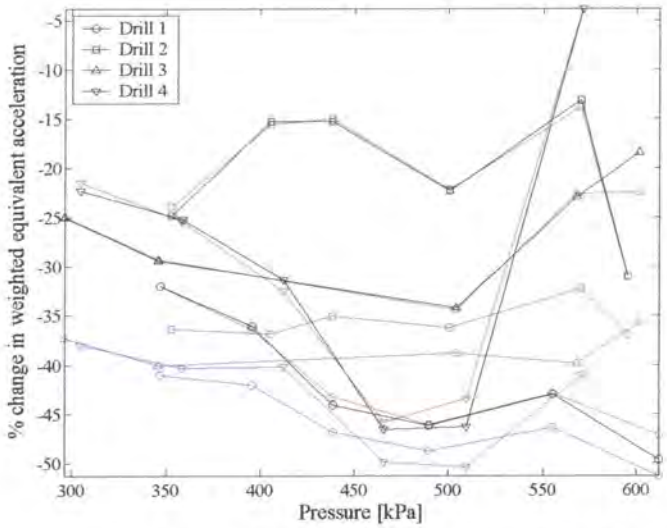

Figure 4.62: Percentage change in the weighted equivalent acceleration with the addition of a type II AVAI using the supply line for tuning (red), tuning the device using the excitation frequency (black) and perfect tuning (blue)

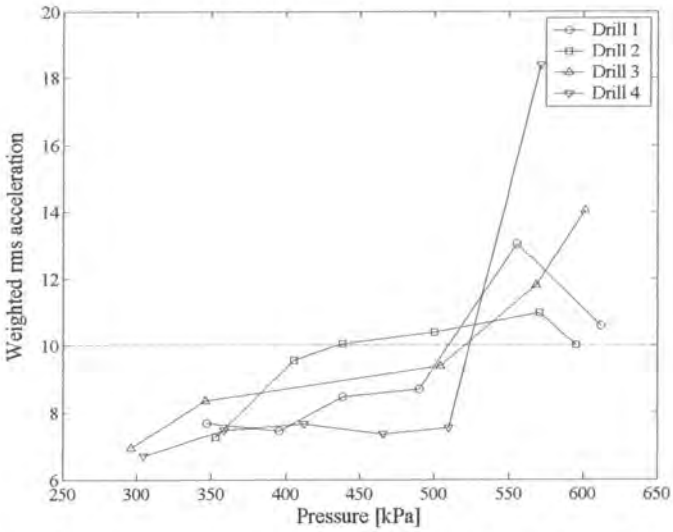

Figure 4.63: Simulated weighted rms acceleration for a type II AVAI tuned using the supply line pressure (PSD method)

4.6 Conclusion

This chapter introduced the concepts applicable to the design of a vibration-isolated handle. The vibration levels of pneumatic rock drills used in the South-African mining industry were shown to be in excess of the exposure limit for short duration rms weighted acceleration permitted under the proposed European Union legislation. Maximum measured values on these drills were 18.72 m/s^2. Two types of vibration absorber were designed and evaluated. Simulation showed that by using a type I AVAI the acceleration levels could be reduced significantly but not to the required levels for all the

drills. The type II AVAI levels were reduced to below 10 m/s^2 up to a pressure of 500 kPa for three of the drills tested. Supply line pressure at the rock face is in South African mines are mostly below 400 kPa.

5 Experimental results

5.1 Introduction

This chapter documents the experimental results of the two AVAIs. The experiments measured the transmissibility in the frequency domain. The results were processed to obtain the parameters that were uncertain during the design process by fitting the analytical models to the experimental results. This will aid future designs of similar absorbers since more accurate models will be available. The experimental set-up measured transmissibility as shown in Figure 5.1. The AVAI was fitted to a hydraulic actuator. Both Zonic and Schenck actuators were used, which were controlled by a custom built PID controller. It was not possible to recreate the amplitudes that the AVAI would experience on a drill, but it was sufficient for characterisation. The air spring was fitted to a 6 bar air supply via a Festo pressure control valve. Accurate pressure readings of the supply pressure were obtained from a strain gauge type GEM pressure transducer. An assortment of PCB ICP accelerometers and signal conditioners were used. A Spectral Dynamics Siglab 20-42 FFT analyser sampled the data. It was also used to supply the various excitation signals.

In the second part of this chapter the manual pressure regulator was replaced by a servo operated valve system that could be controlled with a National Instruments 6024E DAQ card. This was done to show that the device could be used in a closed-loop sense in a system where the excitation frequency can vary arbitrarily.

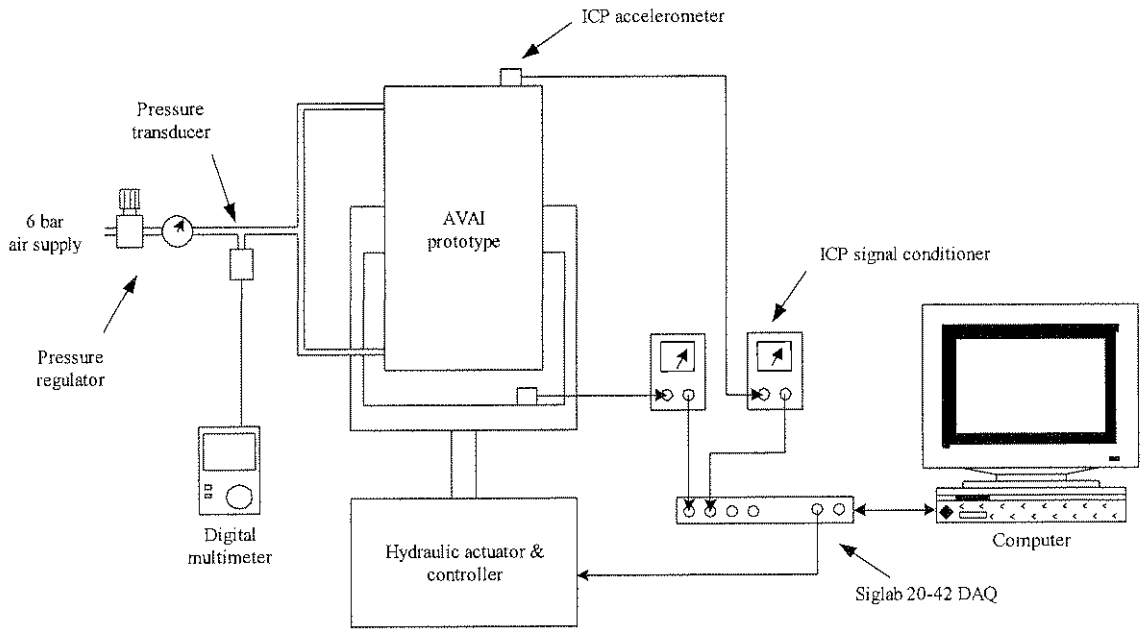

Figure 5.1: Transmissibility measurement set-up

5.2 Type I AVAI

5.2.1 Experimental results

The experimental set-up is shown in Figure 5.2. Here the AVAI was fitted to a Zonic hydraulic actuator and controller. Four 10 kg weights were incrementally added to the AVAI (recall that the mass of the AVAI on the isolated side is 7.5 kg). The stepped sine excitation method was used with a 0.2 Hz frequency resolution from 10 to 70 Hz. This method gave good results, with the lowest correlation measured being 0.98. Acceleration measurements were done with 100 mV/g PCB ICP accelerometers. The pressure was varied using a manual pressure regulator in increments of ~50 kPa from 0 to 600 kPa.

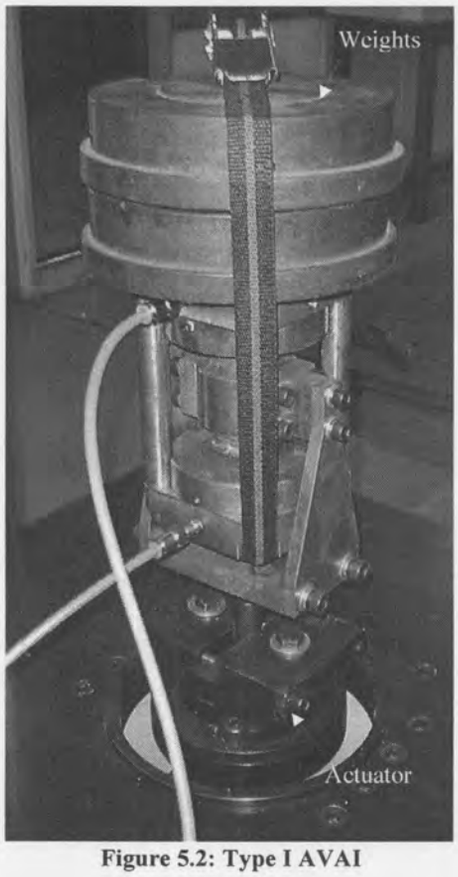

Figure 5.2: Type I AVAI

A set of transmissibility curves measured in this way is shown in Figure 5.3, where it is compared to an undamped conventional isolator with a similar natural frequency as reference. Also shown is a straight-line curve fit through the points off minimum transmissibility at each frequency. These points do not necessarily coincide with the isolation frequency since the minimum transmissibility is also a function of pressure. The points were calculated by finding the intercept of the slope of each curve with the following curve. The envelopes of all the curves are shown in Figure 5.4. As could be expected, the transmissibility is lower as the isolated mass is increased.

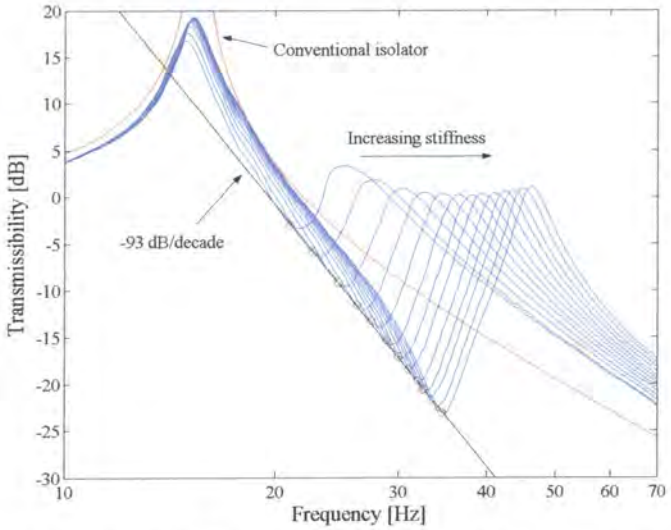

Figure 5.3: Change in transmissibility as the air spring stiffness is increased for a 37.5 kg isolated mass (The red circle indicates the lowest transmissibility at a specific frequency, p_s = ~0..600 kPa)

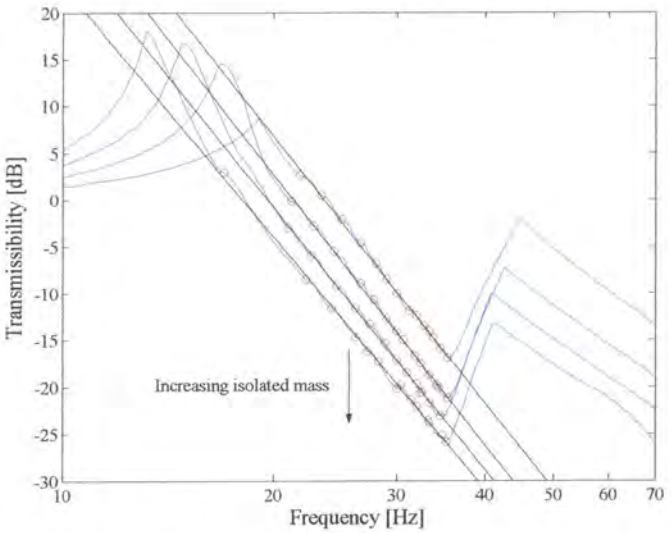

Figure 5.4: Transmissibility curve envelopes for the 4 isolated masses (The red circle indicates the lowest transmissibility at a specific frequency)

When compared to an undamped conventional isolator over the frequency range of the AVAI the performance is significantly better. The calculated roll-off is summarised in Table 5.1.

Table 5.1: Roll-off results

Isolated mass [kg]	Roll-off [dB/decade]
17.5	-94.7
27.5	-95.9
37.5	-93.0
47.5	-89.3

To calculate the isolation frequency and bandwidth from the measured data it was necessary to fit a curve through the data to find an accurate estimate. A typical result of one such 2nd degree polynomial curve fit is shown in Figure 5.5. A number of data points close to the isolation frequency were used for the curve fit. The resulting polynomial was used to find the isolation frequency as well as the frequencies defining the bandwidth (ω_1 and ω_2).

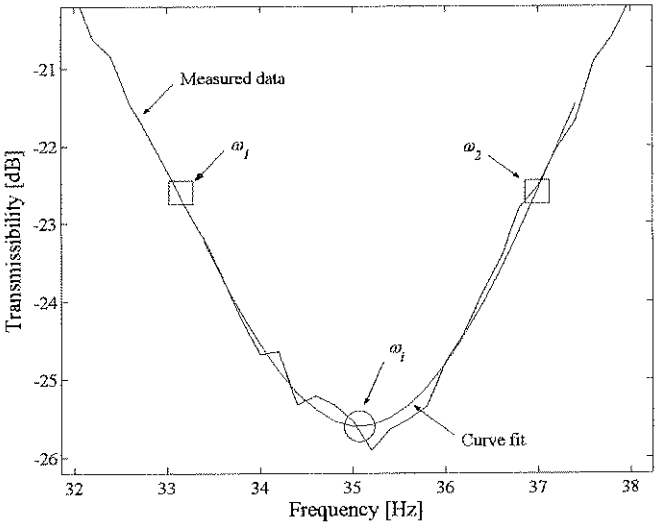

Figure 5.5: Curve fit to calculate the isolation frequency and bandwidth

The isolation frequencies as a function of pressure calculated using this method is shown in Figure 5.6. The AVAI covered a frequency range of ~12 Hz. By fitting a 2nd degree polynomial through the data the following relationship between the supply pressure (p_s in bar) and excitation frequency (f_e in Hz) was found:

$$p_s = 0.0247 f_e^2 - 0.9884 f_e + 9.8658 \tag{5.1}$$

This equation can be used in an open-loop control system.

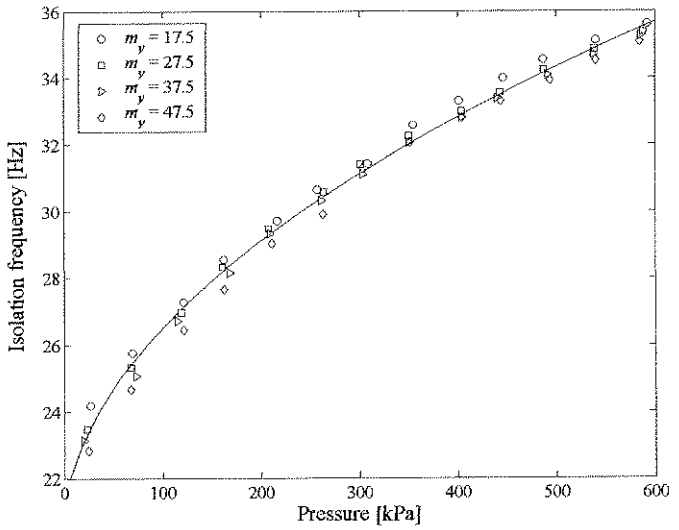

Figure 5.6: Isolation frequency curve fit

The robustness and bandwidth are calculated using the definitions in Equation (2.20) and Equation (2.21) and are shown in Figure 5.7.

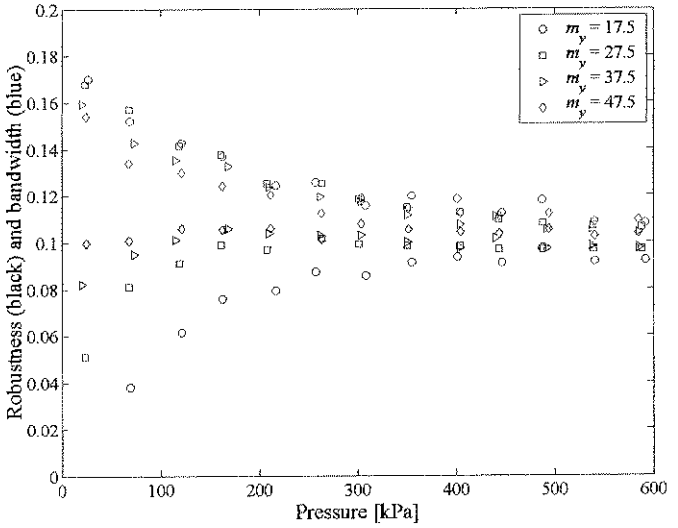

Figure 5.7: Robustness and bandwidth *vs.* supply pressure

The frequency range of the absorber is compared to the drill excitation frequency in Figure 5.8. With some modification it should be possible to ensure that the isolation frequency falls within the 95% confidence intervals of the excitation frequency.

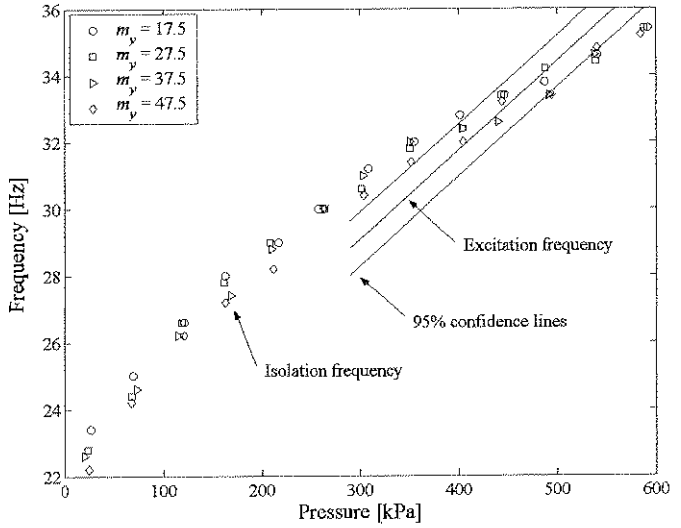

Figure 5.8: Isolation frequency *vs.* supply pressure

5.2.2 Parameter estimation

The parameters were estimated by fitting theoretical models to the experimental data. The purpose was to extract the unknown physical properties, namely stiffness and damping. Mass values were not fitted but rather measured, since this significantly improved the quality of the curve fit. The curve fit method

chosen minimised the sum of the least squares error between the predicted and measured values at each measured frequency. The value at each frequency was normalised by the sum of the squares in order to allow equal weight of values at maximum as well as minimum transmissibility. This allowed a good fit over the entire measured frequency band. The objective function used is:

$$F = \sum_{f=f_1}^{f_2} \frac{\left[|T_r'(f)| - |T_r(f)|\right]^2}{\left[|T_r'(f)| + |T_r(f)|\right]^2} \tag{5.2}$$

where T_r' is the measured transmissibility, T_r is the predicted transmissibility and f the frequency. Only the absolute values of the transmissibility were used. The standard Matlab optimisation algorithm `fmincon.m` was used to minimise the objective function. It was found that good initial values are essential for a converged solution. Several models were fitted to the measured data. Although some of the curve fits provided results that appeared valid, on closer inspection this was found not to be the case. The main problem was how to compensate for the effects of spring and membrane geometry. Initial attempts used a compensation factor for membrane size as a variable in the optimisation algorithm, but these did not provide accurate estimates of the membrane stiffness. Finally an accurate model accounting for both membrane and spring geometry was developed (refer to Appendix E). The model is shown in Figure 5.9.

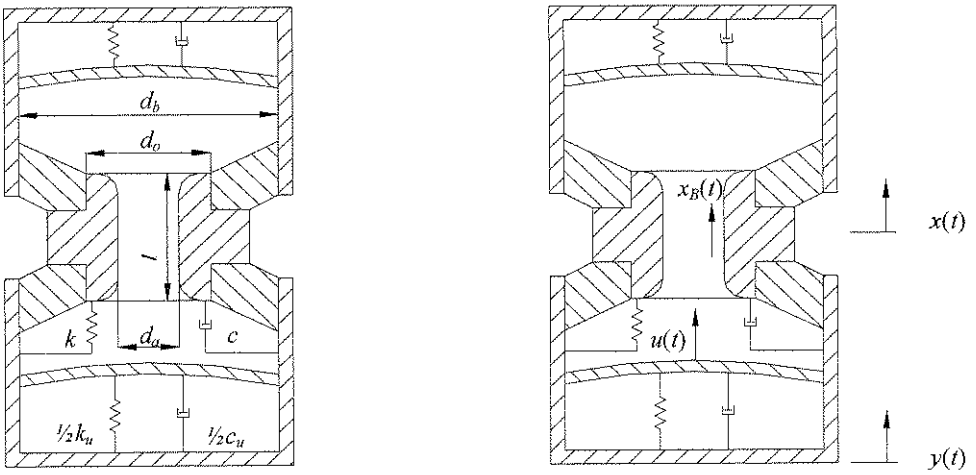

Figure 5.9: Type I AVAI model accounting for geometrical effects

The main difference in this model is that the effect of the conical primary spring geometry as well as the deformed shape of the membrane is taken into account when calculating the continuity equation [Equation (E.10)]:

$$x_B = C_1 y - C_2 x + C_3 u$$

$$\text{where: } C_1 = \frac{1}{3}\frac{A_b}{A_a}\left[\left(\frac{d_o}{d_b}\right)^2 + \frac{d_o}{d_b} + 1 - S_f\right]$$

$$C_2 = \frac{1}{3}\frac{A_b}{A_a}\left[\left(\frac{d_o}{d_b}\right)^2 + \frac{d_o}{d_b} + 1\right] - 1 \tag{5.3}$$

$$C_3 = S_f \frac{A_b}{A_a}$$

S_f is the membrane shape factor and is 1 if the membrane edge has the same displacement as its centre, ½ if its deformation approximates a paraboloid and ⅓ if a fixed (no rotation) boundary condition is assumed (Appendix E).

If excitation occurs at the x degree of freedom the transmissibility is [Equation (E.23)]:

$$\frac{Y}{X}=\frac{-\omega^2 m_B C_2 C_3\left(k_u+i\omega c_u+\omega^2 m_B C_1 C_3\right)+\left(k_u+i\omega c_u-\omega^2 m_B C_3^2\right)\left(k+i\omega c-\omega^2 m_B C_1 C_2\right)}{\left(k_u+i\omega c_u-\omega^2 m_B C_3^2\right)\left[k+k_u+i\omega\left(c+c_u\right)-\omega^2\left(m_y+m_B C_1^2\right)\right]-\left(k_u+i\omega c_u+\omega^2 m_B C_1 C_3\right)^2} \tag{5.4}$$

The constant values used in the fitting procedure are shown in Table 5.2. The values for the remaining parameters were found with the curve fit procedure. Typical curve fits for a 47.5 kg isolated mass at 585 kPa and a 17.5 kg isolated mass at 592 kPa are shown in Figure 5.10. The complete dataset was used for the curve fits resulting in a compromised fit over the frequency band. If an accurate fit of the natural frequency is required the weight for that frequency range can be increased, but this will result in lower correlation at other frequencies.

Table 5.2: Constants in curve fitting

	Variable	Value
Port diameter [m]	d_a	0.014
Reservoir diameter [m]	d_b	0.063
Spring outer diameter [m]	d_o	0.050
Isolated mass [kg]	m_y	17.5 27.5 37.5 47.5
Density [kg/m^3]	ρ	1000
Port length [m]	l	0.1
Membrane shape factor	S_f	⅓

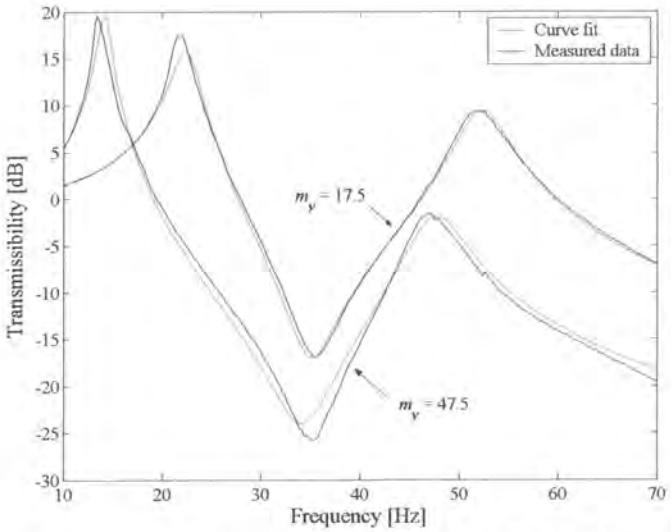

Figure 5.10: Typical curve fits for 47.5 kg at 585 kPa and 17.5 kg at 592 kPa

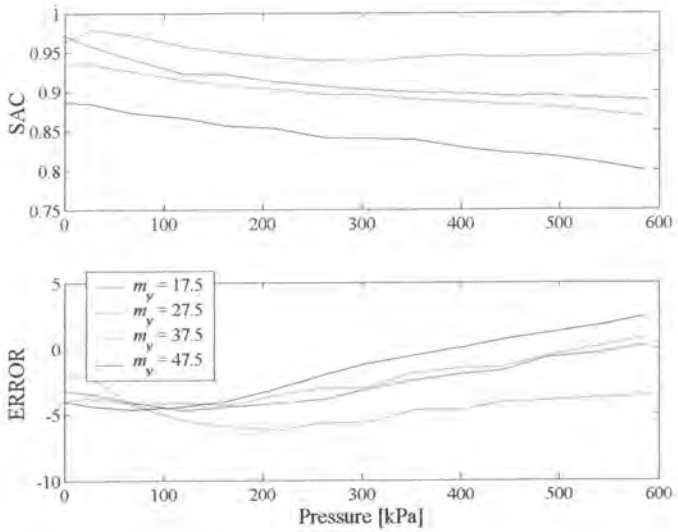

Figure 5.11: SAC and ERROR values *vs.* supply pressure

The quality of the curve fits was assessed by calculating the signature assurance criterion (SAC) and the ERROR values. These values are defined as (Dascotte & Strobbe, 1999):

$$\text{SAC} = \frac{\left|\alpha_X^H \alpha_A\right|^2}{\left(\alpha_X^H \alpha_X\right)\left(\alpha_A^H \alpha_A\right)}$$
$$\text{ERROR} = 100 \cdot \frac{\sum_{j=1}^{M} \alpha_{A_j} - \sum_{i=1}^{N} \alpha_{X_i}}{\sum_{i=1}^{N} \alpha_{X_i}} \tag{5.5}$$

α_X and α_A are the experimental and predicted transmissibilities respectively, and ^{H} denotes the Hermitian transpose. A SAC value of 1 indicates perfect correlation while the ERROR value should ideally be zero. The SAC and ERROR values are shown in Figure 5.11. The figure indicates good correlation between the model and the measured data. The correlation is better at lower isolated mass values. This can be explained by the deformation of the primary spring under static load, the effect of which can also be seen in the fitted parameter values shown in Figure 5.12. The primary system spring stiffness is a function of material property and geometry. It was observed that the geometry of the spring changes substantially due to static deflection, which explains the different values obtained. The maximum difference was 20%. The difference in values with pressure can also be explained by a change in geometry due to the pressure differential between the reservoir and atmosphere. The variation in primary system damping was less and because the damping is not expected to be a function of geometry. For the four isolated masses used the membrane stiffness was found to be similar in each case and consistently increased with pressure.

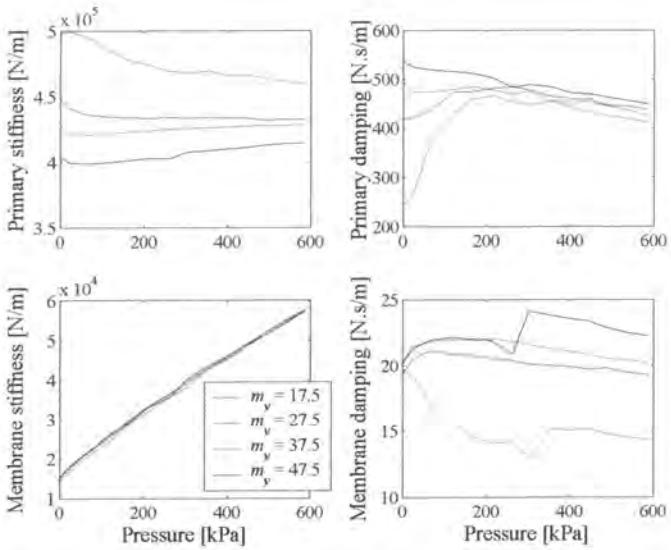

Figure 5.12: Fitted parameters

5.3 Type II AVAI

5.3.1 Experimental results

For these tests the AVAI was fitted to an Schenck hydraulic actuator. Random excitation was used and the 100 mV/g PCB ICP accelerometers were sampled with a frequency resolution of 0.156 Hz. The pressure was varied using a manual pressure regulator in increments of ~50 kPa from 0 to 519 kPa. Figure 5.13 shows the change in transmissibility as the supply pressure is increased. The envelope of these curves is shown in Figure 5.14. From this figure it is clear that the minimum transmissibility is a function of pressure. This is not predicted by the theory presented in Chapter 2 and is a result of the implementation. In contrast with the approach followed with the type I AVAI, in this case the theoretical model will not be updated to describe this effect since it is unwanted and it is believed that it will be possible to eliminate it by design. The device must therefore be changed to more closely represent the theoretical model and not the other way around. This approach will be followed in future work. Clearly there is a diminishing return in tuning since the transmissibility at the isolation frequency increases with increasing pressure.

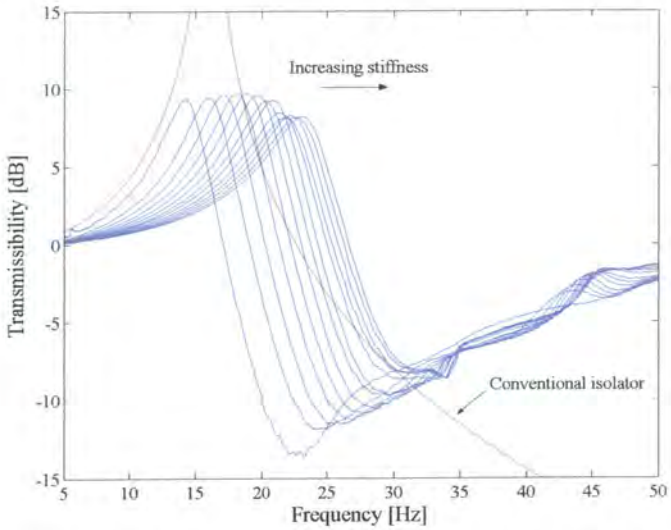

Figure 5.13: Change in transmissibility as the air spring stiffness is increased

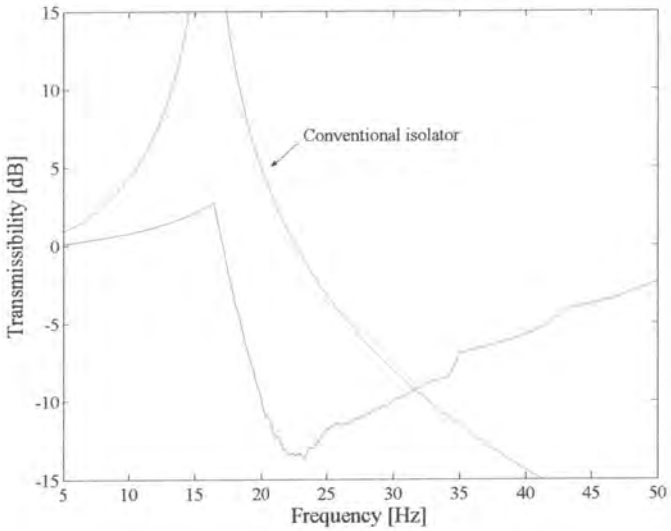

Figure 5.14: Transmissibility envelope

The isolation frequency was calculated as shown before in Figure 5.5, but in this case a 3rd degree polynomial was used since it was found to be more realistic. The relationship between isolation frequency and pressure is shown in Figure 5.15. The frequency range was between 23 at 32 Hz which is slightly too low for the pneumatic drill, but this can easily be remedied by reducing the air spring volume.

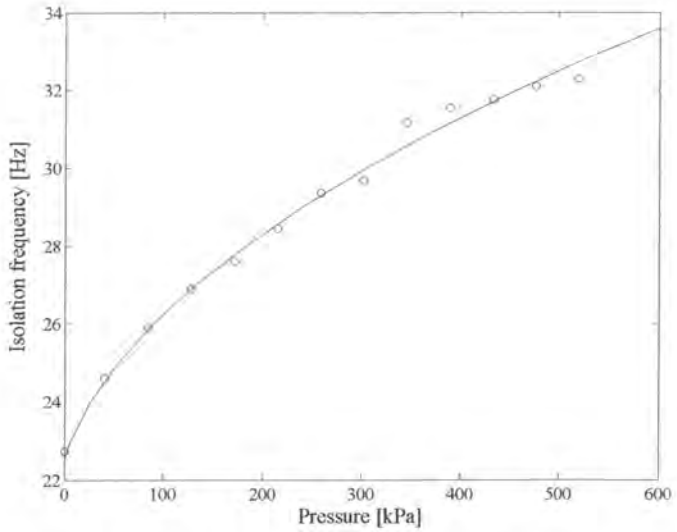

Figure 5.15: Isolation frequency *vs.* supply pressure

The supply pressure (p_s in bar) excitation frequency (f_e in Hz) relationship is:

$$p_s = 0.0371 f_e^2 - 1.5421 f_e + 15.8923 \tag{5.6}$$

It was found that the the bandwidth and robustness was not influenced by pressure as illustrated in Figure 5.16.

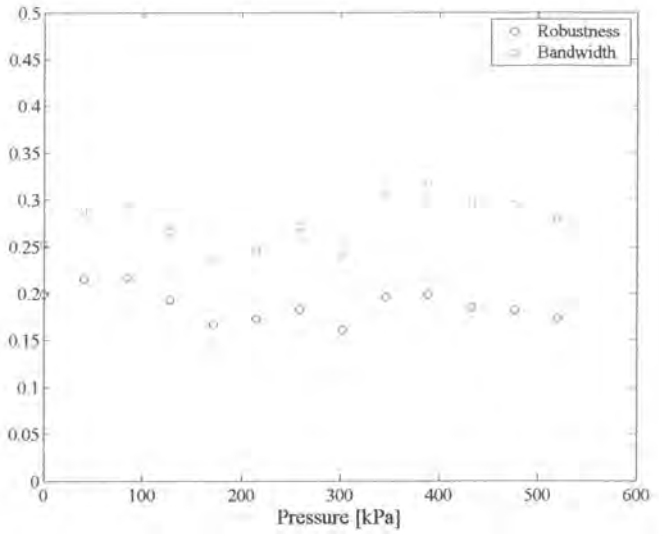

Figure 5.16: Bandwidth and robustness *vs.* supply pressure

5.3.2 Parameter estimation

The same parameter estimation procedure as for the type I AVAI was followed. In this case there are only two unknown parameters, namely the stiffness and damping. The constant values used for the curve fit are shown in Table 5.3. Again several models were fitted and it was found that some

inaccuracy is present in the area ratio estimation. The effective reservoir area ratio can be calculated as was shown in Chapter 4 by assuming a conical deformation of the membrane, while the maximum area ratio is given by reservoir area. If the area ratio varies with pressure then it will be expected to fall somewhere between these values.

Table 5.3: Constants used for curve fitting

	Variable	Value
Slug diameter [m]	d_a	0.02
Reservoir outer diameter [m]	d_b	0.05
Reservoir inner diameter [m]	d_i	0.032
Isolated mass [kg]	m	3.5
Density [kg/m^3]	ρ	14500
Slug length [m]	l_s	0.06
Effective area ratio	A_e/A_a	4.27
Maximum area ratio	A_b/A_a	6.25

A typical curve fit for various area ratios is shown in Figure 5.17. The red curve is the result when the area ratio is treated as a variable in the optimisation process. Normally one would not consider the area ratio to be variable, but due to the construction of the type II AVAI it is possible that small variations in area ratio can exist. This is due to air trapped in the reservoir region that will have an influence on continuity at low air spring pressures.

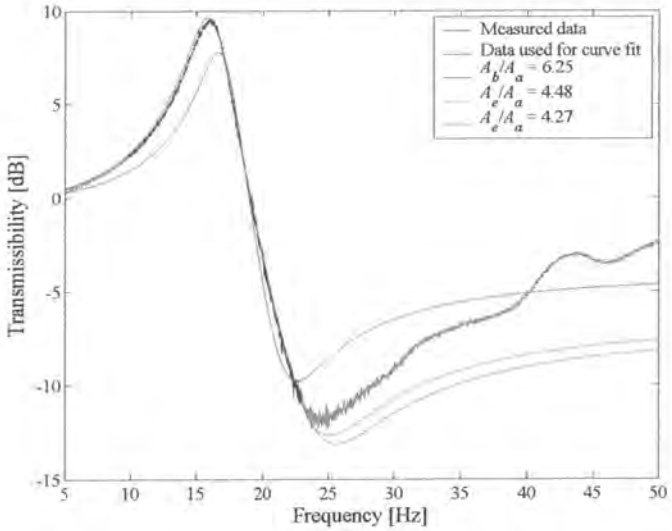

Figure 5.17: Curve fit comparison at 41 kPa

The fitted parameter results are shown in Figure 5.18. The stiffness was changed 3.6 times from 72 to 265 kN/m. At the normal operating pressure of the rock drill the stiffness is 187 kN/m, which is more than adequate since it resulted in a static deflection of 1.6 mm at 30 kg of force. The damping ratio is fairly constant at ~0.1, which is low, as would be expected from an air spring. The maximum difference between the calculated and effective area ratios is 30%. The area ratio remains a concern since it has a large influence on the design while it turned out to be difficult to estimate accurately. In future designs it should be considered to remove this uncertainty by using an additional convolution in

the bellow in the reservoir region. For such a case the area ratio is the average of the inner and outer diameters. The air trapped in the reservoir region should also be limited. Although attempts have been made to minimise any trapped air, additional measures such as pressurising the reservoir can be considered.

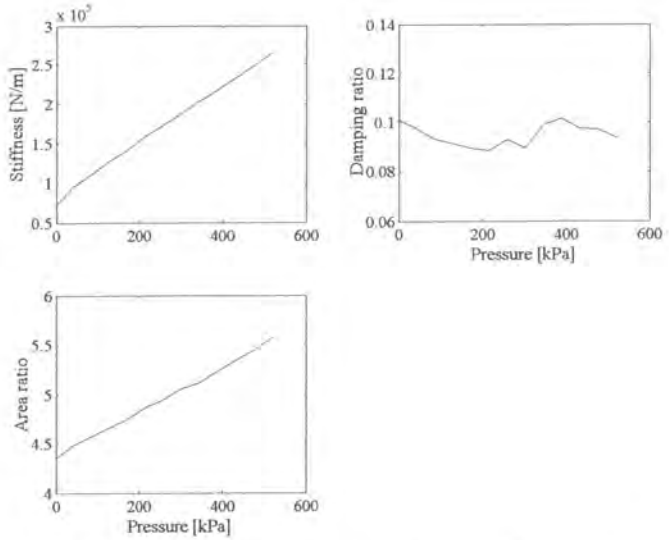

Figure 5.18: Fitted values for stiffness, damping and area ratio *vs.* supply pressure

The quality of the curve fits is not as good as for the type I AVAI as shown by the SAC and ERROR values in Figure 5.19. These values confirm that the variable area ratio fit is more accurate and therefore the parameters for stiffness and damping ratio for this model are believed to be more precise (Figure 5.18).

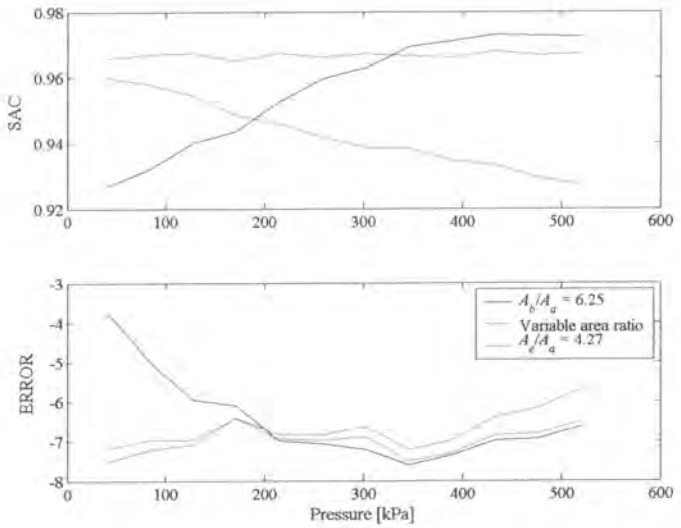

Figure 5.19: SAC and ERROR values *vs.* supply pressure

5.4 Control

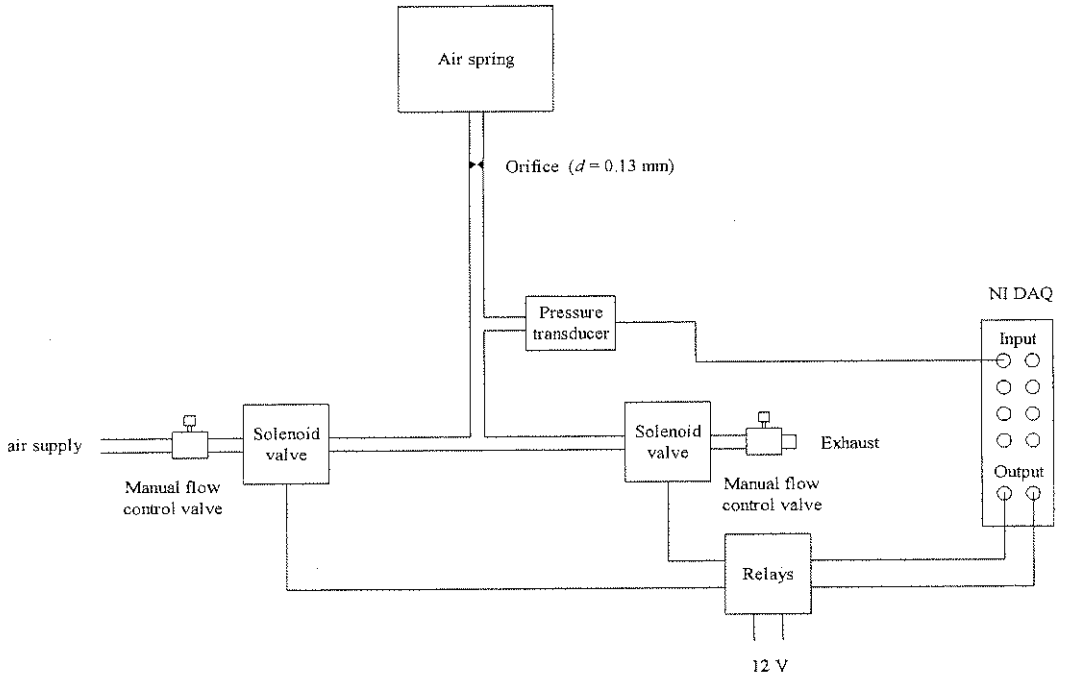

Figure 5.20: Pressure control valve

To demonstrate that the AVAI can be controlled to minimise the transmission of varying tonal excitation, the experimental set-up of Figure 5.1 was modified such that the manual pressure regulator was replaced by electronically controlled solenoid valves as shown in Figure 5.20. Although electronic pressure regulators are available as standard items from pneumatic equipment suppliers, it was decided to build one using components that were readily available. The advantage of this decision was cost effectiveness, but the time needed to change the pressure was significantly longer. Since the objective of this experiment was to show that the control method works and not the speed at which it could change the isolation frequency, the valve system was considered adequate.

The operation of the control system for the supply pressure is explained in Figure 5.20. The National Instruments 6024E DAQ card was nsed to open the appropriate valve and sample the pressure transducer simultaneously. The pressure transducer is located in the supply line before the orifice and not inside the airspring. This location is necessary to make sure that the pressure fluctuation in the airspring, as it is compressed, does not inflnence the measurements. The fluctuation in the supply line due to the air spring operation will of course be a lot less because of the orifice. Once the pressure reached the command pressure within adeqnate accuracy, the valve was closed. After the valve is closed leak-flow will occur to or from the air spring through the orifice resulting in the pressure changing to a value outside the specified tolerance. To make sure that the command pressure is reached the pressure is sampled again after a short delay and reset if necessary. This procedure continued until the pressure stabilised. In practice the pressure was set after ~5 attempts. The pressure set procedure is explained in the flow diagram shown in Figure 5.21.

A practical aspect to consider when setting the pressure is the case where the optimisation algorithm calculates a pressure that cannot be obtained physically. If, for instance, a pressure of 700 kPa is computed, the pressure set algorithm will be sent into an endless loop since the supply pressure is only 600 kPa. This can, of course, be remedied easily by using a constraint on the maximum stiffness, hut even here caution is necessary. If, for instance, the algorithm uses a penalty function approach it could calculate a stiffness value outside the achievable range. Another such case occurs when a finite difference calculation tries to use an out-of-range stiffness value to calculate the derivative. The above issues are particular to the algorithm used and each design must therefore be carefully studied to ensure safe operation under all conditions.

Only the type I AVAI was used to demonstrate the controllability. The standard Matlab optimisation algorithm `fmincon.m` was used for this purpose. This function is an implementation of the sequential quadratic programming (SQP) optimisation algorithm and can handle constraints. Since it is assumed that the excitation is tonal, it is possible to calculate the transmissibility in the time domain by simply dividing the rms output by the rms input value of a short set of sampled values, as was explained in Chapter 3. It would be possible to minimise the rms output only, but that would not take account of varying input amplitude. The objective function used is:

$$f(p) = \frac{\frac{1}{T}\sum_{i=1}^{N} \ddot{y}_i^2}{\frac{1}{T}\sum_{i=1}^{N} \ddot{x}_i^2} \tag{5.7}$$

where $\ddot{x}$ is the input and $\ddot{y}$ the output acceleration.

The excitation frequency can be estimated using zero-crossings, which is a fast and effective technique for tonal signals. Using an FFT can also be considered, but it does have some disadvantages, notably the time required for an accurate estimate. For this experiment the mean period of a number of zero-crossings was used to calculate the excitation frequency. To make sure that the measured signal does not contain frequencies other than the excitation frequency, a 6^{th} order Butterworth band-pass filter was applied before the estimation process.

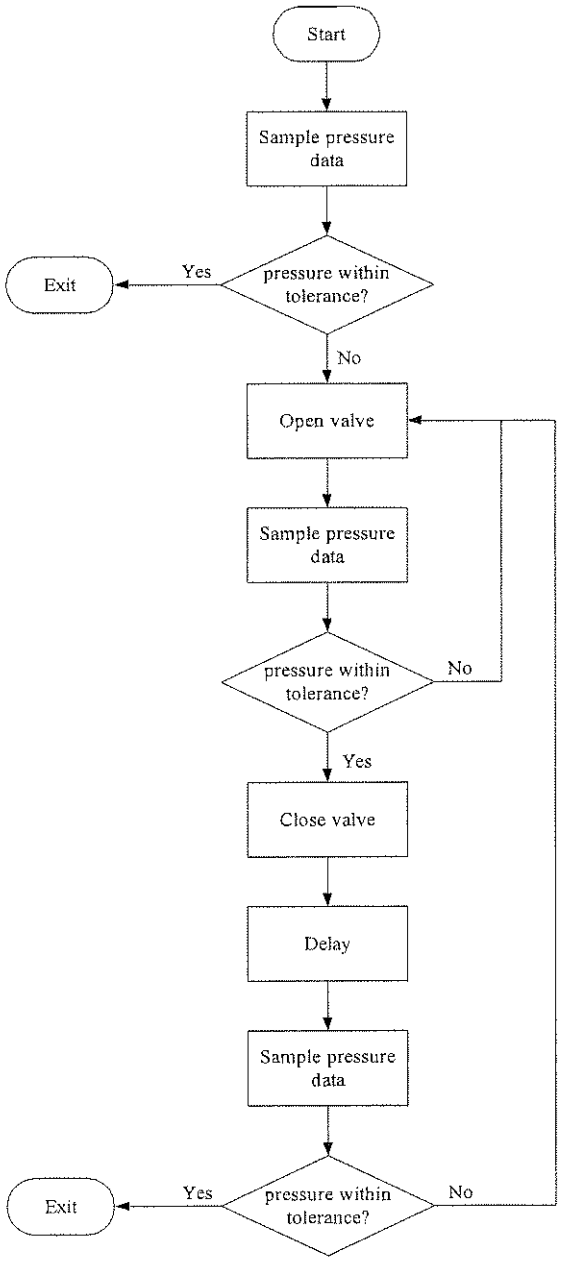

Figure 5.21: Pressure set flow diagram

The flow diagram of the control process is shown in Figure 5.22. Initially the device is tuned using the isolation frequency obtained from the characterisation test. After the pressure is set using this open loop technique, the optimisation algorithm is started in an attempt to find a better solution. The excitation frequency is calculated for each measurement of the objective function and if a change of more than 10% is observed the optimisation problem is restarted. For a practical system the change in excitation frequency allowed will be set according to the system bandwidth and the expected rate of change in excitation frequency. In the control process a constraint on the stiffness value was calculated to ensure that a too low stiffness does not make convergence impossible. The need for the constraint

was discussed in Chapter 3. The experimental 2nd frequency of maximum transmissibility value calculated from the characterisation test was used as the constraint:

$$\hat{p}_s = 0.66 f_e^2 - 22.03 f_e + 135.42 \tag{5.8}$$

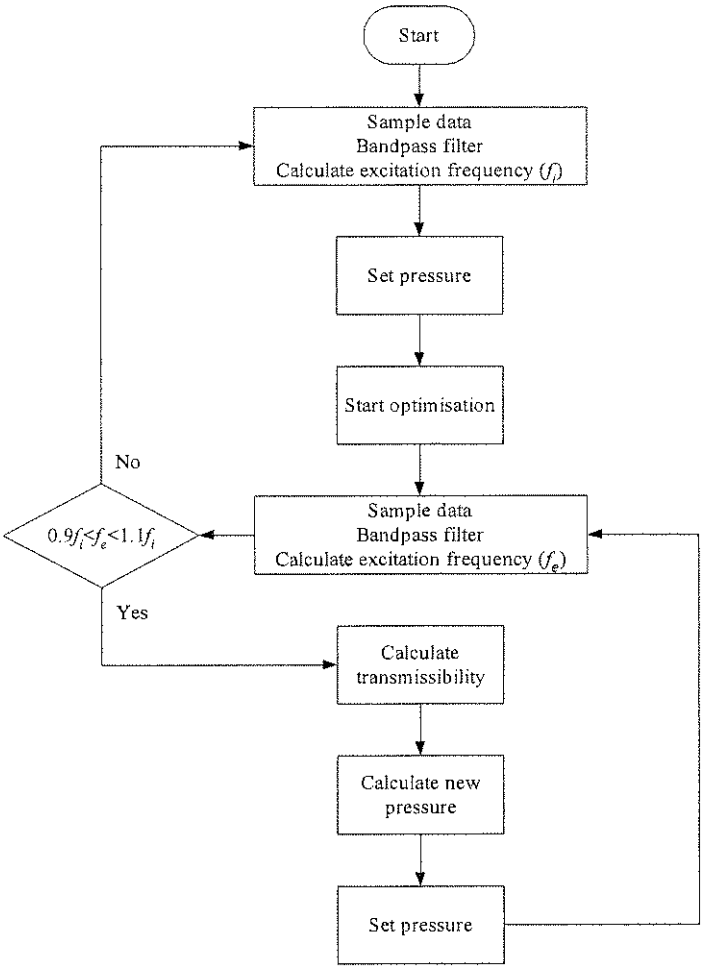

Figure 5.22: Control flow diagram

The results for a frequency step from 30 to 35 Hz are shown in Figure 5.23. The result is only used to illustrate that the method can work and was not fine-tuned to give the best result possible. All the issues regarding different algorithms were discussed in Chapter 3 and the advice contained therein should be followed when a control system is designed for the AVAI.

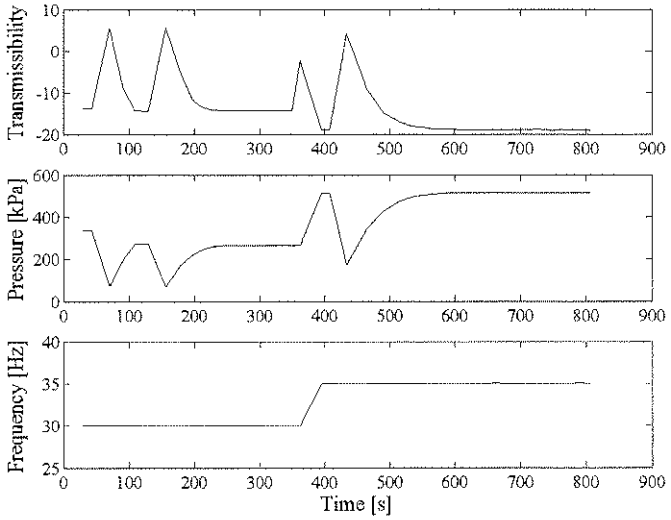

Figure 5.23: Control result when changing the excitation frequency from 30 to 35 Hz

5.5 Conclusion

This chapter verified the mathematical models used for the two AVAIs by using experiments. In both cases the effects seen in experiments were not fully explained in the initial mathematical models and these had to be modified. The modified models represent a reasonable estimate of the actual system behaviour and can be used to design the AVAIs. Due to various practical aspects it will not be possible to eliminate testing entirely and some tuning would still be required for new designs. It is, however, believed that the models suggested will minimise the amount of modification needed after such testing.

This chapter also confirmed experimentally that the system could be controlled successfully. Control was only implemented for the type I AVAI so as to demonstrate the method. The experiment sbowed that it is possible to detect a step change in frequency and that the device can successfully be tuned to the new excitation frequency.

6 Conclusions

The ideal isolator is one that will support the equipment being isolated without transmitting any dynamic forces. An isolator with infinite static stiffness and zero dynamic stiffness will achieve this goal. Although this ideal isolation cannot be obtained in practice, it can be approximated through a wide range of devices. The approximation occurs over a limited frequency band and methods of increasing this band were investigated. The methods were classified as passive, adaptive and active techniques. Passive techniques offer no flexibility, while active techniques approach optimal isolation performance. Adaptive techniques can be seen as a compromise of flexibility and cost.

The isolation philosophy introduced the concept of adapting the isolator properties by considering both the input characteristics and a set of evaluation criteria. The criteria could typically be represented by a filter that would weigh the frequencies according to their importance. An optimisation technique can then be applied to find the optimal set of isolator parameters that will minimise the criteria. The system functions on-line in such a way that near optimal performance can be guaranteed as the input or isolator characteristics vary with time.

Chapter 1 compared a wide range of isolators concepts, starting at the most simple passive isolator and ending with the active amplified vibration-absorbing isolator. To compare the various devices the non-dimensional blocked transfer dynamic stiffness was defined. This quantity was found to represent the isolator properties without the additional complication of the equipment being isolated, as happens in traditional transmissibility methods. Some isolation methods cannot be explained by considering the dynamic stiffness alone and only in those cases were the transmissibility calculated. Methods used to improve vibration absorbers were adapted to isolators with interesting results, which can be investigated in future work. The focus of this work was the broadening of the effective low stiffness bandwidth of the amplified vibration-absorbing isolator by adapting system parameters. A sensitivity study showed that the isolation frequency is the most sensitive to geometric variables, but these cannot be changed easily in practice. A considerable amount of work has been published on variable stiffness devices. The range of stiffness values that can be attained and the speed at which it can be realised remains a problem.

In chapter 2 time and frequency-domain methods were used to study two novel adaptive amplified vibration-absorbing isolators. The type I AVAI used flexible reservoir walls to adapt the isolation frequency. The type II device incorporated a heavy metal slug. Both devices used variable pressure air springs to change the stiffness. The use of air springs was convenient, offered low damping and had the ability to be used with the pneumatic rock drill to eliminate the need for a control system. Conceptual design methodologies were illustrated for both damped and undamped fixed and adaptive isolation frequency AVAIs. To determine the effects of tuning, the equations were transformed in terms of constant frequency ratios and the stiffness ratio. The stiffness ratio was the only tuning parameter considered.

To design the type I AVAI for fixed frequency excitation, optimisation was employed. This approach made it possible to set goals for the required bandwidth and the proximity of the frequencies of

maximum transmissibility to the isolation frequency. For the adaptive AVAI it was shown that specific choice of the area and mass ratios could influence the tuning range. For the damped adaptive AVAI the transmissibility at the isolation frequency was minimised when the area ratio was minimised and the mass ratio maximised. This AVAI had a constant static deflection, which could be advantageous in practice.

For the type II AVAI the main spring stiffness was made adaptive. The design methodology is different from the type I because the travel of the slug is restricted and must enter the design process to ensure that realistic area ratios are chosen. A design methodology was proposed that starts with the overall device size and calculates the port diameter required. It was shown that a maximum of two solutions could exist for each specified set of outside dimensions. Three additional models were analysed each considering specific refinements to the basic model. The first investigated the effect of rubber stops as an alternative to slug springs as a method for keeping the slug centred vertically. The second took account of leakage between the port and the slug, which was shown to increase the isolation frequency. It was concluded that the gap should be minimised. The third showed the effect of using rolling diaphragm seals to eliminate leakage. The rolling diaphragm seal will result in a larger device since the effective mass is reduced.

Chapter 3 showed how optimisation could be used as a control method for the AVAI. Several objective functions were investigated including a ratio of output to input rms acceleration, quadrature of the input and output accelerations and the H_1 transmissibility estimator. Quadrature can only be used if the damping is small, while the rms method will be easy to implement for a damped device. The H1 estimator was considered to be the most accurate. Four separate scenarios were considered. The first case assumed that the device needed to be tuned at start-up only. It was shown that as long as the initial condition is appropriate and the step size can be controlled, the device could be tuned successfully. For the type I device the initial condition had to be the maximum stiffness ratio that could be achieved, while for the type II it must he the minimum. The second case considered a sudden change in excitation frequency. For this case it was found that standard algorithms would not be successful. The lfopc algorithm could be used in this case. The third case considered a slow change in either the excitation frequency or the system properties. Due to incorrect gradient information this case cannot be handled using the optimisation method. Lastly, a general method was proposed where open-loop tuning was used as a first stage and optimisation as fine-tuning during a second stage. The open-loop tuning is done using a look-up table established from a characterisation test. The look-up table is updated with the information from the subsequent optimisation procedure if a lower transmissibility is found. This method will be fast and will maintain its accuracy over time.

Chapter 4 showed how the design of an AVAI could be applied to a practical isolation problem. Pneumatic rock drills are commonly used in the South African gold mining industry. It has been found that the operators of these drills are exposed to harmful vibration levels. The maximum weighted equivalent acceleration value measured on these drills at a test facility was 18.72 m/s^2. The excitation of these drills has a large tonal component, but also consists of wide-band noise. The tonal component contributes ~50% to the overall weighted equivalent acceleration and any isolation method must therefore address it with care. Measurements showed that the frequency of the tonal component is a function of supply air pressure. It was shown theoretically that both the AVAIs considered would have a lower weighted acceleration that an equivalent isolator, depending on the amount of damping

included. Subsequently, a simulation of the actual system behaviour showed that both AVAIs would reduce the handle response. Three tuning methods were compared. The first used the supply line pressure only, the second calculated the excitation frequency and tuned the device accordingly, while the third adapted both stiffness and damping to minimise the weighted equivalent acceleration. The last method resulted in the best performance, but using the supply line was adequate and has a major cost advantage. The type II AVAI acceleration levels were reduced to below 10 m/s^2 up to a pressure of 500 kPa for three of the drills simulated.

In chapter 5 the mathematical models used for the two AVAIs were verified using experiments. In both cases the effects seen in experiments were not fully explained in the initial mathematical models and these had to be modified. The modified models represent a reasonable estimate of the actual system behaviour and can be used to design the AVAIs. Due to various practical aspects it will not be possible to eliminate testing entirely and some tuning would still be required for new designs. It is, however, believed that the models suggested will minimise the amount of modification needed after such testing.

This chapter also confirmed experimentally that the system can be controlled successfully. Control was only implemented for the type I AVAI so as to demonstrate the method. The experiment showed that a step change in frequency could be detected and that the device could successfully be tuned to the new excitation frequency.

Future work on vibration-absorbing isolators:

1. The two AVAIs that were proposed in this work should be made more robust and must be tested on an actual pneumatic drill at the amplitudes experienced in practice.
2. The augmentation of the AVAIs to reduce the response at resonance must be investigated. This should include the addition of "skyhook" dampers etc.
3. The characteristics of the springs should be investigated so that stiffness and damping values can be predicted with greater accuracy.
4. The reduction of damping at all possible sources and under all loading conditions must be explored.

The innovative use of vibration absorbers as isolators shows promise for solving the more demanding isolation problems that exist today in a cost effective manner.

7 References

Ahmadian, M. & Ahn, Y.K. 1999. Performance analysis of magneto-rheological mounts, *Journal of Intelligent Material Systems and Structures*, Vol. 10, pp. 248-256.

Alabuzhev, P., Gritchin, A., Kim, L., Migirenko, G., Chon V. & Stepanov, P. 1989. *Vibration Protecting and Measuring Systems with Quasi-zero Stiffness*, Hemisphere Publishing Corporation: New York.

Andersson, E.R. 1990. Design and testing of a vibration attenuating handle, *International Journal of Industrial Ergonomics*, Vol. 6, pp. 119-125.

Babitsky, V.I. & Veprik, A.M. 1998. Universal bumpered vibration isolator for severe environment, *Journal of Sound and Vibration*, 218(2), pp. 269-292.

Barber, A. 1992. *Handbook of Shock and Vibration Control*, Elsevier Science Publishers: Oxford.

Bisutti, G. 2001. Power tool, *US patent no. 6,321,854.*

Braun, D. 1980. Development of anti-resonance force isolators for helicopter vibration reduction, *Sixth European rotorcraft and powered lift aircraft forum*, Bristol, England, September 16-19.

Brennan, M.J. 1997a. Characteristics of a wideband vibration neutraliser, *Noise Control Engineering Journal*, 45(5), pp. 201-207.

Brennan, M.J. 1997b. Vibration control using a tunable vibration neutralizer, *Proceeding of the Institution of Mechanical Engineers Part C: Journal of Mechanical Engineering Science*, Vol. 211, pp. 91-108.

Burdisso, R.A. & Heilmann, J.D. 1998. A new dual-reaction mass dynamic vibration absorber actuator for active vibration control, *Journal of Sound and Vibration*, 214(5), pp. 817-831.

Cavanaugh, R.D. 1976. Air suspension and servo-controlled isolation systems, In: C.M. Harris & C.E. Crede, *Shock and Vibration Handbook*, New York: McGraw-Hill, pp. 33-1-26.

Commission of European Communities. 1994. Amended proposal for an Council Directive on the minimum Health and Safety requirements regarding the exposure of workers to the risks arising from physical agents – Individual Directive in relation to article 16 of Directive 89/391/EEC, *Official Journal of the European Communities*, No. C 230, 19.8.94, pp. 3-29.

Cunha, S.S. Jr. & Rade, D.A. 2002. Numerical and experimental evaluation of an active dynamic vibration absorber, *Proceedings of ISMA2002*, Leuven, September, Vol. I, pp. 131-140.

Dascotte, E. & Strobbe, J. 1999. Updating finite element models using FRF correlation functions. *Proceedings of the 17th International Modal Analysis Conference (IMAC)*, February, Kissimmee, Florida.

Davey, A.B. & Payne, A.R. 1964. *Rubber in Engineering Practice*, London: Applied Science Publishers.

Desanghere, G. & Vansevenant, E. 1994. An adaptive tuned vibration absorber inside a rotating spindle of a machine tool, *ISMA19 - Tools for Noise and Vibration Analysis*. Leuven, Belgium, September, pp. 597-605.

Desjardins, R.A. & Hooper, W.E. 1976. Rotor isolation of the hingeless rotor B0-105 and YUH-61A helicopters, *2nd European Rotorcraft and Powered Lift Aircraft Forum*, Buckeburg, F.R.G., September.

Desjardins, R.A. & Sankewitsch, V. 1982. Vibration isolation system, *U.S. patent no. 4,311,213.*

Du Plooy, N.F. 1999. The Development of a Vibration Absorber for Vibrating Screens. *M.Eng Thesis*, University of Pretoria.

Duclos, T.G., Hodgson, D.A. & Carlson, J.D. 1988. Tunable electrorheological fluid mount, *US patent no. 4,733,758.*

Ewins, D.J. 2000. *Modal testing theory and practice*, 2nd Edition, Research Studies Press: Baldcock.

Filipović, D. & Schröder, D. 1998. Bandpass vibration absorber, *Journal of Sound and Vibration*, 214(3), pp. 553-566.

Flatau, A.B., Dapino, M.J. & Calkins, F.T. 1998. High bandwidth tunability in a smart vibration absorber, *Proceedings of SPIE: Smart Structures and Materials*, Paper no. 3329-19/3327-42, pp. 1-11.

Frahm, H. 1909. Device for damping vibrations of bodies, *U.S. Patent no. 989958.*

Franchek, M.A., Ryan, M.W. & Bernhard, R.J. 1995. Adaptive passive vibration control, *Journal of Sound and Vibration*, 189(5), pp. 565-585.

Fuller, C.R., Elliot, S.J. & Nelson P.A. 1996. *Active Control of Vibration*, London: Academic Press.

Gere, J.M. & Timoshenko, S.P. 1991. *Mechanics of materials*, London: Chapman & Hall.

Grace, H.P. & Lapple, C.E. 1951. Discharge coefficients for small-diameter orifices and flow nozzles, *Transactions of the ASME*, Vol. 73, pp. 639-647.

Griffen, M.J. 1990. *Handbook of Human Vibration*, Academic Press: London.

Griffen, M.J. 1998. Fundamentals of human responses to vibration, In: Fahy, F. & Walker, J. (Eds), *Fundamentals of Noise and Vibration*, E & FN Spon: London, pp. 179-223.

Gwinn, J.T. & Marjoram, R.H. 1999. Isolated hand-held vibrating device, *US patent no. 5,927,407.*

Halwes, D.R. & Simmons, W.A. 1980. Vibration suppression system, *US patent no. 4,236,607.*

Halwes, D.R. 1981a. Total main rotor isolation system analysis, Bell Helicopter Textron, *NASA Contractor Report No. 165667*, Langley Research Center, Hampton, Virginia, June.

Halwes, D.R. 1981b. Total main rotor isolation system analysis, *American Helicopter Society*, Hartford, Connecticut, November, pp. 1-7.

Hodgson, D.A. & Duclos, T.G. 1990. Mount with adjustable length inertia track, *US patent no. 4,969,632.*

Hunt, J.B. & Nissen, J.-C. 1982. The broadband dynamic vibration absorber, *Journal of Sound and Vibration*, 83(4), pp. 573-578.

Igusa, T. & Xu, K. 1991. Vibration reduction characteristics of distributed tuned mass dampers, *Proceedings of the 4th International Conference on Structural Dynamics: Recent Advances*, Southampton, 15-18 July, pp. 596-605.

ISO 5349:1986(E). Mechanical vibration – Guidelines for the measurement and the assessment of human exposure to hand-transmitted vibration.

ISO 5349-1:2001(E). Mechanical vibration – Measurement and evaluation of human exposure to hand-transmitted vibration – Part 1: General requirements.

Jensen, W.S. 1999. Adaptive tuned vibration absorber, system utilising same and method of controlling vibration therewith, *US patent no. 5,954,169.*

Jolly, M.R., Carlson, J.D. & Muñoz, B.C. 1996. A model of the behaviour of magnetorheological materials, *Smart Materials and Structures*, 5, pp. 607-614.

Karnopp, D. 1995. Active and semi-active vibration isolation, *Transaction of the ASME: Special 50th Anniversary Design Isssue*, Vol. 117. pp. 177-185.

Ketema, Y. 1998. A viscoelastic dynamic vibration absorber with adaptable suppression band: a feasibility study, *Journal of Sound and Vibration*, 216(1), pp. 133-145.

Kidner, M. & Brennan, M.J. 1999. Improving the performance of a vibration neutralizer by actively removing damping, *Journal of Sound and Vibration*, 221(4), pp. 587-606.

Long, T., Brennan, M.J., Day, M.J. & Elliot, S.J. 1994. Adaptive control of pneumatic vibration absorbers, *International conference on system engineering*, Coventry, UK, September, pp. 741-748.

Longbottom, C.J., Day, M.J. & Rider, E. 1987. A self-tuning vibration absorber, *UK patent no. 2,189,573B.*

Luo, H. & Hanagud, S. 1998. On the dynamics of vibration absorbers with motion limiting stops, *Transactions of the ASME: Journal of applied mechanics*, Vol. 65, March, pp. 223-233.

Margolis D.L. & Baker, D. 1992. The variable fulcrum isolator: A low power, nonlinear, vibration control component, *Transactions of the ASME: Journal of Dynamic Systems, Measurement and Control*, 114, pp. 148-154.

McKeown, W.L., Smith, M.R. & Stamps, F.B. 1995. Hydraulic inertial vibration isolator, *US patent no. 5,439,082.*

Mead, D.J. 2000. *Passive Vibration Control*, Chichester: John Wiley & Sons.

Miller, H.T. 1987. Fluid filled vibration isolator having precisely adjustable dynamic operating characteristics, *US patent no. 4,712,777.*

Miller, L.R. & Ahmadian, M. 1992. Active mounts – a discussion of future technological trends, *Inter Noise*, Toronto, Canada, July 20-22, pp. 421-426.

Miller, L.R., Ahmadian, M., Nobles, C.M. & Swanson, D.A. 1995. *Transaction of the ASME: Journal of Vibration and Acoustics*, Vol. 117, July, pp. 272-278.

Mizuno, T. & Araki, K. 1993. Control system design of a dynamic vibration absorber with an electromagnetic servomechanism, *Mechanical Systems and Signal Processing*, 7(4), pp. 293-306.

Nocedal, J. & Wright, S.J. 1999. *Numerical Optimisation*, Springer-Verlag: New York.

Olgac, N. & Holm-Hansen, B.T. 1993. Vibration absorbers utilizing only position measurements for time varying excitation frequencies, *ASME Symposium on Mechatronics*.

Ormondroyd, J. & Den Hartog, J.P. 1928. The theory of the dynamic vibration absorber, *Transactions of the American Society of Mechanical Engineers*, APM-50-7.

Oyadiji, S.O. & Tomlinson, G.R. 1994. Relating the complex moduli of viscoelastic to the complex stiffness of anti-vibration mounts, *Proceedings of SPIE: Smart Structures and Materials: Passive Damping,* Vol. 2193, pp. 226-237.

Palej, R., Piotrowski, S. & Stojek, M. 1993. Mechanical properties of an active pneumatic spring, *Journal of Sound and Vibration*, 168(2), pp. 299-306.

Prajapati, K. & Hes, P. 1999. Reduction of hand-arm transmitted vibration on jackleg rock drills, *CIM Conference,* Paper no. 4MPM2-47, 2-5 May, Calgary Canada.

Rao, S.S. 1990. *Mechanical Vibrations*, 2nd Edition, New York: Addison Wesley.

Raw, S. 1999. Ergonomic had-grip for attenuating vibrations in hand held power tools, *Health and Safety*, May, p. 57.

Ribakov, Y. & Gluck, J. 1998. Optimal design of base isolated active controlled MDOF structures, *Proceedings of ISMA23*, Leuven, September.

Rivin, E. 2001. Vibration isolation theory, In: S.G. Braun *et. al.* (Eds), *Encyclopaedia of Vibration*, Academic Press: London, pp. 1487-1506.

Smith, M.R. & Stamps, F.N. 1988. Vibration isolation system, *US patent no. 5,788,029.*

Snyman, J.A. 1982. A new and dynamic method for unconstrained minimization, *Applied mathematical modelling*, Vol. 6, December.

Sommmerfeldt, S.D. & Tichy, J. 1990. Adaptive control of a two-stage vibration isolation mount, *Journal of the Acoustical Society of America*, 88(2), August, pp. 938-944.

Storn, R. 1996. http://www.icsi.berkeley.edu/~storn/code.html

Strydom, J.P.D. 2000. Development of a vibration absorbing handle for rock drills. *M.Eng Thesis*, University of Pretoria.

Sun, J.Q., Jolly, M.R. & Norris, M.A. 1995. Passive, adaptive and active tuned vibration absorbers – a survey, *Transactions of the ASME – Special 50th Anniversary Design Issue*, Vol. 117, June.

Ting-Kong, C. 1999. Design of an adaptive dynamic vibration absorber, *M.Eng Thesis*, The University of Adelaide.

Van Niekerk, J.L., Heyns, P.S. & Heyns, M. 2000. Human vibration levels in South African mining industry, *Journal of the South African Institute of Mining and Metallurgy*, Vol. 100, Nr. 4, July/August, pp. 235-241.

Von Flotow, A.H., Beard, A. & Bailey, D. 1994. Adaptive tuned vibration absorbers: Tuning laws, tracking agility, sizing and physical implementations, *Proceedings of Noise-Con 94*, Ft. Lauderdale, Florida, pp. 437-454.

Walsh, P.L. & Lamancusa, J.S. 1992. A variable stiffness vibration absorber for minimisation of transient, *Journal of Sound and Vibration*, 158(2), pp. 195-211.

Wang, Y-T. & Singh, R. 1987. Frequency response of a nonlinear pneumatic system, *Journal of Applied Mechanics*, Vol. 54, pp. 209-214.

Waterman, E.H. 1988. Vibration absorber with controllable resonance frequency, *US patent no. 4,724,923*.

Watts, P. 1883. On a method for reducing the rolling of ships at sea, *Transactions of the Institution of Naval Architects*, 24, pp. 165-190.

White, F.M. 1988. *Fluid Mechanics*, 2nd Edition, Singapore: McGraw-Hill.

Williams, K.A., Chiu, G.T.-C. & Bernhard, R.J. 2000. Controlled continuous tuning of an adaptively tunable vibration absorber incorporating shape memory alloys, *Proceedings of SPIE: Mathematics and Control in Smart Structures*, Vol. 3984, March.

Young, W.C. & Budynas, R.G. 2002. *Roark's Formulas for Stress and Strain*, 7th Edition, Singapore: McGraw-Hill International Edition.

Yu, Y., Naganathan, N.G. & Dukkipati, R.V. 2001. A literature review of automotive vehicle engine mounting systems, *Mechanism and Machine Theory*, Vol. 36, pp. 123-142.

APPENDIX A

Derivations for chapter 1

A.1 Background (dynamic stiffness of the relaxation model)

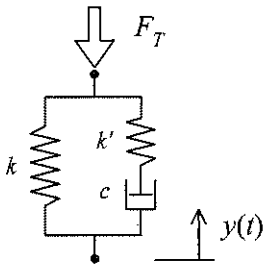

Figure A.1: Mechanical model of a relaxation isolator

Since the spring k' is in series with the dashpot, the force generated by each must be equal:

$$\begin{aligned} c(\dot{y}-\dot{u}) &= k'u \\ i\omega c(Y-U) &= k'U \\ i\omega cY &= (k'+i\omega c)U \\ U &= \frac{i\omega c}{k'+i\omega c}Y \end{aligned} \tag{A.1}$$

The total force of the two elements in parallel is:

$$\begin{aligned} F_T &= kY + k'U \\ &= kY + k'\frac{i\omega c}{k'+i\omega c}Y \end{aligned} \tag{A.2}$$

The above equation can be written in non-dimensional form by dividing with k:

$$\begin{aligned} \frac{F_T}{kY} &= 1+\frac{k'}{k}\frac{i\omega\frac{c}{k'}}{1+i\omega\frac{c}{k'}} \\ &= 1+\frac{k'}{k}\frac{i\omega\frac{c}{k}}{\frac{k'}{k}+i\omega\frac{c}{k}} \end{aligned} \tag{A.3}$$

A.2 Isolators

A.2.1 Passive isolator (intermediate mass isolator)

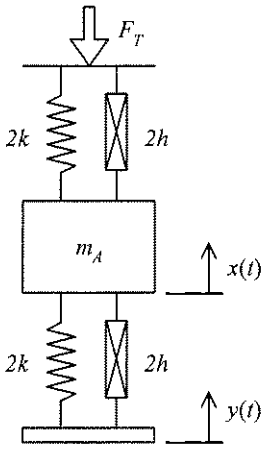

Figure A.2: Mechanical model of an intermediate mass isolator

The equation of motion is:

$$\begin{aligned} m_A\ddot{x} + 2k(1+i\eta)x &= -2k(1+i\eta)(x-y) \\ m_A\ddot{x} + 4k(1+i\eta)x &= 2k(1+i\eta)y \end{aligned} \tag{A.4}$$

The equation of motion can be rewritten in the frequency domain:

$$\left[4k(1+i\eta) - \omega^2 m_A\right]X = 2k(1+i\eta)Y \tag{A.5}$$

The transmissibility is now:

$$\frac{X}{Y} = \frac{2k(1+i\eta)}{4k(1+i\eta) - \omega^2 m_A} \tag{A.6}$$

The dynamic stiffness is a function of the displacement of mass m_A:

$$F_T = 2k(1+i\eta)X \tag{A.7}$$

Using the transmissibility the equation can be written in terms of the input displacement amplitude Y:

$$F_T = 2k(1+i\eta)\left[\frac{2k(1+i\eta)}{4k(1+i\eta) - \omega^2 m}\right]Y \tag{A.8}$$

When normalised, the above equation becomes:

$$\frac{F_T}{kY} = \frac{(1+i\eta)^2}{1+i\eta-\left(\frac{\omega}{\omega_n}\right)^2} \qquad \text{(A.9)}$$

where: $\omega_n = \sqrt{\frac{4k}{m_A}}$

A.2.2 Active isolator (absolute velocity feedback isolator)

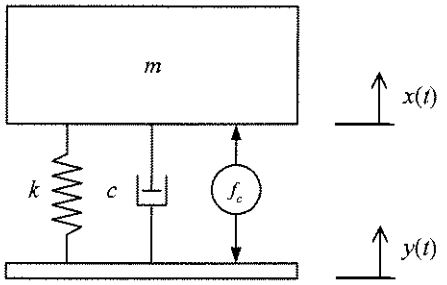

Figure A.3: Mechanical model with skyhook damping

The control force is proportional to the velocity, but in the opposite direction:

$$f_c(t) = -\beta\dot{x} \qquad \text{(A.10)}$$

The equation of motion including the control force is:

$$\begin{aligned} m\ddot{x} + c\dot{x} + kx &= c\dot{y} + ky - \beta\dot{x} \\ m\ddot{x} + (c-\beta)\dot{x} + kx &= c\dot{y} + ky \end{aligned} \qquad \text{(A.11)}$$

Transforming the equation to the frequency domain:

$$\left[-\omega^2 m + i\omega(c+\beta) + k\right]X = (i\omega c + k)Y \qquad \text{(A.12)}$$

The transmissibility is:

$$\frac{X}{Y} = \frac{k + i\omega c}{k + i\omega(c+\beta) - \omega^2 m} \qquad \text{(A.13)}$$

When normalised, the above equation becomes:

$$\frac{X}{Y} = \frac{1 + i2\frac{\omega}{\omega_n}\zeta}{1 + i2\frac{\omega}{\omega_n}(\zeta + \zeta_\beta) - \left(\frac{\omega}{\omega_n}\right)^2} \qquad \text{(A.14)}$$

where: $\omega_n = \sqrt{\frac{k}{m}}$, $\zeta = \frac{c}{2m\omega_n}$, $\zeta_\beta = \frac{\beta}{2m\omega_n}$

A.2.3 Active isolator (general feedforward active isolator)

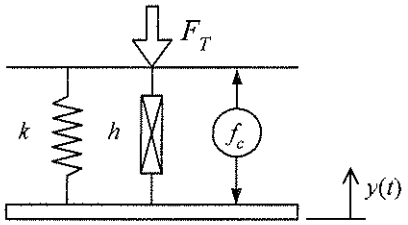

Figure A.4: Mechanical model of an active isolator

The control force is:

$$f_c(t) = \alpha\ddot{y} + (\gamma + i\beta)y \tag{A.15}$$

The total force transmitted is the sum of the spring, damper and control force:

$$\begin{aligned} f_t &= k(1+i\eta)y + \alpha\ddot{y} + (\gamma + i\beta)y \\ &= (k+\gamma)y + i(k\eta + \beta)y + \alpha\ddot{y} \end{aligned} \tag{A.16}$$

When transformed to the frequency domain the above equation becomes:

$$F_T = (k+\gamma)Y + i(k\eta + \beta)Y - \alpha\omega^2 Y \tag{A.17}$$

When normalised, the above equation becomes:

$$\begin{aligned} \frac{F_T}{(k+\gamma)Y} &= 1 + i\frac{k\eta + \beta}{k+\gamma} - \frac{\alpha}{k+\gamma}\omega^2 \\ &= 1 + i\frac{k\eta + \beta}{k+\gamma} - \left(\frac{\omega}{\omega_i'}\right)^2 \end{aligned} \tag{A.18}$$

where: $\omega_i' = \sqrt{\dfrac{k+\gamma}{\alpha}}$

A.3 Vibration-absorbing isolators

A.3.1 Passive vibration-absorbing isolator

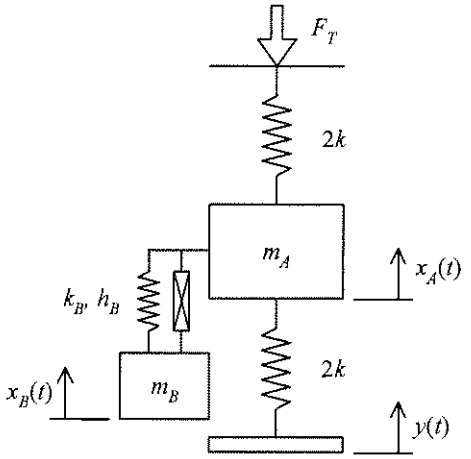

Figure A.5: Mechanical model of a passive vibration-absorbing isolator

The kinetic energy of the system is:

$$T = \frac{1}{2}\left(m_A\dot{x}_A^2 + m_B\dot{x}_B^2\right) \tag{A.19}$$

From the above equation the derivatives can be found:

$$\begin{aligned}\frac{d}{dt}\left(\frac{\partial T}{\partial \dot{x}_A}\right) &= m_A\ddot{x}_A \\ \frac{d}{dt}\left(\frac{\partial T}{\partial \dot{x}_B}\right) &= m_B\ddot{x}_B\end{aligned} \tag{A.20}$$

The potential energy is:

$$\begin{aligned}V &= \frac{1}{2}\left[2k\left(x_A - y\right)^2 + 2kx_A^2 + k_B\left(x_A - x_B\right)^2\right] \\ &= \frac{1}{2}\left[2k\left(x_A^2 - x_A y + y^2\right) + 2kx_A^2 + k_B\left(x_A^2 - x_A x_B + x_B^2\right)\right]\end{aligned} \tag{A.21}$$

From the above equation the derivatives can be found:

$$\begin{aligned}\frac{\partial V}{\partial x_A} &= 2kx_A - 2ky + 2kx_A - k_B x_B - k_B x_A = \left(4k - k_B\right)x_A - k_B x_B - 2ky \\ \frac{\partial V}{\partial x_B} &= -k_B x_A + k_B x_B\end{aligned} \tag{A.22}$$

The equation of motion can be found by substituting the derivates in Lagrange's equations and incorporating a hysteretic damping model:

$$\begin{bmatrix} m_A & 0 \\ 0 & m_B \end{bmatrix}\begin{bmatrix} \ddot{x}_A \\ \ddot{x}_B \end{bmatrix}+\begin{bmatrix} 4k(1+i\eta)+k_B(1+i\eta_B) & -k_B(1+i\eta_B) \\ -k_B(1+i\eta_B) & k_B(1+i\eta_B) \end{bmatrix}\begin{bmatrix} x_A \\ x_B \end{bmatrix}=\begin{bmatrix} 2k(1+i\eta)y \\ 0 \end{bmatrix} \tag{A.23}$$

The second equation can be rewritten in the frequency domain as:

$$\begin{aligned} -k_B(1+i\eta_B)X_A+\left[k_B(1+i\eta_B)-\omega^2 m_B\right]X_B&=0 \\ X_B&=\frac{k_B(1+i\eta_B)}{k_B(1+i\eta_B)-\omega^2 m_B}X_A \end{aligned} \tag{A.24}$$

By substituting for X_B in the first equation the response of X_A to the input Y can be found:

$$\begin{aligned} &\left[4k(1+i\eta)+k_B(1+i\eta_B)-\omega^2 m_A\right]X_A-k_B(1+i\eta_B)\frac{k_B(1+i\eta_B)}{k_B(1+i\eta_B)-\omega^2 m_B}X_A=2k(1+i\eta)Y \\ &\left\{\left[4k(1+i\eta)+k_B(1+i\eta_B)-\omega^2 m_A\right]\left[k_B(1+i\eta_B)-\omega^2 m_B\right]-k_B^2(1+i\eta_B)^2\right\}X_A \\ &\qquad =2k(1+i\eta)\left[k_B(1+i\eta_B)-\omega^2 m_B\right]Y \\ &\frac{X_A}{Y}=\frac{2k(1+i\eta)\left[k_B(1+i\eta_B)-\omega^2 m_B\right]}{\left[4k(1+i\eta)+k_B(1+i\eta_B)-\omega^2 m_A\right]\left[k_B(1+i\eta_B)-\omega^2 m_B\right]-k_B^2(1+i\eta_B)^2} \end{aligned} \tag{A.25}$$

The transmitted force can now be found in terms of the input by using the above transmissibility:

$$\begin{aligned} F_T&=2k(1+i\eta)X_A \\ &=\frac{4k^2(1+i\eta)^2\left[k_B(1+i\eta_B)-\omega^2 m_B\right]}{\left[4k(1+i\eta)+k_B(1+i\eta_B)-\omega^2 m_A\right]\left[k_B(1+i\eta_B)-\omega^2 m_B\right]-k_B^2(1+i\eta_B)^2}Y \end{aligned} \tag{A.26}$$

Rearranging the above equation gives the normalised dynamic stiffness:

$$\frac{F_T}{kY}=\frac{4k(1+i\eta)k_B(1+i\eta_B)\left(1+i\eta_B-\omega^2\frac{m_B}{k_B}\right)}{4k(1+i\eta)k_B(1+i\eta_B)\left\{\left[1+i\eta+\frac{1}{4}\frac{k_B}{k}(1+i\eta_B)-\omega^2\frac{m_A}{4k}\right]\left(1+i\eta_B-\omega^2\frac{m_B}{k_B}\right)-\frac{1}{4}\frac{k_B}{k}(1+i\eta_B)\right\}} \tag{A.27}$$

This equation can further be manipulated to be a function of non-dimensional terms only by introducing the natural frequencies:

$$\frac{F_T}{kY}=\frac{1+i\eta_B-\left(\frac{\omega}{\omega_B}\right)^2}{\left[1+i\eta+\frac{1}{4}\frac{k_B}{k}(1+i\eta_B)-\left(\frac{\omega}{\omega_A}\right)^2\right]\left[1+i\eta_B-\left(\frac{\omega}{\omega_B}\right)^2\right]-\frac{1}{4}\frac{k_B}{k}(1+i\eta_B)} \tag{A.28}$$

where: $\omega_A=\sqrt{\frac{4k_A}{m_A}}\quad \omega_B=\sqrt{\frac{k_B}{m_B}}$

The frequencies at which the dynamic stiffness is equal to 1 can be calculated to define the bandwidth of the device. For an undamped system the condition is:

$$\left|\frac{F_T}{kY}\right| = 1$$
$$\therefore \frac{F_T}{kY} = \pm 1 \tag{A.29}$$

The stiffness ratio is given by $\mu_k = k_B/k_A$. For $F_T/kY = 1$:

$$\frac{F_T}{kY} = \frac{1-\left(\frac{\omega}{\omega_B}\right)^2}{\left[1+\frac{1}{4}\mu_k-\left(\frac{\omega}{\omega_A}\right)^2\right]\left[1-\left(\frac{\omega}{\omega_B}\right)^2\right]-\frac{1}{4}\mu_k} = 1$$
$$1-\left(\frac{\omega}{\omega_B}\right)^2 = 1-\left(\frac{\omega}{\omega_B}\right)^2+\frac{1}{4}\mu_k-\frac{1}{4}\mu_k\left(\frac{\omega}{\omega_B}\right)^2-\left(\frac{\omega}{\omega_A}\right)^2+\left(\frac{\omega}{\omega_A}\right)^2\left(\frac{\omega}{\omega_B}\right)^2-\frac{1}{4}\mu_k$$
$$\frac{1}{4}\mu_k\left(\frac{1}{\omega_B}\right)^2+\left(\frac{1}{\omega_A}\right)^2 = \left(\frac{1}{\omega_A}\right)^2\left(\frac{1}{\omega_B}\right)^2\omega^2 \tag{A.30}$$
$$\left[\frac{1}{4}\mu_k\frac{1}{\omega_B^2}+\frac{1}{\omega_A^2}\right]\omega_B^2\omega_A^2 = \omega^2$$
$$\omega^2 = \left[\frac{1}{4}\mu_k\omega_A^2+\omega_B^2\right]$$
$$\omega_1 = 0, \quad \frac{\omega_2}{\omega_A} = \sqrt{\frac{1}{4}\mu_k+\left(\frac{\omega_B}{\omega_A}\right)^2}$$

For $F_T/kY = -1$:

$$\frac{F_T}{kY}\frac{1-\left(\frac{\omega}{\omega_B}\right)^2}{\left[1+\frac{1}{4}\mu_k-\left(\frac{\omega}{\omega_A}\right)^2\right]\left[1-\left(\frac{\omega}{\omega_B}\right)^2\right]-\frac{1}{4}\mu_k} = -1$$
$$1-\left(\frac{\omega}{\omega_B}\right)^2 = -1+\left(\frac{\omega}{\omega_B}\right)^2-\frac{1}{4}\mu_k+\frac{1}{4}\mu_k\left(\frac{\omega}{\omega_B}\right)^2+\left(\frac{\omega}{\omega_A}\right)^2-\left(\frac{\omega}{\omega_A}\right)^2\left(\frac{\omega}{\omega_B}\right)^2+\frac{1}{4}\mu_k \tag{A.31}$$
$$0 = \omega^4-\left(\frac{1}{4}\mu_k\omega_A^2+2\omega_A^2+\omega_B^2\right)\omega^2+2\omega_A^2\omega_B^2$$

The solution for the above equation is:

$$\omega^2 = \frac{-b \pm \sqrt{b^2 - 4ac}}{2a}$$

$$= \frac{\frac{1}{4}\mu_k\omega_A^2 + 2\omega_A^2 + \omega_B^2 \pm \sqrt{\left(\frac{1}{4}\mu_k\omega_A^2 + 2\omega_A^2 + \omega_B^2\right)^2 - 8\omega_A^2\omega_B^2}}{2}$$

$$\frac{\omega_3}{\omega_A} = \sqrt{\frac{\frac{1}{4}\mu_k + 2 + \left(\frac{\omega_B}{\omega_A}\right)^2 - \sqrt{\left(\frac{1}{4}\mu_k + 2 + \left(\frac{\omega_B}{\omega_A}\right)^2\right)^2 - 8\left(\frac{\omega_B}{\omega_A}\right)^2}}{2}} \qquad \text{(A.32)}$$

$$\frac{\omega_4}{\omega_A} = \sqrt{\frac{\frac{1}{4}\mu_k + 2 + \left(\frac{\omega_B}{\omega_A}\right)^2 + \sqrt{\left(\frac{1}{4}\mu_k + 2 + \left(\frac{\omega_B}{\omega_A}\right)^2\right)^2 - 8\left(\frac{\omega_B}{\omega_A}\right)^2}}{2}}$$

A.3.2 Passive vibration-absorbing isolator (multiple-absorber VAI)

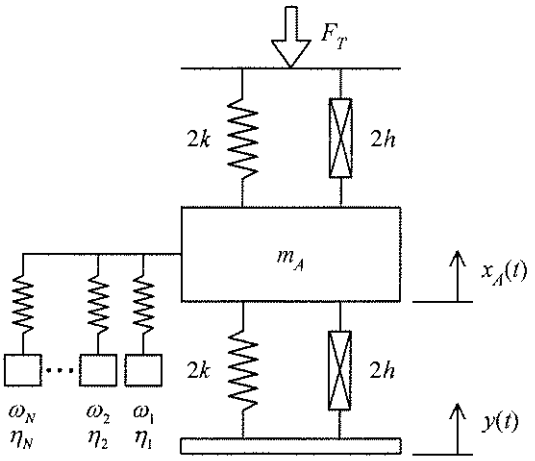

Figure A.6: Mechanical model of a multiple-absorber VAI

The derivation follows from the previous case where one absorber was considered. The kinetic energy is:

$$T = \frac{1}{2}\left(m_A\dot{x}_A^2 + \sum_{q=1}^{N} m_i\dot{x}_i^2\right) \qquad \text{(A.33)}$$

From the above equation the derivatives can be found:

$$\frac{d}{dt}\left(\frac{\partial T}{\partial \dot{x}_A}\right) = m_A\ddot{x}_A$$

$$\frac{d}{dt}\left(\frac{\partial T}{\partial \dot{x}_q}\right) = m_q\ddot{x}_q \qquad \text{(A.34)}$$

The potential energy is:

$$\begin{aligned} V &= \frac{1}{2}\left[2k\left(x_A - y\right)^2 + 2kx_A^2 + \sum_{q=1}^{N} k_q\left(x_A - x_q\right)^2\right] \\ &= \frac{1}{2}\left[4kx_A^2 - 4kx_A y + 2ky^2 + \sum_{q=1}^{N} k_q x_A^2 - 2k_q x_q x_A + k_q x_q^2\right] \end{aligned} \tag{A.35}$$

From the above equation the derivatives can be found:

$$\begin{aligned} \frac{\partial V}{\partial x_A} &= \left(4k + \sum_{q=1}^{N} k_q\right)x_A - \sum_{q=1}^{N} k_q x_q - 2ky \\ \frac{\partial V}{\partial x_q} &= -k_q x_A + k_q x_q \end{aligned} \tag{A.36}$$

The equation of motion can be found by substituting the derivates in Lagrange's equations and incorporating a hysteretic damping model:

$$\begin{bmatrix} m_A & 0 & 0 & \cdots & 0 \\ 0 & m_1 & 0 & \cdots & 0 \\ 0 & 0 & m_2 & \cdots & 0 \\ \vdots & \vdots & \vdots & \ddots & 0 \\ 0 & 0 & 0 & 0 & m_N \end{bmatrix}\begin{bmatrix} \ddot{x}_A \\ \ddot{x}_1 \\ \ddot{x}_2 \\ \vdots \\ \ddot{x}_N \end{bmatrix} + \begin{bmatrix} 4k(1+i\eta) + \sum_{q=1}^{N} k_q(1+i\eta_q) & -k_1(1+i\eta_1) & -k_2(1+i\eta_2) & \cdots & -k_N(1+i\eta_N) \\ -k_1(1+i\eta_1) & k_1(1+i\eta_1) & 0 & \cdots & 0 \\ -k_2(1+i\eta_2) & 0 & k_2(1+i\eta_2) & \cdots & 0 \\ \vdots & \vdots & \vdots & \ddots & 0 \\ -k_N(1+i\eta_N) & 0 & 0 & 0 & k_N(1+i\eta_N) \end{bmatrix}\begin{bmatrix} x_A \\ x_1 \\ x_2 \\ \vdots \\ x_N \end{bmatrix} = \begin{bmatrix} 2k(1+i\eta) \\ 0 \\ 0 \\ 0 \\ 0 \end{bmatrix} y \tag{A.37}$$

The first equation can be transformed to the frequency domain:

$$\left[1 + i\eta + \frac{1}{4}\sum_{q=1}^{N}\frac{k_q}{k}(1+i\eta_q) - \left(\frac{\omega}{\omega_A}\right)^2\right]X_A - \frac{1}{4}\sum_{q=1}^{N}\frac{k_q}{k}(1+i\eta_q)X_q = \frac{1}{2}(1+i\eta)Y \tag{A.38}$$

The q^{th} equation in the frequency domain is:

$$-k_q(1+i\eta_q)X_A + \left[k_q(1+i\eta_q) - \omega^2 m_q\right]X_q = 0 \tag{A.39}$$

The displacement X_q can now be found:

$$X_q = \frac{k_q(1+i\eta_q)}{k_q(1+i\eta_q) - \omega^2 m_q}X_A \tag{A.40}$$

This equation can be used to eliminate the X_q degree of freedom from Equation (A.38):

$$\left[1 + i\eta + \frac{1}{4}\sum_{q=1}^{N}\frac{k_q}{k}(1+i\eta_q) - \left(\frac{\omega}{\omega_A}\right)^2 - \frac{1}{4}\sum_{q=1}^{N}\frac{k_q}{k}\frac{(1+i\eta_q)^2}{1+i\eta_q - \left(\frac{\omega}{\omega_q}\right)^2}\right]X_A = \frac{1}{2}(1+i\eta)Y \tag{A.41}$$

The transmissibility between the intermediate mass and the excitation point is therefore:

$$\frac{X_A}{Y} = \frac{\frac{1}{2}(1+i\eta)}{1+i\eta+\frac{1}{4}\sum_{q=1}^{N}\frac{k_q}{k}(1+i\eta_q)-\left(\frac{\omega}{\omega_A}\right)^2-\frac{1}{4}\sum_{q=1}^{N}\frac{k_q}{k}\frac{(1+i\eta_q)^2}{1+i\eta_q-\left(\frac{\omega}{\omega_q}\right)^2}} \tag{A.42}$$

The force transmitted is:

$$F_T = 2k(1+i\eta)X_A \tag{A.43}$$

From which the normalised dynamic stiffness can be found:

$$\frac{F_T}{kY} = \frac{(1+i\eta)^2}{\left[1+i\eta+\frac{1}{4}\sum_{q=1}^{N}\frac{k_q}{k}(1+i\eta_q)-\left(\frac{\omega}{\omega_A}\right)^2\right]-\frac{1}{4}\sum_{q=1}^{N}\frac{k_q}{k}\frac{(1+i\eta_q)^2}{1+i\eta_q-\left(\frac{\omega}{\omega_q}\right)^2}} \tag{A.44}$$

A.3.3 Passive vibration-absorbing isolator (non-linear VAI)

For this case the auxiliary spring in Figure A.5 is assumed to exhibit Duffing non-linearity and the auxiliary system is viscously damped while the primary system is undamped. The equation of motion for the intermediate mass is:

$$\begin{aligned}
m_A\ddot{x}_A + c_B(\dot{x}_A-\dot{x}_B)+4kx_A+k_B(x_A-x_B)+\alpha k_B(x_A-x_B)^3 &= 2ky\\
\frac{m_A}{4k}\ddot{x}_A+\frac{c_B}{4k}(\dot{x}_A-\dot{x}_B)+x_A+\frac{k_B}{4k}(x_A-x_B)+\alpha\frac{k_B}{4k}(x_A-x_B)^3 &= \frac{1}{2}y\\
\frac{1}{\omega_A^2}\ddot{x}_A+\frac{1}{4}\frac{k_B}{k}\frac{2\zeta_B}{\omega_B}(\dot{x}_A-\dot{x}_B)+x_A+\frac{1}{4}\frac{k_B}{k}(x_A-x_B)+\alpha\frac{1}{4}\frac{k_B}{k}(x_A-x_B)^3 &= \frac{1}{2}y\\
\ddot{x}_A+\frac{1}{4}\frac{k_B}{k}\frac{2\zeta_B}{\omega_B}\omega_A^2(\dot{x}_A-\dot{x}_B)+\omega_A^2x_A+\frac{1}{4}\frac{k_B}{k}\omega_A^2(x_A-x_B)+\alpha\frac{1}{4}\frac{k_B}{k}\omega_A^2(x_A-x_B)^3 &= \frac{1}{2}\omega_A^2y
\end{aligned} \tag{A.45}$$

The auxiliary system equation of motion is:

$$\begin{aligned}
m_B\ddot{x}_B - c_B(\dot{x}_A-\dot{x}_B)-k_B(x_A-x_B)-\alpha k_B(x_A-x_B)^3 &= 0\\
\ddot{x}_B-2\zeta_B\omega_B(\dot{x}_A-\dot{x}_B)-\omega_B^2(x_A-x_B)-\alpha\omega_B^2(x_A-x_B)^3 &= 0\\
\ddot{x}_B-2\zeta_B\omega_B(\dot{x}_A-\dot{x}_B)-\omega_B^2\left[(x_A-x_B)+\alpha(x_A-x_B)^3\right] &= 0
\end{aligned} \tag{A.46}$$

The force transmitted can be calculated by solving for x_A in the above equations and then applying:

$$\frac{f_T}{k} = 2x_A \tag{A.47}$$

A.3.4 Adaptive vibration-absorbing isolator

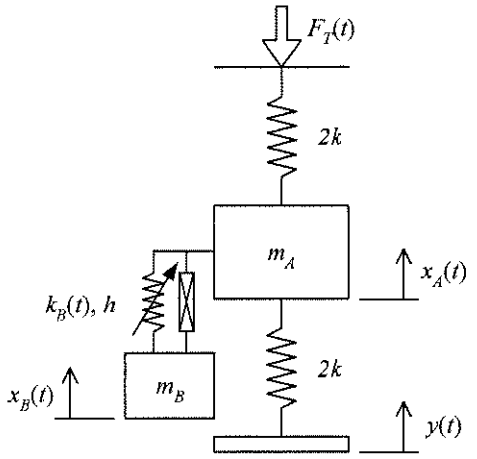

Figure A.7: Mechanical model of a tuneable VAI

The equation of motion for mass m_A can be written using Equation (A.45):

$$\begin{aligned} &m_A\ddot{x}_A + c_B\left(\dot{x}_A - \dot{x}_B\right) + 4kx_A + k_B\left(x_A - x_B\right) = 2ky \\ &\frac{m_A}{4k}\ddot{x}_A + \frac{c_B}{4k}\left(\dot{x}_A - \dot{x}_B\right) + x_A + \frac{k_B}{4k}\left(x_A - x_B\right) = \frac{1}{2}y \end{aligned} \tag{A.48}$$

The damping terms can be written in terms of the primary system stiffness so that it is independent of the stiffness ratio:

$$\begin{aligned} &\frac{c_B}{4k} = \frac{1}{4}\frac{2\bar{\zeta}_B m_B \bar{\omega}_B}{k} = \frac{1}{2}\frac{\bar{\zeta}_B}{\bar{\omega}_B} \\ &\text{where: } \bar{\zeta}_B = \frac{c_B}{2m_B\bar{\omega}_B}, \quad \bar{\omega}_B = \sqrt{\frac{k}{m_B}} \end{aligned} \tag{A.49}$$

Introducing this relationship and the primary system natural frequency into the equation of motion produces:

$$\begin{aligned} &\frac{1}{\omega_A^2}\ddot{x}_A + \frac{1}{2}\frac{\bar{\zeta}_B}{\bar{\omega}_B}\left(\dot{x}_A - \dot{x}_B\right) + x_A + \frac{1}{4}\mu_k\left(x_A - x_B\right) = \frac{1}{2}y \\ &\ddot{x}_A + \frac{1}{2}\frac{\bar{\zeta}_B}{\bar{\omega}_B}\omega_A^2\left(\dot{x}_A - \dot{x}_B\right) + \omega_A^2 x_A + \frac{1}{4}\mu_k\omega_A^2\left(x_A - x_B\right) = \frac{1}{2}\omega_A^2 y \\ &\text{where: } \omega_A = \sqrt{\frac{4k}{m_A}} \end{aligned} \tag{A.50}$$

The damping term can further be simplified in terms of the mass ratio:

$$\frac{1}{2}\bar{\zeta}_B\frac{\omega_A}{\bar{\omega}_B}\omega_A = \frac{1}{2}\bar{\zeta}_B 2\sqrt{\mu_m}\omega_A = \bar{\zeta}_B\sqrt{\mu_m}\omega_A$$

$$\text{where: } \frac{\omega_A}{\bar{\omega}_B} = \frac{\sqrt{\frac{4k}{m_A}}}{\sqrt{\frac{k}{m_B}}} = 2\sqrt{\frac{k}{m_A}\frac{m_B}{k}} = 2\sqrt{\mu_m} \tag{A.51}$$

The equation of motion is now:

$$\ddot{x}_A + \sqrt{\mu_m}\bar{\zeta}_B\omega_A(\dot{x}_A - \dot{x}_B) + \omega_A^2 x_A + \frac{1}{4}\mu_k\omega_A^2(x_A - x_B) = \frac{1}{2}\omega_A^2 y \tag{A.52}$$

where the stiffness ratio is the only parameter that is a function of time.

The equation of motion for the auxiliary mass can be found from Equation (A.46):

$$\begin{aligned} m_B\ddot{x}_B - c_B(\dot{x}_A - \dot{x}_B) - k_B(x_A - x_B) &= 0 \\ \frac{m_B}{k_B}\ddot{x}_B - \frac{c_B}{k_B}(\dot{x}_A - \dot{x}_B) - (x_A - x_B) &= 0 \end{aligned} \tag{A.53}$$

The damping term can be simplified as follows:

$$\frac{c_B}{k_B} = 4\frac{k}{k_B}\frac{c_B}{4k} = \frac{4}{\mu_k}\frac{1}{2}\frac{\bar{\zeta}_B}{\bar{\omega}_B} = \frac{2}{\mu_k}\frac{\bar{\zeta}_B}{\bar{\omega}_B} \tag{A.54}$$

Substitution in the equation of motion yields:

$$\begin{aligned} \frac{1}{\omega_B^2}\ddot{x}_B - \frac{2}{\mu_k}\frac{\bar{\zeta}_B}{\bar{\omega}_B}(\dot{x}_A - \dot{x}_B) - (x_A - x_B) &= 0 \\ \ddot{x}_B - \frac{2}{\mu_k}\frac{\bar{\zeta}_B}{\bar{\omega}_B}\omega_B^2(\dot{x}_A - \dot{x}_B) - \omega_B^2(x_A - x_B) &= 0 \end{aligned} \tag{A.55}$$

The following two natural frequency ratios can be written in terms of the mass and stiffness ratios:

$$\begin{aligned} \frac{\omega_B^2}{\bar{\omega}_B^2} &= \frac{\frac{k_B}{m_B}}{\frac{k}{m_B}} = \frac{k_B}{k} = \mu_k \\ \frac{\omega_A^2}{\omega_B^2} &= 4\frac{\frac{k}{m_A}}{\frac{k_B}{m_B}} = 4\frac{m_B}{m_A}\frac{k}{k_B} = 4\frac{\mu_m}{\mu_k} \end{aligned} \tag{A.56}$$

Substitution in the equation of motion yields:

$$\begin{aligned}
&\ddot{x}_B - \frac{2}{\mu_k}\bar{\zeta}_B \frac{\omega_B}{\bar{\omega}_B}\omega_B\left(\dot{x}_A - \dot{x}_B\right) - \frac{1}{4}\frac{\mu_k}{\mu_m}\omega_A^2\left(x_A - x_B\right) = 0 \\
&\ddot{x}_B - \frac{2}{\mu_k}\bar{\zeta}_B\sqrt{\mu_k}\frac{1}{2}\frac{\sqrt{\mu_k}}{\sqrt{\mu_m}}\omega_A\left(\dot{x}_A - \dot{x}_B\right) - \frac{1}{4}\frac{\mu_k}{\mu_m}\omega_A^2\left(x_A - x_B\right) = 0 \\
&\ddot{x}_B - \frac{\bar{\zeta}_B}{\sqrt{\mu_m}}\omega_A\left(\dot{x}_A - \dot{x}_B\right) - \frac{1}{4}\frac{\mu_k}{\mu_m}\omega_A^2\left(x_A - x_B\right) = 0
\end{aligned} \tag{A.57}$$

In the frequency domain, when using the hysteretic damping, the normalised dynamic stiffness can be written in terms of the mass and stiffness ratios. The equation for a passive VAI (Equation (A.28)) can be rewritten using the relationship in Equation (A.56), yielding:

$$\frac{F_T}{kY} = \frac{1 + i\eta_B - \frac{\mu_m}{\mu_k}\left(\frac{\omega}{\omega_A}\right)^2}{\left[1 + \frac{1}{4}\mu_k\left(1 + i\eta_B\right) - \left(\frac{\omega}{\omega_A}\right)^2\right]\left[1 + i\eta_B - \frac{\mu_m}{\mu_k}\left(\frac{\omega}{\omega_A}\right)^2\right] - \frac{1}{4}\mu_k\left(1 + i\eta_B\right)^2} \tag{A.58}$$

where: $\mu_m = \frac{m_B}{m_A}, \quad \mu_k = \frac{k_B}{k}$

The undamped frequencies of maximum dynamic stiffness can be found by equating the denominator of Equation (A.58) to zero:

$$\begin{aligned}
&\left[1 + \frac{1}{4}\mu_k - \left(\frac{\omega}{\omega_A}\right)^2\right]\left[1 - 4\frac{\mu_m}{\mu_k}\left(\frac{\omega}{\omega_A}\right)^2\right] - \frac{1}{4}\mu_k = 0 \\
&1 + \frac{1}{4}\mu_k - \left(\frac{\omega}{\omega_A}\right)^2 - 4\frac{\mu_m}{\mu_k}\left(\frac{\omega}{\omega_A}\right)^2 - 4\frac{\mu_m}{\mu_k}\left(\frac{\omega}{\omega_A}\right)^2\frac{1}{4}\mu_k + 4\frac{\mu_m}{\mu_k}\left(\frac{\omega}{\omega_A}\right)^2\left(\frac{\omega}{\omega_A}\right)^2 - \frac{1}{4}\mu_k = 0 \\
&1 - \left(\frac{\omega}{\omega_A}\right)^2 - 4\frac{\mu_m}{\mu_k}\left(\frac{\omega}{\omega_A}\right)^2 - \mu_m\left(\frac{\omega}{\omega_A}\right)^2 + 4\frac{\mu_m}{\mu_k}\left(\frac{\omega}{\omega_A}\right)^2\left(\frac{\omega}{\omega_A}\right)^2 = 0 \\
&\omega_A^4 - \omega^2\omega_A^2 - 4\frac{\mu_m}{\mu_k}\omega^2\omega_A^2 - \mu_m\omega^2\omega_A^2 + 4\frac{\mu_m}{\mu_k}\omega^4 = 0 \\
&4\frac{\mu_m}{\mu_k}\omega^4 - \left(\omega_A^2 + 4\frac{\mu_m}{\mu_k}\omega_A^2 + \mu_m\omega_A^2\right)\omega^2 + \omega_A^4 = 0 \\
&\omega^4 - \left(\frac{1}{4}\frac{\mu_k}{\mu_m}\omega_A^2 + \omega_A^2 + \frac{1}{4}\mu_k\omega_A^2\right)\omega^2 + \frac{1}{4}\frac{\mu_k}{\mu_m}\omega_A^4 = 0
\end{aligned} \tag{A.59}$$

The positive roots of the above polynomial are:

$$\begin{aligned}
\Omega_1^2, \Omega_2^2 &= \frac{-b \pm \sqrt{b^2 - 4ac}}{2a} \\
\Omega_1^2, \Omega_2^2 &= \frac{\frac{1}{4}\frac{\mu_k}{\mu_m}\omega_A^2 + \omega_A^2 + \frac{1}{4}\mu_k\omega_A^2 \pm \sqrt{\left(\frac{1}{4}\frac{\mu_k}{\mu_m}\omega_A^2 + \omega_A^2 + \frac{1}{4}\mu_k\omega_A^2\right)^2 - \frac{\mu_k}{\mu_m}\omega_A^4}}{2} \\
\Omega_1^2, \Omega_2^2 &= \omega_A^2\frac{\frac{1}{4}\frac{\mu_k}{\mu_m} + 1 + \frac{1}{4}\mu_k \pm \sqrt{\left(\frac{1}{4}\frac{\mu_k}{\mu_m} + 1 + \frac{1}{4}\mu_k\right)^2 - \frac{\mu_k}{\mu_m}}}{2}
\end{aligned} \tag{A.60}$$

The above equation can be normalised as follows:

$$\frac{\Omega_1}{\omega_A},\frac{\Omega_2}{\omega_A}=\sqrt{\frac{\frac{1}{4}\frac{\mu_k}{\mu_m}+1+\frac{1}{4}\mu_k \pm\sqrt{\left(\frac{1}{4}\frac{\mu_k}{\mu_m}+1+\frac{1}{4}\mu_k\right)^2-\frac{\mu_k}{\mu_m}}}{2}} \tag{A.61}$$

A.3.5 Active vibration-absorbing isolator (acceleration and displacement feedback)

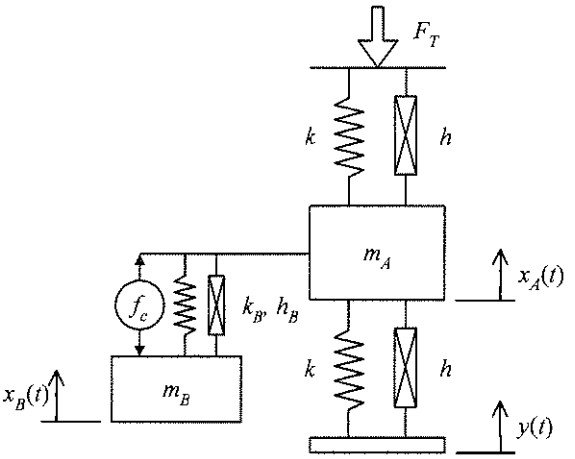

Figure A.8: Mechanical model of an active vihration-absorbing isolator

The control force is using relative acceleration and displacement feedback with gains α and γ:

$$f_c(t)=\alpha\left(\ddot{x}_B-\ddot{x}_A\right)+\gamma\left(x_B-x_A\right) \tag{A.62}$$

The force can be introduced on the right hand side of Equation (A.23). This leads to:

$$\begin{bmatrix} m_A & 0 \\ 0 & m_B \end{bmatrix}\begin{bmatrix} \ddot{x}_A \\ \ddot{x}_B \end{bmatrix}+\begin{bmatrix} 4k(1+i\eta)+k_B(1+i\eta_B) & -k_B(1+i\eta_B) \\ -k_B(1+i\eta_B) & k_B(1+i\eta_B) \end{bmatrix}\begin{bmatrix} x_A \\ x_B \end{bmatrix}=\begin{bmatrix} 2k(1+i\eta)y+f_c \\ -f_c \end{bmatrix} \tag{A.63}$$

When simplified, the above equation becomes:

$$\begin{bmatrix} m_A+\alpha & -\alpha \\ -\alpha & m_B+\alpha \end{bmatrix}\begin{bmatrix} \ddot{x}_A \\ \ddot{x}_B \end{bmatrix}+\begin{bmatrix} 4k(1+i\eta)+k_B(1+i\eta_B)+\gamma & -k_B(1+i\eta_B)-\gamma \\ -k_B(1+i\eta_B)-\gamma & k_B(1+i\eta_B)+\gamma \end{bmatrix}\begin{bmatrix} x_A \\ x_B \end{bmatrix}=\begin{bmatrix} 2k(1+i\eta)y \\ 0 \end{bmatrix} \tag{A.64}$$

In the frequency domain the above equation yields:

$$\begin{aligned} &\left[4k(1+i\eta)+k_B(1+i\eta_B)+\gamma-\omega^2(m_A+\alpha)\right]X_A-\left[k_B(1+i\eta_B)+\gamma\right]X_B=2k(1+i\eta)Y \\ &-\left[k_B(1+i\eta_B)+\gamma\right]X_A+\left[k_B(1+i\eta_B)+\gamma-\omega^2(m_B+\alpha)\right]X_B=0 \end{aligned} \tag{A.65}$$

The second equation can be simplified to give an expression for X_B:

$$X_B=\frac{k_B(1+i\eta_B)+\gamma}{k_B(1+i\eta_B)+\gamma-\omega^2(m_B+\alpha)}X_A \tag{A.66}$$

Introducing the above equation into the first equation yields the transmissibility:

$$\left[4k(1+i\eta)+k_B(1+i\eta_B)+\gamma-\omega^2(m_A+\alpha)\right]X_A-\left[k_B(1+i\eta_B)+\gamma\right]X_B=2k(1+i\eta)Y$$

$$\left[4k(1+i\eta)+k_B(1+i\eta_B)+\gamma-\omega^2(m_A+\alpha)\right]X_A-\left[k_B(1+i\eta_B)+\gamma\right]\frac{k_B(1+i\eta_B)+\gamma}{k_B(1+i\eta_B)+\gamma-\omega^2(m_B+\alpha)}X_A=2k(1+i\eta)Y$$

$$\frac{X_A}{Y}=\frac{2k(1+i\eta)\left[k_B(1+i\eta_B)+\gamma-\omega^2(m_B+\alpha)\right]}{\left[4k(1+i\eta)+k_B(1+i\eta_B)+\gamma-\omega^2(m_A+\alpha)\right]\left[k_B(1+i\eta_B)+\gamma-\omega^2(m_B+\alpha)\right]-\left[k_B(1+i\eta_B)+\gamma\right]^2} \tag{A.67}$$

For the undamped case the force transmitted is:

$$F_T=2kX_A \tag{A.68}$$

Substituting for the displacement of the intermediate mass in terms of the excitation:

$$\frac{F_T}{Y}=\frac{4k^2\left[k_B+\gamma-\omega^2(m_B+\alpha)\right]}{\left[4k+k_B+\gamma-\omega^2(m_A+\alpha)\right]\left[k_B+\gamma-\omega^2(m_B+\alpha)\right]-\left[k_B+\gamma\right]^2} \tag{A.69}$$

The above equation can be non-dimensionalised:

$$\begin{aligned}\frac{F_T}{kY}&=\frac{1-\omega^2\dfrac{m_B+\alpha}{k_B+\gamma}}{\left(1+\dfrac{k_B+\gamma}{4k}-\omega^2\dfrac{m_A+\alpha}{4k}\right)\left(1-\omega^2\dfrac{m_B+\alpha}{k_B+\gamma}\right)-\dfrac{k_B+\gamma}{4k}}\\&=\frac{1-\left(\dfrac{\omega}{\omega_B'}\right)^2}{\left[1+\dfrac{1}{4}\dfrac{k_B}{k}\left(1+\dfrac{\gamma}{k_B}\right)-\left(\dfrac{\omega}{\omega_A}\right)^2\right]\left[1-\left(\dfrac{\omega}{\omega_B'}\right)^2\right]-\dfrac{1}{4}\dfrac{k_B}{k}\left(1+\dfrac{\gamma}{k_B}\right)}\end{aligned} \tag{A.70}$$

where: $\omega_A=\sqrt{\dfrac{4k}{m_A+\alpha}}$, $\omega_B'=\sqrt{\dfrac{k_B\left(1+\dfrac{\gamma}{k_B}\right)}{m_B\left(1+\dfrac{\alpha}{m_B}\right)}}=\omega_B\sqrt{\dfrac{1+\dfrac{\gamma}{k_B}}{1+\dfrac{\alpha}{m_B}}}$

The Routh-Hurwitz stability criterion is evaluated using the characteristic equation and the sub-determinants defined by the coefficients of the characteristic equation. The characteristic equation can be found from the determinant of the equation of motion, which for the undamped case is:

$$\begin{aligned}D(s)&=\begin{vmatrix}4k+k_B+\gamma+s^2(m_A+\alpha) & -k_B-\gamma-s^2\alpha\\ -k_B-\gamma-s^2\alpha & k_B+\gamma+s^2(m_B+\alpha)\end{vmatrix}\\&=\left[4k+k_B+\gamma+s^2(m_A+\alpha)\right]\left[k_B+\gamma+s^2(m_B+\alpha)\right]-\left[-k_B-\gamma-s^2\alpha\right]^2\\&=\left[m_Bm_A+\alpha(m_A+m_B)\right]s^4+\left[4m_Bk+4k\alpha+(m_B+m_A)(k_B+\gamma)\right]s^2+4kk_B+4k\gamma\end{aligned} \tag{A.71}$$

The Routh-Hurwitz criterion requires that the coefficients of the characteristic equation be larger than zero (Rao, 1990):

$$\begin{aligned} a_0 &= m_B m_A + \alpha\left(m_A + m_B\right) > 0 \\ &\therefore \alpha > -\frac{m_B m_A}{m_A + m_B} \\ a_2 &= 4m_B k + 4k\alpha + k_B m_B + \gamma m_B + k m_B + m_A \gamma > 0 \\ &\therefore 4km_B^2 > 0 \\ a_4 &= 4kk_B + 4k\gamma > 0 \\ &\therefore \frac{\gamma}{k_B} > -1 \end{aligned} \tag{A.72}$$

Additionally for a two degree of freedom system the following inequality must be satisfied:

$$a_1 a_2 a_3 > a_0 a_3^2 + a_4 a_1^2 \tag{A.73}$$

The above condition is not satisfied and it is concluded that the system is marginally stable.

A.3.6 Active vibration-absorbing isolator (relative velocity feedback)

For a control force defined by the relative velocity feedback is:

$$f_c(t) = \beta\left(\dot{x}_B - \dot{x}_A\right) \tag{A.74}$$

The equation of motion must necessarily include a viscous damping model:

$$\begin{bmatrix} m_A & 0 \\ 0 & m_B \end{bmatrix}\begin{bmatrix} \ddot{x}_A \\ \ddot{x}_B \end{bmatrix} + \begin{bmatrix} 4c + c_B & -c_B \\ -c_B & c_B \end{bmatrix}\begin{bmatrix} \dot{x}_A \\ \dot{x}_B \end{bmatrix} + \begin{bmatrix} 4k + k_B & -k_B \\ -k_B & k_B \end{bmatrix}\begin{bmatrix} x_A \\ x_B \end{bmatrix} = \begin{bmatrix} 2ky + 2c\dot{y} + \beta\left(\dot{x}_B - \dot{x}_A\right) \\ -\beta\left(\dot{x}_B - \dot{x}_A\right) \end{bmatrix} \tag{A.75}$$

When transformed to the frequency domain the above equation becomes:

$$\begin{bmatrix} 4k + k_B + i\omega\left(4c + c_B + \beta\right) - \omega^2 m_A & -k_B - i\omega\left(c_B + \beta\right) \\ -k_B - i\omega\left(c_B + \beta\right) & k_B + i\omega\left(c_B + \beta\right) - \omega^2 m_B \end{bmatrix}\begin{bmatrix} X_A \\ X_B \end{bmatrix} = \begin{bmatrix} 2\left(k + i\omega c\right) \\ 0 \end{bmatrix} Y \tag{A.76}$$

The second equation can be used to find an expression for the absorber displacement:

$$\begin{aligned} -\left[k_B + i\omega\left(c_B + \beta\right)\right] X_A + \left[k_B + i\omega\left(c_B + \beta\right) - \omega^2 m_B\right] X_B &= 0 \\ X_B &= \frac{k_B + i\omega\left(c_B + \beta\right)}{k_B + i\omega\left(c_B + \beta\right) - \omega^2 m_B} X_A \end{aligned} \tag{A.77}$$

When the absorber displacement is eliminated from the first equation of Equation (A.76):

$$\left[4k+k_B+i\omega\left(4c+c_B+\beta\right)-\omega^2 m_A\right]X_A-\left[k_B+i\omega\left(c_B+\beta\right)\right]X_B=2\left(k+i\omega c\right)Y$$

$$\left[4k+k_B+i\omega\left(4c+c_B+\beta\right)-\omega^2 m_A\right]X_A-\left[k_B+i\omega\left(c_B+\beta\right)\right]\frac{k_B+i\omega\left(c_B+\beta\right)}{k_B+i\omega\left(c_B+\beta\right)-\omega^2 m_B}X_A=2\left(k+i\omega c\right)Y$$

$$\left\{\left[4k+k_B+i\omega\left(4c+c_B+\beta\right)-\omega^2 m_A\right]\left[k_B+i\omega\left(c_B+\beta\right)-\omega^2 m_B\right]-\left[k_B+i\omega\left(c_B+\beta\right)\right]^2\right\}X_A=\quad(A.78)$$

$$2\left(k+i\omega c\right)\left[k_B+i\omega\left(c_B+\beta\right)-\omega^2 m_B\right]Y$$

$$X_A=\frac{2\left(k+i\omega c\right)\left[k_B+i\omega\left(c_B+\beta\right)-\omega^2 m_B\right]}{\left[4k+k_B+i\omega\left(4c+c_B+\beta\right)-\omega^2 m_A\right]\left[k_B+i\omega\left(c_B+\beta\right)-\omega^2 m_B\right]-\left[k_B+i\omega\left(c_B+\beta\right)\right]^2}Y$$

The force transmitted is:

$$F_T=2\left(k+i\omega c\right)X_A \quad (A.79)$$

When substituting the intermediate mass displacement, this equation becomes:

$$\frac{F_T}{Y}=2\left(k+i\omega c\right)\frac{2\left(k+i\omega c\right)\left[k_B+i\omega\left(c_B+\beta\right)-\omega^2 m_B\right]}{\left[4k+k_B+i\omega\left(4c+c_B+\beta\right)-\omega^2 m_A\right]\left[k_B+i\omega\left(c_B+\beta\right)-\omega^2 m_B\right]-\left[k_B+i\omega\left(c_B+\beta\right)\right]^2} \quad (A.80)$$

The equation can be normalised as follows:

$$\frac{F_T}{Y}=\frac{4k^2k_B\left(1+i2\frac{\omega}{\omega_A}\zeta\right)^2\left[1+i2\frac{\omega}{\omega_B}\zeta_B-\left(\frac{\omega}{\omega_B}\right)^2\right]}{4k\left[1+\frac{1}{4}\frac{k_B}{k}+i2\left(\frac{\omega}{\omega_A}\zeta+\frac{\omega}{\omega_B}\frac{k_B}{k}\zeta_B\right)-\left(\frac{\omega}{\omega_A}\right)^2\right]k_B\left[1+i2\frac{\omega}{\omega_B}\zeta_B-\left(\frac{\omega}{\omega_B}\right)^2\right]-k_B^2\left(1+i2\frac{\omega}{\omega_B}\zeta_B\right)^2}$$

$$\frac{F_T}{kY}=\frac{\left(1+i2\frac{\omega}{\omega_A}\zeta\right)^2\left[1+i2\frac{\omega}{\omega_B}\zeta_B-\left(\frac{\omega}{\omega_B}\right)^2\right]}{\left[1+\frac{1}{4}\frac{k_B}{k}+i2\left(\frac{\omega}{\omega_A}\zeta+\frac{\omega}{\omega_B}\frac{k_B}{k}\zeta_B\right)-\left(\frac{\omega}{\omega_A}\right)^2\right]\left[1+i2\frac{\omega}{\omega_B}\zeta_B-\left(\frac{\omega}{\omega_B}\right)^2\right]-\frac{1}{4}\frac{k_B}{k}\left(1+i2\frac{\omega}{\omega_B}\zeta_B\right)^2} \quad (A.81)$$

where: $\zeta=\frac{c}{2m_A\omega_A}$ $\zeta_B=\frac{c_B+\beta}{2m_B\omega_B}$

The characteristic equation is:

$$\begin{aligned}D(s)&=\begin{vmatrix}4k+k_B+s\left(4c+c_B+\beta\right)+s^2m_A & -k_B-s\left(c_B+\beta\right)\\ -k_B-s\left(c_B+\beta\right) & k_B+s\left(c_B+\beta\right)+s^2m_B\end{vmatrix}\\&=\left[4k+k_B+s\left(4c+c_B+\beta\right)+s^2m_A\right]\left[k_B+s\left(c_B+\beta\right)+s^2m_B\right]-\left[k_B+s\left(c_B+\beta\right)\right]^2 \quad (A.82)\\&=m_Am_Bs^4+\left(4cm_B+c_Bm_B+m_Ac_B+m_A\beta+\beta m_B\right)s^3+\left(4km_B+m_Ak_B+4cc_B+4c\beta+k_Bm_B\right)s^2\\&\quad+\left(4ck_B+4kc_B+4k\beta\right)s+4kk_B\end{aligned}$$

The Routh-Hurwitz criterion requires that the coefficients of the characteristic equation be larger than zero:

$$\begin{aligned}
a_0 &= m_A m_B > 0 \\
a_1 &= 4cm_B + c_B m_B + m_A c_B + m_A \beta + \beta m_B > 0 \\
&\therefore \beta > -c_B - 4c\frac{m_B}{m_A + m_B} \\
a_2 &= 4km_B + m_A k_B + 4cc_B + 4c\beta + k_B m_B > 0 \\
&\therefore \beta > -c_B - \frac{k_B m_B}{4c} - \frac{km_B}{c} - \frac{m_A k_B}{4c} \\
a_3 &= 4ck_B + 4kc_B + 4k\beta > 0 \\
&\therefore \beta > -c_B - c\frac{k_B}{k} \\
a_4 &= 4kk_B > 0
\end{aligned} \tag{A.83}$$

Additionally for a two degree of freedom system the following inequality must be satisfied:

$$\begin{aligned}
&a_1 a_2 a_3 > a_0 a_3^2 + a_4 a_1^2 \\
&\left(4cm_B + c_B m_B + m_A c_B + m_A \beta + \beta m_B\right)\left(4km_B + m_A k_B + 4cc_B + 4c\beta + k_B m_B\right)\left(4ck_B + 4kc_B + 4k\beta\right) \\
&> m_A m_B \left(4ck_B + 4kc_B + 4k\beta\right)^2 + 4kk_B \left(4cm_B + c_B m_B + m_A c_B + m_A \beta + \beta m_B\right)^2
\end{aligned} \tag{A.84}$$

The worst case occurs when the intermediate mass damping is equal to zero and then:

$$\beta > -c_B \tag{A.85}$$

A.3.7 Active vibration-absorbing isolator (absolute velocity feedback)

The control force when using absolute absorber velocity feedback is:

$$f_c(t) = \beta \dot{x}_B \tag{A.86}$$

The equation of motion is:

$$\begin{bmatrix} m_A & 0 \\ 0 & m_B \end{bmatrix}\begin{bmatrix} \ddot{x}_A \\ \ddot{x}_B \end{bmatrix} + \begin{bmatrix} 4c + c_B & -c_B \\ -c_B & c_B \end{bmatrix}\begin{bmatrix} \dot{x}_A \\ \dot{x}_B \end{bmatrix} + \begin{bmatrix} 4k + k_B & -k_B \\ -k_B & k_B \end{bmatrix}\begin{bmatrix} x_A \\ x_B \end{bmatrix} = \begin{bmatrix} 2ky + 2c\dot{y} + \beta \dot{x}_B \\ -\beta \dot{x}_B \end{bmatrix} \tag{A.87}$$

When transformed to the frequency domain, the above equation becomes:

$$\begin{bmatrix} 4k + k_B + i\omega\left(4c + c_B\right) - \omega^2 m_A & -k_B - i\omega\left(c_B + \beta\right) \\ -k_B - i\omega c_B & k_B + i\omega\left(c_B + \beta\right) - \omega^2 m_B \end{bmatrix}\begin{bmatrix} X_A \\ X_B \end{bmatrix} = \begin{bmatrix} 2\left(k + i\omega c\right) \\ 0 \end{bmatrix} Y \tag{A.88}$$

The second equation yields the absorber displacement:

$$X_B = \frac{k_B + i\omega c_B}{k_B + i\omega\left(c_B + \beta\right) - \omega^2 m_B} X_A \tag{A.89}$$

Introducing the above equation into the first equation yields the transmissibility:

$$\left[4k+k_B+i\omega\left(4c+c_B\right)-\omega^2 m_A\right]X_A-\left[k_B+i\omega\left(c_B+\beta\right)\right]X_B=2\left(k+i\omega c\right)Y$$

$$\left[4k+k_B+i\omega\left(4c+c_B\right)-\omega^2 m_A\right]X_A-\left[k_B+i\omega\left(c_B+\beta\right)\right]\frac{k_B+i\omega c_B}{k_B+i\omega\left(c_B+\beta\right)-\omega^2 m_B}X_A=2\left(k+i\omega c\right)Y$$

$$\left\{\left[4k+k_B+i\omega\left(4c+c_B\right)-\omega^2 m_A\right]\left[k_B+i\omega\left(c_B+\beta\right)-\omega^2 m_B\right]-\left[k_B+i\omega\left(c_B+\beta\right)\right]\left(k_B+i\omega c_B\right)\right\}X_A \qquad (A.90)$$

$$=2\left(k+i\omega c\right)\left[k_B+i\omega\left(c_B+\beta\right)-\omega^2 m_B\right]Y$$

$$\frac{X_A}{Y}=\frac{2\left(k+i\omega c\right)\left[k_B+i\omega\left(c_B+\beta\right)-\omega^2 m_B\right]}{\left[4k+k_B+i\omega\left(4c+c_B\right)-\omega^2 m_A\right]\left[k_B+i\omega\left(c_B+\beta\right)-\omega^2 m_B\right]-\left[k_B+i\omega\left(c_B+\beta\right)\right]\left(k_B+i\omega c_B\right)}$$

The force transmitted is:

$$F_T=2\left(k+i\omega c\right)X_A \qquad (A.91)$$

Substituting for the displacement of the intermediate mass in terms of the excitation:

$$\frac{F_T}{Y}=\frac{4\left(k+i\omega c\right)^2\left[k_B+i\omega\left(c_B+\beta\right)-\omega^2 m_B\right]}{\left[4k+k_B+i\omega\left(4c+c_B\right)-\omega^2 m_A\right]\left[k_B+i\omega\left(c_B+\beta\right)-\omega^2 m_B\right]-\left[k_B+i\omega\left(c_B+\beta\right)\right]\left(k_B+i\omega c_B\right)}$$

$$\frac{F_T}{kY}=\frac{\left(1+i\omega\frac{c}{k}\right)^2\left[1+i\omega\frac{c_B+\beta}{k_B}-\omega^2\frac{m_B}{k_B}\right]}{\left[1+\frac{1}{4}\frac{k_B}{k}+i\omega\left(\frac{4c+c_B}{4k}\right)-\omega^2\frac{m_A}{4k}\right]\left[1+i\omega\frac{c_B+\beta}{k_B}-\omega^2\frac{m_B}{k_B}\right]-\frac{1}{4}\frac{k_B}{k}\left[1+i\omega\frac{c_B+\beta}{k_B}\right]\left(1+i\omega\frac{c_B}{k_B}\right)} \qquad (A.92)$$

The above equation can be non-dimensionalised as follows:

$$\frac{F_T}{kY}=\frac{\left(1+i2\zeta\frac{\omega}{\omega_A}\right)^2\left[1+i2\frac{\omega}{\omega_B}\zeta_B\left(1+\frac{\beta}{c_B}\right)-\left(\frac{\omega}{\omega_B}\right)^2\right]}{\left[1+\frac{1}{4}\frac{k_B}{k}+i2\left(\frac{\omega}{\omega_A}\zeta+\frac{1}{4}\frac{k_B}{k}\frac{\omega}{\omega_B}\zeta_B\right)-\left(\frac{\omega}{\omega_A}\right)^2\right]\left[1+i2\frac{\omega}{\omega_B}\zeta_B\left(1+\frac{\beta}{c_B}\right)-\left(\frac{\omega}{\omega_B}\right)^2\right]-\frac{1}{4}\frac{k_B}{k}\left[1+i2\frac{\omega}{\omega_B}\zeta_B\left(1+\frac{\beta}{c_B}\right)\right]\left(1+i2\frac{\omega}{\omega_B}\zeta_B\right)} \qquad (A.93)$$

where: $\zeta_B=\frac{c_B}{2m_B\omega_B}$, $\zeta=\frac{c}{2m_A\omega_A}$

The characteristic equation is:

$$D(s)=\begin{vmatrix}4k+k_B+s\left(4c+c_B\right)+s^2m_A & -k_B-s\left(c_B+\beta\right)\\ -k_B-sc_B & k_B+i\omega\left(c_B+\beta\right)+s^2m_B\end{vmatrix}$$

$$=\left[4k+k_B+s\left(4c+c_B\right)+s^2m_A\right]\left[k_B+s\left(c_B+\beta\right)+s^2m_B\right]-\left(k_B+sc_B\right)\left[k_B+s\left(c_B+\beta\right)\right] \qquad (A.94)$$

$$=s^4m_Am_B+(4cm_B+c_Bm_B+m_Ac_B+m_A\beta)s^3+(4km_B+k_Bm_B+4cc_B+4c\beta+m_Ak_B)s^2$$

$$+(4kc_B+4k\beta+4ck_B)s+4kk_B$$

The Routh-Hurwitz criterion requires that the coefficients of the characteristic equation be larger than zero:

$$\begin{aligned}
&a_0 = m_A m_B > 0 \\
&a_1 = 4cm_B + c_B m_B + m_A c_B + m_A \beta > 0 \\
&\quad \therefore \beta > -c_B \left(1 + \frac{m_B}{m_A}\right) - 4c\frac{m_B}{m_A} \\
&a_2 = 4km_B + k_B m_B + 4cc_B + 4c\beta + m_A k_B > 0 \\
&\quad \therefore \beta > -c_B - \frac{km_B}{c} - \frac{k_B m_B}{4c} - \frac{m_A k_B}{4c} \\
&a_3 = 4kc_B + 4k\beta + 4ck_B > 0 \\
&\quad \therefore \beta > -c_B - c\frac{k_B}{k} \\
&a_4 = 4kk_B > 0
\end{aligned} \tag{A.95}$$

Additionally for a two degree of freedom system the following inequality must be satisfied:

$$\begin{aligned}
&a_1 a_2 a_3 > a_0 a_3^2 + a_4 a_1^2 \\
&\left(4cm_B + c_B m_B + m_A c_B + m_A \beta\right)\left(4km_B + k_B m_B + 4cc_B + 4c\beta + m_A k_B\right)\left(4kc_B + 4k\beta + 4ck_B\right) \\
&> m_A m_B \left(4kc_B + 4k\beta + 4ck_B\right)^2 + 4kk_B \left(4cm_B + c_B m_B + m_A c_B + m_A \beta\right)^2
\end{aligned} \tag{A.96}$$

The worst case occurs when the intermediate mass damping is equal to zero and then:

$$\beta > -c_B \tag{A.97}$$

A.4 Amplified vibration-absorbing isolators

A.4.1 Passive amplified vibration-absorbing isolator

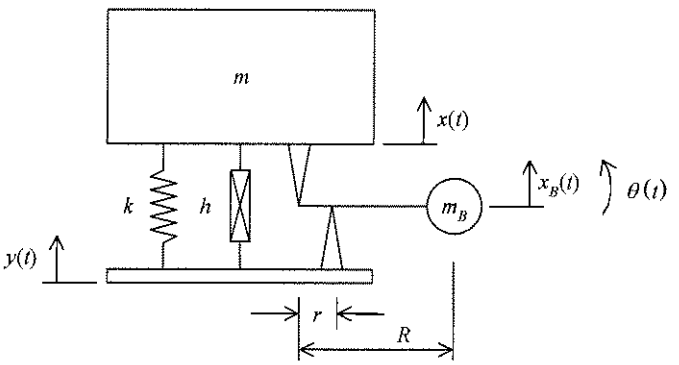

Figure A.9: Mechanical model of a pendulum AVAI

The continuity between the response excitation and the pendulum displacement can be written by considering Figure A.10.

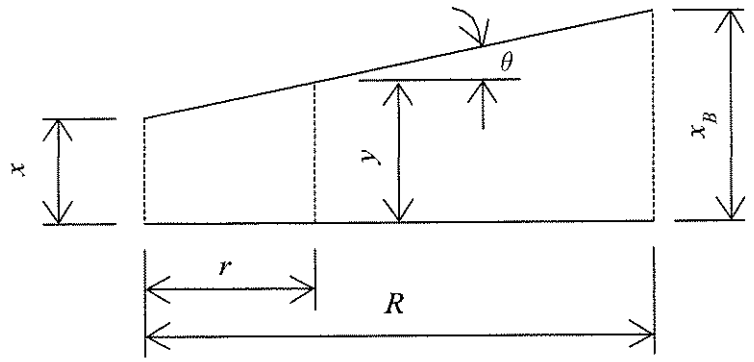

Figure A.10: Continuity description

The distance travelled by the absorber mass and its angle of rotation can be written as:

$$x_B = \left(1-\frac{R}{r}\right)x + \frac{R}{r}y$$
$$\theta = \frac{y-x}{r} \tag{A.98}$$

The kinetic energy can be found in terms of the excitation and response degrees of freedom by substituting the absorber degrees of freedom using the continuity equations:

$$\begin{aligned} T &= \frac{1}{2}\left(m\dot{x}^2 + m_B\dot{x}_B^2 + I_G\dot{\theta}^2\right) \\ &= \frac{1}{2}\left[m + m_B\left(1-\frac{R}{r}\right)^2 + \frac{I_G}{r^2}\right]\dot{x}^2 + \left[m_B\left(1-\frac{R}{r}\right)\frac{R}{r} - \frac{I_G}{r^2}\right]\dot{x}\dot{y} + \frac{1}{2}\left[m_B\left(\frac{R}{r}\right)^2 + \frac{I_G}{r^2}\right]\dot{y}^2 \end{aligned} \tag{A.99}$$

From the above equation the derivatives can be found:

$$\begin{aligned} \frac{d}{dt}\left(\frac{\partial T}{\partial \dot{x}}\right) &= \left[m + m_B\left(1-\frac{R}{r}\right)^2 + \frac{I_G}{r^2}\right]\ddot{x} + \left[m_B\left(1-\frac{R}{r}\right)\frac{R}{r} - \frac{I_G}{r^2}\right]\ddot{y} \\ \frac{d}{dt}\left(\frac{\partial T}{\partial \dot{y}}\right) &= \left[m_B\left(\frac{R}{r}\right)^2 + \frac{I_G}{r^2}\right]\ddot{y} + \left[m_B\left(1-\frac{R}{r}\right)\frac{R}{r} - \frac{I_G}{r^2}\right]\ddot{x} \end{aligned} \tag{A.100}$$

The potential energy is:

$$V = \frac{1}{2}k\left(x-y\right)^2 \tag{A.101}$$

From the above equation the derivatives can be found:

$$\frac{\partial V}{\partial x} = k\left(x-y\right)$$
$$\frac{\partial V}{\partial y} = k\left(y-x\right) \tag{A.102}$$

The Rayleigh term is:

$$R = \frac{1}{2} c (\dot{x} - \dot{y})^2 \tag{A.103}$$

From the above equation the derivatives can be found:

$$\begin{aligned} \frac{\partial R}{\partial \dot{x}} &= c(\dot{x} - \dot{y}) \\ \frac{\partial R}{\partial \dot{y}} &= c(\dot{y} - \dot{x}) \end{aligned} \tag{A.104}$$

The most general case including both viscous and hysteretic damping gives:

$$\begin{bmatrix} m + m_B\left(1 - \frac{R}{r}\right)^2 + \frac{I_G}{r^2} & m_B\left(1 - \frac{R}{r}\right)\frac{R}{r} - \frac{I_G}{r^2} \\ m_B\left(1 - \frac{R}{r}\right)\frac{R}{r} - \frac{I_G}{r^2} & m_B\left(\frac{R}{r}\right)^2 + \frac{I_G}{r^2} \end{bmatrix} \begin{bmatrix} \ddot{x} \\ \ddot{y} \end{bmatrix} + \begin{bmatrix} c & -c \\ -c & c \end{bmatrix} \begin{bmatrix} \dot{x} \\ \dot{y} \end{bmatrix} + \begin{bmatrix} k(1+\eta) & -k(1+\eta) \\ -k(1+\eta) & k(1+\eta) \end{bmatrix} \begin{bmatrix} x \\ y \end{bmatrix} = \begin{bmatrix} f_x \\ f_y \end{bmatrix} \tag{A.105}$$

If the y degree of freedom is prescribed and no external forces are acting on the system the second equation must be neglected and the equation of motion becomes:

$$\left[m + m_B\left(1 - \frac{R}{r}\right)^2 + \frac{I_G}{r^2}\right]\ddot{x} + c\dot{x} + k(1+\eta)x = -\left[m_B\left(1 - \frac{R}{r}\right)\frac{R}{r} - \frac{I_G}{r^2}\right]\ddot{y} + c\dot{y} + k(1+\eta)y \tag{A.106}$$

In the frequency domain the above equation can be used to give the transmissibility:

$$\frac{X}{Y} = \frac{k(1+\eta) + i\omega c - \omega^2\left[m_B\left(\frac{R}{r} - 1\right)\frac{R}{r} + \frac{I_G}{r^2}\right]}{k(1+\eta) + i\omega c - \omega^2\left[m + m_B\left(1 - \frac{R}{r}\right)^2 + \frac{I_G}{r^2}\right]} \tag{A.107}$$

The above equation can be non-dimensionalised by introducing the isolation and natural frequencies:

$$\frac{X}{Y} = \frac{1 + i\eta + i2\frac{\omega}{\omega_n}\zeta - \left(\frac{\omega}{\omega_i}\right)^2}{1 + i\eta + i2\frac{\omega}{\omega_n}\zeta - \left(\frac{\omega}{\omega_n}\right)^2} \tag{A.108}$$

where: $\omega_n = \sqrt{\dfrac{k}{m + m_B\left(\frac{R}{r} - 1\right)^2 + \frac{I_G}{r^2}}}$, $\omega_i = \sqrt{\dfrac{k}{m_B\left(\frac{R}{r} - 1\right)\frac{R}{r} + \frac{I_G}{r^2}}}$, $\zeta = \dfrac{c}{2\left[m + m_B\left(\frac{R}{r} - 1\right)^2 + \frac{I_G}{r^2}\right]\omega_n}$

The invariant frequency can be calculated by setting the absolute value of the transmissibility equal to 1. For transmissibility equal to 1 the trivial solution of zero results. When the transmissibility is equal to -1:

$$\begin{aligned}
\frac{1-\left(\frac{\omega_A}{\omega_i}\right)^2}{1-\left(\frac{\omega_A}{\omega_n}\right)^2} &= -1 \\
\omega_n^2\omega_i^2 - \omega_n^2\omega_A^2 &= -\omega_n^2\omega_i^2 + \omega_i^2\omega_A^2 \\
2\omega_n^2\omega_i^2 &= \left(\omega_n^2 + \omega_i^2\right)\omega_A^2 \\
\frac{\omega_A^2}{\omega_i^2} &= \frac{2}{1+\frac{\omega_i^2}{\omega_n^2}} \\
\frac{\omega_A}{\omega_i} &= \sqrt{\frac{2}{1+\left(\frac{\omega_i}{\omega_n}\right)^2}}
\end{aligned} \tag{A.109}$$

The force transmitted can be calculated by using the first equation of Equation (A.105) and calculating the force f_x needed to restraint the displacement x to zero:

$$\left[m_B\left(\frac{R}{r}-1\right)\frac{R}{r}+\frac{I_G}{r^2}\right]\ddot{y} - c\dot{y} - k\left(1+\eta\right)y = f_x \tag{A.110}$$

When transformed to the frequency domain, substituting the external force (F_x) with the transmitted force ($-F_T$) and neglecting the viscous damping, the above equation becomes:

$$\begin{aligned}
\left\{\omega^2\left[m_B\left(\frac{R}{r}-1\right)\frac{R}{r}+\frac{I_G}{r^2}\right]-k\left(1+i\eta\right)\right\}Y &= F_x \\
\frac{F_T}{Y} &= k\left(1+i\eta\right)-\omega^2\left[m_B\left(\frac{R}{r}-1\right)\frac{R}{r}+\frac{I_G}{r^2}\right]
\end{aligned} \tag{A.111}$$

Which can then be non-dimensionalised as follows:

$$\frac{F_T}{kY} = 1 + i\eta - \left(\frac{\omega}{\omega_i}\right)^2 \tag{A.112}$$

The damped natural and isolation frequencies can be calculated setting the derivative of the transmissibility equal to zero:

$$\frac{\partial}{\partial\omega}\left|\frac{X}{Y}\right| = \frac{\partial}{\partial\omega}\left\{\frac{\left[1-\left(\frac{\omega}{\omega_i}\right)^2\right]^2+4\left(\frac{\omega}{\omega_n}\zeta\right)^2}{\left[1-\left(\frac{\omega}{\omega_n}\right)^2\right]^2+4\left(\frac{\omega}{\omega_n}\zeta\right)^2}\right\}^{\frac{1}{2}} = 0$$

$$\frac{1}{2}\left\{\frac{\left[1-\left(\frac{\omega}{\omega_i}\right)^2\right]^2+4\left(\frac{\omega}{\omega_n}\zeta\right)^2}{\left[1-\left(\frac{\omega}{\omega_n}\right)^2\right]^2+4\left(\frac{\omega}{\omega_n}\zeta\right)^2}\right\}^{-\frac{1}{2}}\left\{\frac{\frac{\partial}{\partial\omega}\left\{\left[1-\left(\frac{\omega}{\omega_i}\right)^2\right]^2+4\left(\frac{\omega}{\omega_n}\zeta\right)^2\right\}\left\{\left[1-\left(\frac{\omega}{\omega_n}\right)^2\right]^2+4\left(\frac{\omega}{\omega_n}\zeta\right)^2\right\}-\frac{\partial}{\partial\omega}\left\{\left[1-\left(\frac{\omega}{\omega_n}\right)^2\right]^2+4\left(\frac{\omega}{\omega_n}\zeta\right)^2\right\}\left\{\left[1-\left(\frac{\omega}{\omega_i}\right)^2\right]^2+4\left(\frac{\omega}{\omega_n}\zeta\right)^2\right\}}{\left\{\left[1-\left(\frac{\omega}{\omega_n}\right)^2\right]^2+4\left(\frac{\omega}{\omega_n}\zeta\right)^2\right\}^2}\right\} = 0$$

$$\frac{\partial}{\partial\omega}\left\{1-2\left(\frac{\omega}{\omega_i}\right)^2+\left(\frac{\omega}{\omega_i}\right)^4+4\zeta^2\left(\frac{\omega}{\omega_n}\right)^2\right\}\left\{1-2\left(\frac{\omega}{\omega_n}\right)^2+\left(\frac{\omega}{\omega_n}\right)^4+4\zeta^2\left(\frac{\omega}{\omega_n}\right)^2\right\}-\frac{\partial}{\partial\omega}\left\{1-2\left(\frac{\omega}{\omega_n}\right)^2+\left(\frac{\omega}{\omega_n}\right)^4+4\zeta^2\left(\frac{\omega}{\omega_n}\right)^2\right\}\left\{1-2\left(\frac{\omega}{\omega_i}\right)^2+\left(\frac{\omega}{\omega_i}\right)^4+4\zeta^2\left(\frac{\omega}{\omega_n}\right)^2\right\} = 0$$

$$\left\{\frac{8\zeta^2}{\omega_n^2}-\frac{4}{\omega_i^2}+\frac{4}{\omega_i^4}\omega^2\right\}\left\{1+\frac{4\zeta^2-2}{\omega_n^2}\omega^2+\frac{1}{\omega_n^4}\omega^4\right\}-\left\{\frac{8\zeta^2}{\omega_n^2}-\frac{4}{\omega_n^2}+\frac{4}{\omega_n^4}\omega^2\right\}\left\{1+\left(\frac{4\zeta^2}{\omega_n^2}-\frac{2}{\omega_i^2}\right)\omega^2+\frac{1}{\omega_i^4}\omega^4\right\} = 0$$

$$\frac{1}{\omega_n^2}-\frac{1}{\omega_i^2}+\left(\frac{1}{\omega_i^4}-\frac{1}{\omega_n^4}\right)\omega^2+\left(-\frac{2\zeta^2}{\omega_n^6}+\frac{1}{\omega_i^2\omega_n^4}-\frac{1}{\omega_n^2\omega_i^4}+\frac{2\zeta^2}{\omega_i^4\omega_n^2}\right)\omega^4 = 0$$

$$\frac{\Omega_n}{\omega_n},\frac{\Omega_i}{\omega_n} = \sqrt{\frac{-\left(\frac{\omega_n}{\omega_i}\right)^2-1\pm\sqrt{\left[\left(\frac{\omega_n}{\omega_i}\right)^2-1\right]^2+8\zeta^2\left[\left(\frac{\omega_n}{\omega_i}\right)^2+1\right]}}{4\zeta^2+4\zeta^2\left(\frac{\omega_n}{\omega_i}\right)^2-2\left(\frac{\omega_n}{\omega_i}\right)^2}}$$

(A.113)

A.4.2 Passive amplified vibration-absorbing isolator (multiple absorbers fitted)

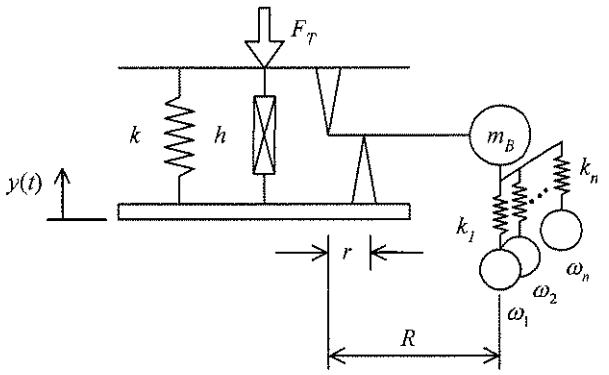

Figure A.11: Mechanical model of multiple absorbers fitted to a pendulum

The continuity is again given by Equation (A.98). The kinetic energy is:

$$T = \frac{1}{2}\left(m\dot{x}^2 + m_B\dot{x}_B^2 + I_G\dot{\theta}^2 + \sum_{i=1}^{n} m_q\dot{x}_q^2 \right)$$
$$\frac{1}{2}\left\{ \left[m + m_B\left(1-\frac{R}{r}\right)^2 + \frac{I_G}{r^2} \right]\dot{x}^2 + 2\left[m_B\left(1-\frac{R}{r}\right)\frac{R}{r} - \frac{I_G}{r^2} \right]\dot{x}\dot{y} + \left[m_B\left(\frac{R}{r}\right)^2 + \frac{I_G}{r^2} \right]\dot{y}^2 + \sum_{q=1}^{n} m_q\dot{x}_q^2 \right\} \quad \text{(A.114)}$$

From the above equation the derivatives can be found:

$$\frac{d}{dt}\left(\frac{\partial T}{\partial \dot{x}}\right) = \left[m + m_B\left(1-\frac{R}{r}\right)^2 + \frac{I_G}{r^2} \right]\ddot{x} + \left[m_B\left(1-\frac{R}{r}\right)\frac{R}{r} - \frac{I_G}{r^2} \right]\ddot{y}$$
$$\frac{d}{dt}\left(\frac{\partial T}{\partial \dot{y}}\right) = \left[m_B\left(\frac{R}{r}\right)^2 + \frac{I_G}{r^2} \right]\ddot{y} + \left[m_B\left(1-\frac{R}{r}\right)\frac{R}{r} - \frac{I_G}{r^2} \right]\ddot{x} \quad \text{(A.115)}$$
$$\frac{d}{dt}\left(\frac{\partial T}{\partial \dot{x}_q}\right) = m_q\ddot{x}_q$$

The potential energy is:

$$V = \frac{1}{2}\left[k(x-y)^2 + \sum_{q=1}^{n} k_q\left(x_B - x_q\right)^2 \right]$$
$$= \frac{1}{2}\left\{ k\left(x^2 - 2xy - y^2\right) + \sum_{q=1}^{n} k_q\left[\left(1-\frac{R}{r}\right)x + \frac{R}{r}y - x_q \right]^2 \right\}$$
$$= \frac{1}{2}\left\{ k\left(x^2 - 2xy - y^2\right) + \sum_{q=1}^{n} k_q\left[\left(1-\frac{R}{r}\right)^2 x^2 + 2\left(1-\frac{R}{r}\right)\frac{R}{r}xy + \left(\frac{R}{r}\right)^2 y^2 - 2\left(1-\frac{R}{r}\right)xx_q - \frac{R}{r}yx_q + x_q^2 \right] \right\} \quad \text{(A.116)}$$
$$= \frac{1}{2}\left\{ k\left(x^2 - 2xy - y^2\right) + \left(1-\frac{R}{r}\right)^2 x^2\sum_{q=1}^{n} k_q + 2\left(1-\frac{R}{r}\right)\frac{R}{r}xy\sum_{q=1}^{n} k_q + \left(\frac{R}{r}\right)^2 y^2\sum_{q=1}^{n} k_q - 2\left(1-\frac{R}{r}\right)x\sum_{q=1}^{n} k_q x_q \right.$$
$$\left. - \frac{R}{r}y\sum_{q=1}^{n} k_q x_q + \sum_{q=1}^{n} k_q x_q^2 \right\}$$

From the above equation the derivatives can be found:

$$\frac{\partial V}{\partial x} = \left(k + \left(1 - \frac{R}{r}\right)^2 \sum_{q=1}^{n} k_q \right) x + \left(-k + \left(1 - \frac{R}{r}\right) \frac{R}{r} \sum_{q=1}^{n} k_q \right) y - \left(1 - \frac{R}{r}\right) \sum_{q=1}^{n} k_q x_q$$

$$\frac{\partial V}{\partial y} = \left[-k + \left(1 - \frac{R}{r}\right) \frac{R}{r} \sum_{q=1}^{n} k_q \right] x + \left[k + \left(\frac{R}{r}\right)^2 \sum_{q=1}^{n} k_q \right] y - \frac{R}{r} \sum_{q=1}^{n} k_q x_q \qquad \text{(A.117)}$$

$$\frac{\partial V}{\partial x_q} = -k_q \left(1 - \frac{R}{r}\right) x - k_q \frac{R}{r} y + k_q x_q$$

The complete undamped equation of motion is:

$$\begin{bmatrix} m+m_B\left(\frac{R}{r}-1\right)^2+\frac{I_G}{r^2} & 0 & 0 & \cdots & 0 \\ 0 & m_1 & 0 & \cdots & 0 \\ 0 & 0 & m_2 & \cdots & 0 \\ \vdots & \vdots & \vdots & \ddots & 0 \\ 0 & 0 & 0 & 0 & m_q \end{bmatrix} \begin{Bmatrix} \ddot{x} \\ \ddot{x}_1 \\ \ddot{x}_2 \\ \vdots \\ \ddot{x}_q \end{Bmatrix} + \begin{bmatrix} k+i\eta+\left(\frac{R}{r}-1\right)^2\sum_{i=1}^{q}k_q+i\eta_q & \left(\frac{R}{r}-1\right)k_1(1+i\eta_1) & \left(\frac{R}{r}-1\right)k_2(1+i\eta_2) & \cdots & \left(\frac{R}{r}-1\right)k_q(1+i\eta_q) \\ \left(\frac{R}{r}-1\right)k_1(1+i\eta_1) & k_1 & 0 & \cdots & 0 \\ \left(\frac{R}{r}-1\right)k_2(1+i\eta_2) & 0 & k_2 & \cdots & 0 \\ \vdots & \vdots & \vdots & \ddots & 0 \\ \left(\frac{R}{r}-1\right)k_q(1+i\eta_q) & 0 & 0 & 0 & k_q \end{bmatrix} \begin{Bmatrix} x \\ x_1 \\ x_2 \\ \vdots \\ x_q \end{Bmatrix} = \begin{bmatrix} m_B\left(\frac{R}{r}-1\right)\frac{R}{r}+\frac{I_G}{r^2} \\ 0 \\ 0 \\ \vdots \\ 0 \end{bmatrix} \ddot{y} + \begin{bmatrix} k+\left(\frac{R}{r}-1\right)\frac{R}{r}\sum_{q=1}^{n}k_q \\ k_1\frac{R}{r} \\ k_2\frac{R}{r} \\ \vdots \\ k_q\frac{R}{r} \end{bmatrix} y + \begin{bmatrix} f_x \\ 0 \\ 0 \\ 0 \\ 0 \end{bmatrix} \tag{A.118}$$

With the x degree of freedom forced to zero by the force f_x the first equation of the above set of equations can be transformed to the frequency domain:

$$F_x = \sum_{q=1}^{n}\left(\frac{R}{r}-1\right)k_q(1+i\eta_q)X_q - \left\{k+i\eta+\left(\frac{R}{r}-1\right)\frac{R}{r}\sum_{q=1}^{n}k_q(1+i\eta_q)-\omega^2\left[m_B\left(\frac{R}{r}-1\right)\frac{R}{r}+\frac{I_G}{r^2}\right]\right\}Y \tag{A.119}$$

The 2nd to q^{th} equation is given by:

$$\left[k_q(1+i\eta_q)-\omega^2 m_q\right]X_q = \frac{R}{r}k_q(1+i\eta_q)Y$$

$$X_q = \frac{\frac{R}{r}(1+i\eta_q)}{1+i\eta_q-\left(\frac{\omega}{\omega_q}\right)^2}Y \tag{A.120}$$

By substituting the above equation into Equation (A.119) and noting that $F_T = -F_x$ the normalised dynamic stiffness can be written as:

$$\frac{F_T}{kY} = 1+i\eta+\left(\frac{R}{r}-1\right)\frac{R}{r}\sum_{q=1}^{n}\frac{k_q}{k}(1+i\eta_q)-\left(\frac{\omega}{\omega_i}\right)^2-\frac{R}{r}\left(\frac{R}{r}-1\right)\sum_{q=1}^{n}\frac{k_q}{k}\frac{(1+i\eta_q)^2}{1+i\eta_q-\left(\frac{\omega}{\omega_q}\right)^2} \tag{A.121}$$

The undamped frequencies of zero dynamic stiffness can be found by setting the above equation to zero. For one absorber attached to the pendulum mass the two frequencies are:

$$1+\left(\frac{R}{r}-1\right)\frac{R}{r}\sum_{q=1}^{n}\frac{k_1}{k}-\left(\frac{\omega}{\omega_i}\right)^2-\frac{R}{r}\left(\frac{R}{r}-1\right)\frac{k_1}{k}\frac{1}{1-\left(\frac{\omega}{\omega_1}\right)^2}=0$$

$$\omega^4-\left[\omega_i^2+\left(\frac{R}{r}-1\right)\frac{R}{r}\frac{k_1}{k}\omega_i^2+\omega_1^2\right]\omega^2+\omega_i^2\omega_1^2=0 \qquad \text{(A.122)}$$

$$(\omega_1')^2,(\omega_2')^2=\frac{\left(\frac{R}{r}-1\right)\frac{R}{r}\frac{k_1}{k}\omega_i^2+\omega_i^2+\omega_1^2\pm\sqrt{\left[\left(\frac{R}{r}-1\right)\frac{R}{r}\frac{k_1}{k}\omega_i^2+\omega_i^2+\omega_1^2\right]^2-4\omega_i^2\omega_1^2}}{2}$$

A.4.3 Passive amplified vibration-absorbing isolator (non-linear)

For a system with Duffing type non-linearity the equation of motion is:

$$\left[m+m_B\left(1-\frac{R}{r}\right)^2+\frac{I_G}{r^2}\right]\ddot{x}+\left[m_B\left(1-\frac{R}{r}\right)\frac{R}{r}-\frac{I_G}{r^2}\right]\ddot{y}+c(\dot{x}-\dot{y})+k(x-y)+\alpha k_B(x-y)^3=0 \qquad \text{(A.123)}$$

This equation can be non-dimensionalised as follows:

$$\frac{\left[m+m_B\left(1-\frac{R}{r}\right)^2+\frac{I_G}{r^2}\right]}{k}\ddot{x}+\frac{\left[m_B\left(1-\frac{R}{r}\right)\frac{R}{r}-\frac{I_G}{r^2}\right]}{k}\ddot{y}+\frac{c}{k}(\dot{x}-\dot{y})+(x-y)+\alpha(x-y)^3=0$$

$$\frac{1}{\omega_n^2}\ddot{x}-\frac{1}{\omega_i^2}\ddot{y}+\frac{c}{k}(\dot{x}-\dot{y})+(x-y)+\alpha(x-y)^3=0 \qquad \text{(A.124)}$$

$$\ddot{x}-\left(\frac{\omega_n}{\omega_i}\right)^2\ddot{y}+2\zeta\omega_n(\dot{x}-\dot{y})+\omega_n^2\left[(x-y)+\alpha(x-y)^3\right]=0$$

A.4.4 Passive amplified vibration-absorbing isolator (motion transformation system)

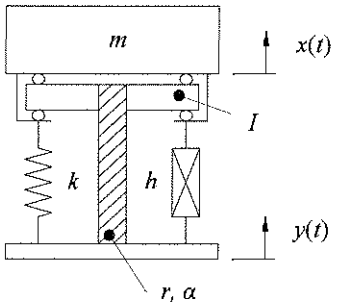

Figure A.12: Mechanical model of motion transformation system

Continuity between the input, output and the rotation angle of the mass can be written as:

$$\phi = \frac{x - y}{r \tan \alpha} \tag{A.125}$$

where r is the mean thread radius and α the helix angle of the thread.

The kinetic energy is:

$$\begin{aligned} T &= \frac{1}{2}\left[m\dot{x}^2 + I\dot{\phi}^2 \right] \\ &= \frac{1}{2}\left[m\dot{x}^2 + \frac{I}{r^2 \tan^2 \alpha}\left(\dot{x}^2 - 2\dot{x}\dot{y} + \dot{y}^2 \right) \right] \end{aligned} \tag{A.126}$$

From the above equation the derivative is:

$$\frac{d}{dt}\left(\frac{\partial T}{\partial \dot{x}} \right) = \left(m + \frac{I}{r^2 \tan^2 \alpha} \right)\ddot{x} - \frac{I}{r^2 \tan^2 \alpha}\ddot{y} \tag{A.127}$$

The potential energy is simply:

$$V = \frac{1}{2}k(x - y)^2 \tag{A.128}$$

From the above equation the derivative is:

$$\frac{\partial V}{\partial x} = kx - ky \tag{A.129}$$

The equation of motion can now be found:

$$\left(m + \frac{I}{r^2 \tan^2 \alpha} \right)\ddot{x} + k(1 + i\eta)x = \frac{I}{r^2 \tan^2 \alpha}\ddot{y} + k(1 + i\eta)y \tag{A.130}$$

The equation of motion can be transformed to the frequency domain:

$$\left[k(1 + i\eta) - \omega^2 \left(m + \frac{I}{r^2 \tan^2 \alpha} \right) \right] X = \left[k(1 + i\eta) - \omega^2 \frac{I}{r^2 \tan^2 \alpha} \right] Y \tag{A.131}$$

Form the above equation the transmissibility can be found:

$$\frac{X}{Y} = \frac{k(1 + i\eta) - \omega^2 \dfrac{I}{r^2 \tan^2 \alpha}}{k(1 + i\eta) - \omega^2 \left(m + \dfrac{I}{r^2 \tan^2 \alpha} \right)} \tag{A.132}$$

The undamped isolation frequency is found by equating the numerator to zero:

$$\omega_i = \sqrt{\frac{k}{\dfrac{I}{r^2 \tan^2 \alpha}}} \tag{A.133}$$

A.4.5 Adaptive amplified vibration-absorbing isolator

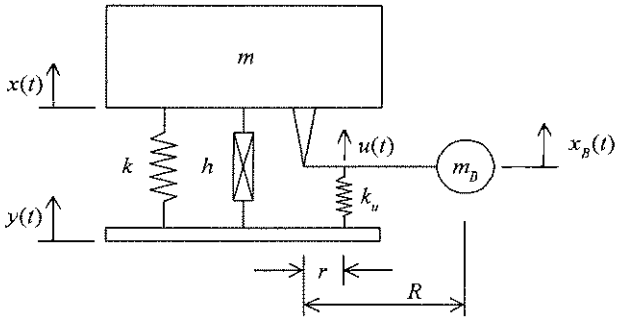

Figure A.13: Mechanical model of an AVAI with flexible fulcrum

The continuity between the x_B, x and u can be written as:

$$\begin{aligned} x_B &= \frac{R}{r}u + \left(1-\frac{R}{r}\right)x \\ \theta &\approx \frac{u-x}{r} \end{aligned} \tag{A.134}$$

The kinetic energy is:

$$\begin{aligned} T &= \frac{1}{2}\left\{m\dot{x}^2 + m_B\dot{x}_B^2 + I_G\dot{\theta}^2\right\} \\ &= \frac{1}{2}\left\{m\dot{x}^2 + m_B\left[\left(1-\frac{R}{r}\right)^2\dot{x}^2 + 2\left(1-\frac{R}{r}\right)\frac{R}{r}\dot{x}\dot{u} + \left(\frac{R}{r}\right)^2\dot{u}^2\right] + \frac{I_G}{r^2}\left(\dot{u}^2 - 2\dot{u}\dot{x} + \dot{x}^2\right)\right\} \end{aligned} \tag{A.135}$$

From the above equation the derivates can be found:

$$\begin{aligned} \frac{d}{dt}\left(\frac{\partial T}{\partial \dot{u}}\right) &= \left[m_B\left(1-\frac{R}{r}\right)\frac{R}{r} - \frac{I_G}{r^2}\right]\ddot{x} + \left[m_B\left(\frac{R}{r}\right)^2 + \frac{I_G}{r^2}\right]\ddot{u} \\ \frac{d}{dt}\left(\frac{\partial T}{\partial \dot{x}}\right) &= \left[m + m_B\left(1-\frac{R}{r}\right)^2 + \frac{I_G}{r^2}\right]\ddot{x} + \left[m_B\left(1-\frac{R}{r}\right)\frac{R}{r} - \frac{I_G}{r^2}\right]\ddot{u} \end{aligned} \tag{A.136}$$

The potential energy is:

$$\begin{aligned} V &= \frac{1}{2}\left[k\left(x-y\right)^2 + k_u\left(u-y\right)^2\right] \\ &= \frac{1}{2}\left(kx^2 - 2kxy + \left(k+k_u\right)y^2 - 2k_uuy + k_uu^2\right) \end{aligned} \tag{A.137}$$

From the above equation the derivates can be found:

$$\begin{aligned}\frac{\partial V}{\partial y} &= (k+k_u)y - k_u u - kx \\ \frac{\partial V}{\partial u} &= k_u u - k_u y \\ \frac{\partial V}{\partial x} &= kx - ky\end{aligned} \tag{A.138}$$

The complete equation of motion (assuming excitation at the y-degree of freedom) is:

$$\begin{bmatrix} m+m_B\left(1-\frac{R}{r}\right)^2+\frac{I_G}{r^2} & m_B\left(1-\frac{R}{r}\right)\frac{R}{r}-\frac{I_G}{r^2} \\ m_B\left(1-\frac{R}{r}\right)\frac{R}{r}-\frac{I_G}{r^2} & m_B\left(\frac{R}{r}\right)^2+\frac{I_G}{r^2} \end{bmatrix}\begin{bmatrix}\ddot{x}\\ \ddot{u}\end{bmatrix}+\begin{bmatrix} k(1+\eta) & 0 \\ 0 & k_u(1+\eta_u)\end{bmatrix}\begin{bmatrix}x\\u\end{bmatrix}=\begin{bmatrix}k(1+\eta)y+f_x\\ k_u(1+\eta_u)y\end{bmatrix} \tag{A.139}$$

In the frequency domain the U degree of freedom can be found in terms of X using the second equation in the set shown above:

$$\begin{aligned}&-\omega^2\left[m_B\left(1-\frac{R}{r}\right)\frac{R}{r}-\frac{I_G}{r^2}\right]X+\left\{-\omega^2\left[m_B\left(\frac{R}{r}\right)^2+\frac{I_G}{r^2}\right]+k_u(1+i\eta_u)\right\}U=k_u(1+i\eta_u)Y \\ &U=\frac{k_u(1+i\eta_u)Y-\omega^2\left[m_B\left(\frac{R}{r}-1\right)\frac{R}{r}+\frac{I_G}{r^2}\right]}{k_u(1+i\eta_u)-\omega^2\left[m_B\left(\frac{R}{r}\right)^2+\frac{I_G}{r^2}\right]}X\end{aligned} \tag{A.140}$$

The U degree of freedom can now be eliminated from the first equation, yielding the transmissibility between the excitation and the response (assuming the force acting on m is zero):

$$\left[m_B\left(\frac{R}{r}-1\right)\frac{R}{r}+\frac{I_G}{r^2}\right]U+\left\{k(1+i\eta)-\omega^2\left[m+m_B\left(1-\frac{R}{r}\right)^2+\frac{I_G}{r^2}\right]\right\}X=k(1+i\eta)Y$$

$$\left\{k_u(1+i\eta_u)-\omega^2\left[m_B\left(\frac{R}{r}\right)^2+\frac{I_G}{r^2}\right]\right\}\left\{k(1+i\eta)-\omega^2\left[m+m_B\left(1-\frac{R}{r}\right)^2+\frac{I_G}{r^2}\right]\right\}X-\left\{\omega^2\left[m_B\left(\frac{R}{r}-1\right)\frac{R}{r}+\frac{I_G}{r^2}\right]\right\}^2X$$

$$=\left\{k_u(1+i\eta_u)-\omega^2\left[m_B\left(\frac{R}{r}\right)^2+\frac{I_G}{r^2}\right]\right\}k(1+i\eta)Y-\omega^2\left[m_B\left(\frac{R}{r}-1\right)\frac{R}{r}+\frac{I_G}{r^2}\right]k_u(1+i\eta_u)Y$$

$$\frac{X}{Y}=\frac{k(1+i\eta)\left\{k_u(1+i\eta_u)-\omega^2\left[m_B\left(\frac{R}{r}\right)^2+\frac{I_G}{r^2}\right]\right\}-\omega^2k_u(1+i\eta_u)\left[m_B\left(\frac{R}{r}-1\right)\frac{R}{r}+\frac{I_G}{r^2}\right]}{\left\{k_u(1+i\eta_u)-\omega^2\left[m_B\left(\frac{R}{r}\right)^2+\frac{I_G}{r^2}\right]\right\}\left\{k(1+i\eta)-\omega^2\left[m+m_B\left(1-\frac{R}{r}\right)^2+\frac{I_G}{r^2}\right]\right\}+\omega^4\left[m_B\left(\frac{R}{r}-1\right)\frac{R}{r}+\frac{I_G}{r^2}\right]^2} \tag{A.141}$$

The dynamic stiffness can be calculated by finding the force acting on the mass m that will force it to zero from the first equation defined by Equation (A.139):

$$\left\{k_u\left(1+i\eta_u\right)-\omega^2\left[m_B\left(\frac{R}{r}\right)^2+\frac{I_G}{r^2}\right]\right\}k\left(1+i\eta\right)Y-\omega^2\left[m_B\left(\frac{R}{r}-1\right)\frac{R}{r}+\frac{I_G}{r^2}\right]k_u\left(1+i\eta_u\right)Y$$
$$+F_x\left\{k_u\left(1+i\eta_u\right)-\omega^2\left[m_B\left(\frac{R}{r}\right)^2+\frac{I_G}{r^2}\right]\right\}=0 \qquad \text{(A.142)}$$

$$\frac{F_T}{Y}=k\left(1+i\eta\right)-\frac{\omega^2\left[m_B\left(\frac{R}{r}-1\right)\frac{R}{r}+\frac{I_G}{r^2}\right]k_u\left(1+i\eta_u\right)}{k_u\left(1+i\eta_u\right)-\omega^2\left[m_B\left(\frac{R}{r}\right)^2+\frac{I_G}{r^2}\right]}$$

The above equation can be normalised as follows:

$$\frac{F_T}{kY}=1+i\eta-\frac{\left(\frac{\omega}{\omega_i}\right)^2\left(1+i\eta_u\right)}{1+i\eta_u-\left(\frac{\omega}{\omega_u}\right)^2} \qquad \text{(A.143)}$$

where: $\omega_i=\sqrt{\dfrac{k}{m_B\left(\frac{R}{r}-1\right)\frac{R}{r}+\frac{I_G}{r^2}}}$ $\omega_u=\sqrt{\dfrac{k_u}{m_B\left(\frac{R}{r}\right)^2+\frac{I_G}{r^2}}}$

The frequency ω_u can be eliminated by introducing the stiffness ratio k_u/k:

$$\frac{F_T}{kY}=1+i\eta-\frac{\left(\frac{\omega}{\omega_i}\right)^2\left(1+i\eta_u\right)}{1+i\eta_u-\frac{k}{k_u}\left(\frac{\frac{R}{r}}{\frac{R}{r}-1}\right)\left(\frac{\omega}{\omega_i}\right)^2} \qquad \text{(A.144)}$$

A.4.6 Active AVAI (acceleration and displacement feedback)

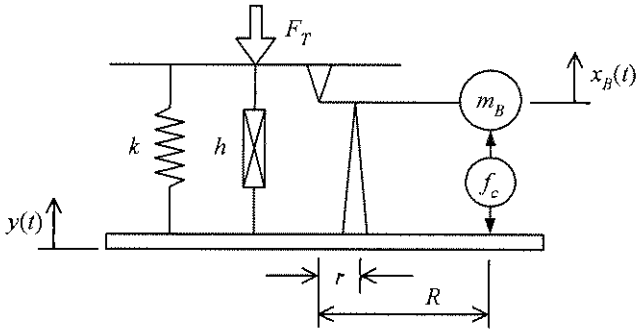

Figure A.14: Mechanical model of an active AVAI

For a control force given by the acceleration and displacement of the input y:

$$f_c = \alpha\ddot{y} + \gamma y \tag{A.145}$$

The dynamic stiffness can be found by using the first equation of the set defined by Equation (A.105) and adding the control force to the right hand side. The control force contribution to the transmitted force is calculated by taking the mechanical advantage of the pendulum into account. The equation is now:

$$\left[m_B\left(1-\frac{R}{r}\right)\frac{R}{r}-\frac{I_G}{r^2}\right]\ddot{y}-k(1+\eta)y = f_x - f_c\left(\frac{R}{r}-1\right) \tag{A.146}$$

On substitution of the control force the above equation becomes:

$$\begin{aligned}&\left[m_B\left(1-\frac{R}{r}\right)\frac{R}{r}-\frac{I_G}{r^2}\right]\ddot{y}-k(1+i\eta)y = f_x-(\alpha\ddot{y}+\gamma y)\left(\frac{R}{r}-1\right)\\&\left[m_B\left(1-\frac{R}{r}\right)\frac{R}{r}-\frac{I_G}{r^2}+\alpha\left(\frac{R}{r}-1\right)\right]\ddot{y}-\left[k(1+i\eta)-\gamma\left(\frac{R}{r}-1\right)\right]y = f_x\end{aligned} \tag{A.147}$$

By substituting the transmitted force and transforming to the frequency domain the above equation becomes:

$$\frac{F_T}{Y} = k-\gamma\left(\frac{R}{r}-1\right)+ik\eta-\omega^2\left[m_B\left(\frac{R}{r}-1\right)\frac{R}{r}+\frac{I_G}{r^2}-\alpha\left(\frac{R}{r}-1\right)\right] \tag{A.148}$$

The equation can be normalised if divided by the static stiffness:

$$\frac{F_T}{\left[k-\gamma\left(\frac{R}{r}-1\right)\right]Y}=1+i\frac{\eta}{1-\frac{\gamma}{k}\left(\frac{R}{r}-1\right)}-\left(\frac{\omega}{\omega_i'}\right)^2$$

$$\omega_i'=\sqrt{\frac{k-\gamma\left(\frac{R}{r}-1\right)}{m_B\left(\frac{R}{r}-1\right)\frac{R}{r}+\frac{I_G}{r^2}-\alpha\left(\frac{R}{r}-1\right)}} \tag{A.149}$$

The stability of the system must be analysed by using the equation of motion when a mass is attached to the system. The equation of motion is (Equation (A.152)):

$$\left[m+m_B\left(\frac{R}{r}-1\right)^2+\frac{I_G}{r^2}\right]\ddot{x}+c\dot{x}+kx=\left[m_B\left(\frac{R}{r}-1\right)\frac{R}{r}+\frac{I_G}{r^2}\right]\ddot{y}+c\dot{y}+ky-(\alpha\ddot{y}+\gamma y)\left(\frac{R}{r}-1\right) \tag{A.150}$$

Since no gains appear on the left hand side of the above equation the system is unconditionally stable.

A.4.7 Active AVAI (relative velocity feedback)

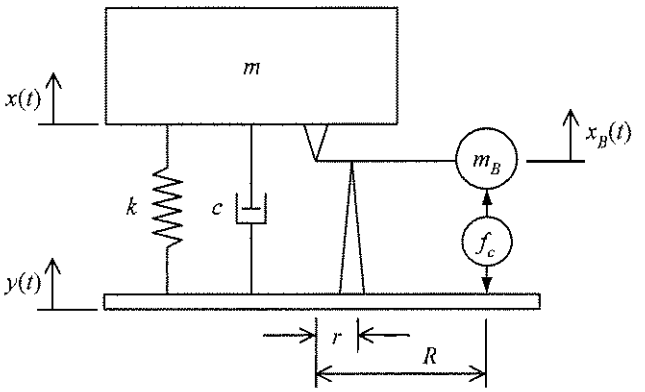

Figure A.15: Mechanical model of an active AVAI for transmissibility

The control force is:

$$f_c=\beta(\dot{x}-\dot{y}) \tag{1.151}$$

Equation (A.105) can be rewritten to include the control force:

$$\left[m+m_B\left(\frac{R}{r}-1\right)^2+\frac{I_G}{r^2}\right]\ddot{x}+c\dot{x}+kx=\left[m_B\left(\frac{R}{r}-1\right)\frac{R}{r}+\frac{I_G}{r^2}\right]\ddot{y}+c\dot{y}+ky-f_c\left(\frac{R}{r}-1\right) \tag{A.152}$$

By substituting the control force it follows that:

$$\begin{aligned}\left[m+m_B\left(\frac{R}{r}-1\right)^2+\frac{I_G}{r^2}\right]\ddot{x}+c\dot{x}+kx&=\left[m_B\left(\frac{R}{r}-1\right)\frac{R}{r}+\frac{I_G}{r^2}\right]\ddot{y}+c\dot{y}+ky-\beta(\dot{x}-\dot{y})\left(\frac{R}{r}-1\right)\\ \left[m+m_B\left(\frac{R}{r}-1\right)^2+\frac{I_G}{r^2}\right]\ddot{x}+\left[c+\beta\left(\frac{R}{r}-1\right)\right]\dot{x}+kx&=\left[m_B\left(\frac{R}{r}-1\right)\frac{R}{r}+\frac{I_G}{r^2}\right]\ddot{y}+\left[c+\beta\left(\frac{R}{r}-1\right)\right]\dot{y}+ky\end{aligned} \tag{A.153}$$

By transforming to the frequency domain:

$$\frac{X}{Y}=\frac{k+i\omega\left[c+\beta\left(\frac{R}{r}-1\right)\right]-\omega^2\left[m_B\left(\frac{R}{r}-1\right)\frac{R}{r}+\frac{I_G}{r^2}\right]}{k+i\omega\left[c+\beta\left(\frac{R}{r}-1\right)\right]-\omega^2\left[m+m_B\left(\frac{R}{r}-1\right)^2+\frac{I_G}{r^2}\right]} \tag{A.154}$$

By introducing some non-dimensional parameters:

$$\frac{X}{Y}=\frac{1+i2\frac{\omega}{\omega_n}\left[\zeta+\zeta_\beta\left(\frac{R}{r}-1\right)\right]-\left(\frac{\omega}{\omega_t}\right)^2}{1+i2\frac{\omega}{\omega_n}\left[\zeta+\zeta_\beta\left(\frac{R}{r}-1\right)\right]-\left(\frac{\omega}{\omega_n}\right)^2} \tag{A.155}$$

$$\text{where: } \zeta_\beta=\frac{\beta}{2\left[m+m_B\left(\frac{R}{r}-1\right)^2+\frac{I_G}{r^2}\right]\omega_n}$$

The stability can be analysed by considering the characteristic equation:

$$\left[m+m_B\left(\frac{R}{r}-1\right)^2+\frac{I_G}{r^2}\right]s^2+\left[c+\beta\left(\frac{R}{r}-1\right)\right]s+k=0 \tag{A.156}$$

The roots are:

$$\begin{aligned}s_1,s_2&=\frac{-b\pm\sqrt{b^2-4ac}}{2a}\\&=\frac{-\left[c+\beta\left(\frac{R}{r}-1\right)\right]\pm\sqrt{\left[c+\beta\left(\frac{R}{r}-1\right)\right]^2-4\left[m+m_B\left(\frac{R}{r}-1\right)^2+\frac{I_G}{r^2}\right]k}}{2\left[m+m_B\left(\frac{R}{r}-1\right)^2+\frac{I_G}{r^2}\right]}\end{aligned} \tag{A.157}$$

The above equation will have at least one positive real part if $-b > 0$. To be stable the real part must be negative:

$$\begin{aligned}-\left[c+\beta\left(\frac{R}{r}-1\right)\right]&<0\\ \beta&>-\frac{c}{\left(\frac{R}{r}-1\right)}\end{aligned} \tag{A.158}$$

A.4.8 Active AVAI (absolute velocity feedback)

The system is described by Figure A.15 in §A.4.7. The control force is:

$$f_c = \beta \dot{x} \tag{A.159}$$

Equation (A.105) can be rewritten to include the control force:

$$\left(m + m_B\left(\frac{R}{r}-1\right)^2 + \frac{I_G}{r^2}\right)\ddot{x} + c\dot{x} + kx = \left(m_B\left(\frac{R}{r}-1\right)\frac{R}{r} + \frac{I_G}{r^2}\right)\ddot{y} + c\dot{y} + ky - f_c\left(\frac{R}{r}-1\right) \tag{A.160}$$

By substituting the control force it follows that:

$$\begin{aligned}
&\left[m + m_B\left(\frac{R}{r}-1\right)^2 + \frac{I_G}{r^2}\right]\ddot{x} + c\dot{x} + kx = \left[m_B\left(\frac{R}{r}-1\right)\frac{R}{r} + \frac{I_G}{r^2}\right]\ddot{y} + c\dot{y} + ky - \beta\dot{x}\left(\frac{R}{r}-1\right) \\
&\left[m + m_B\left(\frac{R}{r}-1\right)^2 + \frac{I_G}{r^2}\right]\ddot{x} + \left[c + \beta\left(\frac{R}{r}-1\right)\right]\dot{x} + kx = \left[m_B\left(\frac{R}{r}-1\right)\frac{R}{r} + \frac{I_G}{r^2}\right]\ddot{y} + c\dot{y} + ky
\end{aligned} \tag{A.161}$$

By transforming to the frequency domain:

$$\frac{X}{Y} = \frac{k + i\omega c - \omega^2\left[m_B\left(\frac{R}{r}-1\right)\frac{R}{r} + \frac{I_G}{r^2}\right]}{k + i\omega\left[c + \beta\left(\frac{R}{r}-1\right)\right] - \omega^2\left[m + m_B\left(\frac{R}{r}-1\right)^2 + \frac{I_G}{r^2}\right]} \tag{A.162}$$

By introducing some non-dimensional parameters:

$$\frac{X}{Y} = \frac{1 + i2\frac{\omega}{\omega_n}\zeta - \left(\frac{\omega}{\omega_i}\right)^2}{1 + i2\frac{\omega}{\omega_n}\left[\zeta + \zeta_\beta\left(\frac{R}{r}-1\right)\right] - \left(\frac{\omega}{\omega_n}\right)^2} \tag{A.163}$$

where: $\zeta_\beta = \dfrac{\beta}{2\left[m + m_B\left(\frac{R}{r}-1\right)^2 + \frac{I_G}{r^2}\right]\omega_n}$

The stability criterion is the same as for the relative feedback case, but is irrelevant in any case since positive feedback will be used and stability will therefore not be a concern.

APPENDIX B

Derivations for chapter 2

B.1 Adaptive AVAI with variable reservoir wall flexibility (Type I)

B.1.1 Reservoir flexibility covering full wall

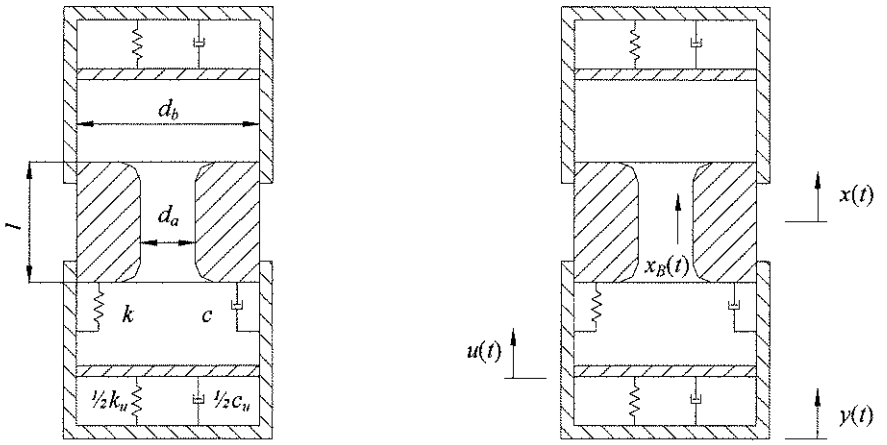

Figure B.1 Mechanical model of an adaptive AVAI with flexibility covering the complete reservoir wall

In Figure B.1 the displacement of the top reservoir wall is equal to the bottom reservoir wall (u), because the fluid is incompressible. Continuity gives the displacement of the fluid in the port:

$$\begin{aligned} uA_b &= (A_b - A_a)x + A_a x_B \\ x_B &= \left(1 - \frac{A_b}{A_a}\right)x + \frac{A_b}{A_a}u \end{aligned} \tag{B.1}$$

$$\text{where:} \quad A_a = \pi\frac{d_a^2}{4}, \quad A_b = \pi\frac{d_b^2}{4},$$

The total kinetic energy is:

$$\begin{aligned} T &= \frac{1}{2}\left(m_x\dot{x}^2 + m_y\dot{y}^2 + m_B\dot{x}_B^2\right) \\ &= \frac{1}{2}\left\{m_x\dot{x}^2 + m_y\dot{y}^2 + m_B\left[\left(1 - \frac{A_b}{A_a}\right)^2\dot{x}^2 + 2\left(1 - \frac{A_b}{A_a}\right)\frac{A_b}{A_a}\dot{x}\dot{u} + \left(\frac{A_b}{A_a}\right)^2\dot{u}^2\right]\right\} \end{aligned} \tag{B.2}$$

From the above equation the derivatives can be calculated:

$$\begin{aligned} \frac{d}{dt}\left(\frac{\partial T}{\partial \dot{y}}\right) &= m_y\ddot{y} \\ \frac{d}{dt}\left(\frac{\partial T}{\partial \dot{u}}\right) &= m_B\left(1 - \frac{A_b}{A_a}\right)\frac{A_b}{A_a}\ddot{x} + m_B\left(\frac{A_b}{A_a}\right)^2\ddot{u} \\ \frac{d}{dt}\left(\frac{\partial T}{\partial \dot{x}}\right) &= \left[m_x + m_B\left(1 - \frac{A_b}{A_a}\right)^2\right]\ddot{x} + m_B\left(1 - \frac{A_b}{A_a}\right)\frac{A_b}{A_a}\ddot{u} \end{aligned} \tag{B.3}$$

The potential energy is:

$$\begin{aligned} V &= \frac{1}{2}\left[k\left(x-y\right)^2 + k_u\left(u-y\right)^2\right] \\ &= \frac{1}{2}\left(kx^2 - 2kxy + \left(k+k_u\right)y^2 - 2k_u uy + k_u u^2\right) \end{aligned} \tag{B.4}$$

From the above equation the derivatives can be calculated:

$$\begin{aligned} \frac{\partial V}{\partial y} &= \left(k+k_u\right)y - k_u u - kx \\ \frac{\partial V}{\partial u} &= k_u u - k_u y \\ \frac{\partial V}{\partial x} &= kx - ky \end{aligned} \tag{B.5}$$

The Rayleigh term is:

$$\begin{aligned} R &= \frac{1}{2}\left[c\left(\dot{x}-\dot{y}\right)^2 + c_u\left(\dot{u}-\dot{x}\right)^2\right] \\ &= \frac{1}{2}\left[c\dot{x} - 2c\dot{x}\dot{y} + c\dot{y}^2 + c_u\dot{u} - 2c_u\dot{u}\dot{y} + c_u\dot{y}^2\right] \end{aligned} \tag{B.6}$$

From the above equation the derivatives can be calculated:

$$\begin{aligned} \frac{\partial R}{\partial \dot{y}} &= \left(c+c_u\right)\dot{y} - c_u\dot{u} - c\dot{x} \\ \frac{\partial R}{\partial \dot{u}} &= c_u\dot{u} - c_u\dot{y} \\ \frac{\partial R}{\partial \dot{x}} &= c\dot{x} - c\dot{y} \end{aligned} \tag{B.7}$$

Lagrange's equations are defined as (Rao, 1990):

$$\frac{d}{dt}\left(\frac{\partial T}{\partial \dot{x}_j}\right) - \frac{\partial T}{\partial x_j} + \frac{\partial V}{\partial x_j} = Q_j^{(n)} \quad j = 1,2,\ldots,n \tag{B.8}$$

The equation of motion can be derived by substituting the derivatives into Lagrange's equations:

$$\begin{bmatrix} m_y & 0 & 0 \\ 0 & m_x + m_B\left(1-\frac{A_b}{A_a}\right)^2 & m_B\left(1-\frac{A_b}{A_a}\right)\frac{A_b}{A_a} \\ 0 & m_B\left(1-\frac{A_b}{A_a}\right)\frac{A_b}{A_a} & m_B\left(\frac{A_b}{A_a}\right)^2 \end{bmatrix} \begin{bmatrix} \ddot{y} \\ \ddot{x} \\ \ddot{u} \end{bmatrix} + \begin{bmatrix} c+c_u & -c & -c_u \\ -c & c & 0 \\ -c_u & 0 & c_u \end{bmatrix} \begin{bmatrix} \dot{y} \\ \dot{x} \\ \dot{u} \end{bmatrix} + \begin{bmatrix} k+k_u & -k & -k_u \\ -k & k & 0 \\ -k_u & 0 & k_u \end{bmatrix} \begin{bmatrix} y \\ x \\ u \end{bmatrix} = \begin{bmatrix} f_y \\ f_x \\ 0 \end{bmatrix} \tag{B.9}$$

If the forces f_y and f_x are zero and the y-displacement is prescribed, the equation for the y degree of freedom can be eliminated from the equation of motion:

$$\begin{bmatrix} m_x + m_B\left(1-\frac{A_b}{A_a}\right)^2 & m_B\left(1-\frac{A_b}{A_a}\right)\frac{A_b}{A_a} \\ m_B\left(1-\frac{A_b}{A_a}\right)\frac{A_b}{A_a} & m_B\left(\frac{A_b}{A_a}\right)^2 \end{bmatrix}\begin{bmatrix}\ddot{x}\\ \ddot{u}\end{bmatrix}+\begin{bmatrix} c & 0 \\ 0 & c_u\end{bmatrix}\begin{bmatrix}\dot{x}\\ \dot{u}\end{bmatrix}+\begin{bmatrix} k & 0 \\ 0 & k_u\end{bmatrix}\begin{bmatrix}x\\ u\end{bmatrix}=\begin{bmatrix} c\dot{y}+ky \\ c_u\dot{y}+k_u y\end{bmatrix} \tag{B.10}$$

The above equation can be transformed to the frequency domain by assuming harmonic excitation:

$$\begin{bmatrix} k+i\omega c-\omega^2\left[m_x+m_B\left(1-\frac{A_b}{A_a}\right)^2\right] & -\omega^2 m_B\left(1-\frac{A_b}{A_a}\right)\frac{A_b}{A_a} \\ -\omega^2 m_B\left(1-\frac{A_b}{A_a}\right)\frac{A_b}{A_a} & k_u+i\omega c_u-\omega^2 m_B\left(\frac{A_b}{A_a}\right)^2\end{bmatrix}\begin{bmatrix}X\\ U\end{bmatrix}=\begin{bmatrix} i\omega c+k \\ i\omega c_u+k_u\end{bmatrix}Y \tag{B.11}$$

The second equation in the set defined above can be used to find an expression for the U degree of freedom:

$$U=\frac{\left(i\omega c_u+k_u\right)Y+\omega^2 m_B\left(1-\frac{A_b}{A_a}\right)\frac{A_b}{A_a}X}{k_u+i\omega c_u-\omega^2 m_B\left(\frac{A_b}{A_a}\right)^2} \tag{B.12}$$

The above equation can be used to eliminate the U degree of freedom from the first equation in the set defined by Equation (B.11), which leads to the transmissibility:

$$\frac{X}{Y}=\frac{\left(k+i\omega c\right)\left[k_u+i\omega c_u-\omega^2 m_B\left(\frac{A_b}{A_a}\right)^2\right]+\omega^2\left(k_u+i\omega c_u\right)m_B\left(1-\frac{A_b}{A_a}\right)\frac{A_b}{A_a}}{\left[k_u+i\omega c_u-\omega^2 m_B\left(\frac{A_b}{A_a}\right)^2\right]\left\{k+i\omega c-\omega^2\left[m_x+m_B\left(1-\frac{A_b}{A_a}\right)^2\right]\right\}-\left[\omega^2 m_B\left(1-\frac{A_b}{A_a}\right)\frac{A_b}{A_a}\right]^2} \tag{B.13}$$

The next section will assume that the excitation occurs at the x degree of freedom as this was the preferred orientation as explained in Chapter 2. If the forces f_y and f_x are zero and the x-displacement is prescribed, the equation for the x degree of freedom can be eliminated from Equation (B.9):

$$\begin{bmatrix} m_y & 0 \\ 0 & m_B\left(\frac{A_b}{A_a}\right)^2\end{bmatrix}\begin{bmatrix}\ddot{y}\\ \ddot{u}\end{bmatrix}+\begin{bmatrix} c+c_u & -c_u \\ -c_u & c_u\end{bmatrix}\begin{bmatrix}\dot{y}\\ \dot{u}\end{bmatrix}+\begin{bmatrix} k+k_u & -k_u \\ -k_u & k_u\end{bmatrix}\begin{bmatrix}y\\ u\end{bmatrix}=\begin{bmatrix} c\dot{x}+kx \\ -m_B\left(1-\frac{A_b}{A_a}\right)\frac{A_b}{A_a}\ddot{x}\end{bmatrix} \tag{B.14}$$

The above equation can be transformed to the frequency domain by assuming harmonic excitation:

$$\begin{bmatrix} k+k_u+i\omega\left(c+c_u\right)-\omega^2 m_y & -\left(k_u+i\omega c_u\right) \\ -\left(k_u+i\omega c_u\right) & k_u+i\omega c_u-\omega^2 m_B\left(\frac{A_b}{A_a}\right)^2\end{bmatrix}\begin{bmatrix}Y\\ U\end{bmatrix}=\begin{bmatrix} k+i\omega c \\ \omega^2 m_B\left(1-\frac{A_b}{A_a}\right)\frac{A_b}{A_a}\end{bmatrix}X \tag{B.15}$$

The second equation in the set defined above can be used to find an expression for the U degree of freedom:

$$U = \frac{\omega^2 m_B \left(1 - \frac{A_b}{A_a}\right)\frac{A_b}{A_a} X + \left(k_u + i\omega c_u\right) Y}{k_u + i\omega c_u - \omega^2 m_B \left(\frac{A_b}{A_a}\right)^2} \tag{B.16}$$

The above equation can be used to eliminate the U degree of freedom from the first equation in the set defined by Equation (B.15), which leads to the transmissibility:

$$\frac{Y}{X} = \frac{\left(k + i\omega c\right)\left[k_u + i\omega c_u - \omega^2 m_B \left(\frac{A_b}{A_a}\right)^2\right] + \left(k_u + i\omega c_u\right)\omega^2 m_B \left(1 - \frac{A_b}{A_a}\right)\frac{A_b}{A_a}}{\left[k_u + i\omega c_u - \omega^2 m_B \left(\frac{A_b}{A_a}\right)^2\right]\left[k + k_u + i\omega\left(c + c_u\right) - \omega^2 m_y\right] - \left(k_u + i\omega c_u\right)^2} \tag{B.17}$$

For the undamped case non-dimensionalisation of Equation (B.17) yields:

$$\begin{aligned}
\frac{Y}{X} &= \frac{k\left[k_u - \omega^2 m_B \left(\frac{A_b}{A_a}\right)^2\right] + k_u \omega^2 m_B \left(1 - \frac{A_b}{A_a}\right)\frac{A_b}{A_a}}{\left[k_u - \omega^2 m_B \left(\frac{A_b}{A_a}\right)^2\right]\left[k + k_u - \omega^2 m_y\right] - k_u^2} \\
&= \frac{kk_u\left\{1 - \omega^2 \frac{m_B \left(\frac{A_b}{A_a}\right)^2}{k_u} + \omega^2 \frac{m_B \left(1 - \frac{A_b}{A_a}\right)\frac{A_b}{A_a}}{k}\right\}}{kk_u\left\{\left[1 - \omega^2 \frac{m_B \left(\frac{A_b}{A_a}\right)^2}{k_u}\right]\left(1 + \frac{k_u}{k} - \omega^2 \frac{m_y}{k}\right) - \frac{k_u}{k}\right\}} \\
&= \frac{1 - \omega^2 \frac{m_B \left(\frac{A_b}{A_a}\right)^2}{k_u} + \omega^2 \frac{m_B \left(1 - \frac{A_b}{A_a}\right)\frac{A_b}{A_a}}{k}}{\left[1 - \omega^2 \frac{m_B \left(\frac{A_b}{A_a}\right)^2}{k_u}\right]\left(1 + \frac{k_u}{k} - \omega^2 \frac{m_y}{k}\right) - \frac{k_u}{k}} \\
&= \frac{1 - \left(\frac{\omega}{\omega_2}\right)^2 - \left(\frac{\omega}{\bar{\omega}_i}\right)^2}{\left[1 - \left(\frac{\omega}{\omega_2}\right)^2\right]\left[1 + \mu_k - \left(\frac{\omega}{\omega_1}\right)^2\right] - \mu_k}
\end{aligned}$$

$$\text{where:} \quad \omega_1^2 = \frac{k}{m_y}, \quad \omega_2^2 = \mu_k \frac{k}{m_B \left(\frac{A_b}{A_a}\right)^2}, \quad \bar{\omega}_i^2 = \frac{k}{m_B \left(\frac{A_b}{A_a} - 1\right)\frac{A_b}{A_a}} \tag{B.18}$$

If the area ratio is much larger than 1 then ω_2 and $\bar{\omega}_i$ are related:

$$\omega_2^2 = \mu_k \frac{k}{m_B\left(\frac{A_b}{A_a}\right)^2} = \mu_k \bar{\omega}_2^2 \approx \mu_k \bar{\omega}_i^2 \tag{B.19}$$

The isolation frequency can be calculated by setting the numerator in Equation (B.18) equal to zero:

$$\begin{aligned} 1 - \left(\frac{\omega}{\omega_2}\right)^2 - \left(\frac{\omega}{\bar{\omega}_i}\right)^2 &= 0 \\ \omega^2\left[\frac{\omega_1^2}{\bar{\omega}_i^2} + \frac{\omega_1^2}{\omega_2^2}\right] &= \omega_1^2 \\ \frac{\omega_i^2}{\omega_1^2} &= \frac{1}{\left(\frac{\omega_1}{\bar{\omega}_i}\right)^2 + \frac{1}{\mu_k}\left(\frac{\omega_1}{\bar{\omega}_2}\right)^2} \end{aligned} \tag{B.20}$$

The frequency ratio $\omega_1/\bar{\omega}_i$ can be written in terms of the mass (μ_m) and area (μ_A) ratios:

$$\left(\frac{\omega_1}{\bar{\omega}_i}\right)^2 = \frac{\frac{k}{m_y}}{\frac{k}{m_B\left(\frac{A_b}{A_a} - 1\right)\frac{A_b}{A_a}}} = \frac{k}{m_y}\frac{m_B\left(\frac{A_b}{A_a} - 1\right)\frac{A_b}{A_a}}{k} = \frac{m_B}{m_y}\left(\frac{A_b}{A_a} - 1\right)\frac{A_b}{A_a} = \mu_m\left(\mu_A - 1\right)\mu_A \tag{B.21}$$

The frequency ratio $\omega_1/\bar{\omega}_2$ can be written in terms of the mass and area ratios:

$$\left(\frac{\omega_1}{\bar{\omega}_2}\right)^2 = \frac{\frac{k}{m_y}}{\frac{k}{m_B\left(\frac{A_b}{A_a}\right)^2}} = \frac{k}{m_y}\frac{m_B\left(\frac{A_b}{A_a}\right)^2}{k} = \frac{m_B}{m_y}\left(\frac{A_b}{A_a}\right)^2 = \mu_m\mu_A^2 \tag{B.22}$$

Using the above two relations the isolation frequency can be rewritten as:

$$\begin{aligned} \left(\frac{\omega_i}{\omega_1}\right)^2 &= \frac{1}{\frac{m_B}{m_y}\left(\frac{A_b}{A_a} - 1\right)\frac{A_b}{A_a} + \frac{1}{\mu_k}\frac{m_B}{m_y}\left(\frac{A_b}{A_a}\right)^2} \\ &= \frac{1}{\mu_m\left(\mu_A - 1\right)\mu_A + \frac{\mu_m\mu_A^2}{\mu_k}} \end{aligned} \tag{B.23}$$

The undamped frequencies of maximum transmissibility can be found by equating the denominator of Equation (B.18) to zero:

$$\left[1-\left(\frac{\omega}{\omega_2}\right)^2\right]\left[1+\mu_k-\left(\frac{\omega}{\omega_1}\right)^2\right]-\mu_k=0$$

$$\frac{1}{\omega_2^2\omega_1^2}\omega^4-\left[\left(\frac{1}{\omega_2}\right)^2(1+\mu_k)+\left(\frac{1}{\omega_1}\right)^2\right]\omega^2+1=0$$

$$\left(\frac{\omega_1}{\omega_2}\right)^2\left(\frac{\omega}{\omega_1}\right)^4-\left[\left(\frac{\omega_1}{\omega_2}\right)^2(1+\mu_k)+1\right]\left(\frac{\omega}{\omega_1}\right)^2+1=0 \tag{B.24}$$

$$\left(\frac{\Omega_1}{\omega_1}\right)^2,\left(\frac{\Omega_2}{\omega_1}\right)^2=\frac{\left(\frac{\omega_1}{\omega_2}\right)^2(1+\mu_k)+1\mp\sqrt{\left[\left(\frac{\omega_1}{\omega_2}\right)^2(1+\mu_k)+1\right]^2-4\left(\frac{\omega_1}{\omega_2}\right)^2}}{2\left(\frac{\omega_1}{\omega_2}\right)^2}$$

The following two relations will assist in writing the equation in terms of the stiffness ratio ($\mu_k = k_u/k$) and constant frequency ratios:

$$\frac{\omega_1}{\omega_2}=\frac{1}{\sqrt{\mu_k}}\frac{\omega_1}{\bar{\omega}_2} \tag{B.25}$$

$$\zeta_2=\frac{1}{\sqrt{\mu_k}}\frac{c_u}{2m_p\left(\frac{A_b}{A_a}\right)^2\bar{\omega}_2}=\frac{1}{\sqrt{\mu_k}}\bar{\zeta}_2 \tag{B.26}$$

When introducing Equation (B.25) in Equation (B.24) the frequencies of maximum transmissibility can be written in terms of the stiffness ratio:

$$\left(\frac{\Omega_1}{\omega_1}\right)^2,\left(\frac{\Omega_2}{\omega_1}\right)^2=\frac{\frac{1}{\mu_k}\left(\frac{\omega_1}{\bar{\omega}_2}\right)^2(1+\mu_k)+1\mp\sqrt{\left[\frac{1}{\mu_k}\left(\frac{\omega_1}{\bar{\omega}_2}\right)^2(1+\mu_k)+1\right]^2-4\frac{1}{\mu_k}\left(\frac{\omega_1}{\bar{\omega}_2}\right)^2}}{2\frac{1}{\mu_k}\left(\frac{\omega_1}{\bar{\omega}_2}\right)^2}$$

$$=\frac{\frac{1+\mu_k}{\mu_k}\left(\frac{\omega_1}{\bar{\omega}_2}\right)^2+1\mp\sqrt{\left[\frac{1+\mu_k}{\mu_k}\left(\frac{\omega_1}{\bar{\omega}_2}\right)^2+1\right]^2-\frac{4}{\mu_k}\left(\frac{\omega_1}{\bar{\omega}_2}\right)^2}}{\frac{2}{\mu_k}\left(\frac{\omega_1}{\bar{\omega}_2}\right)^2} \tag{B.27}$$

$$=\frac{(1+\mu_k)\left(\frac{\omega_1}{\bar{\omega}_2}\right)^2+\mu_k\mp\sqrt{\left[(1+\mu_k)\left(\frac{\omega_1}{\bar{\omega}_2}\right)^2+\mu_k\right]^2-4\mu_k\left(\frac{\omega_1}{\bar{\omega}_2}\right)^2}}{2\left(\frac{\omega_1}{\bar{\omega}_2}\right)^2}$$

For the damped case Equation (B.17) can be non-dimensionalised as follows:

$$\frac{Y}{X}=\frac{\left(1+i\omega\frac{c}{k}\right)\left[1+i\omega\frac{c_u}{k_u}-\omega^2\frac{m_B\left(\frac{A_b}{A_a}\right)^2}{k_u}\right]-\left(1+i\omega\frac{c_u}{k_u}\right)\omega^2\frac{m_B\left(\frac{A_b}{A_a}-1\right)\frac{A_b}{A_a}}{k}}{\left[1+i\omega\frac{c_u}{k_u}-\omega^2\frac{m_B\left(\frac{A_b}{A_a}\right)^2}{k_u}\right]\left[1+\frac{k_u}{k}+i\omega\frac{(c+c_u)}{k}-\omega^2\frac{m_y}{k}\right]-\frac{k_u}{k}\left(1+i\omega\frac{c_u}{k_u}\right)^2}$$

$$=\frac{\left(1+i2\frac{\omega}{\omega_1}\zeta_1\right)\left[1+i2\frac{\omega}{\omega_2}\zeta_2-\left(\frac{\omega}{\omega_2}\right)^2\right]-\left(1+i2\frac{\omega}{\omega_2}\zeta_2\right)\left(\frac{\omega}{\bar{\omega}_i}\right)^2}{\left[1+\frac{k_u}{k}+i2\left(\frac{\omega}{\omega_1}\zeta_1+\frac{k_u}{k}\frac{\omega}{\omega_2}\zeta_2\right)-\left(\frac{\omega}{\omega_1}\right)^2\right]\left[1+i2\frac{\omega}{\omega_2}\zeta_2-\left(\frac{\omega}{\omega_2}\right)^2\right]-\frac{k_u}{k}\left(1+i2\frac{\omega}{\omega_2}\zeta_2\right)^2} \quad \text{(B.28)}$$

where: $\zeta_1=\frac{c}{2m_y\omega_1}$, $\zeta_2=\frac{c_u}{2m_B\left(\frac{A_b}{A_a}\right)^2\omega_2}$

Equation (B.28) can be written in terms of frequency and damping ratios that are independent of the stiffness ratio:

$$\frac{Y}{X}=\frac{\left(1+i2\frac{\omega}{\omega_1}\zeta_1\right)\left[1+i\frac{2}{\mu_k}\frac{\omega_1}{\bar{\omega}_2}\frac{\omega}{\omega_1}\bar{\zeta}_2-\frac{1}{\mu_k}\left(\frac{\omega_1}{\bar{\omega}_2}\right)^2\left(\frac{\omega}{\omega_1}\right)^2\right]-\left(1+i\frac{2}{\mu_k}\frac{\omega_1}{\bar{\omega}_2}\frac{\omega}{\omega_1}\bar{\zeta}_2\right)\left(\frac{\omega_1}{\bar{\omega}_i}\right)^2\left(\frac{\omega}{\omega_1}\right)^2}{\left[1+\mu_k+i2\frac{\omega}{\omega_1}\left(\zeta_1+\frac{\omega_1}{\bar{\omega}_2}\bar{\zeta}_2\right)-\left(\frac{\omega}{\omega_1}\right)^2\right]\left[1+i\frac{2}{\mu_k}\frac{\omega_1}{\bar{\omega}_2}\frac{\omega}{\omega_1}\bar{\zeta}_2-\frac{1}{\mu_k}\left(\frac{\omega_1}{\bar{\omega}_2}\right)^2\left(\frac{\omega}{\omega_1}\right)^2\right]-\mu_k\left(1+i\frac{2}{\mu_k}\frac{\omega_1}{\bar{\omega}_2}\frac{\omega}{\omega_1}\bar{\zeta}_2\right)^2} \quad \text{(B.29)}$$

Equation (B.14) can be non-dimensionalised as follows for the first equation:

$$m_y\ddot{y}+(c+c_u)\dot{y}-c_u\dot{u}+(k+k_u)y-k_uu=c\dot{x}+kx$$

$$\frac{m_y}{k}\ddot{y}+\left(\frac{c}{k}+\mu_k\frac{c_u}{k_u}\right)\dot{y}-\mu_k\frac{c_u}{k_u}\dot{u}+(1+\mu_k)y-\mu_ku=\frac{c}{k}\dot{x}+x$$

$$\frac{1}{\omega_1^2}\ddot{y}+2\left(\frac{\zeta_1}{\omega_1}+\mu_k\frac{\zeta_2}{\omega_2}\right)\dot{y}-2\mu_k\frac{\zeta_2}{\omega_2}\dot{u}+(1+\mu_k)y-\mu_ku=2\frac{\zeta_1}{\omega_1}\dot{x}+x$$

$$\ddot{y}+2\left(\zeta_1+\mu_k\frac{\omega_1}{\omega_2}\zeta_2\right)\omega_1\dot{y}-2\mu_k\frac{\omega_1}{\omega_2}\zeta_2\omega_1\dot{u}+\omega_1^2(1+\mu_k)y-\omega_1^2\mu_ku-2\zeta_1\omega_1\dot{x}-\omega_1^2x=0 \quad \text{(B.30)}$$

$$\ddot{y}+2\left(\zeta_1+\frac{\omega_1}{\bar{\omega}_2}\bar{\zeta}_2\right)\omega_1\dot{y}-2\frac{\omega_1}{\bar{\omega}_2}\bar{\zeta}_2\omega_1\dot{u}+\omega_1^2(1+\mu_k)y-\omega_1^2\mu_ku-2\zeta_1\omega_1\dot{x}-\omega_1^2x=0$$

where: $\frac{\zeta_2}{\omega_2}=\frac{\frac{1}{\sqrt{\mu_k}}\bar{\zeta}_2}{\sqrt{\mu_k}\bar{\omega}_2}=\frac{1}{\sqrt{\mu_k}}\bar{\zeta}_2\frac{1}{\sqrt{\mu_k}\bar{\omega}_2}=\frac{1}{\mu_k}\frac{\bar{\zeta}_2}{\bar{\omega}_2}$

And as follows for the second equation:

$$
\begin{aligned}
&m_B\left(\frac{A_b}{A_a}\right)^2\ddot{u}+c_u(\dot{u}-\dot{y})+k_u(u-y)-m_B\left(\frac{A_b}{A_a}-1\right)\frac{A_b}{A_a}\ddot{x}=0\\
&\frac{m_B\left(\frac{A_b}{A_a}\right)^2}{k_u}\ddot{u}+\frac{c_u}{k_u}(\dot{u}-\dot{y})+u-y-\frac{m_B\left(\frac{A_b}{A_a}-1\right)\frac{A_b}{A_a}}{k_u}\ddot{x}=0\\
&\frac{1}{\omega_2^2}\ddot{u}+2\frac{\zeta_2}{\omega_2}(\dot{u}-\dot{y})+u-y-\frac{1}{\mu_k}\frac{1}{\bar{\omega}_i^2}\ddot{x}=0\\
&\ddot{u}+2\zeta_2\omega_2(\dot{u}-\dot{y})+\omega_2^2(u-y)-\frac{1}{\mu_k}\left(\frac{\omega_2}{\bar{\omega}_i}\right)^2\ddot{x}=0\\
&\ddot{u}+2\bar{\zeta}_2\bar{\omega}_2(\dot{u}-\dot{y})+\mu_k\bar{\omega}_2^2(u-y)-\left(\frac{\bar{\omega}_2}{\bar{\omega}_i}\right)^2\ddot{x}=0\\
&\text{where: }\ \zeta_2\omega_2=\frac{1}{\sqrt{\mu_k}}\bar{\zeta}_2\sqrt{\mu_k}\bar{\omega}_2=\bar{\zeta}_2\bar{\omega}_2
\end{aligned}
\tag{B.31}
$$

B.1.2 Reduced-area reservoir wall stiffness

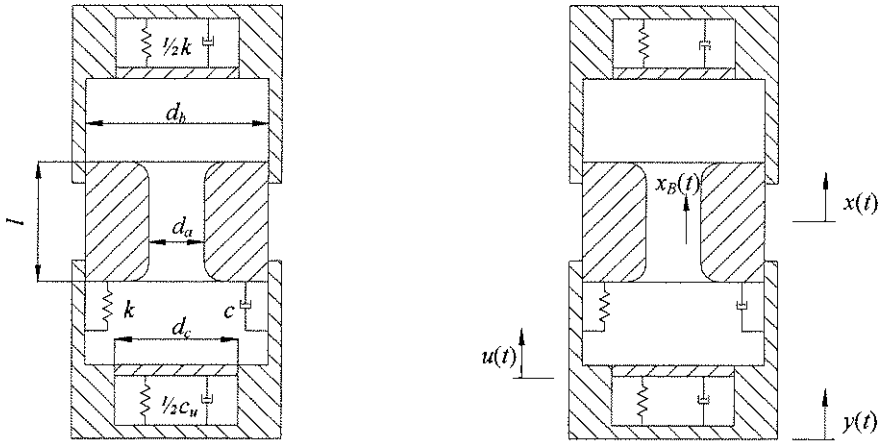

Figure B.2: Mechanical model of an AVAI with reduced-area reservoir wall stiffness

The fluid continuity through the port is changed with the reduced area give by A_c:

$$
\begin{aligned}
&y(A_b-A_c)+uA_c=(A_b-A_a)x+A_ax_B\\
&x_B=\left(1-\frac{A_b}{A_a}\right)x+\frac{A_b-A_c}{A_a}y+\frac{A_c}{A_a}u\\
&\text{where: }\ A_a=\pi\frac{d_a^2}{4},\quad A_b=\pi\frac{d_b^2}{4},\quad A_c=\pi\frac{d_c^2}{4}
\end{aligned}
\tag{B.32}
$$

The above equation reduces to Equation (B.1) when the reduced area covers the full wall (i.e. $A_c = A_b$).

The continuity equation will be used to eliminate the fluid motion (x_B) from the equations of motion. The equation of motion is derived using Lagrange's equations. The kinetic energy is:

$$\begin{aligned} T &= \frac{1}{2}\left\{m_y\dot{y}^2 + m_x\dot{x}^2 + m_B\dot{x}_B^2\right\} \\ &= \frac{1}{2}\left\{m_y\dot{y}^2 + m_x\dot{x}^2 + m_B\left[\left(1-\frac{A_b}{A_a}\right)^2\dot{x}^2 + 2\left(1-\frac{A_b}{A_a}\right)\frac{A_b-A_c}{A_a}\dot{x}\dot{y} + \left(\frac{A_b-A_c}{A_a}\right)^2\dot{y}^2\right.\right. \\ &\qquad \left.\left. + 2\left(1-\frac{A_b}{A_a}\right)\frac{A_c}{A_a}\dot{x}\dot{u} + 2\left(\frac{A_b-A_c}{A_a}\right)\frac{A_c}{A_a}\dot{u}\dot{y} + \left(\frac{A_c}{A_a}\right)^2\dot{u}^2\right]\right\} \end{aligned} \tag{B.33}$$

The derivates are:

$$\begin{aligned} \frac{d}{dt}\left(\frac{\partial T}{\partial \dot{y}}\right) &= \left[m_y + m_B\left(\frac{A_b-A_c}{A_a}\right)^2\right]\ddot{y} + m_B\left[\left(1-\frac{A_b}{A_a}\right)\left(\frac{A_b-A_c}{A_a}\right)\ddot{x} + \left(\frac{A_b-A_c}{A_a}\right)\frac{A_c}{A_a}\right]\ddot{u} \\ \frac{d}{dt}\left(\frac{\partial T}{\partial \dot{x}}\right) &= \left[m + m_B\left(1-\frac{A_b}{A_a}\right)^2\right]\ddot{x} + m_B\left[\left(1-\frac{A_b}{A_a}\right)\frac{A_b-A_c}{A_a}\ddot{y} + \left(1-\frac{A_b}{A_a}\right)\frac{A_c}{A_a}\ddot{u}\right] \\ \frac{d}{dt}\left(\frac{\partial T}{\partial \dot{u}}\right) &= m_B\left[\frac{A_c}{A_a}\left(1-\frac{A_b}{A_a}\right)\ddot{x} + \frac{A_c}{A_a}\left(\frac{A_b-A_c}{A_a}\right)\ddot{y} + \left(\frac{A_c}{A_a}\right)^2\ddot{u}\right] \end{aligned} \tag{B.34}$$

The potential energy and Rayleigh terms do not depend on the continuity equation and are therefore exactly as before (refer §B.1.1). The equation of motion can be derived using Lagrange's equations and by assuming that the x degree of freedom is prescribed:

$$\begin{aligned} &\begin{bmatrix} m_y + m_B\left(\frac{A_b-A_c}{A_a}\right)^2 & m_B\left(\frac{A_b-A_c}{A_a}\right)\frac{A_c}{A_a} \\ m_B\left(\frac{A_b-A_c}{A_a}\right)\frac{A_c}{A_a} & m_B\left(\frac{A_c}{A_a}\right)^2 \end{bmatrix}\begin{bmatrix}\ddot{y}\\ \ddot{u}\end{bmatrix} + \begin{bmatrix} c+c_u & -c_u \\ -c_u & c_u\end{bmatrix}\begin{bmatrix}\dot{y}\\ \dot{u}\end{bmatrix} + \begin{bmatrix} k+k_u & -k_u \\ -k_u & k_u\end{bmatrix}\begin{bmatrix}y\\ u\end{bmatrix} \\ &= \begin{bmatrix} m_B\left(\frac{A_b}{A_a}-1\right)\left(\frac{A_b-A_c}{A_a}\right)\ddot{x} + c\dot{x} + kx \\ m_B\left(\frac{A_b}{A_a}-1\right)\frac{A_c}{A_a}\ddot{x}\end{bmatrix} \end{aligned} \tag{B.35}$$

Transforming the above equation to the frequency domain yields:

$$\begin{aligned} &\begin{bmatrix} k+k_u+i\omega(c+c_u) - \omega^2\left[m_y + m_B\left(\frac{A_b-A_c}{A_a}\right)^2\right] & -k_u - i\omega c_u - \omega^2 m_B\left(\frac{A_b-A_c}{A_a}\right)\frac{A_c}{A_a} \\ -k_u - i\omega c_u - \omega^2 m_B\left(\frac{A_b-A_c}{A_a}\right)\frac{A_c}{A_a} & k_u + i\omega c_u - \omega^2 m_B\left(\frac{A_c}{A_a}\right)^2\end{bmatrix}\begin{bmatrix}Y\\ U\end{bmatrix} \\ &= \begin{bmatrix} \omega^2 m_B\left(1-\frac{A_b}{A_a}\right)\left(\frac{A_b-A_c}{A_a}\right) + i\omega c + k \\ \omega^2 m_B\left(1-\frac{A_b}{A_a}\right)\frac{A_c}{A_a}\end{bmatrix}X \end{aligned} \tag{B.36}$$

The second equation in the set described above can be used to eliminate the U degree of freedom.

The non-dimensional transmissibility can be found as follows:

$$\frac{Y}{X}=\frac{\left[k+i\omega c-\omega^2 m_B\left(\frac{A_b}{A_a}-1\right)\left(\frac{A_b-A_c}{A_a}\right)\right]\left[k_u+i\omega c_u-\omega^2 m_B\left(\frac{A_c}{A_a}\right)^2\right]-\omega^2 m_B\left(\frac{A_b}{A_a}-1\right)\frac{A_c}{A_a}\left[k_u+i\omega c_u+\omega^2 m_B\left(\frac{A_b-A_c}{A_a}\right)\frac{A_c}{A_a}\right]}{\left\{k+k_u+i\omega\left(c+c_u\right)-\omega^2\left[m_y+m_B\left(\frac{A_b-A_c}{A_a}\right)^2\right]\right\}\left[k_u+i\omega c_u-\omega^2 m_B\left(\frac{A_c}{A_a}\right)^2\right]-\left[k_u+i\omega c_u+\omega^2 m_B\left(\frac{A_b-A_c}{A_a}\right)\frac{A_c}{A_a}\right]^2}$$

$$=\frac{\left[1+i\omega\frac{c}{k}-\omega^2(1-\lambda)\frac{m_B\left(\frac{A_b}{A_a}-1\right)\left(\frac{A_b}{A_a}\right)}{k}\right]\left[1+i\omega\frac{c_u}{k_u}-\omega^2\lambda^2\frac{m_B\left(\frac{A_b}{A_a}\right)^2}{k_u}\right]-\omega^2\lambda\frac{m_B\left(\frac{A_b}{A_a}-1\right)\frac{A_b}{A_a}}{k}\left[1+i\omega\frac{c_u}{k_u}+\omega^2(1-\lambda)\lambda\frac{m_B\left(\frac{A_b}{A_a}\right)^2}{k_u}\right]}{\left\{1+\frac{k_u}{k}+i\omega\frac{c+c_u}{k}-\omega^2\left[\frac{m_y}{k}+\frac{m_B(1-\lambda)^2\left(\frac{A_b}{A_a}\right)^2}{k}\right]\right\}\left[1+i\omega\frac{c_u}{k_u}-\omega^2\lambda^2\frac{m_B\left(\frac{A_b}{A_a}\right)^2}{k_u}\right]-\frac{k_u}{k}\left[1+i\omega\frac{c_u}{k_u}+\omega^2(1-\lambda)\lambda\frac{m_B\left(\frac{A_b}{A_a}\right)^2}{k_u}\right]^2}$$

$$=\frac{\left[1+i2\frac{\omega}{\omega_1}\zeta_1-(1-\lambda)\left(\frac{\omega}{\bar{\omega}_i}\right)^2\right]\left[1+i2\frac{\omega}{\omega_2}\zeta_2-\lambda^2\left(\frac{\omega}{\omega_2}\right)^2\right]-\lambda\left(\frac{\omega}{\bar{\omega}_i}\right)^2\left[1+i2\frac{\omega}{\omega_2}\zeta_2+(1-\lambda)\lambda\left(\frac{\omega}{\omega_2}\right)^2\right]}{\left\{1+\frac{k_u}{k}+i2\left(\frac{\omega}{\omega_1}\zeta_1+\frac{k_u}{k}\frac{\omega}{\omega_2}\zeta_2\right)-\left[\left(\frac{\omega}{\omega_1}\right)^2+(1-\lambda)^2\frac{k_u}{k}\left(\frac{\omega}{\omega_2}\right)^2\right]\right\}\left[1+i2\frac{\omega}{\omega_2}\zeta_2-\lambda^2\left(\frac{\omega}{\omega_2}\right)^2\right]-\frac{k_u}{k}\left[1+i2\frac{\omega}{\omega_2}\zeta_2+(1-\lambda)\lambda\left(\frac{\omega}{\omega_2}\right)^2\right]^2}$$

where: $\lambda=\frac{A_c}{A_b}$ (B.37)

The transmissibility can be written in terms of the stiffness ratio and constants defined by Equation (B.25) and (B.26):

$$\frac{Y}{X}=\frac{\left[1+i2\frac{\omega}{\omega_1}\zeta_1-(1-\lambda)\left(\frac{\omega_1}{\bar{\omega}_i}\right)^2\left(\frac{\omega}{\omega_1}\right)^2\right]\left[1+i\frac{2}{\mu_k}\frac{\omega_1}{\bar{\omega}_2}\frac{\omega}{\omega_1}\bar{\zeta}_2-\frac{\lambda^2}{\mu_k}\left(\frac{\omega_1}{\bar{\omega}_2}\right)^2\left(\frac{\omega}{\omega_1}\right)^2\right]-\lambda\left(\frac{\omega_1}{\bar{\omega}_i}\right)^2\left(\frac{\omega}{\omega_1}\right)^2\left[1+i\frac{2}{\mu_k}\frac{\omega_1}{\bar{\omega}_2}\frac{\omega}{\omega_1}\bar{\zeta}_2+(1-\lambda)\frac{\lambda}{\mu_k}\left(\frac{\omega_1}{\bar{\omega}_2}\right)^2\left(\frac{\omega}{\omega_1}\right)^2\right]}{\left\{1+\mu_k+i2\frac{\omega}{\omega_1}\left(\zeta_1+\frac{\omega_1}{\bar{\omega}_2}\bar{\zeta}_2\right)-\left[\left(\frac{\omega}{\omega_1}\right)^2+(1-\lambda)^2\left(\frac{\omega_1}{\bar{\omega}_2}\right)^2\left(\frac{\omega}{\omega_1}\right)^2\right]\right\}\left[1+i\frac{2}{\mu_k}\frac{\omega_1}{\bar{\omega}_2}\frac{\omega}{\omega_1}\bar{\zeta}_2-\frac{\lambda^2}{\mu_k}\left(\frac{\omega_1}{\bar{\omega}_2}\right)^2\left(\frac{\omega}{\omega_1}\right)^2\right]-\mu_k\left[1+i\frac{2}{\mu_k}\frac{\omega_1}{\bar{\omega}_2}\frac{\omega}{\omega_1}\bar{\zeta}_2+(1-\lambda)\frac{\lambda}{\mu_k}\left(\frac{\omega_1}{\bar{\omega}_2}\right)^2\left(\frac{\omega}{\omega_1}\right)^2\right]^2} \quad \text{(B.38)}$$

B.2 Adaptive AVAI with slug (Type II)

B.2.1 Slug springs

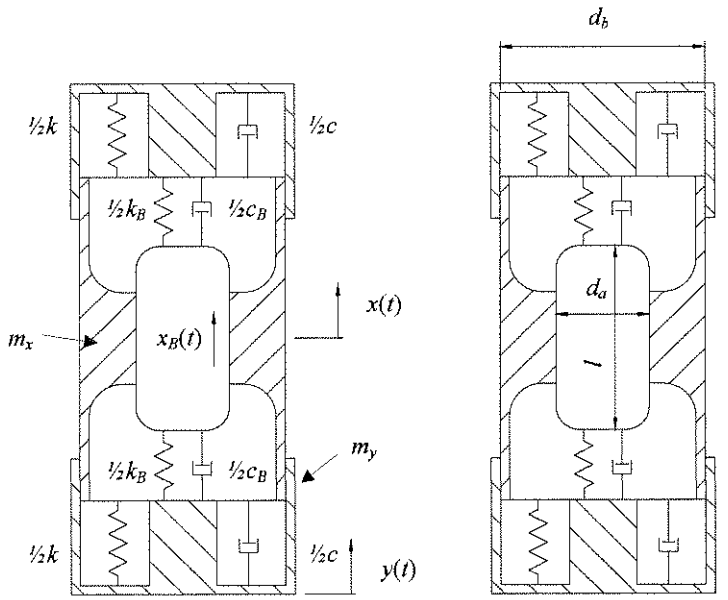

Figure B.3: Mechanical model of an adaptive AVAI with a slug

The equations of motion will be derived using Lagrange's equations. The equations of motion for this configuration can also be derived by considering force balance as shown by Halwes (1981a). The fluid continuity through the port is:

$$\begin{aligned} yA_b &= (A_b - A_a)x + A_a x_B \\ x_B &= \left(1 - \frac{A_b}{A_a}\right)x + \frac{A_b}{A_a}y \end{aligned} \tag{B.39}$$

The kinetic energy is:

$$\begin{aligned} T &= \frac{1}{2}\left(m_x\dot{x}^2 + m_B\dot{x}_B^2 + m_y\dot{y}^2\right) \\ &= \frac{1}{2}\left\{m_x\dot{x}^2 + m_B\left[\left(\frac{A_b}{A_a} - 1\right)^2\dot{x}^2 - 2\left(\frac{A_b}{A_a} - 1\right)\frac{A_b}{A_a}\dot{x}\dot{y} + \left(\frac{A_b}{A_a}\right)^2\dot{y}^2\right] + m_y\dot{y}^2\right\} \end{aligned} \tag{B.40}$$

where: $m_B = \rho A_a l$

From the previous equation the derivatives can be found:

$$\begin{aligned}\frac{d}{dt}\left(\frac{\partial T}{\partial \dot{x}}\right) &= \left[m_x + m_B\left(\frac{A_b}{A_a}-1\right)^2\right]\ddot{x} + m_B\left(\frac{A_b}{A_a}-1\right)\frac{A_b}{A_a}\ddot{y} \\ \frac{d}{dt}\left(\frac{\partial T}{\partial \dot{y}}\right) &= m_B\left(\frac{A_b}{A_a}-1\right)\frac{A_b}{A_a}\ddot{x} + \left[m_y + m_B\left(\frac{A_b}{A_a}\right)^2\right]\ddot{y}\end{aligned} \tag{B.41}$$

The potential energy is:

$$\begin{aligned}V &= \frac{1}{2}\left[k\left(x-y\right)^2 + k_B\left(x_B - y\right)^2\right] \\ &= \frac{1}{2}\left[k + k_B\left(1-\frac{A_b}{A_a}\right)^2\right]\left(x^2 - 2xy + y^2\right)\end{aligned} \tag{B.42}$$

From the previous equation the derivatives can be found:

$$\begin{aligned}\frac{\partial V}{\partial x} &= \left[k + k_B\left(1-\frac{A_b}{A_a}\right)^2\right]x - \left[k + k_B\left(1-\frac{A_b}{A_a}\right)^2\right]y \\ \frac{\partial V}{\partial y} &= -\left[k + k_B\left(1-\frac{A_b}{A_a}\right)^2\right]x + \left[k + k_B\left(1-\frac{A_b}{A_a}\right)^2\right]y\end{aligned} \tag{B.43}$$

The complete equation of motion can be found using Lagrange's equations:

$$\begin{aligned}&\begin{bmatrix} m_x + m_B\left(\frac{A_b}{A_a}-1\right)^2 & -m_B\left(\frac{A_b}{A_a}-1\right)\frac{A_b}{A_a} \\ -m_B\left(\frac{A_b}{A_a}-1\right)\frac{A_b}{A_a} & m_y + m_B\left(\frac{A_b}{A_a}\right)^2 \end{bmatrix}\begin{bmatrix}\ddot{x}\\ \ddot{y}\end{bmatrix} + \begin{bmatrix} c + c_B\left(\frac{A_b}{A_a}-1\right)^2 & -\left[c + c_B\left(\frac{A_b}{A_a}-1\right)^2\right] \\ -\left[c + c_B\left(\frac{A_b}{A_a}-1\right)^2\right] & c + c_B\left(\frac{A_b}{A_a}-1\right)^2 \end{bmatrix}\begin{bmatrix}\dot{x}\\ \dot{y}\end{bmatrix} \\ &+ \begin{bmatrix} k + k_B\left(\frac{A_b}{A_a}-1\right)^2 & -\left[k + k_B\left(\frac{A_b}{A_a}-1\right)^2\right] \\ -\left[k + k_B\left(\frac{A_b}{A_a}-1\right)^2\right] & k + k_B\left(\frac{A_b}{A_a}-1\right)^2 \end{bmatrix}\begin{bmatrix}x\\ y\end{bmatrix} = \begin{bmatrix}0\\ 0\end{bmatrix}\end{aligned} \tag{B.44}$$

Assuming that excitation occurs at the y degree of freedom, the second equation is eliminated:

$$\begin{aligned}&\left[m_x + m_B\left(\frac{A_b}{A_a}-1\right)^2\right]\ddot{x} + \left[c + c_B\left(\frac{A_b}{A_a}-1\right)^2\right]\dot{x} + \left[k + k_B\left(\frac{A_b}{A_a}-1\right)^2\right]x \\ &= m_B\left(\frac{A_b}{A_a}-1\right)\frac{A_b}{A_a}\ddot{y} + \left[c + c_B\left(\frac{A_b}{A_a}-1\right)^2\right]\dot{y} + \left[k + k_B\left(\frac{A_b}{A_a}-1\right)^2\right]y\end{aligned} \tag{B.45}$$

The equation of motion can be non-dimensionalised by introducing the damping ratio and the isolation and natural frequencies:

$$\ddot{x}+2\zeta\omega_n\dot{x}+\omega_n^2 x=\left(\frac{\omega_n}{\omega_i}\right)^2\ddot{y}+2\zeta\omega_n\dot{y}+\omega_n^2 y$$

$$\text{where:}\quad \omega_i=\sqrt{\frac{k+k_B\left(\frac{A_b}{A_a}-1\right)^2}{m_B\left(\frac{A_b}{A_a}-1\right)\frac{A_b}{A_a}}},\quad \omega_n=\sqrt{\frac{k+k_B\left(\frac{A_b}{A_a}-1\right)^2}{m_x+m_B\left(\frac{A_b}{A_a}-1\right)^2}},\quad \zeta=\frac{c+c_B\left(\frac{A_b}{A_a}-1\right)^2}{2\left[m_x+m_B\left(\frac{A_b}{A_a}-1\right)^2\right]\omega_n} \tag{B.46}$$

The transmissibility is:

$$\frac{X}{Y}=\frac{1+i2\frac{\omega}{\omega_n}\zeta-\left(\frac{\omega}{\omega_i}\right)^2}{1+i2\frac{\omega}{\omega_n}\zeta-\left(\frac{\omega}{\omega_n}\right)^2} \tag{B.47}$$

Assuming that excitation occurs at the x degree of freedom, the first equation is eliminated:

$$\begin{aligned}&\left[m_y+m_B\left(\frac{A_b}{A_a}\right)^2\right]\ddot{y}+\left[c+c_B\left(\frac{A_b}{A_a}-1\right)^2\right]\dot{y}+\left[k+k_B\left(\frac{A_b}{A_a}-1\right)^2\right]y\\&=m_B\left(\frac{A_b}{A_a}-1\right)\frac{A_b}{A_a}\ddot{x}+\left[c+c_B\left(\frac{A_b}{A_a}-1\right)^2\right]\dot{x}+\left[k+k_B\left(\frac{A_b}{A_a}-1\right)^2\right]x\end{aligned} \tag{B.48}$$

The equation of motion can be non-dimensionalised by introducing the damping ratio and the isolation and natural frequencies:

$$\ddot{y}+2\zeta\omega_n\dot{y}+\omega_n^2 y=\left(\frac{\omega_n}{\omega_i}\right)^2\ddot{x}+2\zeta\omega_n\dot{x}+\omega_n^2 x$$

$$\text{where:}\quad \omega_i=\sqrt{\frac{k+k_B\left(\frac{A_b}{A_a}-1\right)^2}{m_B\left(\frac{A_b}{A_a}-1\right)\frac{A_b}{A_a}}},\quad \omega_n=\sqrt{\frac{k+k_B\left(\frac{A_b}{A_a}-1\right)^2}{m_y+m_B\left(\frac{A_b}{A_a}\right)^2}},\quad \zeta=\frac{c+c_B\left(\frac{A_b}{A_a}-1\right)^2}{2\left[m_y+m_B\left(\frac{A_b}{A_a}\right)^2\right]\omega_n} \tag{B.49}$$

The equation is the same as when the x degree of freedom is the excitation degree of freedom, except for the definition of the natural frequency and damping ratio. In the analysis that follows the ratio X/Y can therefore be inverted as long as the corresponding definition of the natural frequency and damping ratio is used. The transmissibility can be rewritten in terms of the isolation frequency by introducing the frequency ratio:

$$\frac{X}{Y}=\frac{1+i2\frac{\omega_i}{\omega_n}\frac{\omega}{\omega_i}\zeta-\left(\frac{\omega}{\omega_i}\right)^2}{1+i2\frac{\omega_i}{\omega_n}\frac{\omega}{\omega_i}\zeta-\left(\frac{\omega_i}{\omega_n}\right)^2\left(\frac{\omega}{\omega_i}\right)^2} \tag{B.50}$$

The frequency ratio is a function of the mass and area ratio only. For excitation at y:

$$\left(\frac{\omega_n}{\omega_i}\right)^2 = \frac{m_B\left(\frac{A_b}{A_a}-1\right)\frac{A_b}{A_a}}{m_x + m_B\left(\frac{A_b}{A_a}-1\right)^2} = \frac{\frac{m_B}{m_x}\left(\frac{A_b}{A_a}-1\right)\frac{A_b}{A_a}}{1+\frac{m_B}{m_x}\left(\frac{A_b}{A_a}-1\right)^2} = \frac{\mu_m(\mu_A-1)\mu_A}{1+\mu_m(\mu_A-1)^2} \tag{B.51}$$

where: $\mu_m = \frac{m_B}{m_x}, \quad \mu_A = \frac{A_b}{A_a}$

and for excitation at x:

$$\left(\frac{\omega_n}{\omega_i}\right)^2 = \frac{m_B\left(\frac{A_b}{A_a}-1\right)\frac{A_b}{A_a}}{m_y + m_B\left(\frac{A_b}{A_a}\right)^2} = \frac{\frac{m_B}{m_y}\left(\frac{A_b}{A_a}-1\right)\frac{A_b}{A_a}}{1+\frac{m_B}{m_y}\left(\frac{A_b}{A_a}\right)^2} = \frac{\mu_m(\mu_A-1)\mu_A}{1+\mu_m\mu_A^2} \tag{B.52}$$

where: $\mu_m = \frac{m_B}{m_y}, \quad \mu_A = \frac{A_b}{A_a}$

The frequency ratio must be as small as possible, which can be achieved if the denominator is much larger than the numerator of the previous 2 equations. Considering the first equation:

$$\begin{aligned} \frac{\mu_m(\mu_A-1)\mu_A}{1+\mu_m(\mu_A-1)^2} &\square\ 1 \\ \mu_m(\mu_A-1)\mu_A - \mu_m(\mu_A-1)^2 &\square\ 1 \\ \mu_m(\mu_A-1)\left[\mu_A-(\mu_A-1)\right] &\square\ 1 \\ \mu_m(\mu_A-1) &\square\ 1 \end{aligned} \tag{B.53}$$

condition met if $\mu_m \to 0$ and/or $\mu_A \to 1$

The second equation follows similarly. The current natural and isolation frequencies can be written in terms of their initial values (before changes to the stiffness ratio) indicated by the prime:

$$\begin{aligned} \omega_n^2 &= \frac{k+k_B\left(\frac{A_b}{A_a}-1\right)^2}{k'+k'_B\left(\frac{A_b}{A_a}-1\right)^2}\frac{k'+k'_B\left(\frac{A_b}{A_a}-1\right)^2}{m+m_B\left(\frac{A_b}{A_a}-1\right)^2} = \mu_k\omega_n'^2 \\ \omega_i^2 &= \frac{k+k_B\left(\frac{A_b}{A_a}-1\right)^2}{k'+k'_B\left(\frac{A_b}{A_a}-1\right)^2}\frac{k'+k'_B\left(\frac{A_b}{A_a}-1\right)^2}{m+m_B\left(\frac{A_b}{A_a}-1\right)\frac{A_b}{A_a}} = \mu_k\omega_i'^2 \end{aligned} \tag{B.54}$$

$$\zeta = \frac{\omega_n'}{\omega_n}\frac{c}{2\left[m_x + m_B\left(\frac{A_b}{A_a}-1\right)^2\right]\omega_n'} = \frac{1}{\sqrt{\mu_k}}\zeta'$$

The transmissibility can conveniently be written in terms of the stiffness ratio:

$$\frac{X}{Y} = \frac{1+i2\dfrac{\omega}{\omega_n'}\dfrac{\omega_n'}{\omega_n}\zeta - \left(\dfrac{\omega_n'}{\omega_i}\right)^2\left(\dfrac{\omega}{\omega_n'}\right)^2}{1+i2\dfrac{\omega}{\omega_n'}\dfrac{\omega_n'}{\omega_n}\zeta - \left(\dfrac{\omega_n'}{\omega_n}\right)^2\left(\dfrac{\omega}{\omega_n'}\right)^2}$$

$$= \frac{1+i2\dfrac{\omega}{\omega_n'}\left(\dfrac{\omega_n'}{\omega_n}\right)^2\zeta' - \dfrac{\omega_n'^2}{\omega_i^2}\left(\dfrac{\omega}{\omega_n'}\right)^2}{1+i2\dfrac{\omega}{\omega_n'}\left(\dfrac{\omega_n'}{\omega_n}\right)^2\zeta' - \dfrac{\omega_n'^2}{\omega_n^2}\left(\dfrac{\omega}{\omega_n'}\right)^2}$$

$$= \frac{1+i2\dfrac{\omega}{\omega_n'}\dfrac{1}{\mu_k}\zeta' - \dfrac{\omega_n'^2}{\mu_k\omega_i'^2}\left(\dfrac{\omega}{\omega_n'}\right)^2}{1+i2\dfrac{\omega}{\omega_n'}\dfrac{1}{\mu_k}\zeta' - \dfrac{\omega_n'^2}{\mu_k\omega_n'^2}\left(\dfrac{\omega}{\omega_n'}\right)^2}$$

$$= \frac{1+i2\dfrac{\omega}{\omega_n'}\dfrac{1}{\mu_k}\zeta' - \dfrac{1}{\mu_k}\left(\dfrac{\omega_n}{\omega_i}\right)^2\left(\dfrac{\omega}{\omega_n'}\right)^2}{1+i2\dfrac{\omega}{\omega_n'}\dfrac{1}{\mu_k}\zeta' - \dfrac{1}{\mu_k}\left(\dfrac{\omega}{\omega_n'}\right)^2}$$

where: $\mu_k = \dfrac{k+k_B\left(\dfrac{A_b}{A_a}-1\right)^2}{k'+k_B'\left(\dfrac{A_b}{A_a}-1\right)^2}$, $\zeta' = \dfrac{c}{2\left[m_x+m_B\left(\dfrac{A_b}{A_a}-1\right)^2\right]\omega_n'}$ (B.55)

The dimensions used in the design of the device are shown in Figure B.4.

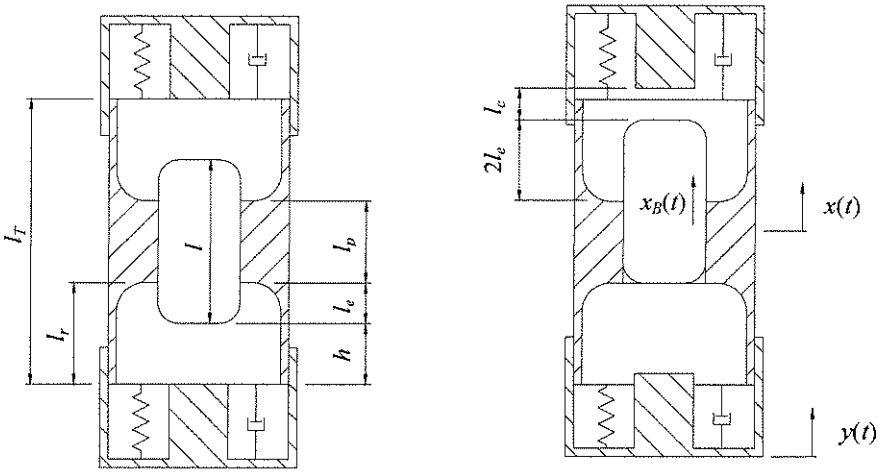

Figure B.4: Definition of dimensions

The isolation frequency can be rewritten to find the slug length:

$$l = \frac{k + k_B\left(\frac{A_b}{A_a} - 1\right)^2}{\omega_i^2\left(\frac{A_b}{A_a} - 1\right)\frac{A_b}{A_a}\rho A_a} \tag{B.56}$$

The slug displacement for an undamped device can be found from the continuity equation:

$$X_B = \frac{A_b}{A_a}Y \tag{B.57}$$

The total length required is a function of the reservoir length (l_r) the protrusion length (l_e) and the slug length (l):

$$l_T = 2l_r - 2l_e + l \tag{B.58}$$

If the length of the protrusion (l_e) is assumed to be equal to the slug displacement:

$$l_T = 2l_r - 2\frac{A_b}{A_a}Y + l \tag{B.59}$$

The length of the reservoir is a function of the compressed length of the spring (l_c):

$$l_r = l_c + 2l_e - Y \tag{B.60}$$

The total length required can be rewritten using the expressions in Equation (B.59) and Equation (B.60):

$$l_T = 2l_c + 2\left(\frac{A_b}{A_a} - 1\right)Y + l \tag{B.61}$$

The port area can now be found in terms of the outside dimensions of the device using the expressions for the slug length Equation (B.56) and the total length Equation (B.61):

$$l_T\omega_i^2\left(\frac{A_b}{A_a} - 1\right)\frac{A_b}{A_a}\rho A_a = 2l_c\omega_i^2\left(\frac{A_b}{A_a} - 1\right)\frac{A_b}{A_a}\rho A_a + 2\left(\frac{A_b}{A_a} - 1\right)Y\omega_i^2\left(\frac{A_b}{A_a} - 1\right)\frac{A_b}{A_a}\rho A_a + k + k_B\left(\frac{A_b}{A_a} - 1\right)^2$$

$$l_T\omega_i^2\frac{A_b}{A_a}A_b\rho - l_T\omega_i^2A_b\rho = 2l_c\omega_i^2\frac{A_b}{A_a}A_b\rho - 2l_c\omega_i^2A_b\rho + 2Y\omega_i^2A_b\rho\left[\left(\frac{A_b}{A_a}\right)^2 - 2\frac{A_b}{A_a} + 1\right] + k + k_B\left[\left(\frac{A_b}{A_a}\right)^2 - 2\frac{A_b}{A_a} + 1\right]$$

$$l_T\omega_i^2\frac{A_b^2}{A_a}\rho - l_T\omega_i^2A_b\rho = 2l_c\omega_i^2\frac{A_b^2}{A_a}\rho - 2l_c\omega_i^2A_b\rho + 2Y\omega_i^2A_b\rho\frac{A_b^2}{A_a^2} - 4Y\omega_i^2A_b\rho\frac{A_b}{A_a} + 2Y\omega_i^2A_b\rho + k + k_B\frac{A_b^2}{A_a^2} - 2k_B\frac{A_b}{A_a} + k_B$$

$$l_T\omega_i^2\rho A_b^2A_a - l_T\omega_i^2A_b\rho A_a^2 - 2l_c\omega_i^2\rho A_b^2A_a + 2l_c\omega_i^2A_b\rho A_a^2 - 2Y\omega_i^2A_b\rho A_b^2 + 4Y\omega_i^2A_b\rho A_bA_a$$
$$- 2Y\omega_i^2A_b\rho A_a^2 - kA_a^2 - k_BA_b^2 + 2k_BA_bA_a - k_BA_a^2 = 0$$

$$\left(2l_c\omega_i^2A_b\rho - 2Y\omega_i^2A_b\rho - l_T\omega_i^2A_b\rho - k - k_B\right)A_a^2 + \left(l_T\omega_i^2\rho A_b^2 - 2l_c\omega_i^2\rho A_b^2 + 4Y\omega_i^2A_b^2\rho + 2k_BA_b\right)A_a - 2Y\omega_i^2\rho A_b^3 - k_BA_b^2 = 0 \tag{B.62}$$

The current isolation frequency can be written in terms of the initial isolation frequency by equating the numerator to zero:

$$\begin{aligned}\left(\frac{\omega_i}{\omega_n'}\right)^2 &= \mu_k\left(\frac{\omega_i'}{\omega_n'}\right)^2 \\ &= \mu_k\left(\frac{\omega_i}{\omega_n}\right)^2 \\ &= \mu_k\frac{1+\mu_m(\mu_A-1)^2}{\mu_m(\mu_A-1)\mu_A} \quad \text{(excitation at } x\text{)} \\ &\text{or} \\ &= \mu_k\frac{1+\mu_m(\mu_A-1)^2}{\mu_m\mu_A^2} \quad \text{(excitation at y)}\end{aligned} \tag{B.63}$$

The damped isolation frequency can be written in terms of the stiffness ratio:

$$\left(\frac{\Omega_i}{\omega_n}\right)^2 = \frac{-\left(\frac{\omega_n}{\omega_i}\right)^2 - 1 - \sqrt{\left[\left(\frac{\omega_n}{\omega_i}\right)^2 - 1\right]^2 + 8\zeta^2\left[\left(\frac{\omega_n}{\omega_i}\right)^2 + 1\right]}}{4\zeta^2 + 4\zeta^2\left(\frac{\omega_n}{\omega_i}\right)^2 - 2\left(\frac{\omega_n}{\omega_i}\right)^2}$$

$$\left(\frac{\Omega_i}{\sqrt{\mu_k}\omega_n'}\right)^2 = \frac{-\left(\frac{\sqrt{\mu_k}\omega_n'}{\sqrt{\mu_k}\omega_i'}\right)^2 - 1 - \sqrt{\left[\left(\frac{\sqrt{\mu_k}\omega_n'}{\sqrt{\mu_k}\omega_i'}\right)^2 - 1\right]^2 + 8\left(\frac{\zeta'}{\sqrt{\mu_k}}\right)^2\left[\left(\frac{\sqrt{\mu_k}\omega_n'}{\sqrt{\mu_k}\omega_i'}\right)^2 + 1\right]}}{4\left(\frac{\zeta'}{\sqrt{\mu_k}}\right)^2 + 4\left(\frac{\zeta'}{\sqrt{\mu_k}}\right)^2\left(\frac{\sqrt{\mu_k}\omega_n'}{\sqrt{\mu_k}\omega_i'}\right)^2 - 2\left(\frac{\sqrt{\mu_k}\omega_n'}{\sqrt{\mu_k}\omega_i'}\right)^2}$$

$$\frac{1}{\mu_k}\left(\frac{\Omega_i}{\omega_n'}\right)^2 = \frac{-\left(\frac{\omega_n'}{\omega_i'}\right)^2 - 1 - \sqrt{\left[\left(\frac{\omega_n'}{\omega_i'}\right)^2 - 1\right]^2 + 8\frac{\zeta'^2}{\mu_k}\left[\left(\frac{\omega_n'}{\omega_i'}\right)^2 + 1\right]}}{4\frac{\zeta'^2}{\mu_k} + 4\frac{\zeta'^2}{\mu_k}\left(\frac{\omega_n'}{\omega_i'}\right)^2 - 2\left(\frac{\omega_n'}{\omega_i'}\right)^2}$$

$$\begin{aligned}\left(\frac{\Omega_i}{\omega_n'}\right)^2 &= \mu_k\frac{-\left(\frac{\omega_n'}{\omega_i'}\right)^2 - 1 - \sqrt{\left[\left(\frac{\omega_n'}{\omega_i'}\right)^2 - 1\right]^2 + 8\frac{\zeta'^2}{\mu_k}\left[\left(\frac{\omega_n'}{\omega_i'}\right)^2 + 1\right]}}{4\frac{\zeta'^2}{\mu_k} + 4\frac{\zeta'^2}{\mu_k}\left(\frac{\omega_n'}{\omega_i'}\right)^2 - 2\left(\frac{\omega_n'}{\omega_i'}\right)^2} \\ &= \mu_k\frac{-\left(\frac{\omega_n}{\omega_i}\right)^2 - 1 - \sqrt{\left[\left(\frac{\omega_n}{\omega_i}\right)^2 - 1\right]^2 + 8\frac{\zeta'^2}{\mu_k}\left[\left(\frac{\omega_n}{\omega_i}\right)^2 + 1\right]}}{4\frac{\zeta'^2}{\mu_k} + 4\frac{\zeta'^2}{\mu_k}\left(\frac{\omega_n}{\omega_i}\right)^2 - 2\left(\frac{\omega_n}{\omega_i}\right)^2}\end{aligned} \tag{B.64}$$

B.2.2 Slug stops

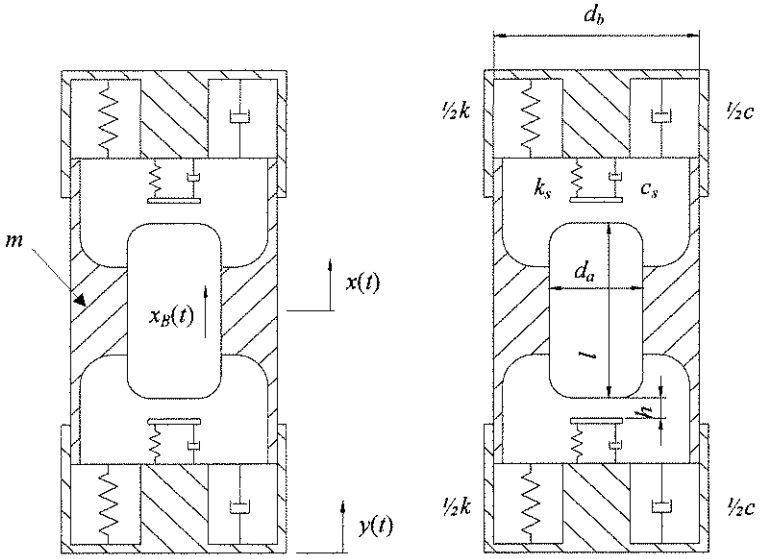

Figure B.5: Mechanical model of a type II AVAI with slug stops

Continuity is described by Equation (B.39). For this derivation it is assumed that the stop will stay in contact with the slug if the relative displacement between the slug and the reservoir is larger than the gap (h). This might not be the situation for high damping ratios, in which case the approach taken by Luo and Hanagud (1998) is more appropriate. For this derivation it will be more convenient to use force balance on the various components rather than Lagrange's equations as was done up till now.

Graphically the stiffness can be represented as shown in Figure B.6, where f_s is the force acting on the slug.

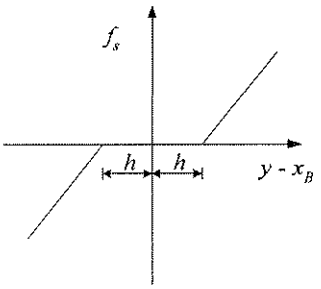

Figure B.6: Graphical representation of stop force

The stop force is:

$$\begin{aligned} f_s &= \beta k_s \left[y - x_B - \text{sign}(y - x_B) h \right] \\ &= \beta k_s \left\{ y - x + \frac{A_b}{A_a}(x - y) - \text{sign}\left[y - x + \frac{A_b}{A_a}(x - y) \right] h \right\} \end{aligned} \tag{B.65}$$

where: $\beta = \begin{cases} 0 \text{ if } \left| y - x + \frac{A_b}{A_a}(x - y) \right| < h \\ 1 \text{ if } \left| y - x + \frac{A_b}{A_a}(x - y) \right| \geq h \end{cases}$

The stop damping force is:

$$\begin{aligned} f_d &= \beta c_s (\dot{y} - \dot{x}_B) \\ &= \beta c_s \left[\dot{y} - \dot{x} + \frac{A_b}{A_a}(\dot{x} - \dot{y}) \right] \end{aligned} \tag{B.66}$$

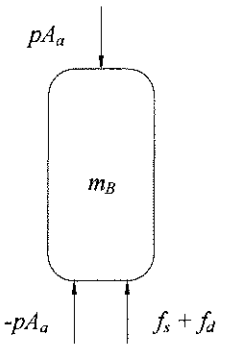

Figure B.7: Forces acting on the slug when in contact with the bottom stop

The forces acting on the slug are:

$$-2pA_a + f_s + f_d = m_B \ddot{x}_B$$

$$p = \frac{k_s}{2A_a}\Delta_d + \frac{c_s}{2A_a}\Delta_v - \frac{m_B}{2A_a}\left[\left(1 - \frac{A_b}{A_a} \right) \ddot{x} + \frac{A_b}{A_a} \ddot{y} \right]$$

where:

$$\Delta_d = \beta \left\{ y - x + \frac{A_b}{A_a}(x - y) - \text{sign}\left[y - x + \frac{A_b}{A_a}(x - y) \right] h \right\} \tag{B.67}$$

$$\Delta_v = \beta \left[\dot{y} - \dot{x} + \frac{A_b}{A_a}(\dot{x} - \dot{y}) \right]$$

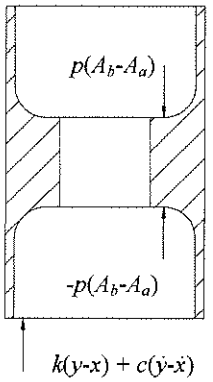

Figure B.8: Forces acting on the port

The forces acting on the port can be found by substituting the expression found for the pressure in Equation (B.67):

$$-2p\left(A_b - A_a\right) + k\left(y - x\right) + c\left(\dot{y} - \dot{x}\right) = m\ddot{x}$$

$$-\left\{\frac{k_s}{A_a}\Delta_d + \frac{c_s}{A_a}\Delta_v - \frac{m_B}{A_a}\left[\left(1 - \frac{A_b}{A_a}\right)\ddot{x} + \frac{A_b}{A_a}\ddot{y}\right]\right\}\left(A_b - A_a\right) + k\left(y - x\right) + c\left(\dot{y} - \dot{x}\right) = m\ddot{x}$$

$$k\left(y - x\right) + c\left(\dot{y} - \dot{x}\right) - k_s\Delta_d\left(\frac{A_b}{A_a} - 1\right) - c_s\Delta_v\left(\frac{A_b}{A_a} - 1\right) - m_B\left[\left(\frac{A_b}{A_a} - 1\right)^2\ddot{x} - \frac{A_b}{A_a}\left(\frac{A_b}{A_a} - 1\right)\ddot{y}\right] = m\ddot{x} \tag{B.68}$$

$$\left[m + m_B\left(\frac{A_b}{A_a} - 1\right)^2\right]\ddot{x} = m_B\left(\frac{A_b}{A_a} - 1\right)\frac{A_b}{A_a}\ddot{y} + k\left(y - x\right) + c\left(\dot{y} - \dot{x}\right) - k_s\Delta_d\left(\frac{A_b}{A_a} - 1\right) - c_s\Delta_v\left(\frac{A_b}{A_a} - 1\right)$$

The above equation can be written in terms of non-dimensional parameters:

$$\ddot{x} = \left(\frac{\omega_n}{\omega_i}\right)^2\ddot{y} - 2\zeta\omega_n\left(\dot{x} - \dot{y}\right) - \omega_n^2\left(x - y\right) - \omega_n^2\frac{k_s}{k}\Delta_d\left(\frac{A_b}{A_a} - 1\right) - 2\zeta_s\omega_n\Delta_v\left(\frac{A_b}{A_a} - 1\right)$$

$$\text{where: } \omega_n = \sqrt{\frac{k}{m + m_B\left(\frac{A_b}{A_a} - 1\right)^2}}, \quad \omega_i = \sqrt{\frac{k}{m_B\left(\frac{A_b}{A_a} - 1\right)\frac{A_b}{A_a}}}, \quad \zeta_s = \frac{c_s}{2\left[m + m_B\left(\frac{A_b}{A_a} - 1\right)^2\right]\omega_n} \tag{B.69}$$

B.2.3 Leakage

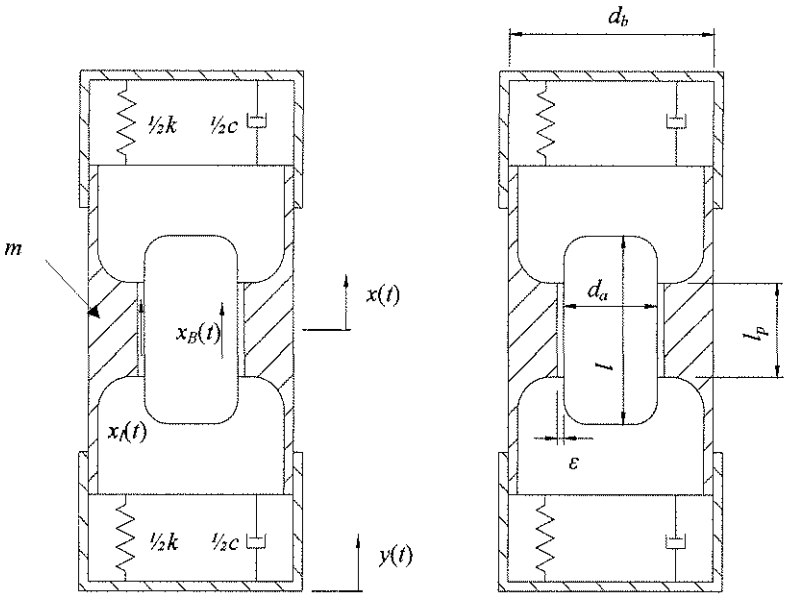

Figure B.9: Mechanical model of a type II AVAI with leakage

The effect of leakage will be studied with this model. It is assumed that the slug is connected to the port through discrete dashpots as shown in Figure B.9. The exact properties of these dashpots can be determined by finding the velocity-dependent shear force acting on the port and the slug. The shear force is a function of the viscosity and the slope of the radial velocity profile in the annulus. The dashpot properties will, however, not be calculated and this model will only be used to make a qualitative assessment of the effect of modelling leakage.

If it is assumed that the gap between the port and the slug is small the leakage area is:

$$A_\varepsilon = \varepsilon \pi d_a \tag{B.70}$$

The continuity equation is:

$$\begin{aligned} yA_b &= x_B A_a + \varepsilon \pi d_a x_l + \left(A_b - A_a - \varepsilon \pi d_a\right) x \\ x_B &= \frac{A_b}{A_a} y + \left(1 + \frac{\varepsilon \pi d_a - A_b}{A_a}\right) x - \frac{\varepsilon \pi d_a}{A_a} x_l \end{aligned} \tag{B.71}$$

If the gap is zero then the above equation reduces to that found in Equation (B.39).

The kinetic energy is:

$$\begin{aligned}T &= \frac{1}{2}\left(m\dot{x}^2 + m_B\dot{x}_B^2 + m_l\dot{x}_l^2\right)\\ &= \frac{1}{2}\left\{m\dot{x}^2 + m_B\left[\frac{A_b}{A_a}\dot{y} - \left(\frac{A_b - \varepsilon\pi d_a}{A_a} - 1\right)\dot{x} - \frac{\varepsilon\pi d_a}{A_a}\dot{x}_l\right]^2 + m_l\dot{x}_l^2\right\}\\ &= \frac{1}{2}\left\{m\dot{x}^2 + m_B\left[\left(\frac{A_b}{A_a}\right)^2\dot{y}^2 + \left(\frac{A_b - \varepsilon\pi d_a}{A_a} - 1\right)^2\dot{x}^2 + \left(\frac{\varepsilon\pi d_a}{A_a}\right)^2\dot{x}_l^2 - 2\frac{A_b}{A_a}\left(\frac{A_b - \varepsilon\pi d_a}{A_a} - 1\right)\dot{x}\dot{y}\right.\right.\\ &\qquad \left.\left. - 2\frac{A_b}{A_a}\frac{\varepsilon\pi d_a}{A_a}\dot{x}_l\dot{y} + 2\left(\frac{A_b - \varepsilon\pi d_a}{A_a} - 1\right)\frac{\varepsilon\pi d_a}{A_a}\dot{x}_l\dot{x}\right] + m_l\dot{x}_l^2\right\}\end{aligned} \tag{B.72}$$

where: $m_B = \rho A_a l, \quad m_l = \rho_f \varepsilon\pi d_a l_p$

The derivatives are:

$$\begin{aligned}\frac{d}{dt}\left(\frac{\partial T}{\partial \dot{x}}\right) &= \left[m + m_B\left(1 + \frac{\varepsilon\pi d_a - A_b}{A_a}\right)^2\right]\ddot{x} + m_B\left(\frac{A_b - \varepsilon\pi d_a}{A_a} - 1\right)\frac{\varepsilon\pi d_a}{A_a}\ddot{x}_l - m_B\frac{A_b}{A_a}\left(\frac{A_b - \varepsilon\pi d_a}{A_a} - 1\right)\ddot{y}\\ \frac{d}{dt}\left(\frac{\partial T}{\partial \dot{x}_l}\right) &= m_B\left(\frac{A_b - \varepsilon\pi d_a}{A_a} - 1\right)\frac{\varepsilon\pi d_a}{A_a}\ddot{x} + \left[m_l + m_B\left(\frac{\varepsilon\pi d_a}{A_a}\right)^2\right]\ddot{x}_l - m_B\frac{A_b}{A_a}\frac{\varepsilon\pi d_a}{A_a}\ddot{y}\\ \frac{d}{dt}\left(\frac{\partial T}{\partial \dot{y}}\right) &= -m_B\frac{A_b}{A_a}\left(\frac{A_b - \varepsilon\pi d_a}{A_a} - 1\right)\ddot{x} - m_B\frac{A_b}{A_a}\frac{\varepsilon\pi d_a}{A_a}\ddot{x}_l + m_B\left(\frac{A_b}{A_a}\right)^2\ddot{y}\end{aligned} \tag{B.73}$$

The potential energy is:

$$\begin{aligned}V &= \frac{1}{2}k\left(x - y\right)^2\\ &= \frac{1}{2}k\left(x^2 - 2xy + y^2\right)\end{aligned} \tag{B.74}$$

The derivatives are:

$$\begin{aligned}\frac{\partial V}{\partial x} &= kx - ky\\ \frac{\partial V}{\partial x_l} &= 0\\ \frac{\partial V}{\partial y} &= -kx + ky\end{aligned} \tag{B.75}$$

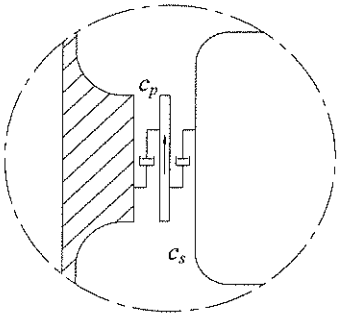

Figure B.10: Fluid damping

The Rayleigh term is:

$$
\begin{aligned}
R &= \frac{1}{2}\left[c\left(\dot{x}-\dot{y}\right)^2 + c_p\left(\dot{x}_l-\dot{x}\right)^2 + c_s\left(\dot{x}_B-\dot{x}_l\right)^2\right] \\
&= \frac{1}{2}\left\{c\left(\dot{x}-\dot{y}\right)^2 + c_p\left(\dot{x}_l-\dot{x}\right)^2 + c_s\left[\frac{A_b}{A_a}\dot{y}-\left(\frac{A_b-\varepsilon\pi d_a}{A_a}-1\right)\dot{x}-\left(\frac{\varepsilon\pi d_a}{A_a}+1\right)\dot{x}_l\right]^2\right\} \\
&= \frac{1}{2}\left\{c\left(\dot{x}^2-\dot{x}\dot{y}+\dot{y}^2\right) + c_p\left(\dot{x}_l^2-\dot{x}_l\dot{x}+\dot{x}^2\right) + c_s\left[\left(\frac{A_b}{A_a}\right)^2\dot{y}^2+\left(\frac{A_b-\varepsilon\pi d_a}{A_a}-1\right)^2\dot{x}^2+\left(\frac{\varepsilon\pi d_a}{A_a}+1\right)^2\dot{x}_l^2-2\frac{A_b}{A_a}\left(\frac{A_b-\varepsilon\pi d_a}{A_a}-1\right)\dot{x}\dot{y}-2\frac{A_b}{A_a}\left(\frac{\varepsilon\pi d_a}{A_a}+1\right)\dot{x}_l\dot{y}+2\left(\frac{A_b-\varepsilon\pi d_a}{A_a}-1\right)\left(\frac{\varepsilon\pi d_a}{A_a}+1\right)\dot{x}_l\dot{x}\right]\right\}
\end{aligned}
\tag{B.76}
$$

From the above equation the derivatives can be found:

$$
\begin{aligned}
\frac{\partial R}{\partial \dot{x}} &= \left[c+c_p+c_s\left(\frac{A_b-\varepsilon\pi d_a}{A_a}-1\right)^2\right]\dot{x}+\left[c_s\left(\frac{A_b-\varepsilon\pi d_a}{A_a}-1\right)\left(\frac{\varepsilon\pi d_a}{A_a}+1\right)-c_p\right]\dot{x}_l-\left[c+c_s\frac{A_b}{A_a}\left(\frac{A_b-\varepsilon\pi d_a}{A_a}-1\right)\right]\dot{y} \\
\frac{\partial R}{\partial \dot{x}_l} &= \left[c_s\left(\frac{A_b-\varepsilon\pi d_a}{A_a}-1\right)\left(\frac{\varepsilon\pi d_a}{A_a}+1\right)-c_p\right]\dot{x}+\left[c_s\left(\frac{\varepsilon\pi d_a}{A_a}+1\right)^2+c_p\right]\dot{x}_l-c_s\frac{A_b}{A_a}\left(\frac{\varepsilon\pi d_a}{A_a}+1\right)\dot{y} \\
\frac{\partial R}{\partial \dot{y}} &= \left[c+c_s\frac{A_b}{A_a}\left(\frac{A_b-\varepsilon\pi d_a}{A_a}-1\right)\right]\dot{x}-c_s\frac{A_b}{A_a}\left(\frac{\varepsilon\pi d_a}{A_a}+1\right)\dot{x}_l+\left[c+c_s\left(\frac{A_b}{A_a}\right)^2\right]\dot{y}
\end{aligned}
\tag{B.77}
$$

The complete equation of motion can now be found by substituting the derivates found above in Lagrange's equations:

$$
\begin{aligned}
&\left[m+m_B\left(1+\frac{\varepsilon\pi d_a-A_b}{A_a}\right)^2\right]\ddot{x}+\left[c+c_p+c_s\left(\frac{A_b-\varepsilon\pi d_a}{A_a}-1\right)^2\right]\dot{x}+m_B\left(\frac{A_b-\varepsilon\pi d_a}{A_a}-1\right)\frac{\varepsilon\pi d_a}{A_a}\ddot{x}_l+\left[c_s\left(\frac{A_b-\varepsilon\pi d_a}{A_a}-1\right)\left(\frac{\varepsilon\pi d_a}{A_a}+1\right)-c_p\right]\dot{x}_l+kx \\
&\qquad = m_B\frac{A_b}{A_a}\left(\frac{A_b-\varepsilon\pi d_a}{A_a}-1\right)\ddot{y}+\left[c+c_s\frac{A_b}{A_a}\left(\frac{A_b-\varepsilon\pi d_a}{A_a}-1\right)\right]\dot{y}+ky \\
&m_B\left(\frac{A_b-\varepsilon\pi d_a}{A_a}-1\right)\frac{\varepsilon\pi d_a}{A_a}\ddot{x}+\left[c_s\left(\frac{A_b-\varepsilon\pi d_a}{A_a}-1\right)\left(\frac{\varepsilon\pi d_a}{A_a}+1\right)-c_p\right]\dot{x}+\left[m_l+m_B\left(\frac{\varepsilon\pi d_a}{A_a}\right)^2\right]\ddot{x}_l+\left[c_s\left(\frac{\varepsilon\pi d_a}{A_a}+1\right)^2+c_p\right]\dot{x}_l \\
&\qquad = m_B\frac{A_b}{A_a}\frac{\varepsilon\pi d_a}{A_a}\ddot{y}+c_s\frac{A_b}{A_a}\left(\frac{\varepsilon\pi d_a}{A_a}+1\right)\dot{y}
\end{aligned}
\tag{B.78}
$$

By transforming to the frequency domain:

$$\left\{k+i\omega\left[c+c_p+c_s\left(\frac{A_b-\varepsilon\pi d_a}{A_a}-1\right)^2\right]-\omega^2\left[m+m_B\left(1+\frac{\varepsilon\pi d_a-A_b}{A_a}\right)^2\right]\right\}X+\left\{i\omega\left[c_s\left(\frac{A_b-\varepsilon\pi d_a}{A_a}-1\right)\left(\frac{\varepsilon\pi d_a}{A_a}+1\right)-c_p\right]-\omega^2 m_B\left(\frac{A_b-\varepsilon\pi d_a}{A_a}-1\right)\frac{\varepsilon\pi d_a}{A_a}\right\}X_l$$
$$=\left\{k+i\omega\left[c+c_s\frac{A_b}{A_a}\left(\frac{A_b-\varepsilon\pi d_a}{A_a}-1\right)\right]-\omega^2 m_B\frac{A_b}{A_a}\left(\frac{A_b-\varepsilon\pi d_a}{A_a}-1\right)\right\}Y$$
$$\left\{i\omega\left[c_s\left(\frac{A_b-\varepsilon\pi d_a}{A_a}-1\right)\left(\frac{\varepsilon\pi d_a}{A_a}+1\right)-c_p\right]-\omega^2 m_B\left(\frac{A_b-\varepsilon\pi d_a}{A_a}-1\right)\frac{\varepsilon\pi d_a}{A_a}\right\}X+\left\{i\omega\left[c_s\left(\frac{\varepsilon\pi d_a}{A_a}+1\right)^2+c_p\right]-\omega^2\left[m_l+m_B\left(\frac{\varepsilon\pi d_a}{A_a}\right)^2\right]\right\}X_l$$
$$=\left\{i\omega c_s\frac{A_b}{A_a}\left(\frac{\varepsilon\pi d_a}{A_a}+1\right)-\omega^2 m_B\frac{A_b}{A_a}\frac{\varepsilon\pi d_a}{A_a}\right\}Y \tag{B.79}$$

The second of Equation (B.79) can be used to find X_l:

$$X_l=\frac{\left\{i\omega c_s\frac{A_b}{A_a}\left(\frac{\varepsilon\pi d_a}{A_a}+1\right)-\omega^2 m_B\frac{A_b}{A_a}\frac{\varepsilon\pi d_a}{A_a}\right\}Y-\left\{i\omega\left[c_s\left(\frac{A_b-\varepsilon\pi d_a}{A_a}-1\right)\left(\frac{\varepsilon\pi d_a}{A_a}+1\right)-c_p\right]-\omega^2 m_B\left(\frac{A_b-\varepsilon\pi d_a}{A_a}-1\right)\frac{\varepsilon\pi d_a}{A_a}\right\}X}{i\omega\left[c_s\left(\frac{\varepsilon\pi d_a}{A_a}+1\right)^2+c_p\right]-\omega^2\left[m_l+m_B\left(\frac{\varepsilon\pi d_a}{A_a}\right)^2\right]} \tag{B.80}$$

Back substitution into the first of Equation (B.79) yields:

$$\left\{k+i\omega\left[c+c_p+c_s\left(\frac{A_b-\varepsilon\pi d_a}{A_a}-1\right)^2\right]-\omega^2\left[m+m_B\left(1+\frac{\varepsilon\pi d_a-A_b}{A_a}\right)^2\right]\right\}\left\{i\omega\left[c_s\left(\frac{\varepsilon\pi d_a}{A_a}+1\right)^2+c_p\right]-\omega^2\left[m_l+m_B\left(\frac{\varepsilon\pi d_a}{A_a}\right)^2\right]\right\}X$$
$$-\left\{i\omega\left[c_s\left(\frac{A_b-\varepsilon\pi d_a}{A_a}-1\right)\left(\frac{\varepsilon\pi d_a}{A_a}+1\right)-c_p\right]-\omega^2 m_B\left(\frac{A_b-\varepsilon\pi d_a}{A_a}-1\right)\frac{\varepsilon\pi d_a}{A_a}\right\}\left\{i\omega\left[c_s\left(\frac{A_b-\varepsilon\pi d_a}{A_a}-1\right)\left(\frac{\varepsilon\pi d_a}{A_a}+1\right)-c_p\right]-\omega^2 m_B\left(\frac{A_b-\varepsilon\pi d_a}{A_a}-1\right)\frac{\varepsilon\pi d_a}{A_a}\right\}X$$
$$=\left\{i\omega\left[c_s\left(\frac{\varepsilon\pi d_a}{A_a}+1\right)^2+c_p\right]-\omega^2\left[m_l+m_B\left(\frac{\varepsilon\pi d_a}{A_a}\right)^2\right]\right\}\left\{k+i\omega\left[c+c_s\frac{A_b}{A_a}\left(\frac{A_b-\varepsilon\pi d_a}{A_a}-1\right)\right]-\omega^2 m_B\frac{A_b}{A_a}\left(\frac{A_b-\varepsilon\pi d_a}{A_a}-1\right)\right\}Y$$
$$-\left\{i\omega\left[c_s\left(\frac{A_b-\varepsilon\pi d_a}{A_a}-1\right)\left(\frac{\varepsilon\pi d_a}{A_a}+1\right)-c_p\right]-\omega^2 m_B\left(\frac{A_b-\varepsilon\pi d_a}{A_a}-1\right)\frac{\varepsilon\pi d_a}{A_a}\right\}\left\{i\omega c_s\frac{A_b}{A_a}\left(\frac{\varepsilon\pi d_a}{A_a}+1\right)-\omega^2 m_B\frac{A_b}{A_a}\frac{\varepsilon\pi d_a}{A_a}\right\}Y \tag{B.81}$$

The following natural frequencies and damping ratios are now defined:

$$\omega_l = \sqrt{\frac{k}{m_l + m_B\left(4\frac{\varepsilon}{d_a}\right)^2}},\quad \omega_l = \sqrt{\frac{k}{m_B\frac{A_b}{A_a}\left(\frac{A_b}{A_a} - 4\frac{\varepsilon}{d_a} - 1\right)}},\quad \omega_\varepsilon = \sqrt{\frac{k}{m_B\left(\frac{A_b}{A_a} - 4\frac{\varepsilon}{d_a} - 1\right)4\frac{\varepsilon}{d_a}}},$$

$$\omega_\varepsilon' = \sqrt{\frac{k}{m_B\frac{A_b}{A_a}4\frac{\varepsilon}{d_a}}},\quad \omega_n = \sqrt{\frac{k}{m + m_B\left(\frac{A_b}{A_a} - 4\frac{\varepsilon}{d_a} - 1\right)^2}},\quad \zeta_s = \frac{c_s}{2\left[m + m_B\left(\frac{A_b}{A_a} - 4\frac{\varepsilon}{d_a} - 1\right)^2\right]\omega_n},\qquad \text{(B.82)}$$

$$\zeta_p = \frac{c_p}{2\left[m + m_B\left(\frac{A_b}{A_a} - 4\frac{\varepsilon}{d_a} - 1\right)^2\right]\omega_n}$$

The transmissibility can be found by using the above non-dimensional relationships:

$$\frac{X}{Y} = \frac{AB - CD}{EF - G^2}$$

$$\frac{A}{k} = i2\frac{\omega}{\omega_n}\left[\zeta_s\left(4\frac{\varepsilon}{d_a} + 1\right)^2 + \zeta_p\right] - \left(\frac{\omega_n}{\omega_l}\right)^2\left(\frac{\omega}{\omega_n}\right)^2$$

$$\frac{B}{k} = 1 + i2\frac{\omega}{\omega_n}\left[\zeta + \zeta_s\frac{A_b}{A_a}\left(\frac{A_b}{A_a} - 4\frac{\varepsilon}{d_a} - 1\right)\right] - \left(\frac{\omega_n}{\omega_l'}\right)^2\left(\frac{\omega}{\omega_n}\right)^2$$

$$\frac{C}{k} = i2\frac{\omega}{\omega_n}\left[\zeta_s\left(\frac{A_b}{A_a} - 4\frac{\varepsilon}{d_a} - 1\right)\left(4\frac{\varepsilon}{d_a} + 1\right) - \zeta_p\right] - \left(\frac{\omega_n}{\omega_\varepsilon}\right)^2\left(\frac{\omega}{\omega_n}\right)^2$$

$$\frac{D}{k} = i2\frac{\omega}{\omega_n}\zeta_s\frac{A_b}{A_a}\left(4\frac{\varepsilon}{d_a} + 1\right) - \left(\frac{\omega_n}{\omega_\varepsilon'}\right)^2\left(\frac{\omega}{\omega_n}\right)^2$$

$$\frac{E}{k} = 1 + i2\frac{\omega}{\omega_n}\left[\zeta + \zeta_p + \zeta_s\left(\frac{A_b}{A_a} - 4\frac{\varepsilon}{d_a} - 1\right)^2\right] - \left(\frac{\omega}{\omega_n}\right)^2$$

$$\frac{F}{k} = i2\frac{\omega}{\omega_n}\left[\zeta_s\left(4\frac{\varepsilon}{d_a} + 1\right)^2 + \zeta_p\right] - \left(\frac{\omega_n}{\omega_l}\right)^2\left(\frac{\omega}{\omega_n}\right)^2$$

$$\frac{G}{k} = i2\frac{\omega}{\omega_n}\left[\zeta_s\left(\frac{A_b}{A_a} - 4\frac{\varepsilon}{d_a} - 1\right)\left(4\frac{\varepsilon}{d_a} + 1\right) - \zeta_p\right] - \left(\frac{\omega_n}{\omega_\varepsilon}\right)^2\left(\frac{\omega}{\omega_n}\right)^2$$

$$\frac{\omega_n}{\omega_l} = \frac{\frac{m_l}{m_B} + \left(4\frac{\varepsilon}{d_a}\right)^2}{\frac{m}{m_B} + \left(\frac{A_b}{A_a} - 4\frac{\varepsilon}{d_a} - 1\right)^2},\quad \frac{\omega_n}{\omega_l'} = \frac{\frac{A_b}{A_a}\left(\frac{A_b}{A_a} - 4\frac{\varepsilon}{d_a} - 1\right)}{\frac{m}{m_B} + \left(\frac{A_b}{A_a} - 4\frac{\varepsilon}{d_a} - 1\right)^2},\qquad \text{(B.83)}$$

$$\frac{\omega_n}{\omega_\varepsilon} = \frac{4\frac{\varepsilon}{d_a}\left(\frac{A_b}{A_a} - 4\frac{\varepsilon}{d_a} - 1\right)}{\frac{m}{m_B} + \left(\frac{A_b}{A_a} - 4\frac{\varepsilon}{d_a} - 1\right)^2},\quad \frac{\omega_n}{\omega_\varepsilon'} = \frac{4\frac{\varepsilon}{d_a}\frac{A_b}{A_a}}{\frac{m}{m_B} + \left(\frac{A_b}{A_a} - 4\frac{\varepsilon}{d_a} - 1\right)^2}$$

B.2.4 Slug with diaphragm seal

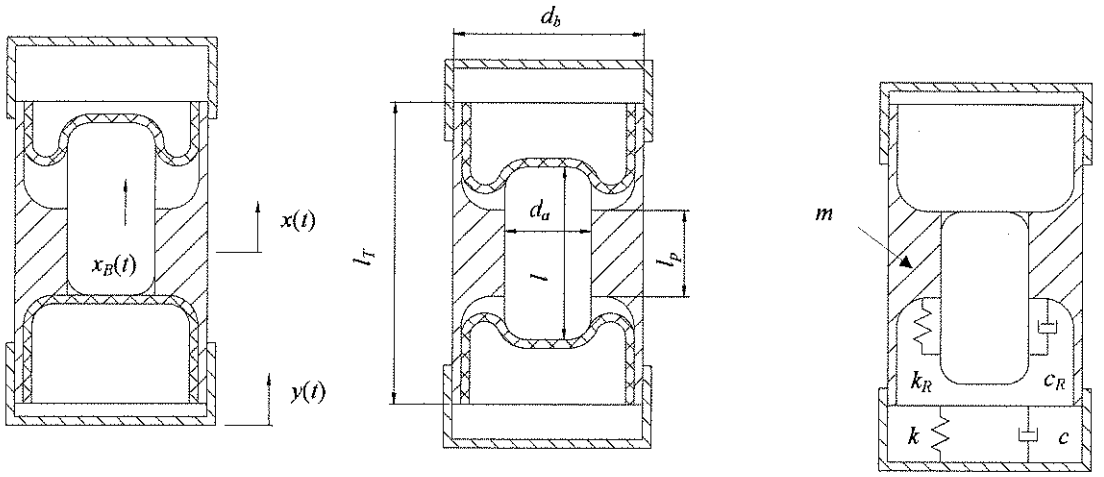

Figure B.11 Mechanical model of a type II AVAI with a rolling diaphragm seal

To derive the continuity equation it must be recognised that the diaphragm cannot stretch and that the relative motion between the slug and the port is:

$$x_R = \frac{1}{2}(x_B + x) \tag{B.84}$$

Considering continuity gives:

$$\begin{aligned} yA_b &= x_B A_a + \frac{1}{2}(x_B + x)(A_b - A_a) \\ x_B &= -\left(\frac{A_b - A_a}{A_b + A_a}\right)x + \frac{2A_b}{A_b + A_a}y \end{aligned} \tag{B.85}$$

The total kinetic energy is:

$$\begin{aligned} T &= \frac{1}{2}\left(m\dot{x}^2 + m_B\dot{x}_B^2\right) \\ T &= \frac{1}{2}\left\{\left[m + m_B\left(\frac{A_b - A_a}{A_b + A_a}\right)^2\right]\dot{x}^2 - m_B\frac{4A_b(A_b - A_a)}{(A_b + A_a)^2}\dot{x}\dot{y} + 4m_B\left(\frac{A_b}{A_b + A_a}\right)^2\dot{y}^2\right\} \end{aligned} \tag{B.86}$$

From the above equation the derivatives can be found:

$$\begin{aligned} \frac{d}{dt}\left(\frac{\partial T}{\partial \dot{x}}\right) &= \left[m + m_B\left(\frac{A_b - A_a}{A_b + A_a}\right)^2\right]\ddot{x} + m_B\frac{4A_b(A_a - A_b)}{(A_b + A_a)^2}\ddot{y} \\ \frac{d}{dt}\left(\frac{\partial T}{\partial \dot{y}}\right) &= m_B\frac{4A_b(A_a - A_b)}{(A_b + A_a)^2}\ddot{x} + 4\left(\frac{A_b}{A_b + A_a}\right)^2\ddot{y} \end{aligned} \tag{B.87}$$

The potential energy is (k_R represents the total stiffness of both diaphragms):

$$\begin{aligned} V &= \frac{1}{2}\left[k\left(x-y\right)^2 + k_R\left(x_B - x\right)^2\right] \\ &= \frac{1}{2}\left[k\left(x-y\right)^2 + k_R\left(\frac{2A_b}{A_b+A_a}y - \left(\frac{A_b-A_a}{A_b+A_a}+1\right)x\right)^2\right] \end{aligned} \tag{B.88}$$

From the above equation the derivatives can be found:

$$\begin{aligned} \frac{\partial V}{\partial x} &= \left[k + k_R\left(\frac{A_b-A_a}{A_b+A_a}\right)^2 - 2k_R\frac{A_b-A_a}{A_b+A_a} + k_R\right]x - \left[k + k_R\frac{2A_b\left(A_b-A_a\right)}{\left(A_b+A_a\right)^2} + k_R\frac{2A_b}{A_b+A_a}\right]y \\ \frac{\partial V}{\partial y} &= -\left[k + k_R\frac{2A_b\left(A_b-A_a\right)}{\left(A_b+A_a\right)^2} + k_R\frac{2A_b}{A_b+A_a}\right]x + \left[k + k_R\left(\frac{2A_b}{A_b+A_a}\right)^2\right]y \end{aligned} \tag{B.89}$$

The Rayleigh term is:

$$\begin{aligned} R &= \frac{1}{2}\left[c\left(\dot{x}-\dot{y}\right)^2 + c_R\left(\dot{x}_B - \dot{x}\right)^2\right] \\ &= \frac{1}{2}\left[c\left(\dot{x}-\dot{y}\right)^2 + c_R\left(\frac{2A_b}{A_b+A_a}\dot{y} - \left(\frac{A_b-A_a}{A_b+A_a}+1\right)\dot{x}\right)^2\right] \end{aligned} \tag{B.90}$$

From the above equation the derivatives can be found:

$$\begin{aligned} \frac{\partial R}{\partial \dot{x}} &= \left[c + c_R\left(\frac{A_b-A_a}{A_b+A_a}\right)^2 - 2c_R\frac{A_b-A_a}{A_b+A_a} + c_R\right]\dot{x} - \left[c + c_R\frac{2A_b\left(A_b-A_a\right)}{\left(A_b+A_a\right)^2} + c_R\frac{2A_b}{A_b+A_a}\right]\dot{y} \\ \frac{\partial R}{\partial \dot{y}} &= -\left[c + c_R\frac{2A_b\left(A_b-A_a\right)}{\left(A_b+A_a\right)^2} + c_R\frac{2A_b}{A_b+A_a}\right]\dot{x} + \left[c + c_R\left(\frac{2A_b}{A_b+A_a}\right)^2\right]\dot{y} \end{aligned} \tag{B.91}$$

The complete equation of motion can now be found by substituting the derivates found above in Lagrange's equations:

$$\begin{aligned} &\left[m + m_B\left(\frac{A_b-A_a}{A_b+A_a}\right)^2\right]\ddot{x} + \left[c + c_R\left(\frac{A_b-A_a}{A_b+A_a}\right)^2 - 2c_R\frac{A_b-A_a}{A_b+A_a} + c_R\right]\dot{x} + \left[k + k_R\left(\frac{A_b-A_a}{A_b+A_a}\right)^2 - 2k_R\frac{A_b-A_a}{A_b+A_a} + k_R\right]x \\ &= -m_B\frac{4A_b\left(A_a-A_b\right)}{\left(A_b+A_a\right)^2}\ddot{y} + \left[c + c_R\frac{2A_b\left(A_b-A_a\right)}{\left(A_b+A_a\right)^2} + c_R\frac{2A_b}{A_b+A_a}\right]\dot{y} + \left[k + k_R\frac{2A_b\left(A_b-A_a\right)}{\left(A_b+A_a\right)^2} + k_R\frac{2A_b}{A_b+A_a}\right]y \end{aligned} \tag{B.92}$$

The transmissibility can now be calculated by transforming the above equation to the frequency domain:

$$\frac{X}{Y} = \frac{k + k_R\frac{2A_b\left(A_b-A_a\right)}{\left(A_b+A_a\right)^2} + k_R\frac{2A_b}{A_b+A_a} + i\omega\left[c + c_R\frac{2A_b\left(A_b-A_a\right)}{\left(A_b+A_a\right)^2} + c_R\frac{2A_b}{A_b+A_a}\right] + \omega^2 m_B\frac{4A_b\left(A_a-A_b\right)}{\left(A_b+A_a\right)^2}}{k + k_R\left(\frac{A_b-A_a}{A_b+A_a}\right)^2 - 2k_R\frac{A_b-A_a}{A_b+A_a} + k_R + i\omega\left[c + c_R\left(\frac{A_b-A_a}{A_b+A_a}\right)^2 - 2c_R\frac{A_b-A_a}{A_b+A_a} + c_R\right] + \omega^2\left[m + m_B\left(\frac{A_b-A_a}{A_b+A_a}\right)^2\right]} \tag{B.93}$$

The isolation frequency is:

$$\omega_i = \sqrt{\frac{k + k_R \dfrac{2A_b\left(A_b - A_a\right)}{\left(A_b + A_a\right)^2} + k_R \dfrac{2A_b}{A_b + A_a}}{m_B \dfrac{4A_b\left(A_a - A_b\right)}{\left(A_b + A_a\right)^2}}} \tag{B.94}$$

The effective mass term can be rewritten as follows:

$$m_B \frac{4A_b\left(A_a - A_b\right)}{\left(A_b + A_a\right)^2}\ddot{x} = m_B \frac{4A_a^2}{\left(A_b + A_a\right)^2}\frac{A_b\left(A_b - A_a\right)}{A_a^2} = \frac{4}{\left(\dfrac{A_b}{A_a} + 1\right)^2} m_B \left(1 - \frac{A_b}{A_a}\right)\frac{A_b}{A_a} \tag{B.95}$$

By comparing the effective absorber mass term in Equation (B.94) with the isolation frequency of a system without a rolling diaphragm an effective mass ratio can be found:

$$M_{ratio} = \frac{4}{\left(\dfrac{A_b}{A_a} + 1\right)^2} \tag{B.96}$$

APPENDIX C

Derivations for chapter 3

C.1 Type I AVAI (equation of motion)

The equation of motion from Appendix B can be non-dimensionalised and written in terms of the stiffness ratio as follows for the first equation:

$$m_y\ddot{y}+(c+c_u)\dot{y}-c_u\dot{u}+(k+k_u)y-k_u u=c\dot{x}+kx$$

$$\frac{m_y}{k}\ddot{y}+\left(\frac{c}{k}+\mu_k\frac{c_u}{k_u}\right)\dot{y}-\mu_k\frac{c_u}{k_u}\dot{u}+(1+\mu_k)y-\mu_k u=\frac{c}{k}\dot{x}+x$$

$$\frac{1}{\omega_1^2}\ddot{y}+2\left(\frac{\zeta_1}{\omega_1}+\mu_k\frac{\zeta_2}{\omega_2}\right)\dot{y}-2\mu_k\frac{\zeta_2}{\omega_2}\dot{u}+(1+\mu_k)y-\mu_k u=2\frac{\zeta_1}{\omega_1}\dot{x}+x$$

$$\ddot{y}+2\left(\zeta_1+\mu_k\frac{\omega_1}{\omega_2}\zeta_2\right)\omega_1\dot{y}-2\mu_k\frac{\omega_1}{\omega_2}\zeta_2\omega_1\dot{u}+\omega_1^2(1+\mu_k)y-\omega_1^2\mu_k u-2\zeta_1\omega_1\dot{x}-\omega_1^2 x=0 \qquad \text{(C.1)}$$

$$\ddot{y}+2\left(\zeta_1+\frac{\omega_1}{\bar{\omega}_2}\bar{\zeta}_2\right)\omega_1\dot{y}-2\frac{\omega_1}{\bar{\omega}_2}\bar{\zeta}_2\omega_1\dot{u}+\omega_1^2(1+\mu_k)y-\omega_1^2\mu_k u-2\zeta_1\omega_1\dot{x}-\omega_1^2 x=0$$

where: $\dfrac{\zeta_2}{\omega_2}=\dfrac{\frac{1}{\sqrt{\mu_k}}\bar{\zeta}_2}{\sqrt{\mu_k}\bar{\omega}_2}=\dfrac{1}{\sqrt{\mu_k}}\bar{\zeta}_2\dfrac{1}{\sqrt{\mu_k}\bar{\omega}_2}=\dfrac{1}{\mu_k}\dfrac{\bar{\zeta}_2}{\bar{\omega}_2}$

And as follows for the second equation:

$$m_B\left(\frac{A_b}{A_a}\right)^2\ddot{u}+c_u(\dot{u}-\dot{y})+k_u(u-y)-m_B\left(\frac{A_b}{A_a}-1\right)\frac{A_b}{A_a}\ddot{x}=0$$

$$\frac{m_B\left(\frac{A_b}{A_a}\right)^2}{k_u}\ddot{u}+\frac{c_u}{k_u}(\dot{u}-\dot{y})+u-y-\frac{m_B\left(\frac{A_b}{A_a}-1\right)\frac{A_b}{A_a}}{k_u}\ddot{x}=0$$

$$\frac{1}{\omega_2^2}\ddot{u}+2\frac{\zeta_2}{\omega_2}(\dot{u}-\dot{y})+u-y-\frac{1}{\mu_k}\frac{1}{\bar{\omega}_i^2}\ddot{x}=0 \qquad \text{(C.2)}$$

$$\ddot{u}+2\zeta_2\omega_2(\dot{u}-\dot{y})+\omega_2^2(u-y)-\frac{1}{\mu_k}\left(\frac{\omega_2}{\bar{\omega}_i}\right)^2\ddot{x}=0$$

$$\ddot{u}+2\bar{\zeta}_2\bar{\omega}_2(\dot{u}-\dot{y})+\mu_k\bar{\omega}_2^2(u-y)-\left(\frac{\bar{\omega}_2}{\bar{\omega}_i}\right)^2\ddot{x}=0$$

where: $\zeta_2\omega_2=\dfrac{1}{\sqrt{\mu_k}}\bar{\zeta}_2\sqrt{\mu_k}\bar{\omega}_2=\bar{\zeta}_2\bar{\omega}_2$

C.2 Type I AVAI (quadrature objective function)

The quadrature objective function can be evaluated by finding the point product of the input and output signals. This must be done over a predetermined time period T. Assuming that the input and output are given by two harmonic functions:

$$\begin{aligned} x(t) &= X\cos(\omega t+\theta) \\ y(t) &= Y\cos(\omega t) \end{aligned} \tag{C.3}$$

where θ is the angle between the response of the system and the input.

The input can be rewritten as:

$$\begin{aligned} x(t) &= X\cos(\omega t+\theta) \\ &= X\cos(\omega t)\cos(\theta) - X\sin(\omega t)\sin(\theta) \end{aligned} \tag{C.4}$$

The point product is (Long *et al.* 1994):

$$\begin{aligned} f &= x(t)\bullet y(t) \\ &= \frac{1}{T}\int_{-T/2}^{T/2}[X\cos(\omega t)\cos(\theta) - X\sin(\omega t)\sin(\theta)]Y\cos(\omega t+\phi)\,dt \\ &= \frac{1}{T}\int_{-T/2}^{T/2} X\cos(\omega t)\cos(\theta)Y\cos(\omega t+\phi) - X\sin(\omega t)\sin(\theta)Y\cos(\omega t+\phi)\,dt \\ &= \frac{XY\cos(\theta)}{2} \\ &= 0 \qquad \text{when} \quad \theta = (2n+1)\frac{\pi}{2} \quad n = 0,1,2... \end{aligned} \tag{C.5}$$

C.3 Type II AVAI (equation of motion)

The equation of motion from Appendix B can be written in terms of the stiffness ratio to make tuning possible. The equation of motion is:

$$\ddot{y} + 2\zeta\omega_n\dot{y} + \omega_n^2 y = \left(\frac{\omega_n}{\omega_i}\right)^2\ddot{x} + 2\zeta\omega_n\dot{x} + \omega_n^2 x \tag{C.6}$$

As before, the current natural frequency and damping ratio can be written in terms of the initial value as follows:

$$\begin{aligned} \zeta &= \frac{1}{\sqrt{\mu_k}}\zeta' \\ \omega_n &= \sqrt{\mu_k}\,\omega_n' \end{aligned} \tag{C.7}$$

Substituting the above relations in the equation of motion:

$$\ddot{y} + 2\zeta'\omega_n'\dot{y} + \mu_k\omega_n' y = \left(\frac{\omega_n'}{\omega_i'}\right)^2\ddot{x} + 2\zeta'\omega_n'\dot{x} + \mu_k\omega_n' x \tag{C.8}$$

APPENDIX D

Derivations for chapter 4

D.1 Vibration measurement of a Boart Longyear S250 rock drill (calibration factors)

Table D.1: Calibration factors

	x-direction	*y*-direction	*z*-direction
Calibration factor [V/g]	0.029176	0.031604	0.031604

D.2 Type I AVAI design (air spring stiffness)

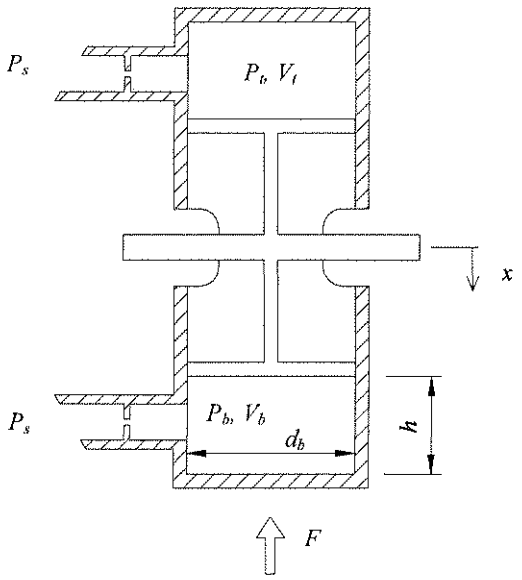

Figure D.1: Double sided air spring

The force balance acting on the piston is:

$$F = \left(P_b - P_t\right) A \tag{D.1}$$

Assuming adiabatic compression the pressure in the top and bottom chambers can be written in terms of the initial pressure (P_i) and volume (V_i):

$$P_b V_b^n = P_i V_i^n \tag{D.2}$$

where n is the ratio of specific heats (1.4 for air).

The force relationship of Equation (D.1) can now be written in terms of the initial pressure and volume values:

$$F = P_i A\left[\left(\frac{V_i}{V_b}\right)^n - \left(\frac{V_i}{V_t}\right)^n\right] = P_i A h^n\left[\left(\frac{1}{h-x}\right)^n - \left(\frac{1}{h+x}\right)^n\right] \quad \text{(D.3)}$$

where h is the initial height.

The stiffness of the spring is the derivative of the force with respect to displacement:

$$k = \frac{dF}{dx} = nP_i A h^n\left[\left(\frac{1}{h-x}\right)^{n+1} + \left(\frac{1}{h+x}\right)^{n+1}\right] \quad \text{(D.4)}$$

At small displacements this reduces to:

$$k = \frac{2nP_i A}{h} \quad \text{(D.5)}$$

D.3 Type I AVAI design (heavy liquid properties)

Table 3.2 Summary of liquid properties at 25°C

Liquid		ρ [kg/m^3]	μ [N.s/m^2]	T_m [°C]	T_b [°C]	Hazard rating*
Water	H_2O	998	1.00×10^{-3}	0	100	0
Bromine	Br_2	3113	0.91×10^{-3}	-7	59	4
Bromoform	$CHBr_3$	2894		N/A	150	3
Carbon tetrachloride	CCl_4	1590	0.97×10^{-3}	-23	76	3
Lead tetrachloride	$PbCl_4$	3174		-15	105	
LST		2954				
Mercury	Hg	13550	1.56×10^{-3}	-38	356	4
Phosphorous tribromide	PBr_3	2846		-40	173	3
Selenium bromide	Se_2Br_2	3597			227	
Selenium monochloride	Se_2Cl_2	2764		-85	130	
Tetrabromoacetylene	$Br_2CHCHBr_2$	2954		0	135	2
Thionyl bromide	$SOBr_2$	2675		-52	138	
Thiophosphorylbromidechloride	$PSBr_2Cl$	2475		-60	95	
Tindibromidedichloride	$SnBr_2Cl_2$	2814		-20	65	

* Baker SAF-T-DATA™ health rating, 0 = no hazard, 4 = extreme hazard.

D.4 Type I AVAI design (forces acting on the drill)

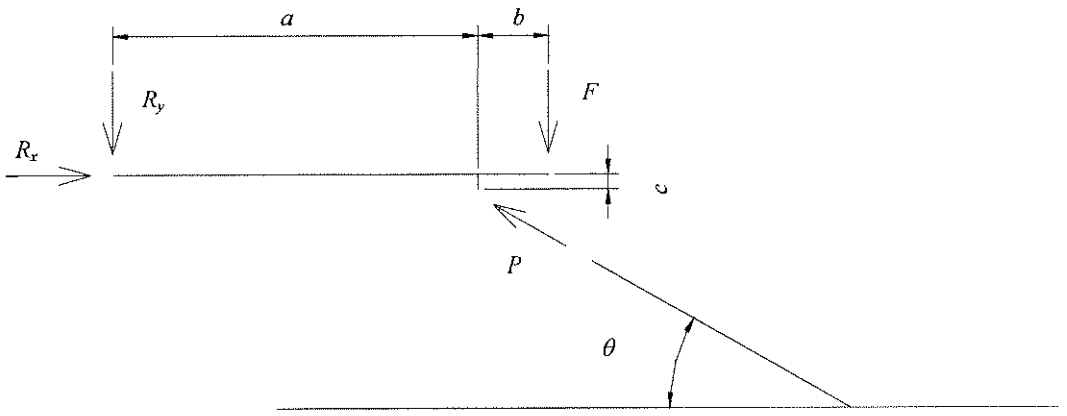

Figure D.2: Forces acting on the drill

The forces acting in the *x*-direction:

$$\begin{aligned}\sum_{\rightarrow} F_x &= 0 \\ &= R_x - P\cos(\theta)\end{aligned} \tag{D.6}$$

The forces acting in the *y*-direction:

$$\begin{aligned}\sum_{\uparrow} F_y &= 0 \\ &= -R_y - F + P\sin(\theta)\end{aligned} \tag{D.7}$$

The moments about *R*:

$$\begin{aligned}\sum_{\circlearrowleft} M &= 0 \\ &= F(a+b) - P\sin(\theta)a + P\cos(\theta)c \\ F &= \frac{P\sin(\theta)a - P\cos(\theta)c}{a+b}\end{aligned} \tag{D.8}$$

Table D.2: Drill dimensions

Dimension	Value [mm]
a	1690
b	330
c	70
Piston diameter	63

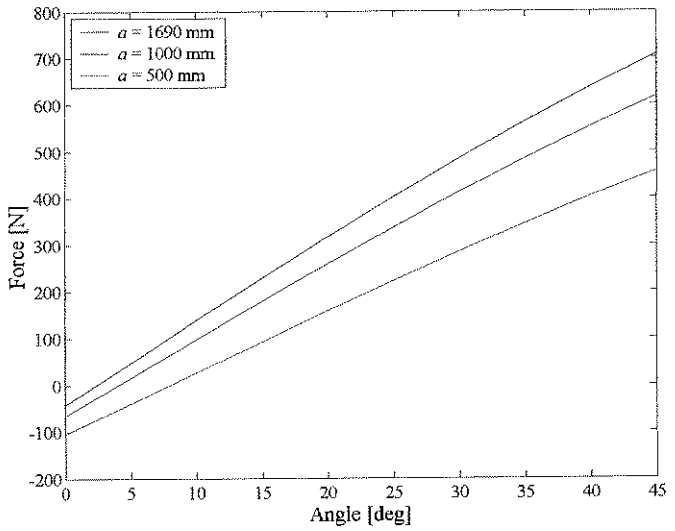

Figure D.3: Force *vs.* angle for a supply pressure of 400 kPa

D.5 Type I AVAI design (forces acting on the handle)

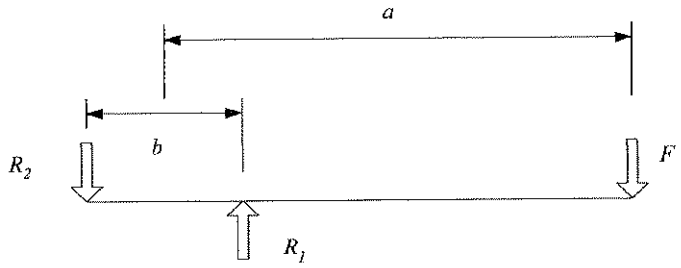

Figure D.4: Moment acting on the handle

The deflection at point R_1 can be calculated using the sum of the moments about R_2:

$$\begin{aligned} \sum M &= 0 \\ &= F\left(a+\frac{b}{2}\right)-R_1 b \\ R_1 &= \frac{F\left(a+\frac{b}{2}\right)}{b} \\ \delta_1 &= \frac{F}{k_1}\left(\frac{a}{b}+\frac{1}{2}\right) \end{aligned} \tag{D.9}$$

The deflection at point R_2 can be calculated using the sum of the moments and force balance in the y-direction:

$$\begin{aligned}\sum_{\uparrow} F_y &= 0 \\ &= -R_2 - R_1 - F \\ R_2 &= -\frac{F\left(a+\frac{b}{2}\right)}{b} - F \\ \delta_2 &= -\frac{F}{k_2}\left(\frac{a}{b}-\frac{1}{2}\right)\end{aligned} \tag{D.10}$$

The rotation angle can now be calculated by using Equation (D.9) and Equation (D.10):

$$\begin{aligned}\theta &= \sin^{-1}\left(\frac{\delta_2-\delta_1}{b}\right) \\ &= \sin^{-1}\left[\frac{-\frac{F}{k_2}\left(\frac{a}{b}-\frac{1}{2}\right)-\frac{F}{k_1}\left(\frac{a}{b}+\frac{1}{2}\right)}{b}\right]\end{aligned} \tag{D.11}$$

D.6 Type II AVAI design (effective area calculation)

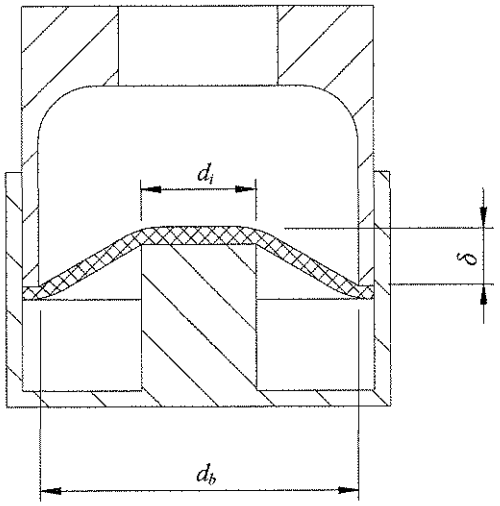

Figure D.5: Definition of dimensions

The volume change due to relative displacement δ is:

$$\Delta V = \frac{1}{3}A_b h - \frac{1}{3}A_i (h-\delta) \tag{D.12}$$

The relationship between h and δ is:

$$\frac{\frac{1}{2}d_b}{h} = \frac{\frac{1}{2}d_b - \frac{1}{2}d_i}{\delta}$$
$$h = \frac{d_b}{d_b - d_i}\delta \tag{D.13}$$

The volume change can now be written as:

$$\begin{aligned}\Delta V &= \frac{1}{3}A_b h - \frac{1}{3}A_i (h-\delta) \\ &= \frac{1}{3}A_b \frac{d_b}{d_b - d_i}\delta - \frac{1}{3}A_i\left(\frac{d_b}{d_b - d_i}\delta - \delta\right) \\ &= \frac{\pi}{12}\left(\frac{d_b^3}{d_b - d_i} - \frac{d_b d_i^2}{d_b - d_i} + d_i^2\right)\delta\end{aligned} \tag{D.14}$$

D.7 Type II AVAI design (damped design method)

The ratio of natural to isolation frequency is independent of the change in stiffness:

$$\frac{\omega_n}{\omega_i} = \sqrt{\frac{m_b \frac{A_b}{A_a}\left(\frac{A_b}{A_a} - 1\right)}{m + m_b\left(\frac{A_b}{A_a}\right)^2}} \tag{D.15}$$

The damped isolation frequency is:

$$\left(\frac{\Omega_i}{\omega_n}\right)^2 = \frac{-\left(\frac{\omega_n}{\omega_i}\right)^2 - 1 - \sqrt{\left[\left(\frac{\omega_n}{\omega_i}\right)^2 - 1\right]^2 + 8\zeta^2\left[\left(\frac{\omega_n}{\omega_i}\right)^2 + 1\right]}}{4\zeta^2 + 4\zeta^2\left(\frac{\omega_n}{\omega_i}\right)^2 - 2\left(\frac{\omega_n}{\omega_i}\right)^2} \tag{D.16}$$

The right hand side of the equation is constant:

$$C = \frac{-\left(\frac{\omega_n}{\omega_i}\right)^2 - 1 - \sqrt{\left[\left(\frac{\omega_n}{\omega_i}\right)^2 - 1\right]^2 + 8\zeta^2\left[\left(\frac{\omega_n}{\omega_i}\right)^2 + 1\right]}}{4\zeta^2 + 4\zeta^2\left(\frac{\omega_n}{\omega_i}\right)^2 - 2\left(\frac{\omega_n}{\omega_i}\right)^2} \tag{D.17}$$

The isolation frequency can be written in terms of the constant C:

$$\begin{aligned}\Omega_i^2 &= \omega_n^2 C \\ \Omega_i^2 &= \frac{k}{m + m_b\left(\frac{A_b}{A_a}\right)^2}C\end{aligned} \tag{D.18}$$

The device has to be designed such that the excitation frequency coincides with the isolation frequency (i.e. $\Omega_i = \Omega_e$). If it is assumed that the stiffness consists of a spring in parallel with the air spring, the stiffness can be written in terms of the pressure:

$$k = k_p P_s + k_c \tag{D.19}$$

Since there are two unknowns, two sets of excitation and pressure values are needed to solve for k_p and k_s. In matrix format the set of equations are:

$$\begin{bmatrix} P_1 & 1 \\ P_2 & 1 \end{bmatrix} \begin{bmatrix} k_p \\ k_s \end{bmatrix} = \frac{\left[m + m_B \left(\frac{A_b}{A_a} \right)^2 \right]}{C} \begin{bmatrix} \Omega_{e1}^2 \\ \Omega_{e2}^2 \end{bmatrix} \tag{D.20}$$

To solve for the stiffness:

$$\begin{bmatrix} k_p \\ k_c \end{bmatrix} = \frac{\left[m + m_b \left(\frac{A_b}{A_a} \right)^2 \right]}{C} \begin{bmatrix} P_1 & 1 \\ P_2 & 1 \end{bmatrix}^{-1} \begin{bmatrix} \Omega_{e1}^2 \\ \Omega_{e2}^2 \end{bmatrix} \tag{D.21}$$

APPENDIX E

Derivations for chapter 5

E.1 Refined model for a type I AVAI

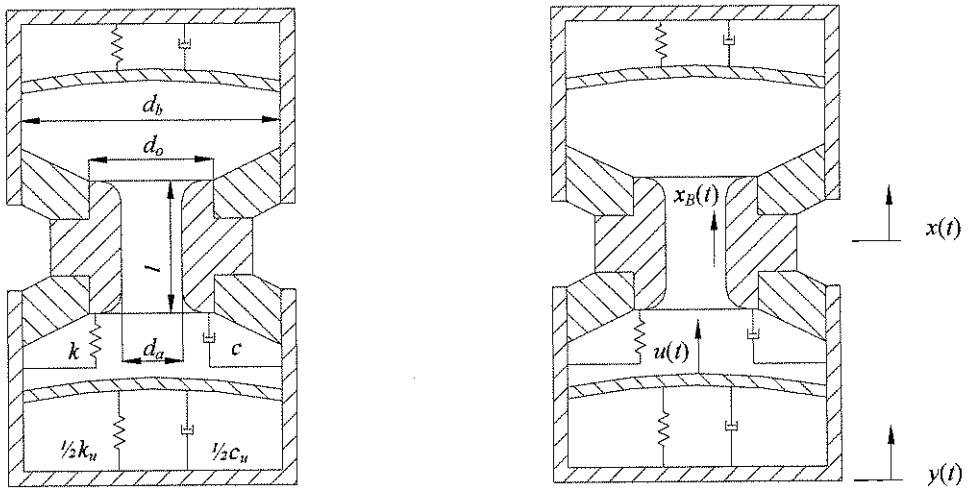

Figure E.1: A liquid vibration absorber system with base excitation

The displacement of the top and bottom elements must be equal under steady-state conditions because the fluid is incompressible. To find the continuity it is necessary to calculate the fluid displaced by the membrane. To do this it is necessary to know the shape of the membrane when deflected. If it is assumed that the displacement of the membrane assumes the shape of a paraboloid, the volume displaced can conveniently be written as:

$$V = \frac{1}{2} A_b h \tag{E.1}$$

with h the height of the paraboloid, which in this case is the relative displacement between u and y. Alternatively, if the membrane behaves as if fixed at the boundary, no rotation is possible and the deflected shape can be calculated (Young & Budynas, 2002).

The shape is a function of the radius:

$$y(r) = y_c + \frac{M_c r^2}{2D(1+\nu)} + LT_y$$

where: $LT_y = -\frac{qr^4}{64D}$

$$y_c = -\frac{qa^4}{64D} \tag{E.2}$$

$$M_c = \frac{qa^2(1+\nu)}{16}$$

$$D = \frac{Et^3}{12(1-\nu^2)}$$

for $r_o = 0$

a is the disk radius, v Poison's ratio, q the distributed load, E is the Young's modulus, t the membrane thickness and y_c the displacement of the centre of the disk. From the above y can be rewritten:

$$\begin{aligned} y &= y_c + \frac{qa^2}{32D} r^2 - \frac{qr^4}{64D} \\ &= y_c \left(1 - \frac{2}{a^2} r^2 + \frac{r^4}{a^4} \right) \end{aligned} \tag{E.3}$$

The displaced volume can now be calculated:

$$\begin{aligned} V &= \int_0^a \int_0^{2\pi} y_c \left(1 - \frac{2}{a^2} r^2 + \frac{r^4}{a^4} \right) r d\theta dr \\ &= 2\pi y_c \int_0^a r - \frac{2}{a^2} r^3 + \frac{r^5}{a^4} dr \\ &= 2\pi y_c \left(\frac{1}{2} r^2 - \frac{1}{2} \frac{r^4}{a^2} + \frac{r^6}{6a^4} \right) \Big|_0^a \\ &= \frac{1}{3} \pi a^2 y_c \\ &= \frac{1}{3} A_b y_c \end{aligned} \tag{E.4}$$

To make provision to test assumption regarding membrane shape the derivation of the equation of motion will be done in terms of a shape factor S_f. The volume is therefore:

$$V = S_f A_b h \tag{E.5}$$

The change in volume can be calculated by subtracting the initial volume from the current volume. In Figure E.2 the initial values are denoted by the subscript i, while the current values are without subscript.

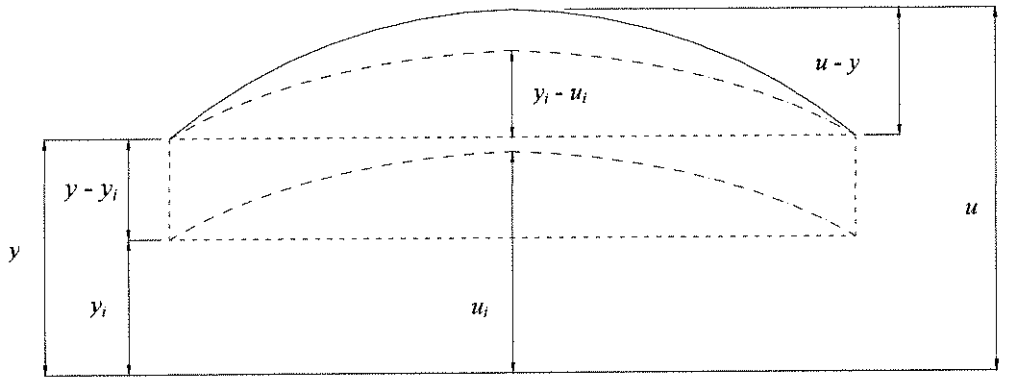

Figure E.2: Membrane displacement

The volume after relative displacement δ is:

$$\begin{aligned} V_s &= \frac{1}{3}A_b h_o - A_o(h-\delta) - \frac{1}{3}A_o(h_o - h + \delta) \\ h_o &= \frac{\delta - h}{\frac{d_o}{d_b} - 1} \\ &= \left(\frac{1}{3}A_b \frac{d_b}{d_b - d_o} - A_o - \frac{1}{3}A_o \frac{d_o}{d_b - d_o}\right)(h-\delta) \end{aligned} \tag{E.8}$$

The change in volume due to the relative displacement δ is:

$$\begin{aligned} \Delta V_\delta &= V_l - V_s \\ &= \left[\frac{A_b d_b - A_o d_o}{3(d_b - d_o)} - A_o\right]\delta \\ &= A_e \delta \end{aligned} \tag{E.9}$$

The total displaced volume is a function of the absolute and relative displacements of both x and y as explained in Figure E.4.

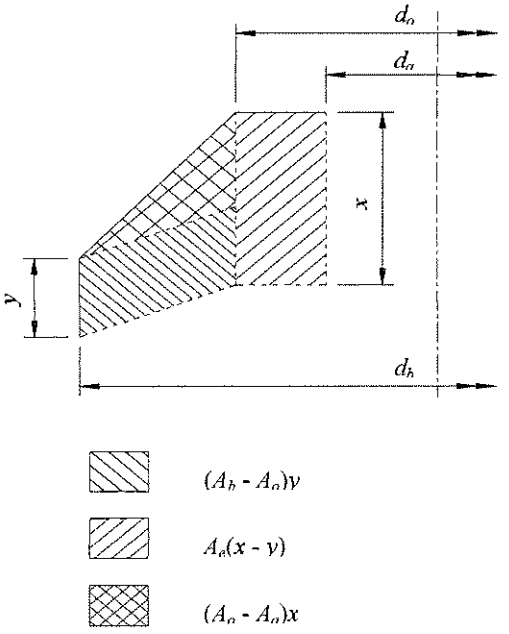

Figure E.4: Total displaced volume

The continuity is now given by:

$$\begin{aligned}
\left(1-S_f\right)A_b y + S_f A_b u &= \left[\frac{A_b d_b - A_o d_o}{3\left(d_b - d_o\right)} - A_a\right]\left(x-y\right) + \left(A_b - A_a\right)y + A_a x_B \\
x_B &= \left[1 - \frac{A_b d_b - A_o d_o}{3A_a\left(d_b - d_o\right)}\right]\left(x-y\right) + \left(1 - \frac{A_b}{A_a}\right)y + \left(1-S_f\right)\frac{A_b}{A_a}y + S_f\frac{A_b}{A_a}u \\
&= \left[\frac{A_b d_b - A_o d_o}{3A_a\left(d_b - d_o\right)} - S_f\frac{A_b}{A_a}\right]y + \left[1 - \frac{A_b d_b - A_o d_o}{3A_a\left(d_b - d_o\right)}\right]x + S_f\frac{A_b}{A_a}u \\
&= C_1 y - C_2 x + C_3 u \qquad \text{(E.10)} \\
C_1 &= \frac{A_b d_b - A_o d_o}{3A_a\left(d_b - d_o\right)} - S_f\frac{A_b}{A_a} = \frac{1}{3}\frac{A_b}{A_a}\left[\left(\frac{d_o}{d_b}\right)^2 + \frac{d_o}{d_b} + 1 - S_f\right] \\
C_2 &= 1 - \frac{A_b d_b - A_o d_o}{3A_a\left(d_b - d_o\right)} = \frac{1}{3}\frac{A_b}{A_a}\left[\left(\frac{d_o}{d_b}\right)^2 + \frac{d_o}{d_b} + 1\right] - 1 \\
C_3 &= S_f\frac{A_b}{A_a}
\end{aligned}$$

The kinetic energy is:

$$\begin{aligned}
T &= \frac{1}{2}m_x\dot{x}^2 + \frac{1}{2}m_y\dot{y}^2 + \frac{1}{2}m_B\dot{x}_B^2 \\
&= \frac{1}{2}m_x\dot{x}^2 + \frac{1}{2}m_y\dot{y}^2 + \frac{1}{2}m_B\left(C_1^2\dot{y}^2 + C_2^2\dot{x}^2 + C_3^2\dot{u}^2 - 2C_1C_2\dot{x}\dot{y} + 2C_1C_3\dot{y}\dot{u} - 2C_2C_3\dot{x}\dot{u}\right)
\end{aligned} \qquad \text{(E.11)}$$

The derivatives are:

$$\begin{aligned}
\frac{d}{dt}\left(\frac{\partial T}{\partial \dot{x}}\right) &= m_x\ddot{x} + m_B\left(C_2^2\ddot{x} - C_1C_2\ddot{y} - C_2C_3\ddot{u}\right) \\
&= -m_BC_1C_2\ddot{y} + \left(m_x + m_BC_2^2\right)\ddot{x} - m_BC_2C_3\ddot{u} \\
\frac{d}{dt}\left(\frac{\partial T}{\partial \dot{y}}\right) &= m_y\ddot{y} + m_B\left(C_1^2\ddot{y} - C_1C_2\ddot{x} + C_1C_3\ddot{u}\right) \\
&= \left(m_y + m_BC_1^2\right)\ddot{y} - m_BC_1C_2\ddot{x} + m_BC_1C_3\ddot{u} \\
\frac{d}{dt}\left(\frac{\partial T}{\partial \dot{u}}\right) &= m_B\left(C_3^2\ddot{u} + C_1C_3\ddot{y} - C_2C_3\ddot{x}\right) \\
&= m_BC_1C_3\ddot{y} - m_BC_2C_3\ddot{x} + m_BC_3^2\ddot{u}
\end{aligned} \qquad \text{(E.12)}$$

The mass matrix is:

$$\begin{bmatrix} M_1 & M_2 & M_3 \\ M_4 & M_5 & M_6 \\ M_7 & M_8 & M_9 \end{bmatrix} = \begin{bmatrix} m_y + m_BC_1^2 & -m_BC_1C_2 & m_BC_1C_3 \\ -m_BC_1C_2 & m_x + m_BC_2^2 & -m_BC_2C_3 \\ m_BC_1C_3 & -m_BC_2C_3 & m_BC_3^2 \end{bmatrix} \qquad \text{(E.13)}$$

The potential energy and Raleigh terms are the same as before (refer to Appendix B). The equation of motion with y prescribed and no external forces acting on the system is:

$$\begin{bmatrix} M_5 & M_6 \\ M_8 & M_9 \end{bmatrix}\begin{bmatrix} \ddot{x} \\ \ddot{u} \end{bmatrix} + \begin{bmatrix} c & 0 \\ 0 & c_u \end{bmatrix}\begin{bmatrix} \dot{x} \\ \dot{u} \end{bmatrix} + \begin{bmatrix} k & 0 \\ 0 & k_u \end{bmatrix}\begin{bmatrix} x \\ u \end{bmatrix} = \begin{bmatrix} ky + c\dot{y} - M_4\ddot{y} \\ k_u y + c_u\dot{y} - M_7\ddot{y} \end{bmatrix} \qquad \text{(E.14)}$$

By transforming to the frequency domain:

$$\begin{bmatrix} k+i\omega c-\omega^2 M_5 & -\omega^2 M_6 \\ -\omega^2 M_8 & k_u+i\omega c_u-\omega^2 M_9 \end{bmatrix}\begin{bmatrix} X \\ U \end{bmatrix}=\begin{bmatrix} k+i\omega c+\omega^2 M_4 \\ k_u+i\omega c_u+\omega^2 M_7 \end{bmatrix}Y \tag{E.15}$$

The membrane displacement is:

$$U=\frac{\left(k+i\omega c+\omega^2 M_4\right)Y-\left(k+i\omega c-\omega^2 M_5\right)X}{-\omega^2 M_6} \tag{E.16}$$

The transmissibility is:

$$\frac{X}{Y}=\frac{\omega^2 M_6\left(k_u+i\omega c_u+\omega^2 M_3\right)+\left(k_u+i\omega c_u-\omega^2 M_9\right)\left(k+i\omega c+\omega^2 M_2\right)}{\left(k_u+i\omega c_u-\omega^2 M_9\right)\left(k+i\omega c-\omega^2 M_5\right)-\left(\omega^2 M_6\right)^2} \tag{E.17}$$

The following natural frequencies can be defined:

$$\omega_1^2=\frac{k}{M_1}=\frac{k}{m_y+m_B C_1^2} \tag{E.18}$$

The transmissibility can now be non-dimensionalised:

$$\begin{aligned}
\frac{X}{Y} &= \frac{\omega^2\frac{M_6}{k_u}\left(1+i\omega\frac{k_u}{k}\frac{c_u}{k_u}+\omega^2\frac{M_3}{k}\right)+\left(1+i\omega\frac{c_u}{k_u}-\omega^2\frac{M_9}{k_u}\right)\left(1+i\omega\frac{c}{k}+\omega^2\frac{M_2}{k}\right)}{\left(1+i\omega\frac{c_u}{k_u}-\omega^2\frac{M_9}{k_u}\right)\left[1+i\omega\frac{c}{k}-\omega^2\frac{M_5}{k}\right]-\frac{k_u}{k}\left(\omega^2\frac{M_6}{k_u}\right)^2} \\
&= \frac{-\omega^2\frac{m_B C_2 C_3}{k_u}\left(1+i\omega\frac{k_u}{k}\frac{c_u}{k_u}+\omega^2\frac{m_B C_1 C_3}{k}\right)+\left(1+i\omega\frac{c_u}{k_u}-\omega^2\frac{m_B C_3^2}{k_u}\right)\left(1+i\omega\frac{c}{k}-\omega^2\frac{m_B C_1 C_2}{k}\right)}{\left(1+i\omega\frac{c_u}{k_u}-\omega^2\frac{m_B C_3^2}{k_u}\right)\left[1+i\omega\frac{c}{k}-\omega^2\frac{m_x+m_B C_2^2}{k}\right]-\frac{k_u}{k}\left(\omega^2\frac{m_B C_2 C_3}{k_u}\right)^2} \\
&= \frac{\frac{C_2}{C_3}\left(\frac{\omega}{\omega_9'}\right)^2\left[1+i2\frac{\omega}{\omega_9'}\frac{k_u}{k}\zeta_u+\frac{k_u}{k}\frac{C_1}{C_3}\left(\frac{\omega}{\omega_9'}\right)^2\right]+\left[1+i2\frac{\omega}{\omega_9'}\zeta_u-\left(\frac{\omega}{\omega_9'}\right)^2\right]\left[1+i2\frac{\omega}{\omega_2}\zeta_2-\left(\frac{\omega}{\omega_2}\right)^2\right]}{\left[1+i2\frac{\omega}{\omega_9'}\zeta_u-\left(\frac{\omega}{\omega_9'}\right)^2\right]\left[1+i2\frac{\omega}{\omega_5}\zeta_5-\left(\frac{\omega}{\omega_5}\right)^2\right]-\frac{k_u}{k}\left[\frac{C_2}{C_3}\left(\frac{\omega}{\omega_9'}\right)^2\right]^2}
\end{aligned}$$

$$\omega_3^2=\frac{k}{M_3}=\frac{k}{m_B C_1 C_3},\quad \omega_2^2=\frac{k}{M_2}=\frac{k}{m_B C_1 C_2},\quad \omega_6'^2=\frac{k_u}{M_6}=\frac{k_u}{m_B C_2 C_3}$$

$$\omega_9'^2=\frac{k_u}{M_9}=\frac{k_u}{m_B C_3^2},\quad \omega_3^2=\frac{k}{k_u}\frac{C_3}{C_1}\omega_9'^2,\quad \omega_1^2=\frac{k}{M_5}=\frac{k}{m_x+m_B C_2^2},\quad \omega_6'^2=\frac{C_3}{C_2}\omega_9'^2$$

$$\zeta_u=\frac{c_u}{2m_B C_3^2\omega_9'},\quad \zeta_5=\frac{c}{2\left(m_x+m_B C_2^2\right)\omega_5},\quad \zeta_2=\frac{c}{2m_B C_1 C_2\omega_2} \tag{E.19}$$

The equation of motion with x prescribed and no external forces acting on the system is:

$$\begin{bmatrix} M_1 & M_3 \\ M_7 & M_9 \end{bmatrix}\begin{bmatrix} \ddot{y} \\ \ddot{u} \end{bmatrix}+\begin{bmatrix} c+c_u & -c_u \\ -c_u & c_u \end{bmatrix}\begin{bmatrix} \dot{y} \\ \dot{u} \end{bmatrix}+\begin{bmatrix} k+k_u & -k_u \\ -k_u & k_u \end{bmatrix}\begin{bmatrix} y \\ u \end{bmatrix}=\begin{bmatrix} kx+c\dot{x}-M_2\ddot{x} \\ -M_8\ddot{x} \end{bmatrix} \tag{E.20}$$

By transforming to the frequency domain:

$$\begin{bmatrix} k+k_u+i\omega(c+c_u)-\omega^2 M_1 & -k_u-i\omega c_u-\omega^2 M_3 \\ -k_u-i\omega c_u-\omega^2 M_7 & k_u+i\omega c_u-\omega^2 M_9 \end{bmatrix}\begin{bmatrix} Y \\ U \end{bmatrix}=\begin{bmatrix} k+i\omega c+\omega^2 M_2 \\ \omega^2 M_8 \end{bmatrix}X \tag{E.21}$$

The membrane displacement can be found from the second equation in the set defined above:

$$U=\frac{\left(k_u+i\omega c_u+\omega^2 M_2\right)X-\left[k+k_u+i\omega(c+c_u)-\omega^2 M_1\right]Y}{-\left(k_u+i\omega c_u+\omega^2 M_3\right)} \tag{E.22}$$

The transmissibility is:

$$\frac{Y}{X}=\frac{\left(k_u+i\omega c_u+\omega^2 M_3\right)\omega^2 M_8+\left(k_u+i\omega c_u-\omega^2 M_9\right)\left(k+i\omega c+\omega^2 M_2\right)}{\left(k_u+i\omega c_u-\omega^2 M_9\right)\left[k+k_u+i\omega(c+c_u)-\omega^2 M_1\right]-\left(k_u+i\omega c_u+\omega^2 M_3\right)^2} \tag{E.23}$$

The transmissibility can now be non-dimensionalised:

$$\begin{aligned}
\frac{Y}{X}&=\frac{\omega^2\frac{M_6}{k_u}\left(1+i\omega\frac{k_u}{k}\frac{c_u}{k_u}+\omega^2\frac{M_3}{k}\right)+\left(1+i\omega\frac{c_u}{k_u}-\omega^2\frac{M_9}{k_u}\right)\left(1+i\omega\frac{c}{k}+\omega^2\frac{M_2}{k}\right)}{\left(1+i\omega\frac{c_u}{k_u}-\omega^2\frac{M_9}{k_u}\right)\left[1+\frac{k_u}{k}+i\omega\left(\frac{c}{k}+\frac{k_u}{k}\frac{c_u}{k_u}\right)-\omega^2\frac{M_1}{k}\right]-\frac{k_u}{k}\left(1+i\omega\frac{c_u}{k_u}+\omega^2\frac{M_3}{k_u}\right)^2} \\
&=\frac{-\omega^2\frac{m_B C_2 C_3}{k_u}\left(1+i\omega\frac{k_u}{k}\frac{c_u}{k_u}+\omega^2\frac{m_B C_1 C_3}{k}\right)+\left(1+i\omega\frac{c_u}{k_u}-\omega^2\frac{m_B C_3^2}{k_u}\right)\left(1+i\omega\frac{c}{k}-\omega^2\frac{m_B C_1 C_2}{k}\right)}{\left(1+i\omega\frac{c_u}{k_u}-\omega^2\frac{m_B C_3^2}{k_u}\right)\left[1+\frac{k_u}{k}+i\omega\left(\frac{c}{k}+\frac{k_u}{k}\frac{c_u}{k_u}\right)-\omega^2\frac{m_y+m_B C_1^2}{k}\right]-\frac{k_u}{k}\left(1+i\omega\frac{c_u}{k_u}+\omega^2\frac{m_B C_1 C_3}{k_u}\right)^2} \\
&=\frac{-\frac{C_2}{C_3}\left(\frac{\omega}{\omega_9'}\right)^2\left[1+i2\frac{\omega}{\omega_9'}\frac{k_u}{k}\zeta_u+\frac{k_u}{k}\frac{C_1}{C_3}\left(\frac{\omega}{\omega_9'}\right)^2\right]+\left[1+i2\frac{\omega}{\omega_9'}\zeta_u-\left(\frac{\omega}{\omega_9'}\right)^2\right]\left[1+i2\frac{\omega}{\omega_2}\zeta_2-\left(\frac{\omega}{\omega_2}\right)^2\right]}{\left[1+i2\frac{\omega}{\omega_9'}\zeta_u-\left(\frac{\omega}{\omega_9'}\right)^2\right]\left[1+\frac{k_u}{k}+i2\left(\frac{\omega}{\omega_1}\zeta_1+\frac{k_u}{k}\frac{\omega}{\omega_9'}\zeta_u\right)-\left(\frac{\omega}{\omega_1}\right)^2\right]-\frac{k_u}{k}\left[1+i2\frac{\omega}{\omega_9'}\zeta_u+\frac{C_1}{C_3}\left(\frac{\omega}{\omega_9'}\right)^2\right]^2}
\end{aligned}$$

$$\omega_3^2=\frac{k}{M_3}=\frac{k}{m_B C_1 C_3},\quad \omega_2^2=\frac{k}{M_2}=\frac{k}{m_B C_1 C_2},\quad \omega_6'^2=\frac{k_u}{M_6}=\frac{k_u}{m_B C_2 C_3},\quad \omega_9'^2=\frac{k_u}{M_9}=\frac{k_u}{m_B C_3^2}$$

$$\omega_3^2=\frac{k}{k_u}\frac{C_3}{C_1}\omega_9'^2,\quad \omega_3'^2=\frac{C_3}{C_1}\omega_9'^2,\quad \omega_1^2=\frac{k}{M_1}=\frac{k}{m_y+m_B C_1^2},\quad \omega_6'^2=\frac{C_3}{C_2}\omega_9'^2$$

$$\zeta_u=\frac{c_u}{2m_B C_3^2\omega_9'},\quad \zeta_1=\frac{c}{2\left(m_y+m_B C_1^2\right)\omega_1},\quad \zeta_2=\frac{c}{2m_B C_1 C_2\omega_2} \tag{E.24}$$